Ραδιοσημασμένες ενώσεις στη μοριακή απεικόνιση του αδενοκαρκινώματος του παγκρέατος

Radiolabeled compounds in molecular imaging of pancreatic adenocarcinoma

Κανελλόπουλος Παναγιώτης

Kanellopoulos Panagiotis

School of Medicine, University of Crete

2022

Three-member consultant committee

Prof. Liapakis G.
(School of Medicine, University of Crete)

Prof. Koukouraki S.
(School of Medicine, University of Crete)

Dr. Maina Nock T.
(INRASTES, NCSR "Demokritos")

Rest of the examining seven-member committee

Prof. Kampa M.E.
(School of Medicine, University of Crete)

Prof. Mavromoustakos T.
(Department of Chemistry, University of Athens)

Prof. Venihaki M.
(School of Medicine, University of Crete)

Dr. Nock B.A.
(INRASTES, NCSR "Demokritos")

Acknowledgments

List of tables

List of images

Table of Contents

Περίληψη

Ο παγκρεατικός καρκίνος (PC) καταγράφηκε ως ο $10^{ος}$ σε συχνότητα καρκίνος στον άνθρωπο και ως $4^η$ αιτία θανάτου από καρκίνο στις ΗΠΑ το 2018. Ο ασυμπτωματικός χαρακτήρας του PC σε συνδυασμό με την έλλειψη επαρκών διαγνωστικών μεθόδων για την έγκαιρη διάγνωση συμβάλλουν σε αυτήν την κατάσταση. Η πρόσφατη τεχνολογική πρόοδος στις απεικονιστικές διατάξεις της πυρηνικής ιατρικής (τομογραφία ποζιτρονίου (PET), ή υπολογιστική τομογραφία μονοφωτονιακής εκπομπής (SPECT)), παράλληλα με την πρόσφατη έλευση των νέων μοριακών ραδιοφαρμάκων, αναμένεται να προσφέρουν στους κλινικούς γιατρούς εξελιγμένα διαγνωστικά εργαλεία στο άμεσο μέλλον. Έτσι, αναμένεται να καταστεί δυνατή η απεικόνιση πρωτογενών και μεταστατικών εστιών PC μη παρεμβατικά, γρήγορα και με ευκολία, με την αλληλεπίδραση ραδιοσημασμένων μορίων (π.χ. ραδιοσημασμένων πεπτιδίων) με ειδικά βιομόρια – "στόχους" (π.χ. υποδοχείς πεπτιδίων), χαρακτηριστικών για τον καρκίνο. Σήμερα υπάρχει επείγουσα ανάγκη για νέα ραδιοφάρμακα για εφαρμογή στην ακριβή και αξιόπιστη διάγνωση του PC, και ιδιαίτερα του εξωκρινούς ποροειδούς αδενοκαρκινώματος του παγκρέατος (PDAC) που αποτελεί το 95% των περιστατικών PC.

Αξίζει να σημειωθεί ότι ο υποδοχέας 1 της νευροτενσίνης (ή νευροτανσίνης) (NTS$_1$R) αντιπροσωπεύει υποψήφιο βιομοριακό στόχο στη διάγνωση του PDAC, δεδομένου ότι υπερεκφράζεται επιλεκτικά στο 95% των περιστατικών PDAC αλλά όχι στο υγιές πάγκρεας ή σε χρόνια παγκρεατίτιδα. Η ύπαρξη του ενδογενούς πεπτιδικού NTS$_1$R-προσδέτη νευροτενσίνης (NT) και πληθώρας συνθετικών NT-αναλόγων δίνουν το έναυσμα για την ανάπτυξη NT-σχετικών ραδιοφαρμάκων. Όπως όλα τα πεπτίδια, η NT και τα ανάλογα της υφίστανται ταχεία πρωτεολυτική αποικοδόμηση. Δύο κυρίως πεπτιδάσες, η νεπριλυσίνη (NEP) και το μετατρεπτικό ένζυμο της αγγειοτενσίνης (ή αγγειοτασίνης) (ACE) εμπλέκονται στην ταχεία αποικοδόμηση των αναλόγων NT στον οργανισμό. Παρόμοια, ραδιοπεπτίδια στόχευσης του NTS$_1$R αποικοδομούνται κατά την πορεία τους στις καρκινικές εστίες με αρνητικά αποτελέσματα στην ικανότητα πρόσληψης τους εκεί.

Στόχος της παρούσας διατριβής ήταν η ανάπτυξη νέων στρατηγικών ή/και πεπτιδικών ραδιοπροσδετών με βάση το C-τελικό εξαπεπτίδιο NT(8-13), ώστε να βελτιωθεί η *in vivo* σταθερότητα, η στόχευση των όγκων και η ολική φαρμακοκινητική, ώστε να αποβούν κατάλληλα και επιτυχή στην διάγνωση του PC/PDAC με SPECT. Για την επιτυχία αυτού του σκοπού εφαρμόστηκαν δύο μέθοδοι: (1) Επαναξιολόγηση γνωστών [^{99m}Tc]Tc-σημασμένων NT(8-13)-αναλόγων χωρίς ή με *in situ* αναστολή των NEP ή/και ACE. (2) Σχεδιασμός νέων NT-ραδιοπεπτιδίων με δομικές παρεμβάσεις-κλειδιά στο NT(8-13). Η διαγνωστική αξία των αναλόγων αυτών μελετήθηκε και πάλι χωρίς ή με *in situ* αναστολή των NEP ή/και ACE.

Για την επίτευξη του πρώτου στόχου, τα ήδη γνωστά DT1 (N$_4$-Gly-Arg-Arg-Pro-Tyr-Ile-Leu-OH), DT5 (N$_4$-βAla-Arg-Dab-Pro-Tyr-Ile-Leu-OH) και DT6 (N$_4$-βAla-Arg-Dab-Pro-Tyr-Tle-Leu-OH) επισημάνθηκαν με Tc-99m. Έγινε σύγκριση της πρόσληψης τους σε κύτταρα WiDr, της σταθερότητας τους στο αίμα υγιών

ποντικιών και της βιοκατανομής τους σε ανοσοκατεσταλμένα ποντίκια με όγκους WiDr, καταλήγοντας στα ακόλουθα συμπεράσματα: i) Η αντικατάσταση Dab^9/Arg^9 οδήγησε σε χαμηλότερη κυτταρική πρόσληψη *in vitro*, μη μετρήσιμη βελτίωση της μεταβολικής σταθερότητας, χαμηλότερη πρόσληψη σε όγκους WiDr και αυξημένη νεφρική εντόπιση. ii) Η αντικατάσταση Tle^{12}/Ile^{12} αύξησε δραστικά την *in vivo* σταθερότητα, αλλά μείωσε την κυτταρική πρόσληψη *in vitro* και την πρόσληψη στον όγκο *in vivo*. Το [^{99m}Tc]Tc-DT1 εμφάνισε τις καλύτερες *in vitro* ιδιότητες, και συνδύασε άριστη στόχευση των όγκων WiDr με ταχεία φαρμακοκινητική *in vivo* με παράλληλη αναστολή των NEP και ACE. Ως εκ τούτου, [^{99m}Tc]Tc-DT1 επιλέχθηκε ως ένωση αναφοράς για την αξιολόγηση των νέων δομικά τροποποιημένων αναλόγων.

Για την αξιολόγηση όλων των αναλόγων σε αξιόπιστο και πρακτικά εύχρηστο NTS$_1$R-θετικό πρότυπο PC, έγινε σύγκριση της καταλληλότητας τεσσάρων διαφορετικών κυτταρικών σειρών PC: AsPC-1, PANC-1, MiaPaca-2 και Capan-1. Με επώαση του [^{99m}Tc]Tc-DT1 σε αυτά τα κύτταρα προέκυψε η ακόλουθη σειρά μειούμενης κυτταρικής πρόσληψης: κύτταρα AsPC-1 >> PANC-1 >>MiaPaca-2 > CAPAN-1. Επιπλέον, η ανάπτυξη όγκων μετά την εμφύτευση κυττάρων AsPC-1 σε ποντίκια SCID βρέθηκε παρόμοια με των κυττάρων WiDr, με τις δύο κυτταρικές σειρές να χρειάζονται χρονικό διάστημα 3 – 4 εβδομάδων για την ανάπτυξη όγκων στα σημεία της εμφύτευσης. Ως εκ τούτου, τα κύτταρα AsPC-1 επιλέχθηκαν ως η κατάλληλη κυτταρική σειρά PC για την παρούσα διατριβή. Συνολικά, το [^{99m}Tc]Tc-DT1 έδειξε παρόμοια συμπεριφορά *in vitro* και *in vivo* πειραματικά πρότυπα των κυττάρων WiDr και AsPC-1. Παρότι η φωσφοραμιδόνη (PA) έχει μέχρι τώρα χρησιμοποιηθεί με επιτυχία για αναστολή της NEP, αποφασίστηκε αλλαγή προς το εγκεκριμένο αντιϋπερτασικό φάρμακο Entresto$^®$ για τον σκοπό αυτό, προσβλέποντας σε μελλοντική «μετάφραση» της μεθοδολογίας από τα ποντίκια σε ασθενείς. Πράγματι, το Entresto$^®$ αποδείχθηκε εξίσου αποτελεσματικό με το PA, με τις όποιες παρατηρούμενες μικροδιαφορές στην σταθεροποιητική δράση των δύο αυτών αναστολέων να αποδίδονται: i) στον τρόπο χορήγησης (PA – iv, Entresto$^®$ - per os), ii) διαφορές μεταξύ των ζώων και iii) τη μικρή ικανότητα αναστολής του ACE από PA σε υψηλές δόσεις.

Στη δεύτερη ενότητα της διατριβής, επιχειρήθηκαν δομικές παρεμβάσεις στο DT1 σύμφωνα με δύο βασικές στρατηγικές. Επιμήκυνση / αντικατάσταση στο C-τελικό άκρο, ή εισαγωγή πλευρικών ομάδων στην ε-αμινο-ομάδα της Lys^7 μετά από αντικατάσταση της Gly^7 στην αρχική DT1 αλληλουχία. Η πρώτη ομάδα αναλόγων περιέλαβε τα DT7 (N$_4$-Gly-Arg-Arg-Pro-Tyr-Ile-Leu-D-Asn-OH) και DT13 (N$_4$-Gly-Arg-Arg-Pro-Tyr-Ile-β^{3}hLeu-OH), που και τα δύο διατήρησαν υψηλή συγγένεια δέσμευσης στον NTS$_1$R. Οι αντίστοιχοι [^{99m}Tc]Tc-ραδιοπροσδέτες επέδειξαν αυξημένη *in vivo* σταθερότητα στην κυκλοφορία του αίματος σε υγιή ποντίκια, αλλά έφθασαν σε μέγιστη σταθερότητα μόνο μετά τη χορήγηση του συνδυασμού Entresto$^®$+Lis στα ποντίκια. Τα [^{99m}Tc]Tc-DT7 και [^{99m}Tc]Tc-DT13 έδειξαν πολύ χαμηλή πρόσληψη σε κύτταρα AsPC-1 *in vitro*, οπότε δεν επιλέχθηκαν για περαιτέρω μελέτη της βιοκατανομής τους σε ποντίκια με όγκους AsPC-1.

Στη δεύτερη ομάδα Lys^7-τροποποιημένων αναλόγων, αρχικά προσδέθηκε μια πλευρική παλμιτοϋλο-ομάδα – DT8 (N$_4$-Lys(palmitoyl)-Arg-Arg-Pro-Tyr-Ile-Leu-OH), προς μίμηση αναλόγων της contulakin-G, ενός αναλόγου της NT από τα ασπόνδυλα. Το DT8 έδειξε υψηλή συγγένεια δέσμευσης στον NTS1R και το [^{99m}Tc]Tc-DT8 υψηλή πρόσληψη σε κύτταρα AsPC-1. Η σταθερότητα του ραδιοπροσδέτη στην κυκλοφορία του αίματος υγιών ποντικιών ήταν επίσης πολύ υψηλή. Οι ιδιότητες αυτές μεταφράστηκαν σε πολύ ικανοποιητική πρόσληψη του [^{99m}Tc]Tc-DT8 σε ετερομοσχεύματα AsPC-1 σε ποντίκια SCID, όμως συνδυάστηκε με ανεπιθύμητη και επίμονα υψηλή ακτινοβολία υποστρώματος. Συμπεραίνεται, ότι η ισχυρή δέσμευση της παλμιτοϋλο-ομάδας του [^{99m}Tc]Tc-DT8 στην αλβουμίνη και η υψηλή της λιποφιλικότητα τελικά οδήγησαν σε μη επιθυμητή φαρμακοκινητική.

Στη 2^η γενιά αναλόγων με πλευρική ομάδα προσδεμένη στην ε-αμινο-ομάδα της Lys^7: μια ομάδα 4-(4-μεθυλοφαινυλ)βουτυρικού οξέος (MPBA) προσδέθηκε είτε απευθείας – DT9 (N$_4$-Lys(MPBA)-Arg-Arg-Pro-Tyr-Ile-Leu-OH) είτε διαμέσου συνδετικού μορίου PEG4 (πολυαιθυλενογλυκόλη) – DT10 (N$_4$-Lys(PEG4-MPBA)-Arg-Arg-Pro-Tyr-Ile-Leu-OH). Σε τρίτο ανάλογο έγινε πρόσδεση ομάδας PEG6 (CH$_3$-PEG5-CH$_2$-COOH) – DT11 (N$_4$-Lys(PEG6)-Arg-Arg-Pro-Tyr-Ile-Leu-OH). Οι δομικές αυτές τροποποιήσεις δε μείωσαν την αλληλεπίδραση των αναλόγων με τον NTS$_1$R, και τα DT9, DT10 και DT11 επέδειξαν υπονανομοριακή συγγένεια δέσμευσης στον υποδοχέα. Τα [^{99m}Tc]Tc-DT9 and [^{99m}Tc]Tc-DT10 προσλήφθηκαν σε κύτταρα AsPC-1 εξίσου ικανοποιητικά με το [^{99m}Tc]Tc-DT1, ενώ το [^{99m}Tc]Tc-DT11 έδειξε μειωμένη πρόσληψη. Όπως αναμενόταν, οι ραδιοπροσδέτες χωρίς πλευρική ABD-ομάδα, [^{99m}Tc]Tc-DT1 και [^{99m}Tc]Tc-DT11 έδειξαν χαμηλή δέσμευση στην αλβουμίνη. Σε αντίθεση, τα [^{99m}Tc]Tc-DT9 και [^{99m}Tc]Tc-DT10 δεσμεύτηκαν σε ικανοποιητικό ποσοστό στην αλβουμίνη, με το ποσοστό αυτό να μειώνεται με προσθήκη του παυσίπονου ιμπουπτοφένης (ibuprofen), που δεσμεύεται στην αλβουμίνη. Το [^{99m}Tc]Tc-DT9 έδειξε παρόμοια χαμηλή *in vivo* σταθερότητα με το [^{99m}Tc]Tc-DT1 στην κυκλοφορία του αίματος υγιών ποντικιών, με τα [^{99m}Tc]Tc-DT10 και [^{99m}Tc]Tc-DT11 να είναι σημαντικότερα πιο σταθερά, αναδεικνύοντας την επίδραση στερεοχημικών παραγόντων. Όλοι οι ραδιοπροσδέτες έφθασαν στο υψηλότερο ποσοστό σταθερότητας μετά τη χορήγηση του συνδυασμού Entresto$^®$+Lis στα ποντίκια. Είναι αξιοσημείωτο το ότι το [^{99m}Tc]Tc-DT10 μετά τη χορήγηση του Entresto$^®$ μόνο επέτυχε παρόμοια ποσοστά σταθερότητας με αυτά των [^{99m}Tc]Tc-DT9 και [^{99m}Tc]Tc-DT11 μετά την συνδυαστική χορήγηση Entresto$^®$+Lis. Σε ποντίκια SCID με ετερομοσχεύματα AsPC-1 οι τρεις ραδιοπροσδέτες επέδειξαν πολύ ταχύτερη κάθαρση υποστρώματος σε σύγκριση με το [^{99m}Tc]Tc-DT8. Η πρόσληψη των τριών ραδιοπροσδετών στους όγκους AsPC-1 στην ομάδα των μαρτύρων βρέθηκε σημαντικά αυξημένη σε σχέση με το [^{99m}Tc]Tc-DT1, και αυξήθηκε περαιτέρω με εφαρμογή του συνδυασμού Entresto$^®$+Lis ([^{99m}Tc]Tc-DT9 και [^{99m}Tc]Tc-DT11) ή μόνο του Entresto$^®$ ([^{99m}Tc]Tc-DT10). Συμπερασματικά, το [^{99m}Tc]Tc-DT10, ξεπέρασε όλα τα ανάλογα της παρούσας διατριβής με κριτήρια τη σταθερότητα, τη στόχευση των όγκων και της ταχείας κάθαρσης υποστρώματος, ιδιαίτερα μετά την χορήγηση ενός μόνον αναστολέα στα ποντίκια, του εγκεκριμένου φαρμάκου Entresto$^®$.

Τα αποτελέσματα αυτά αναδεικνύουν την αποτελεσματικότητα και σημασία της στρατηγικής της *in situ* σταθεροποίησης ραδιοπεπτιδίων, δεδομένου ότι οδήγησαν σε σημαντικές βελτιώσεις στη συμπεριφορά μεταβολικά ασταθών NTS_1R-ραδιοπροσδετών. Επίσης ανέδειξαν ότι η προσθήκη πλευρικών ομάδων διαμέσου της Lys^7 μετά την εισαγωγή της στην αλυσίδα NT(7-13), ήταν ανεκτή από τον NTS_1R. Η συμπεριφορά των αντίστοιχων ραδιοπροσδετών δείχτηκε ότι εξαρτάται από τις ιδιότητες της πλευρικής ομάδας, όπως η λιποφιλικότητα, η ικανότητα δέσμευσης στην αλβουμίνη και στερεοχημικούς παράγοντες. Η συμπεριφορά του $[^{99m}Tc]$Tc-DT10 ήταν ιδιαίτερα ικανοποιητική σε προκλινικό επίπεδο, ιδιαίτερα σε συνδυασμό με Entresto®, ώστε να ανταγωνίζεται άλλους NTS_1R-ραδιοπροσδέτες ήδη σε κλινική αξιολόγηση με SPECT. Ως εκ τούτου, περαιτέρω μελέτη απαιτείται για τη διερεύνηση της προοπτικής αυτής σε ασθενείς PC.

Summary

Pancreatic cancer (PC) was identified as the 10th most common cancer in humans and 4th cause of cancer deaths in USA in 2018. The asymptomatic character of PC at the early stages in combination with the lack of effective diagnostic tools for its early diagnosis contribute in these poor outcomes. Recent advances in nuclear medicine technology (positron emission tomography (PET) and single positron emission computed tomography (SPECT), alongside with the recent advent of novel molecular radiopharmaceuticals, may offer clinicians better diagnostic tools in near future. In this way, the visualization of primary and metastatic PC lesions may become feasible in a non-invasive, fast and convenient way, after interaction of the radiolabeled probe (e.g. a peptide radioligand) with cancer-related "finger-print" biomolecules – "targets" (e.g. a G – protein coupled receptor or GPCR). Currently, there is an urgent need for new radiolabeled probes for effective and reliable diagnosis of PC, and especially of exocrine pancreatic ductal adenocarcinoma (PDAC) representing 95% of PC cases.

Interestingly, neurotensin subtype 1 receptor (NTS_1R) may serve as a viable biomolecular target in PDAC diagnosis, owing to its overexpression in 95% of PDAC cases in combination with its lack of expression in healthy pancreas and in chronic pancreatitis. The availability of the native NTS_1R peptide ligand neurotensin (NT) and numerous synthetic NT-analogs provide the basis for the development of new NT-like radiopharmaceuticals. Like any peptide, NT and its analogs undergo rapid proteolytic degradation; two major peptidases, neprilysin (NEP) and angiotensin converting enzyme (ACE) are implicated in their rapid breakdown in the body. Likewise, NTS_1R-targeting radiopeptides are degraded on their way to tumor sites with negative impact on their tumor-targeting capabilities.

The aim of the present work was the development of new strategies and/or peptide radioligands based on the C-terminal hexapeptide NT(8-13), to improve *in vivo* stability, enhanced tumor-targeting and favorable overall pharmacokinetics and eventually suitable for accurate PC/PDAC diagnosis with SPECT. Two major approaches were pursued to achieve this goal: (1) Re-evaluation of previously reported [^{99m}Tc]Tc-labeled NT(8-13)-analogs without or during *in situ* inhibition of NEP and/or ACE. (2) Design of new NT-like radiopeptides after key-structural changes of the NT(8-13) motif; the diagnostic efficacy of these analogs was again evaluated without or during *in situ* NEP and/or ACE inhibition.

To address the first task, previously reported NT analogs, DT1 (N_4-Gly^7-Arg^8-Arg^9-Pro^{10}-Tyr^{11}-Ile^{12}-Leu^{13}-OH), DT5 (N_4-βAla-Arg-Dab-Pro-Tyr-Ile-Leu-OH) and DT6 (N_4-βAla-Arg-Dab-Pro-Tyr-Tle-Leu-OH) were labeled with Tc-99m. Their uptake in colon adenocarcinoma WiDr cells, stability in peripheral mice blood and biodistribution in WiDr tumor-bearing mice were compared, leading to the following conclusions: i) The Dab^9/Arg^9-substitution resulted in lower cell uptake *in vitro*, no measurable improvement of metabolic stability, lower uptake in WiDr tumors and elevated renal uptake. ii) the Tle^{12}/Ile^{12}-substitution drastically increased *in*

vivo stability, but led to impaired cell uptake *in vitro* and tumor uptake *in vivo*. [^{99m}Tc]Tc-DT1 showed superior *in vitro* performance, combining excellent WiDr tumor targeting and fast pharmacokinetics *in vivo* during dual NEP and ACE inhibition. Hence [^{99m}Tc]Tc-DT1 was chosen as reference for the evaluation of the new structurally modified analogs.

To test all analogs in a reliable and convenient NTS$_1$R-positive PC model, the suitability of four different PC cell lines was compared: AsPC-1, PANC-1, MiaPaca-2 and Capan-1. By incubating [^{99m}Tc]Tc-DT1 with these cell lines the following rank of cell uptake was established: AsPC-1 >> PANC-1 >>MiaPaca-2 > CAPAN-1 cells. Furthermore, the tumorgenicity of AsPC-1 cells tested in SCID mice was found comparable with that of WiDr cells, with both cell lines requiring a time-span of 3 – 4 weeks for tumors to grow at the inoculation sites. In view of the above, AsPC-1 cells were selected as the PC cell line of choice in this thesis. Overall, the [^{99m}Tc]Tc-DT1 reference displayed similar performance both *in vitro* and *in vivo* between the WiDr and AsPC-1 cell models. Although phosphoramidon (PA) has been successfully applied for NEP inhibition thus far, a switch to the registered antihypertensive drug Entresto® was decided for such purposes, in support of future translation from animals to patients. Interestingly, Entresto® was proven equally effective as PA, with minor differences observed in the stabilization effects of the two agents attributed to: i) the administration routes (PA – iv, Entresto® - per os), ii) individual animal status and iii) the minor ACE-inhibition ability of PA at higher doses.

In the second part of this thesis, structural modifications of the DT1 motif were adopted comprising two major interventions. C-terminal modification (1st group), or introduction of pendant groups at the ε-amine of Lys^7 replacing Gly^7 (2nd group) in the original DT1 template. The first group comprises the analogs DT7 (N$_4$-Gly-Arg-Arg-Pro-Tyr-Ile-Leu-D-Asn-OH) and DT13 (N$_4$-Gly-Arg-Arg-Pro-Tyr-Ile-β^{3}hLeu-OH), both retaining high binding affinity for NTS$_1$R. The respective [^{99m}Tc]Tc-radioligands showed increased *in vivo* stability in peripheral mice blood, although they achieved maximum stability only after treatment of mice with the Entresto®+Lisinopril (Lis) combination. Both [^{99m}Tc]Tc-DT7 and [^{99m}Tc]Tc-DT13 displayed poor uptake in AsPC-1 cells *in vitro*, thereby failing to qualifying for further study of their biodistribution profiles in AsPC-1 tumor-bearing mice.

In the second Lys^7-modified set of compounds, a pendant palmitoyl group was first attached: DT8 (N$_4$-Lys(palmitoyl)-Arg-Arg-Pro-Tyr-Ile-Leu-OH), mimicking analogs of the invertebrate NT-counterpart contulakin-G. DT8 displayed an excellent affinity for NTS$_1$R and [99mTc]Tc-DT8 high uptake in AsPC-1 cells. The radioligand stability in mice peripheral blood was excellent as well. These results translated into a very promising tumor uptake of [^{99m}Tc]Tc-DT8 in AsPC-1 xenografts bearing SCID mice which however was compromised by a very unfavorable and persistently high background radioactivity. Thus, the strong binding of the palmitoyl pendant group of [^{99m}Tc]Tc-DT8 to albumin and its high lipophilicity resulted in poor end-pharmacokinetics.

In the 2nd generation of compounds with a pendant group attached at the ε-amine of Lys[7]: a 4-(4-methylphenyl)butyric acid (MPBA) moiety was attached either directly – DT9 (N_4-Lys(MPBA)-Arg-Arg-Pro-Tyr-Ile-Leu-OH) or via a polyethylenoglycol PEG4-spacer – DT10 (N_4-Lys(PEG4-MPBA)-Arg-Arg-Pro-Tyr-Ile-Leu-OH); in a third analog a PEG6 (Met-PEG5-CH_2-COOH) was introduced – DT11 (N_4-Lys(PEG6)-Arg-Arg-Pro-Tyr-Ile-Leu-OH). These modifications were excellently tolerated by the NTS_1R, with DT9, DT10 and DT11 displaying sub-nanomolar receptor affinities. [^{99m}Tc]Tc-DT9 and [^{99m}Tc]Tc-DT10 were taken up by AsPC-1 cells equally well with [^{99m}Tc]Tc-DT1, while [^{99m}Tc]Tc-DT11 showed lower cell uptake. As expected, the radioligands lacking an albumin binding domain (ABD) -functionality, [^{99m}Tc]Tc-DT1 and [^{99m}Tc]Tc-DT11 demonstrated poor binding to albumin. In contrast, [^{99m}Tc]Tc-DT9 and [^{99m}Tc]Tc-DT10 were well bound to albumin, with their binding being significantly reduced by the albumin-binding pain-killer ibuprofen. While [^{99m}Tc]Tc-DT9 displayed similar *in vivo* stability with the [^{99m}Tc]Tc-DT1 reference in peripheral mice blood, [^{99m}Tc]Tc-DT10 and [^{99m}Tc]Tc-DT11 were significantly more stable, revealing the impact of steric factors. All radiotracers reached their maximum stability by treatment of animals with the Entresto®+Lis combination. It should be noted however that [^{99m}Tc]Tc-DT10 could achieve similar stability levels by Entresto® alone with [^{99m}Tc]Tc-DT9 and [^{99m}Tc]Tc-DT11 during Entresto®+Lis treatment. In SCID mice bearing AsPC-1 xenografts the three radioligands displayed by far a faster clearance from the background compared with [^{99m}Tc]Tc-DT8. In the control animals the uptake of the three new radioligands was higher than the [^{99m}Tc]Tc-DT1 reference, further increasing in the animals treated with the Entresto®+Lis combination ([^{99m}Tc]Tc-DT9 and [^{99m}Tc]Tc-DT11) or with Entresto® only ([^{99m}Tc]Tc-DT10). In conclusion, [^{99m}Tc]Tc-DT10, outperformed all analogs of the thesis in terms of stability, tumor targeting and background clearance, especially after treatment of animals with a single inhibitor, the registered drug Entresto®.

These results emphasize the validity and importance of the *in situ* stabilization approach, leading to notable improvements in performance of biodegradable NTS_1R-targeting radioligands. They have also shown that the introduction of pendant groups at Lys[7] introduced in the NT(8-13) chain, was well tolerated by the NTS_1R. The performance of resulting radioligands was found highly dependent on pendant group features, such as lipophilicity, albumin binding capability and steric factors. The performance of [^{99m}Tc]Tc-DT10 was very promising at the preclinical level, especially in combination with Entresto®, fairly competing with other NTS_1R-targeting SPECT radiotracers already in clinical tests. Further studies are warranted to assess this option in PC patients.

Introduction

Pancreas and pancreatic cancer

Pancreas is a gland, located behind the stomach near its junction with duodenum and its length is approximately 15 cm in adults (**Image I1**). As part of the gastrointestinal track it plays a dual role. On one hand, it functions as an endocrine gland, producing hormones excreted into the bloodstream, and on the other, as an exocrine gland, producing enzymes mandatory for digestion, which are secreted through the ducts to the duodenum (**Image I1**) (1,2) .

The most common diseases associated with the pancreas comprise three major types. First, inflammation of pancreas or pancreatitis (PT), which presents as acute or as chronic. Second, insulin-dependent diabetes or type I diabetes, which in the majority of cases is an autoimmune elimination of β cells. Third, neoplasms which can be either neuroendocrine tumors (NETs) originating from the endocrine part of the pancreas, or exocrine pancreatic ductal adenocarcinoma (PDAC), originating from the exocrine part of the pancreas; the latter type has been the focus of the present work (3,4)
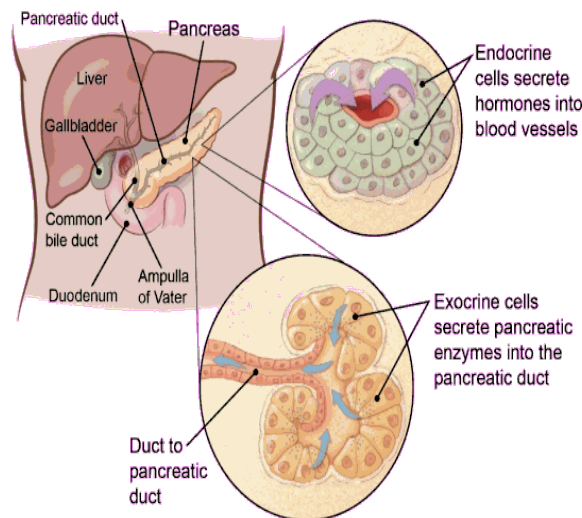
Image I1: Image of human pancreas and its parts. Image from:
https://www.cancer.org/cancer/pancreatic-cancer/about/what-is-pancreatic-cancer.html

Pancreatic cancer (PC) is the 10th most common human cancer and the 4th cause of death from cancer, with a five-year-survival rate reported to be around 10% in the USA in 2018. The greatest concerns in the management of PC are linked to its asymptomatic character up to advanced stages along with the lack of effective diagnostic tools in its early stages (5–7).

Radioactivity and Imaging modalities

Radioactive emission is the emission of radiation after the decay of the radioactive atom. It can be classified in four different types:

- **Alpha or α** is the emission of a helium nucleus, consisting of two neutrons and two protons, deprived of its electrons

- **Beta or β⁻** is the emission of electron(s)

- **Positron or β⁺** is an antimatter particle, a positively charged electron. After traveling some distance in matter dependent on its initial energy, it collides with an electron, whereby both particles are annihilated producing two opposite beams of gamma rays of 511 keV energy each.

- **Gamma or γ** is electromagnetic radiation emitted from a radioactive nucleus. It is a high frequency photon with energy ranging from a few keV up to 8 MeV.

These kinds of radiation have high enough energy to interact with mater and ionize the atoms they come in contact with, directly (α or β⁻) or indirectly through excitation (γ or β⁺). Due to the nature of the emissions, different kinds of radiation are used for different purposes. For instance, particle radiation (α or β⁻) has lower tissue penetration and if in proximity to tumor cells, its interaction with the cell membranes and/or the nucleus can induce apoptosis and cell death, thereby eradicating tumor lesions. On the other hand, electromagnetic radiation (γ or β⁺-induced) can easier penetrate through tissues and diffuse in space, minimizing the interaction with cells, thereby becoming easily detected outside of the body. This gives the opportunity for tumor imaging using the appropriate imaging modalities, as follows:

- **Single photon emission computed tomography or SPECT**, is used in combination with γ emitting radionuclides. After the intravenous (iv) injection of the radiotracer, the patient is placed on the bed of a specially designed imaging device, based on at least one gamma-camera head, detecting the emitted γ photons as it revolves around the bed. The camera head comprises a collimator, a filter made out of lead of a specific thickness and is practically a set of parallel holes allowing only the γ rays falling parallel to the holes to pass through. The selected γ rays reach the Tl-dopped NaI-crystal and are transformed into scintillations (visible light), which are guided and converted into an electric current in the photomultiplier tubes. The resulting electric signal is then processed and converted into an image (scintigram) by a dedicated computer (I**mage I2**).
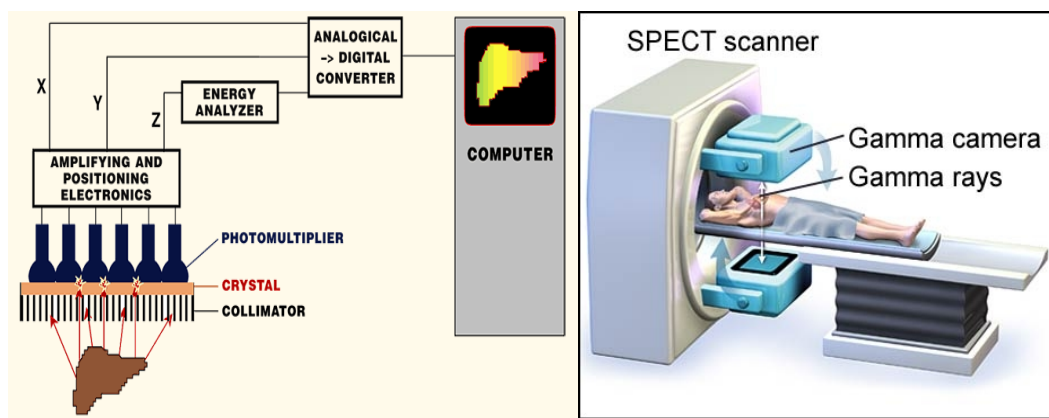
Image I2: (Left) Diagram of a γ-camera head and its basic operational parts (right) image of a SPECT scanner

- **Positron emission tomography or PET** is used in combination with β^+ emitting radionuclides. Its function is based on the simultaneous detection of the two anti-parallel 511 keV γ rays that are produced after the annihilation of the emitted positron. It consists of a ring of detectors made out of scintillation crystals that are connected to a computer. The rays are captured from the detectors and the electrical signal is amplified, but only the rays that are registered simultaneously from a system of opposite detectors are recorded. Then the position and the intensity of the emitting point is calculated (**Image I3**).

Image I3: (Left) Diagram of a PET device and its basic operational parts (right) image of a PET scanner

The above-mentioned technologies can provide not only functional but also biochemical information of disease, on condition that the radiopharmaceutical accumulates at the pathological sites by specific interaction with the target-biomolecules overexpressed therein. Contemporary state-of-the-art devices combine SPECT or PET with modalities that provide spatial information, like magnetic resonance imaging (MRI), or computed tomography (CT). In this way, the location and spread of disease, in our case primary tumor and metastases, can be accurately pin-pointed in the body (8,9).

Radiopharmaceuticals

Nuclear medicine, is a relatively new field of medicine that utilizes radioactive compounds or "radiopharmaceuticals" for non-invasive diagnosis and therapy of human disease, including cancer. The term radiopharmaceutical refers to compounds linked to a radioactive isotope, either covalently (e.g. radiohalogens) or via a chelating agent (e.g. radiometals). After iv injection of radiopharmaceuticals in patients a variety of biological functions and/or diseases can be monitored by exploiting their physical and/or molecular characteristics.

The first generation of radiopharmaceuticals have exploited the physicochemical properties of the radiolabeled molecules, dictating key-pharmacokinetic parameters related to disease, such as disease-linked alterations in the diffusion into tissues or organs of the body following the blood flow. Some examples are the Tc-99m labeled Ceretec® used to monitor blood flow in the brain and TechneScan-MAG3® used to test kidney function (**Image I4**) (10,11).
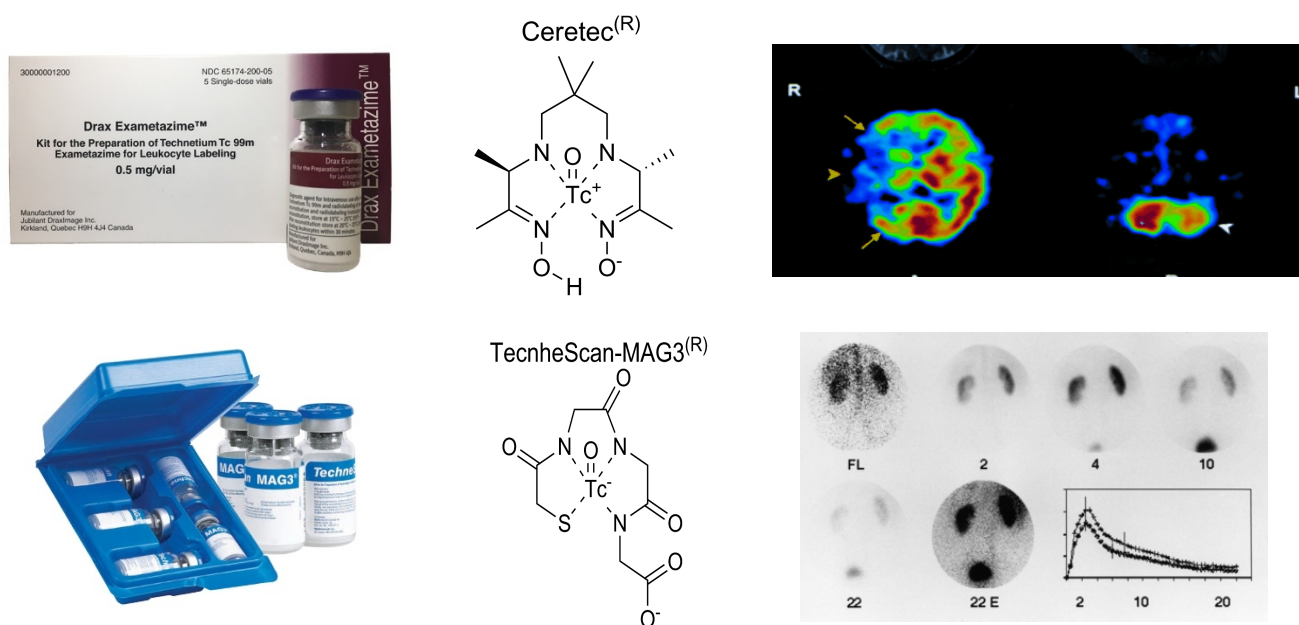
Image I4. Top: Ceretec® and structure of its complex with Tc-99m used in the imaging of regionally altered blood flow in the brain applying SPECT; Bottom: TechneScan-MAG3® and structure of its complex with Tc-99m used in the imaging of kidney function (shape, location, blood flow and delineation of obstructions)

Today's radiopharmaceuticals exploit molecular characteristics – "finger-prints" – of the disease, like cancer. They are specially designed to recognize and interact with specific disease-associated target biomolecules, thereby representing a whole new family of radiopharmaceuticals, the so-called "molecular radiopharmaceuticals" (12–14).

Molecular radiopharmaceuticals

Molecular radiopharmaceuticals" form a distinct category of state-of-the-art radiopharmaceuticals. Based on the concept of the "magic bullet", introduced by Paul Ehrlich in late 1800s (15), "molecular radiopharmaceuticals" are carriers of either a diagnostic or a therapeutic radionuclide specific for a biomolecular target situated on the sites of disease, but not expressed in healthy surrounding tissue. In this way, high disease-to-background contrast imaging can be achieved and radiotoxic payloads can be delivered selectively to pathological sites, sparing healthy tissues.

A good and relatively recent example of such modern radiopharmaceutical is [^{177}Lu]Lu-PSMA-617 (**Image I5**) (16–18), recently approved by FDA for radionuclide therapy of metastatic castration-resistant prostate cancer following PET/CT imaging with [^{68}Ga]Ga-PSMA-11 (also recently FDA-approved) (19–21). These two radiopharmaceuticals represent the diagnostic and therapeutic members of a typical "theranostic pair" used in the management of prostate cancer.

Both [^{68}Ga]Ga-PSMA-11 and [^{177}Lu]Lu-PSMA-617 target a member of the M28 peptidase family, a type II membrane glycoprotein called prostate-specific membrane antigen (PSMA) or folate hydrolase (FOLH1) with a molecular weight of 100-120 kDa. PSMA consists of a intracellular part (18 amino-acids in length), a transmembrane domain (25 amino-acids in length) and a very pronounced extracellular part (707 amino-acids). It is overexpressed on 90% of prostate cancer cases in a 1000-fold higher density than in healthy prostate, although high levels of undesired physiological expression of PSMA have been documented in small intestine, proximal renal tubules and salivary/lacrimal glands, imposing dosimetric concerns during radionuclide therapy (14,22,23).

Both PSMA-11 and PSMA-617 are small-molecule inhibitors for PSMA, based of urea. The PSMA recognition motif is glutamate-urea-lysine, extended in the case of PSMA-617 at the ε-amino group of lysine by a spacer carrying a naphthyl pendant group and a tranexamic acid residue. At the end of the spacer the chelator DOTA (1,4,7,10-tetraazacyclododecane-1,4,7,10-tetraacetic acid), suitable for stable binding of trivalent metals, such as Lu-177, is coupled.
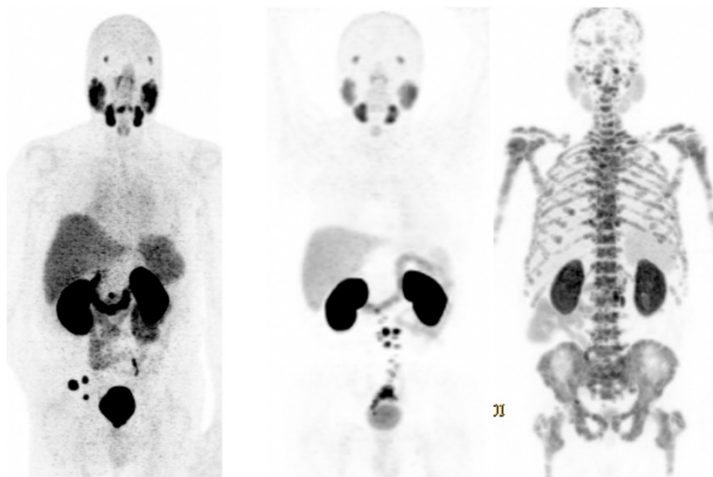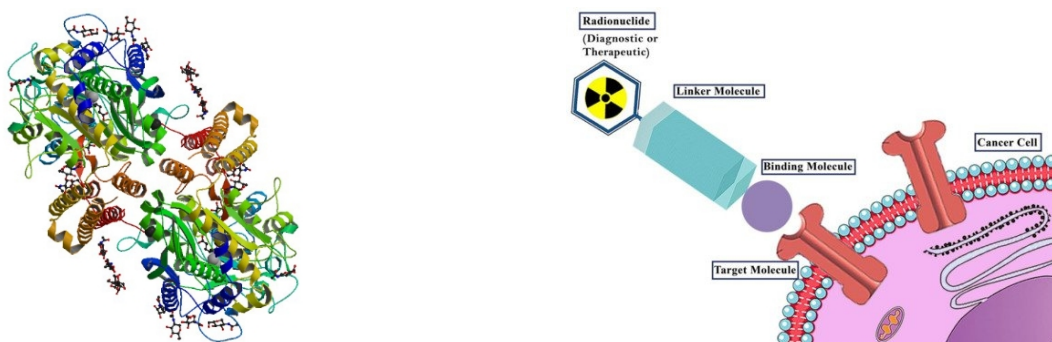
PET/CT imaging of PC in three patients using [^{68}Ga]Ga-PSMA-11 (gallium-68 gozetotide)

PSMA-617

Pulvicto (^{177}Lu-PSMA-617)
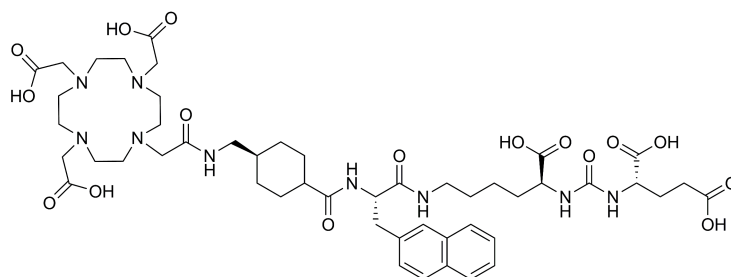
Radionuclide therapy with [^{177}Lu]Lu-PSMA-617 (Pulvicto)

Image I5. Diagnosis (PET/CT) with gallium-68 gozetotide and therapy with pulvicto ([^{177}Lu]Lu-PSMA-617) of prostate cancer via the PSMA target (upper left) overexpressed in cancer cells; both analogs are FDA approved and represent a "theranostic pair" in prostate cancer treatment.

Other examples of molecular radiopharmaceuticals approved or in clinical trials, with their biomolecular target and the types of cancers expressing those targets, are listed at the table below (**Table I1**).

Table I1. Examples of molecular radiopharmaceuticals with their biomolecular targets and the types of cancers overexpressing these targets. The type of vector used in these molecular radiopharmaceuticals is given in parentheses

Radiopharmaceutical	Biomolecular target	Tumor types
[^{111}In]In-DTPA-trastuzumab (antibody) (24)	HER-2 (transmembrane receptor)	breast, esophageal, lung, cervical, endometrial and ovarian cancer
[^{111}In]In-octreotide (peptide) (25)	somatostatin subtype 2 receptor SST$_2$R (GPCR*)	neuroendocrine, gastrointestinal, pancreatic, breast, small-cell lung cancer, non-Hodgkin lymphoma, paraganglioma, melanoma
[^{68}Ga]Ga-NeoBOMB1 (peptide) (26)	gastrin-releasing peptide receptor, GRPR (GPCR)	prostate, breast, pancreatic cancer, small-cell lung, gastrointestinal, colon cancer, glioma
[^{177}Lu]Lu-PSMA-617 (inhibitor, small organic molecule) (17)	prostate-specific membrane antigen, PSMA (type II transmembrane glycoprotein)	prostate cancer

*GPCR: G-protein coupled receptor

A wide variety of biomolecules may serve as targets for diagnostic and/or therapeutic purposes. These biomolecules have to meet certain criteria (12,27) to become eligible targets. First, they have to be overexpressed on tumor-sites, while being absent in measurable amounts in surrounding healthy tissues. Second, they have to keep a stable and high expression throughout the propagation of the disease. Third, they have to be easily accessed by the radiolabeled vectors. Thus, biomolecules with high expression levels on the cell membrane of tumor-cells or cells in the tumor-microenvironment or even on the epithelial cells of the vasculature of tumors are typically preferred. Some examples of biomolecules, used as targets for molecular radiopharmaceuticals are:

- Enzymes located on the external part of the cell-membrane of tumor cells (e.g., PSMA – see above)
- Enzymes located in tumor stroma (e.g., fibroblast activation protein – FAP) (28).
- Transmembrane transporters (e.g., glucose transporters – GLUT (29))
- Cell-surface receptors (e.g., epidermal growth factor receptors – HER2, members of G-protein coupled receptor (GPCR) superfamily – somatostatin subtype 2 receptor (SST$_2$R), gastrin-

releasing peptide receptor (GRPR), neurotensin receptor 1 (NTS$_1$R), cholecystokinin subtype 2/gastrin receptor (CCK$_2$R) etc. (see **Table I2**).

The nature of the target biomolecule guides the selection of vector type. Thus, GPCR-agonists/antagonists, enzyme-inhibitors, transporter substrates or even antibodies may be used as targeting moieties (see below).

Amongst the biomolecules serving as targets, GPCRs are of particular interest. GPCRs are a superfamily of cell-surface membrane receptors (>800 members) with high impact both for classical pharmacology and for radiopharmacy. In fact, they represent the most frequently selected protein family for drug development, with actually more than 50% (30,31) of registered drugs being designed to directly or indirectly target a GPCR. Their structure consists of an extracellular N-terminal domain, followed by seven transmembrane domains, linked with each other with three intra- and three extracellular loops, ending at the C-terminal intracellular domain (**Image I6**). The N-terminus with the extracellular loops contain amino acids essential for ligand recognition, while the seven transmembrane domains form a binding pocket, where the ligand rests upon interacting with the receptor. This interaction gives rise to conformational changes, that lead, in the case of agonists, to activation of the G-protein heterotrimer by the receptor. In turn, the activated G-proteins stimulate various signaling pathways, thus amplifying the extracellular signal (32–34).
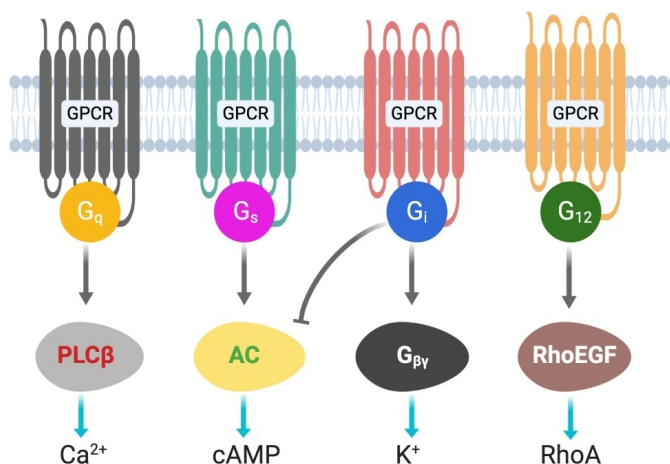
Image I6: Representation of the structure of GPCRs and their major signaling cascades. After agonist ligand – receptor interaction on the four differed types of G proteins are activated, which subsequently interact with other intracellular proteins. Gs activates AC while Gi inactivates it. PLCβ: phospholipase Cβ, AC: adenylyl cyclase, Gβγ: βγ sub-units of G proteins, RhoEFG: guanine nucleotide exchange factors for small GTPases of the Rho family, cAMP: cyclic adenosine monophosphate, RhoA: Transforming protein RhoA. Image from: https://encyclopedia.pub/entry/2907

Design of molecular radiopharmaceuticals

There are some key steps that have to be tackled in the design of molecular radiopharmaceuticals.

- The choice of a biomolecular target (as outlined above)
- Selection of vector (depending upon the target at hand)
- Selection of radionuclide, based on the intended use (diagnosis and/or therapy). For radiopharmaceuticals utilizing radiometals, a suitable combination of chelating agent and radiometal is preferrable
- The biological half-life of the radiolabeled vector has to match the half-life of the radionuclide. For example, the combination of a slow circulating, slow tissue penetration vector (e.g. antibody circulating for days in the blood) cannot be a perfect match to a fast-decaying radionuclide (e.g. F-18 with a half-life of 1.83 h). By the time the radio-fluorinated antibody reaches the target-antigen on tumor sites, radiofluorine will be long gone.
- Sufficient hydrophilicity is essential to ensure a fast-enough excretion of the radiolabeled vector from the body preferably via the kidneys and not the hepatobiliary route, thereby minimizing abdominal retention of radioactivity and enhancing image quality.

In order to achieve an optimal balance between the above attributes, a variety of vectors have been made available in recent years, including peptides, antibodies and small organic molecules to name some of the few (see below) (14,35).

Vector or targeting probe

The role of the vector or targeting probe is to seek and interact with a specific disease-associated biomolecule, serving as the "target". After labeling, the vector will guide the radionuclide to the site(s) of the pathology with high specificity, without interfering with healthy tissues lacking target expression. Radiolabeled vectors used for tumor theranostics (diagnosis or therapy) will seek the target situated on cancer cells, tumor vasculature or peritumoral micro-environment (stroma). Chemically and/or pharmacologically different entities may act as vectors. Thus, antibodies will seek antigens, peptides their cognate GPCR, and small-organic molecules, like enzyme-inhibitors or non-peptide GPCR-ligands, their enzymatic or GPCR target, respectively, all located on tumor-sites. Each of these vectors displays inherent advantages and shortcomings that have to be considered for the intended application:

- **Antibodies** have high specificity for their target-antigen, but display slow blood and body clearance. They cannot penetrate easily through tissues due to their bulky structure and they are linked with high immunogenicity risks. Owing to their highly organized structure they are prone to denaturation at high temperatures or harsh chemical conditions that interrupt their tertiary structure, rendering them inactive. Furthermore, they are costly to produce and modify.

- **Small organic molecules** have faster blood clearance and good tissue penetration compared with antibodies. They tend to be metabolically robust against proteases, non-immunogenic, cheaper to produce and show high affinities for their target (e.g., receptors, enzymes etc.). However, they often show sub-optimal target-selectivity and are prone to off-targeting (31,36,37). Unlike antibodies they can tolerate harsh conditions in most cases.

The present work is focusing on peptide-based molecular radiopharmaceuticals, as radiometal carriers to cancer sites. Such molecules can be divided into the following parts: the peptide moiety, the linker, the bifunctional chelator and the radiometal (**Image I7**) (14,35).

Image I7: Graphical representation of a peptide radioligand targeting a GPCR overexpressed on tumor cells

Peptides as vectors

Peptides are amino-acid polymers, typically containing up to 20-30 monomers linked to each other by the so-called amide or peptide bonds. The majority of endogenous peptides are GPCR ligands, exerting their biological function uponr binding to their target receptor with high affinities. In general, peptides owing to their small size display very rapid body distribution, excellent tissue penetration after iv injection and are not immunogenic. They serve as hormones, neurotransmitters and in general as mediators of signaling between tissues, organs or cells.

In peptide radiopharmaceuticals for molecular targeting of human tumors, a chelator stably binding the radiometal is typically covalently attached at their N-terminus, either directly or via a linker (**Image I7**), away from the C-terminus. In most cases, the latter contains regions essential for the receptor recognition and binding. Some additional advantages of peptides as vectors are the ease and cost-effectiveness of synthesizing peptide analogs, especially when applying contemporary automated

solid phase synthesis techniques and having available a wide range of new materials, protective groups and solid supports. Their above-mentioned fast biodistribution and rapid background clearance, minimizes the time needed to reach their biomolecular target on tumor sites, rendering them suitable for use in combination with shorter-lived radionuclides, at least for diagnostic purposes. As a result, radiation doses to healthy tissues and organs are minimized and hospital logistics with regards to radiation hazards and waste management are simplified.

It should be noted that the action of native peptides is regulated by a variety of mechanisms and mainly by the deployment of a special family of enzymes called proteases or peptidases, hydrolyzing peptide-bonds and causing degradation of peptides in the biological milieu. Peptidases, are widely distributed across the different compartments of the body, either associated with cells (intracellularly or membrane bound) or released in biological fluids, such as the blood, the urine, or the cerebrospinal fluid. This fact represents the major hurdle in the application of peptide radiopharmaceuticals in oncology. Like native peptides, peptide radiopharmaceuticals are prone to degradation by omnipresent peptidases after injection in the body, compromising diagnostic accuracy and therapeutic efficacy. A list of GPCRs over-expressed in various human cancers is included in **Table I2** (13,14,27,35,38)**.**

Table I2. Endogenous peptides used as motifs for molecular radiopharmaceuticals with their native receptors and examples of cancers overexpressing their cognate GPCR-targets (27).

Endogenous peptide	Receptors	Cancer types
neurotensin (NT)	neurotensin receptor 1 (NTS$_1$R)	colon, prostate, breast, pancreatic, small-cell lung cancer, Ewing sarcoma
bombesin (BBN) / gastrin releasing peptide (GRP)	gastrin-releasing peptide receptor, GRPR or bombesin subtype 2 receptor, BB$_2$R	prostate, breast, small-cell lung, gastrointestinal, colon cancer, glioma
gastrin / cholecystokinin (CCK)	cholecystokinin subtype 2 receptor, or gastrin receptor, CCK$_2$R	prostate, breast, pancreatic, colon, gastric, small-cell lung cancer
somatostatin	somatostatin subtype 2 receptor, SST$_2$R	neuroendocrine, gastrointestinal, pancreatic, non-Hodgkin lymphoma, paraganglioma, melanoma, breast, small-cell lung cancer
substance P	neurokinin subtype 1 receptor, NK$_1$R	glioblastoma, astrocytoma, medullary theroid, breast cancer

Recent studies have shown that the enzymes playing a lead role in the rapid degradation of peptide radioligands after injection in animals or patients, are neutral endopeptidase (NEP) in combination or not with angiotensin converting enzyme (ACE), while the action of ubiquitous aminopeptidases is inhibited by the radiometal-chelate attached at the N-terminus (39).

ACE, or peptidyl-dipeptidase A, is a zinc metallopeptidase belonging to the clan MA – family M2 of metalloproteases with a molecular weight of 150 – 180 kDa (40). Three isoforms of the enzyme have been isolated: a) somatic ACE, b) soluble ACE and c) germinal ACE. Somatic ACE consists of two homologous domains, a C- and an N-terminal one, both demonstrating catalytic properties (41,42). These two domains share a 60% homology, rising to 89% for a region of 40 amino acids essential for their active sites, indicating the tandem duplication of an ancestral gene. Both active sites contain the zinc binding motif histidine – glutamic acid – X – X – histidine (43). It is located at the extracellular part of the plasma membrane. It has high expression in the brain, on vascular endothelial cells especially in the lungs, on epithelial cells of the small intestine and the kidneys (44–47). The soluble form, originates from the somatic by proteolytic cleavage of the C-terminus of the enzyme and it is present in a variety of biological fluids, like blood serum, amniotic, seminal and cerebrospinal fluids (48–51). ACE hydrolyzes a wide variety of substrates, but due to its capability to degrade and consistently inactivate angiotensin I and bradykinin, it plays a significant role in blood pressure regulation and water and salt balance (52).
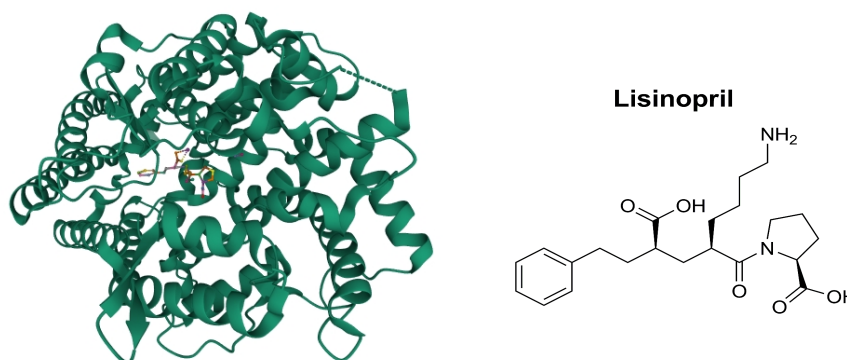
Image I8. (Left) Crystal structure of ACE in complex with the inhibitor lisinopril (right) chemical structure of lisinopril (https://www.uniprot.org/uniprotkb/P12821/entry#structure)

NEP (CALLA or CD10) is also a zinc metallopeptidase and it belongs to clan MA – family M13. It has a molecular weight of 85-110 kDa. It is a type II membrane protein located on the extracellular part of the plasma membrane of cell (53–56). It acts as oligopeptidase, hydrolyzing

peptides up to 40-50 amino-acids in length, with its efficacy declining with the increase in length of the substrates (57). It has a histidine – glutamic acid – X – X – histidine in its active center (58,59), located at the C-terminus, and it displays a broad substrate repertoire, represented by enkephalins, tachykinins (like substance P), endothelins, bradykinin and the atrial natriuretic peptide family (57,58,60). It is abundant in kidneys, liver, intestine, placenta, choroid plexus, on reticular cells, reproductive system, in the lungs and anchored on epithelial cells of blood vessels(60–62).
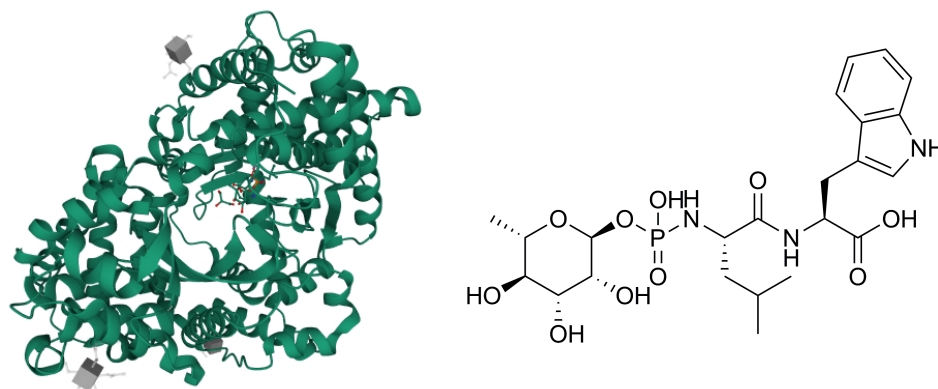
Image I9. (Left) Crystal structure of NEP in complex with the natural inhibitor phosphoramidon (https://www.uniprot.org/uniprotkb/P08473/entry#structure) (right) chemical structure of phosphoramidon.

NEP, either alone or together with ACE, has been associated with poor stability of peptide radioligands in the circulation, compromising efficient delivery of intact radiopeptide to tumor-sites and thereby tumor uptake. In order to mitigate this problem, several strategies involving structural modifications have been pursued in hunt of increased metabolic stability, such as amino-acid replacements, reduction or methylation of peptide bonds, cyclization, or multimerization to name some of the few. However, such changes have been often adopted at the cost of other important biological properties of resulting radioligands, rendering this effort costly, time consuming and frequently unsuccessful. Recently the use of specific NEP (+/-ACE) inhibitors has been shown to effectively stabilize the peptide radioligands *in situ* in experimental animal models (39,63–67) and in man[1], leading to drastic enhancement of tumor uptake (**Image I10**).

---

1   Valkema R. et al. EJNNMI, 2019;46 (Suppl 1), S701-2. DOI: https://doi.org/10.1007/s00259-019-04486-2
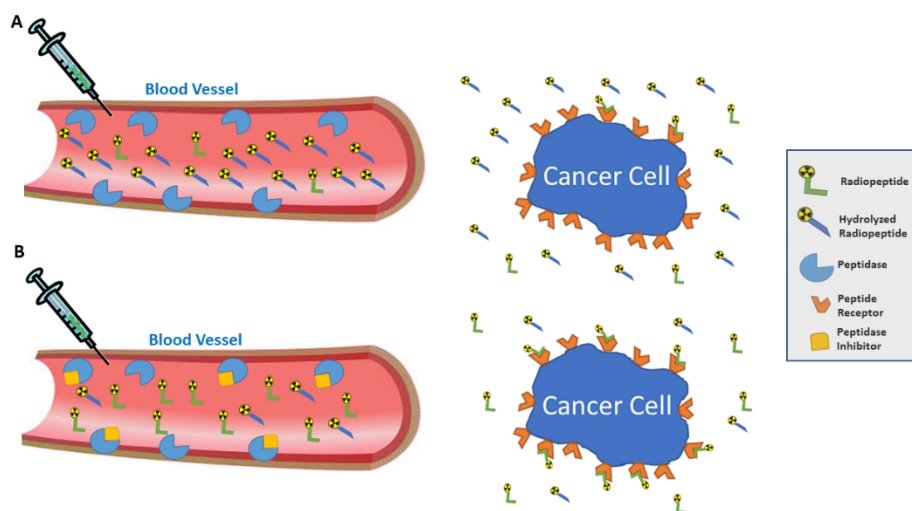
Image I10: *In situ* stabilization of peptide radioligands with the aid of peptidase inhibitor(s) leads to efficient delivery of the radionuclide to tumor sites, enhancing tumor uptake and consequently diagnostic accuracy or therapeutic index

Linker

The role of the linker or spacer is to connect and at the same time separate the targeting moiety with/from the radiometal-chelate. It is covalently attached usually at the N-terminus of the peptide chain. Introduction of the linker may be elegantly operated to modulate several biological properties of the peptide radioligand by incorporating charged residues, hydrophilic/lipophilic domains or even branching for conveying additional functional capabilities to the final molecule, such as conjunction of a dye (for optical imaging) or of another vector (e.g. PSMA-inhibitor and BBN analog heterodimers in prostate cancer targeting). Some commonly used linkers are polyethylene-glycol moieties (PEG), natural or unnatural amino acids or even polyamine chains. The linkers may also serve as pharmacokinetic modifiers, achieving fine tuning of pharmacokinetic parameters, such as diffusion capability, hydrophilicity, excretion route, or binding to plasma proteins. However, such interventions may affect other important pharmacological properties, such as receptor binding affinity, or cell-uptake and internalization rates and should be adopted with caution (18,35,68–70).

24

Bifunctional chelator

The bifunctional chelator is covalently attached to the peptide vector either directly or via a spacer (forming a peptide conjugate) and also stably binds the radiometal of choice (forming a radiometal-chelate). There is a variety of chelators currently in use, either open-chain, macrocyclic, or hybrid (13,35,71). The choice of chelator depends on the radiometal intended in each application and dictates the labeling protocol. Open-chain chelators such as DTPA (diethylenetriaminepentaacetic acid) are suitable for binding In-111 at room temperature, but tend to form weaker complexes with other bi/trivalent metals (**Image I11**) (72,73). For stable binding of the latter, macrocyclics, such as DOTA or NOTA (1,4,7-triazacyclononane-1,4,7-triacetic acid) and their derivatives, are preferred, because they form more substitution-inert complexes with these radiometals. In this case however, for complex formation the radiometal needs to master a higher energy barrier imposed by the rigid structure of the chelator. Hence, unlike open-chain chelators, macrocyclics need elevated temperatures and prolonged incubation times to get over the energy barrier and eventually bind the radiometal. For example, In-111 forms complexes at room temperature with the linear DTPA, but it needs 30 min incubation at 90 $^{\circ}$C for incorporation in macrocyclic DOTA (74,75).

Other important factors with impact on the formation and stability of the radiometal-chelate are the size of the metal ion as well as its coordination number. Clearly, the ionic radius and the coordination number of the radiometal need to match the size of the macrocyclic ring and the number of its donor atoms. For instance, the bulky Lu-177 (ionic radius of 100 pm) with a coordination number of 9, forms stable complexes with DOTA possessing a bigger ring and 8 donor atoms, but it can be poorly bound by NOTA with a much smaller macrocyclic ring and 6 donor atoms only. On the other hand, the macrocyclic ring of DOTA is too big for smaller radiometals, such as Ga-67/68 (ionic radius of 76 pm, coordination number 6), resulting in loosely bound and substitution prone metal-chelate. Instead such radiometals form more robust complexes with NOTA. Interestingly, In-111 (ionic radius of 94 pm, coordination number 7 or 8) having an intermediate size can be bound to both chelators under formation of complexes which turned out to be sufficiently stable in the biological milieu (71,76).
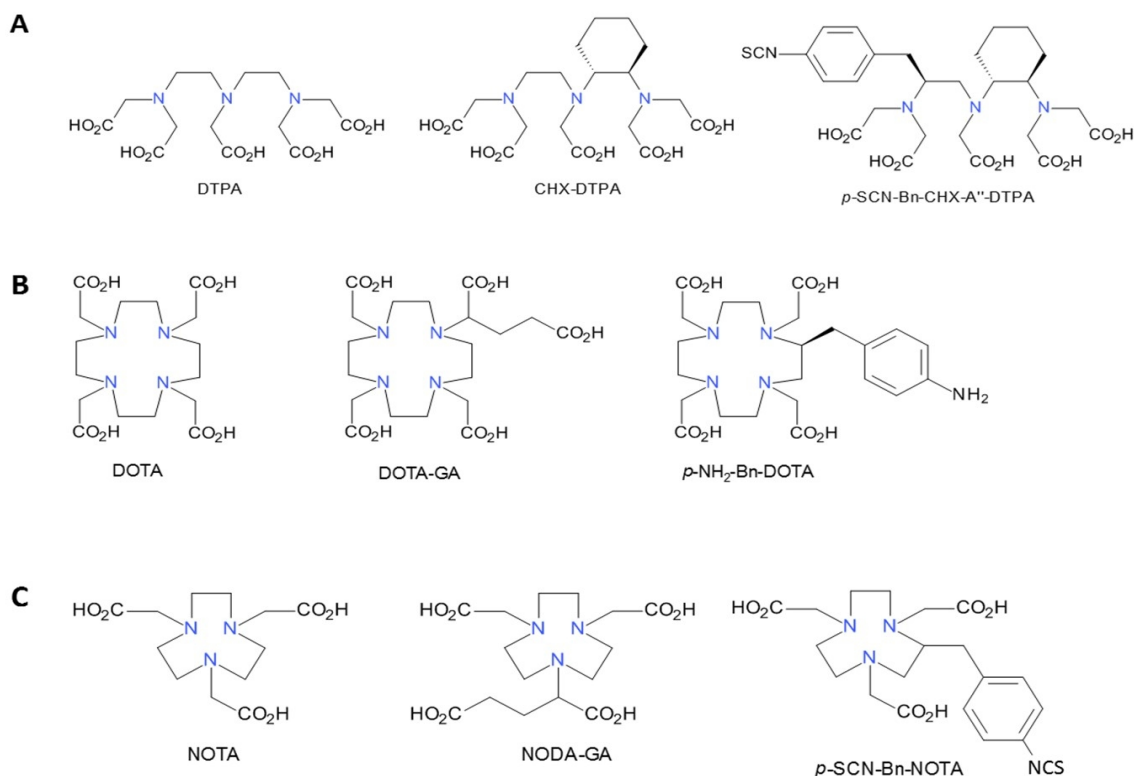
Image I11: Structures of commonly used bifunctional chelators; (A) open chain chelator DTPA (diethylenetriaminepentaacetic acid) and its derivatives for stable binding of In-111, (B) the universal chelator DOTA (1,4,7,10-tetraazacyclododecane-1,4,7,10-tetraacetic acid), (C) NOTA chelator (1,4,7-triazacyclononane-1,4,7-triacetic acid) and their derivatives used for stable binding of bi/trivalent radiometals, such as In-111, Lu-177 or Ga-67/68 (13).

In an effort to combine the benefits from both worlds (high substitution inertness of macrocyclic chelates / ambient labeling temperatures needed for linear chelators) hybrid chelators have been recently emerging. Such examples, are DATA[5M] (6-amino-1,4-diazepine-triacetic acid) (**Image I12**) used for stable binding of the PET radiometal Ga-68, or AAZTA[5] (6-amino-6-methylperhydro-1,4-diazepinetetraacetic acid) suitable for binding the therapeutic radiometal Lu-177. They both contain cyclic and linear parts, making them suitable to bind Ga^{+3} (DATA[5M]) or Lu^{3+} (AAZTA[5]) under mild conditions (77).
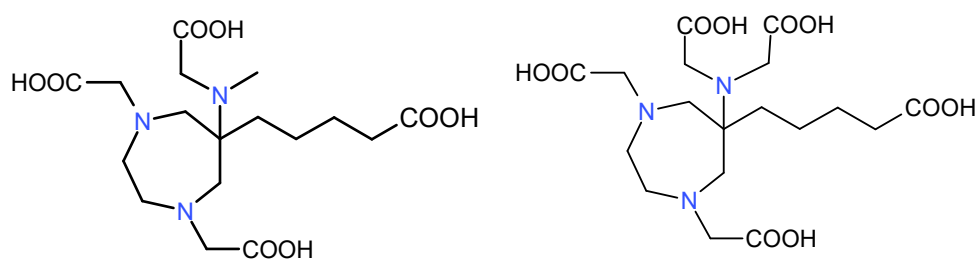
Image I12: Structure of the hybrid chelator DATA[5M] and AAZTA[5], used in combination with Ga-68 or Lu-177, respectively.

26

The forming radiometal chelate may have great impact on the overall performance of the peptide radioligand, affecting important biological responses, such as receptor affinity, cell uptake, *in vivo* stability and overall pharmacokinetics. There are instances whereby the peptide analog after labeling with different radiometals displayed quite different characteristics. For example, the affinity of SB3 (DOTA-p-AMA-DIG-DPhe-Gln-Trp-Ala-Val-Gly-His-Leu-NHEt, AMA: 4-(aminomethyl)alanine, DIG: diglycolic acid, **Image I13**) for GRPR, was altered after binding of different metals (SB3: $IC_{50} =$ 4.6 ± 0.4 nM, Ga-tagged: 1.7 ± 0.03 nM, In-tagged: 2.2 ± 0.2 nM and Lu-tagged: 4.28 ± 0.33 nM and). This pattern followed by the relative cell-uptake of the respective radioligands in PC-3 cells after 1 h incubation at 37 °C ([^{67}Ga]Ga-SB3: 27.7 ± 1.6 %, [^{111}In]In-SB3: 16.23 ± 0.80 % and [^{177}Lu]Lu-SB3: 2.85 ± 0.21 % uptake of the total added radioactivity). Their metabolic stability in mice peripheral blood was also affected ([^{67}Ga]Ga-SB3: >85% intact 5 min pi, [^{111}In]In-SB3: 56 ± 2 % intact and [^{177}Lu]Lu-SB3: 54 ± 7 % intact) revealing different propensity to proteolytic degradation by NEP. Most importantly, the above *in vitro* performance in combination with the metabolic stability translated in different uptake of the three radiopeptides in PC3 tumors in SCID mice 4 h pi ([^{67}Ga]Ga-SB3: 34 ± 6.9 %IA/g (% injected activity / gram tissue), [^{111}In]In-SB3: 8.78 ± 3.03 %IA/g and [^{177}Lu]Lu-SB3: 8.22 ± 1.61 %IA/g). The above example, demonstrates beyond any doubt the impact of the radiometal-chelate on the overall performance of the resulting [^{67}Ga]Ga-/[^{111}In]In-/[^{177}Lu]Lu-radiopeptides, dictated by differences in net charge, charge-density and charge-distribution, size and conformation of forming radiometal-chelate (**Image I13**) (78,79).
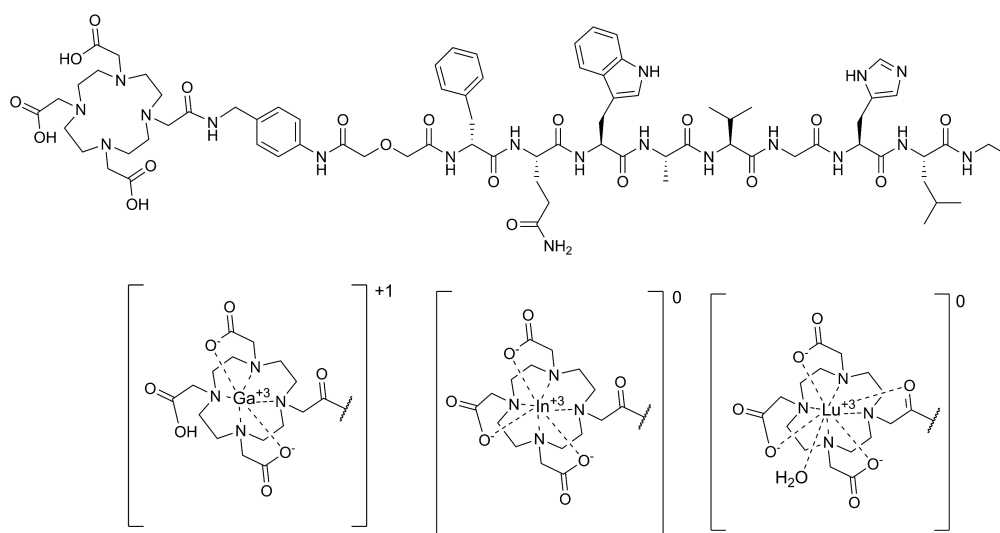
Image I13. (Top) structure of SB3 and (bottom) the metal complexes forming after binding Ga/In/Lu to DOTA

Radiometal

The choice of the radiometal relies on two important factors. First, the decay properties should be suitable for the desired application, especially the type and energy of emission and its half-life. Thus, γ or β^+ (positron) emitters are used in diagnostic imaging and β^- (electron) or α emitters for therapy. Second, the availability (including availability in pharmaceutical grade), cost and logistics for use in the clinic. Some prime examples of radiometals currently in use along with their decay characteristics are listed in the table below (80–83).

Table I3: Radiometals of clinical interest

Intended use	Radiometal	Hal- life ($T_{1/2}$)	Emission (energies, keV)	Production
SPECT	**Tc-99m**	6.01 h	γ (141)	Mo-99/Tc-99m generator
	Ga-67	78.26 h	γ (91, 93, 185, 296, 388)	cyclotron
	In-111	67.9 h	γ (172, 247)	cyclotron
PET	Sc-44	3.97 h	β^+ (632)	Ti-44/Sc-44 generator
	Cu-64	12.7 h	β^+ (653)	reactor
	Ga-68	1.1 h	β^+ (820, 1895)	Ge-68/Ga-99 generator
Therapy	Cu-67	61.83 h	β^- (570)	accelerator
	Y-90	64.05 h	β^- (2270)	Sr-90/Y-90 generator
	Lu-177	6.65 d	β^- (174, 249, 385, 497)	reactor
	Re-186	3.72 d	β^- (306, 359)	reactor
	Re-188	17 h	β^- (729, 795)	W-188/Re-188 generator
	Ac-225	9.920 d	A (5.9351 MeV)	Th-229/Ac-225 generator

It should be noted that the coordination chemistry of the pre-eminent SPECT radionuclide Tc-99m is quite different from most bi/trivalent radiometals used in nuclear medicine, requiring completely different chelator types for stable binding. At this point it is worth noting that Tc-99m has its own therapeutic counterparts, Re-186 and Re-188 (**Table I1**) and accordingly, the option of making available Tc-99m/Re-186/188 theranostic pairs of radiopeptides in oncology in future is valid. Re

belongs in the same group with Tc with the two metals exhibiting similar chemical properties. Re however is positioned in period six under Tc, but due to the lanthanide contraction, it has a similar atomic size with Tc. As a result, the two metals share a similar coordination chemistry. Given that the present work is focused on Tc-99m labeled radiopeptides, a dedicated chapter follows, including a more detailed introduction of technetium in medicine and in chemistry, with information on its oxidation states and chelators.

Technetium and its role in nuclear medicine

Technetium (Tc) belongs to the transition metals, with atomic number forty-three. In the periodic table of elements it is located in group sixteen and in period five, found beneath Manganese (Mn) and above Rhenium (Re). It is the first artificial element, as its name implies («τεχνητός», meaning artificial in Greek) and it was isolated for the first time in 1937. Technetium is the lightest element of the periodic table with all of its isotopes radioactive; the most commonly occurring isotope is Tc-99, or else Tc-99g (ground state Tc-99). As all the transition metals, technetium exhibits various oxidation states, ranging from -1 up to +7, with the most common ones being +4, +5 and +7. The most stable oxidation states for it in aqueous solutions are either +7, as in pertechnetate (TcO_4^-), which is the most prevalent form of Tc, or +4 in the form of TcO_2, which is insoluble in water. For a few decades technetium dominated the fields of nuclear medicine and radiopharmacy with its Tc-99m isotope ("m" – metastable, indicates that the nucleus is in an excited state) (84,85).

One should also comment on the cost-effective and broad availability of Tc-99m in high purity and high specific activity as [^{99m}Tc]TcO_4^- in a sterile and pyrogen free solution through commercial Mo-99/Tc-99m generators (see next subchapter). This last technological breakthrough should be seen together with the development and availability of the so called "technetium kits", which are formulations containing the pro-drug of the actual [^{99m}Tc]Tc-radiopharmaceutical along with a reductant and other excipients in a freeze-dried form. After "kit reconstitution", in else addition of generator eluate, the end-radiopharmaceutical should be ready to be iv injected to patients and consequently, needs to be sterile and pyrogen free. Accordingly, the kits are manufactured abiding to strict European or American Pharmacopoeia good manufacturing practice (GMP) guidelines. Conveniently, kits can be stored for long periods of time in the clinic and can easily yield the desired radiopharmaceutical any time upon demand by mere addition of generator eluate (10,11,86,87). The above benefits, have established Tc-99m as the pre-eminent SPECT radionuclide. It is interesting to see

that still today more than 80% diagnostic nuclear medicine tests worldwide are based on Tc-99m, well-deserving its name as the "workhorse" of nuclear medicine. Examples of freeze-dried kits used with Tc-99m in clinics are Ceretec® and TechneScan-MAG3® ("Radiopharmaceuticals", **Image I4**).

The [^{99}Mo]Mo/[^{99m}Tc]Tc generator

The rationale behind commercial [^{99}Mo]Mo/[^{99m}Tc]Tc-generators is the exploitation of the ß decay of the long-lived "mother" Mo-99 ($t_{1/2}$ = 66 h) to the significantly shorter-lived "daughter" Tc-99m ($t_{1/2}$ = 6 h), which further decays, after emission of a photon, to to the "pseudo"-stable Tc-99 or Tc-99g ($t_{1/2}$ = 2.11×10^5 years to Ru-99) also known as "carrier technetium". The difference in these half-lives allows for "transient equilibrium" to occur, because after some time the growth of Tc-99m and its decay reach equilibrium and thus, the amount of activity of the daughter closely matches that of the mother. (**Image I14**). As long as the system is not disturbed mother and daughter remain in such equilibrium. However, to obtain Tc-99m regularly and separated from the mother, the generator is eluted and equilibrium needs about 24 h (approximately 4 daughter half-lives) to re-establish (88,89).

In a typical [^{99}Mo]Mo/[^{99m}Tc]Tc-generator, Mo-99, in the form of [^{99}Mo][MoO$_4$]$^{2-}$, is adsorbed on the alumina (Al$_2$O$_3$) column and the carrier free daughter Tc-99m accumulates in the form of TcO$_4$$^-$. The latter possesing only one charge, is loosely bound on the alumina and it can be easily eluted in a physiological saline solution, leaving behind the mother which is strongly retained due to its two negative charges. This simple ion exchange system is encased into a hermetically closed plastic housing, armored with sufficient lead shielding to protect users from radiation. Sterility and lack of pyrogens in the eluate is further ensured by the use of a sterile and pyrogen free saline solution for elution as well as a final passage through a 0.22 μm filter of the eluate at the outlet. Two major contaminants are of critical importance: first, the unavoidable leakage of Mo-99, which gets more intense as the generator reaches its expiration date and second, the leakage of alumina traces, potentially affecting labeling yields. Other metal contaminants often compromising the labeling process can be introduced into the eluent from various metallic parts (e.g. needles). In order to minimize the amount of trace metal impurities in the eluate, fractionated elution and discarding of the initial fraction(s) may be helpful.

It should be emphasized that the option to acquire [^{99m}Tc]TcO$_4$$^-$ - rich [^{99m}Tc]Tc-generator eluate at regular intervals is very useful in an operating radiopharmacy – nuclear medicine unit. A generator can have an effective life-span of 2 weeks or more, although the activity of the mother continues to

decrease as it decays and so less of the daughter radionuclide is available from the elution process. Commercial generators have made Tc-99m world-widely available and affordable and thus quite appealing for routine clinical use (85,88,89).
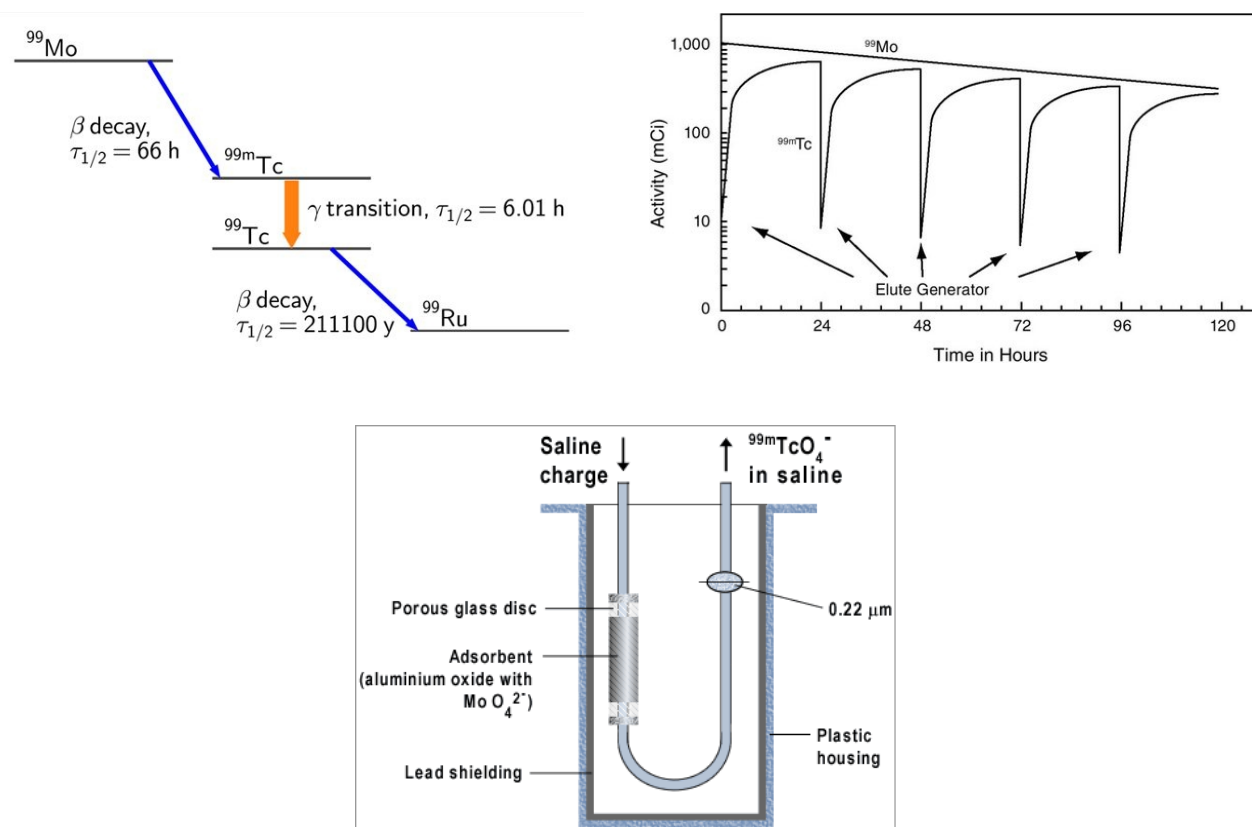
Image I14: Top: Left – Decay of Mo-99 ("mother") to Tc-99m ("daughter"), which further decays to the "pseudo-stable" Tc-99(g). Right – Transient equilibrium scheme, showing Mo-99/Tc-99m/Tc ratios during the life and elution episodes of the generator. Bottom: Diagram of a typical [^{99}Mo]Mo/[^{99m}Tc]Tc-generator, Image from: https://humanhealth.iaea.org/HHW/Radiopharmacy/VirRad/Eluting_the_Generator/Generator_Module/Design_principles/index.html

31

A glimpse at technetium chemistry

Many attempts have been made for development of radiopharmaceuticals exploiting the versatile redox and coordination chemistry of technetium. A wide spectrum of chelating systems have been designed for stable binding the (radio)metal in different oxidation states. Technetium in the form of TcO_4^- in the generator eluate is found at oxidation state +7, unable to form complexes with a chelator. For such purposes, it needs to be reduced to a lower oxidation state, with the most common oxidation state typical in commercial radiopharmaceuticals being +5. In this state the chelator wraps around a Tc^{+5}-core, usually either the mono-oxo (TcO^{3+}) or the *trans*-dioxo (*trans*-$[Tc(O)_2]^+$) (**Image I15**). The coordination sphere of the radiometal is completed by 5 or 6 donor atoms (usually S, O and N), yielding complexes adopting a square pyramidal or an octahedral geometry, respectively. Very often these donor-atoms occupy the equatorial plane and belong to a tetradentate chelator (**Image I16**) (13,38,90).

$$[Tc^{+5}(O)]^{+3} \qquad [Tc^{+5}(O)_2]^+$$
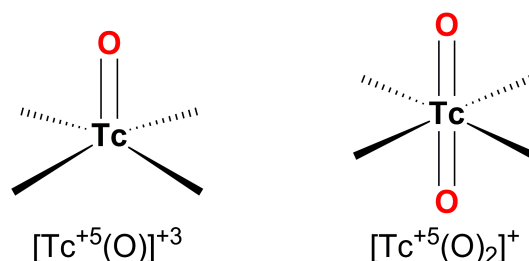
Image I15. Structure of the mono- and *trans*-dioxo cores of Tc^{+5}
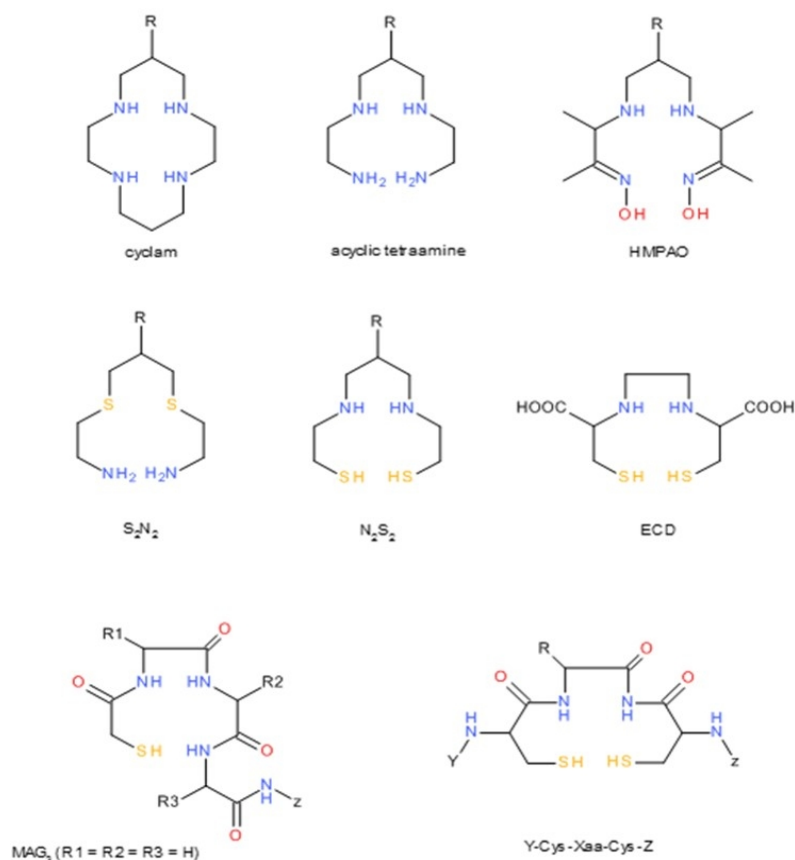
Image I16. Representative cyclic and open-chain chelators combined with the $[TcO]^{3+}$ or *trans*-$[Tc(O)_2]^+$ Tc^{5+}-cores (13)

In the present work, the N_4 (6-carboxy-1,4,8,11-tetraazaundecane) was the bifunctional chelator of choice. Acyclic tetraamines (including N4) form Tc complexes of an octahedral geometry, with the two oxygens of a dioxo-core ($[Tc(O)_2]^+$) occupying the apical positions of the forming octahedron *trans* to one another and the four nitrogen atoms wrapped around the core occupying the equatorial plane (91,92). The net charge of the complex is +1 at pH 7 with Tc at the oxidation state of +5. The +1 charge of the complex, in combination with the two apical oxygens, convey high hydrophilicity of the metal-chelate and thus, $[^{99m}Tc]$Tc-complexes with acyclic tetraamines were proposed as kidney perfusion agents back in the 90's (93).

Due to the two apical oxygen atoms of the *trans*-$[Tc(O)_2]^+$ core in the forming chelate, the electron-deficiency of Tc^{+5} are partially satisfied and accordingly, the electron-pairs from the four nitrogen donor atoms of the tetraamine fully quench the electron demand of the radiometal, without the need to strip them of their hydrogens. Moreover, Tc is hexa-coordinated, forming a strong, substitution-inert complex in the biological milieu. Despite its robustness in physiological pH, the *trans-*

$[Tc(O)_2(N_4)]^+$ complex decomposes in acidic pH after protonation of one of the two oxygens of the core (91,92).

As already mentioned, in order to reduce Tc from +7 oxidation state (found in the generator eluate) to +5 rendering the metal amenable to complex formation, a reducing agent is needed. The most widely used reductant in commercial Tc-kits is stannous chloride ($SnCl_2$), owing to its biocompatibility and safety for iv injection to patients. It should be noted, that often Tc is further reduced to +4, where it forms the so-called "reduced-hydrolyzed technetium", $TcO_2 \times nH_2O$, a common radiochemical impurity during radiolabeling. In this state, Tc becomes unavailable for complex formation. The addition of a "transfer or auxiliary" chelator rapidly forming a "loose" or "intermediate" complex with Tc has been used as a means to stabilize the radiometal at oxidation state 5+, thereby preventing its further reduction to 4+. Given that the forming intermediate complex is prone to transchelation in the presence of the selected chelator under formation of the desired final complex, this strategy has been broadly adopted in radiopharmaceutical design with a variety of transfer chelators, such citrate, tartrate, or gluconate, being a common reagent in most freeze-dried kit formulations (94–96).

In the present work, citrate anions serve as the intermediate chelator, forming a weak Tc^{5+}-citrate complex after reduction of Tc^{7+} in pertechnetate to Tc^{5+} by $SnCl_2$. This offers the time required by the peptide-coupled N_4 to replace the citrate and form the desired product *trans*-$[Tc(O)_2(N_4)]^+$-peptide (**Image I17**). Based on the above, it is reasonable to assume that the labeling reaction mixture of a N_4-carrying peptide with Tc-99m, may contain the following radiochemical impurities: $Tc^{7+}O_4^-$, Tc^{5+}-citrate and reduced-hydrolyzed technetium $Tc^{4+}O_2 \times nH2O$, which should be kept to the minimum by optimizing the ratios of reactants and labeling conditions (e.g. pH, temperature and incubation times).
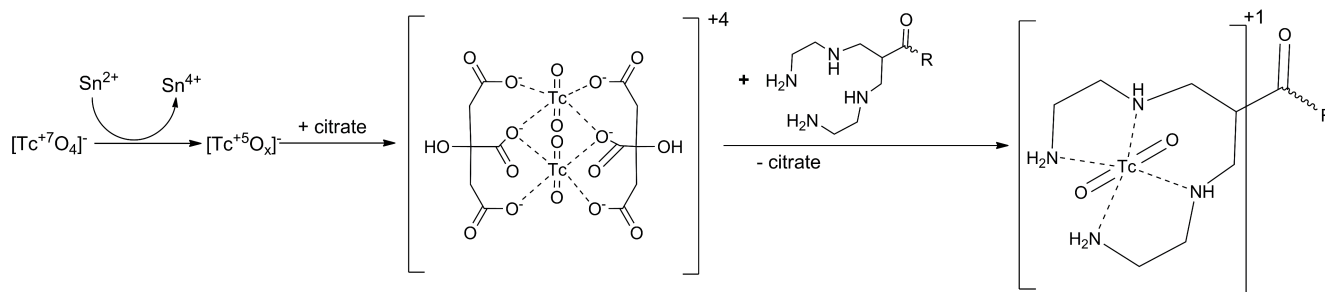
Image I17. Formation of the desired *trans*-$[Tc(O)_2(N_4)]^+$ complex using citrate as transfer chelator

PC diagnostic imaging: current status

In the last few decades, improvements of imaging technologies, such as CT, MRI and ultrasound imaging (UI), have helped clinicians in the detection of PC. Despite their high spatial resolution, these techniques lack diagnostic accuracy or specificity, mainly because they do not provide functional or biochemical information about the disease. Eventually, biopsies are required to unequivocally confirm diagnosis, but they represent an invasive and time-demanding procedure which is highly dependent on sample collection and linked with much patient discomfort. On the other hand, non-invasive nuclear medicine modalities such as PET or SPECT, offer an alternative diagnostic tool likely to deliver vital functional and biochemical information. Indeed, high precision tumor visualization can be achieved when suitably tailored radiolabeled probes are administered to patients, which will seek and specifically interact with PC-located target-biomolecules. Furthermore, when the above-mentioned modalities are combined with high resolution CT or MRI, diagnostic accuracy is drastically enhanced (8,9).

For example, PET and PET/CT imaging with [^{18}F]FDG (fluorodeoxyglucose) reveals locations of increased metabolic rates, including metabolically active tumor lesions. However, [^{18}F]FDG is not a tumor-selective radiopharmaceutical, lacking the ability to distinguish between PC and chronic pancreatitis or to visualize metabolically "silent" cancer sites. Another example is the visualization of NETs in the pancreas, expressing the SST_2R. This type of tumors can be visualized with radiolabeled somatostatin analogs, such as Octreoscan ([^{111}In]In-octreotide, octreotide: DTPA-DPhe-c[Cys-Phe-DTrp-Lys-Thr-Cys]-Thr-OH; **Table I1**) in combination with SPECT or SPECT/CT. However, pancreatic NETs represent only 5% of all PC cases (74,97–99).

Hence, it is evident, that there is an urgent clinical need for new radiolabeled probes capable of providing reliable diagnosis for the rest 95% of PC cases accurately, fast and non-invasively. Accordingly, new biomolecules with high incidence and high density of expression in human PDAC, are currently considered as potential targets for development of new diagnostic radiopharmaceuticals.

NTS₁R as a biomolecular target for PC imaging

As already discussed, sufficient expression levels of the target-biomolecule on the sites of the pathology is a major requirement for the efficacy of any molecular radiopharmaceutical. In the case of PDAC, the biomolecule serving as the target should be selectively expressed on tumor cells, but not in healthy pancreas or in the inflammatory pancreatic tissue of chronic pancreatitis (PT). Such target-candidate is actually the NTS₁R, overexpressed in 95% of human PDAC cases, but not in samples from patients with chronic PT or healthy pancreas (**Images I17 and I18**). This finding in combination with the availability of native peptide ligands, as well as synthetic peptide analogs with high receptor affinity, render NTS₁R a promising biomolecular target for radiopharmaceutical development (100–102).
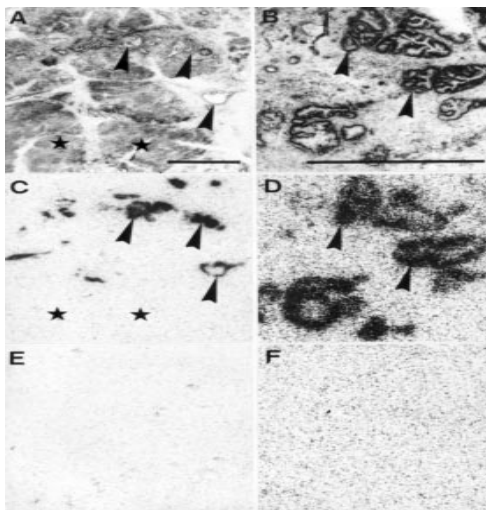
Image I17: (A) and (B) haematoxylin-eosin stained sections Arrowheads: tumor duct-like structures, asterisks: non-neoplastic pancreatic acini; (C) and (D) autoradiograms with [^{125}I]I-[Tyr^3]-NT. Arrowheads: NTS₁Rs in the tumor ducts. Asterisks: NTS1R-free pancreatic acini. (E) and (F) autoradiograms with [^{125}I]I-[Tyr^3]-NT (in the presence of 10^{-6} M NT) (100)
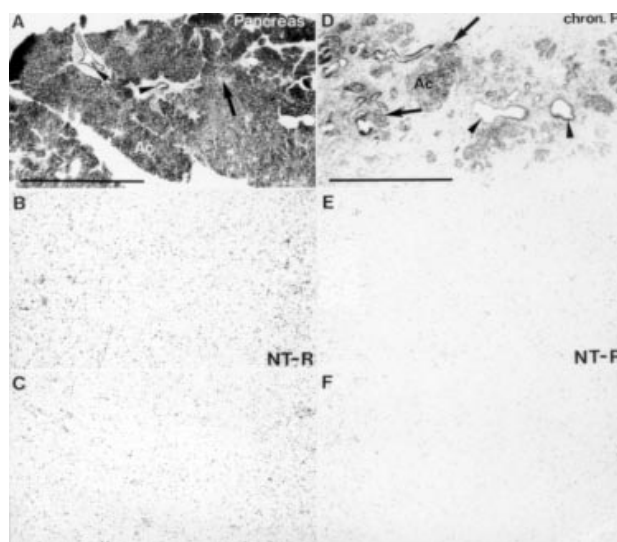
Image I18: Healthy human pancreatic tissue (A–C) and in chronic PT (D–F). (A) & (D) Haematoxylin-eosin-stained sections showing pancreatic acini (Ac), pancreatic ducts (arrowheads), and pancreatic islets (arrows). (B) & (E) Autoradiograms showing total binding of $[^{125}I]I-[Tyr^3]$-NT. (C) & (F) Autoradiograms showing non-specific binding of $[^{125I}]I-[Tyr^3]$-NT (in the presence of 10^{-6} M NT) (100).

NTS$_1$R-directed peptide radiopharmaceuticals can be suitably designed to carry γ or positron emitters on PDAC lesions with a high specificity for diagnostic imaging with SPECT or SPECT/CT and PET or PET/CT, respectively. The visualization of the primary tumor and any existing metastases will allow to determine if the disease is still localized or has already spread in the body as well as to establish the exact position of the lesions. This information can be then elegantly exploited by the oncologist on several levels: i) for guided biopsy and guided surgery, ii) for therapy decision-making depending upon disease progress and dissemination, iii) for planning of radionuclide therapy with the peptide radiopharmaceutical carrying instead a beta or an alpha emitter to pathological sites, according to an integrated theranostic "patient adopted" approach. Furthermore, diagnostic imaging will enable reliable dosimetric calculations prior to radionuclide therapy. Eventually, it will allow non-invasive monitoring of therapeutic responses during radionuclide therapy, chemotherapy etc. Thus, ineffective and patient debilitating therapies can be recognized as such at an early stage and timely discontinued. In conclusion, nuclear medicine diagnostics using suitable NTS$_1$R-targeting peptide radioligands may turn out to be instrumental in establishing the onset, staging and progress of PDAC in a unique and non-invasive manner. They may become essential as well for decision-making with regards to therapy planning and for the assessment of therapeutic efficacy.

Neurotensin and its receptors

Neurotensin (NT, pyroGlu[1]-Leu[2]-Tyr[3]-Glu[4]-Asn[5]-Lys[6]-Pro[7]-Arg[8]-Arg[9]-Pro[10]-Tyr[11]-Ile[12]-Leu[13]-OH) is a thirteen amino acid peptide, first isolated from bovine hypothalami. It has a high degree of preservation across species and it acts as neurotransmitter / neuromodulator both in the central nervous system (CNS) and in the periphery. The smallest fragment of NT that retains its biological function is NT(8-13) (Arg[8]-Arg[9]-Pro[10]-Tyr[11]-Ile[12]-Leu[13]-OH), a six amino acid-long peptide located at the carboxyl terminus of the native NT (**Image I19**). Both of these peptides exert their functions by binding to three different receptors and triggering second message intracellular cascades (103,104).
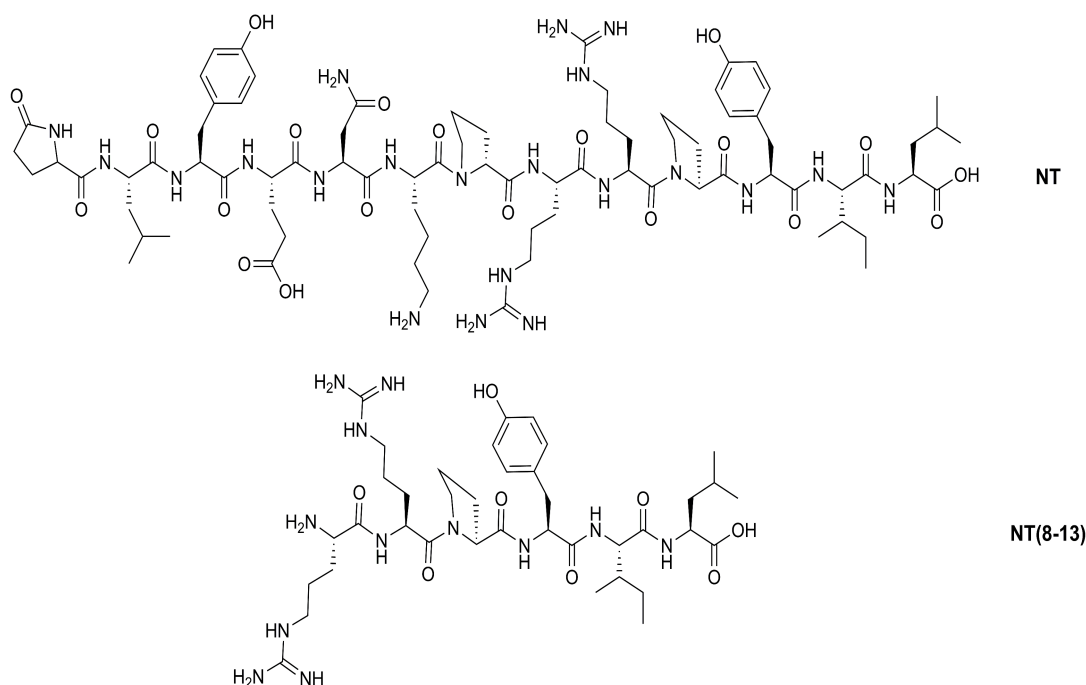
Image I19: Structure of native NT and its C-terminal hexapeptide fragment NT(8-13).

Two neurotensin receptors, belong to the superfamily of GPCRs and they are known as NTS_1R (**Image I20**) and neurotensin receptor 2 (NTS_2R). Both of these receptors are located on the cell membrane and they have the characteristic serpentine structure of the GPCRs (see subchapter "Molecular radiopharmaceuticals"). Upon activation of the receptor by an agonist, a G-protein is activated and gives rise of the second message intracellular cascade. The major signaling pathway for both NTS_1R and NTS_2R starts with the activation of Gq protein, which activates phospholipase C and the production of IP3 (inositol trisphosphate), triggering the increase of intracellular concentration of Ca^{2+}. Although these two receptors share a 60% homology, they differ in their body distribution and

role. Thus, the NTS$_1$R is physiologically expressed throughout the CNS and in the intestines and has a neuroleptic-like action. NTS$_2$R is expressed predominantly in the CNS, functioning mainly as antinociceptive and inducing hypothermia (103–108).
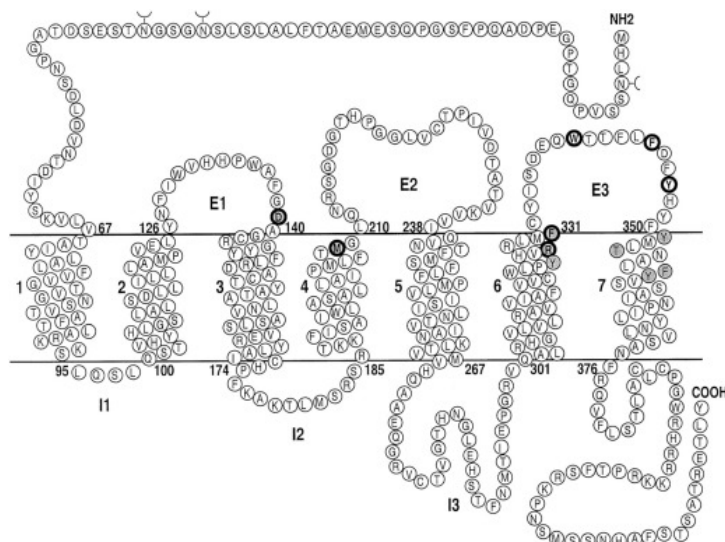
Image I20: Sequence and structure of NTS$_1$R.

The third neurotensin receptor, is a type I sortilin-like receptor, known as neurotensin receptor 3 (NTS$_3$R). It has a single transmembrane domain and is located mostly on intracellular membranes. The sortilin-like family of receptors has a cysteine-rich extracellular domain and a short intracellular one that transduces signals for fast internalization of the receptor. Despite the fast internalization of the receptor, the number of NTS$_3$Rs on the outer cell membrane seems to be constant (around 10% of the whole receptor population), even after its activation by NT. Due to its wide distribution to most tissues of the body and its predominantly intracellular location, the NTS$_3$R is not of any interest as a radiopharmaceutical target (107,109,110).

Therefore, only the NTS$_1$R is of interest for oncological applications amongst the three neurotensin receptor subtypes, owing to its overexpression in PDAC as well as in other human malignancies (**Table I2**). Various efforts to obtain clinically relevant NT-based radioligands for PDAC theranostics have been made thus far, but success has been limited mainly due to their metabolic instability (see below).

Enzymatic degradation of NT

It is common for peptides which act as neurotransmitters, neuromodulators or hormones to have their function regulated by inherent mechanisms, preventing the over-stimulation of their cognate-receptors. The methods involved include: a) the re-uptake of the excreted peptides, b) desensitization of their receptors and c) peptide degradation by peptidases. Peptidases represent a major class of proteolytic enzymes breaking down peptide bonds and can be further divided into metal-based and non-metal-based. Metalloproteases (or metallopeptidases) are using metal ions as part of their catalytic center, while non-metalloproteases are not. Peptidases, like most enzymes, exhibit a variety in their tissue distribution patterns. Some members are localized in specific tissues, organs or cell compartments, while others are abundantly present or even excreted into the bloodstream ("Peptides as vectors").

NT and its NT(8-13) fragment share this metabolic fate, undergoing degradation by peptidases in the biological milieu. It should be noted however that despite the significant number of peptidases potentially participating in the degradation of NT and are expected to degrade NT(8-13)-based radiopharmaceuticals as well, only a few have been identified thus far: a) NEP b) ACE, c) neurolysin (NL) and d) thimet oligopeptidase (TOP). The individual cleavage sites of these enzymes on the NT(8-13) chain are: Pro^{10}-Tyr^{11} and Tyr^{11}-Ile^{12} for NEP, Tyr^{11}-Ile^{12} for ACE, Arg^8-Arg^9 for TOP and Pro^{10}-Tyr^{11} for NL.

It is reasonable to assume that in the brief period of time that a NT(8-13)-based radioligand reaches the tumor after entering the bloodstream only the peptidases coming in contact with it can exert their proteolytic action. Consequently, TOP and NL can be ruled out, since they are located intracellularly. On the other hand, ACE is abundantly present in the blood solute as well as in several tissues, such as the lungs, kidneys, GI. Likewise, NEP is omnipresent in the body, found anchored on the epithelial cells of the blood vessels and major organs, such as liver, intestines, kidneys, in high local concentrations. Thus, NT-based radiotracers will be inevitably exposed to the proteolytic action of both ACE and NEP on their way to the tumor-situated NTS_1R target. Indeed, these two peptidases drastically compromise the efficient delivery of intact radiolabeled NT-based peptides to tumor sites (39,52,118,119,58,111–117).

Enhancing peptide stability

As already discussed (in "Peptides as vectors"), two major routes have been pursued for the stabilization of peptide analogs in the body and can be adopted as well for stabilizing NT(8-13) derived radioligands. The first involves key-structural changes in the peptide chain and the second concerns the transient *in situ* stabilization of the peptide with the aid of suitable NEP and ACE inhibitors (39,63,65). Both strategies have their own advantages and disadvantages.

The use of inhibitors is probably the fastest way to go, at least at the developmental and preclinical level. Considering the fact that both NEP and ACE involved in the degradation of NT(8-13) based radioligands, play a significant role in human disease, there is a plethora of inhibitors available. Interestingly, FDA and EMA-approved inhibitors for NEP and ACE are already in clinical use, since those enzymes are part of the mechanism regulating blood pressure (120–123). Thus, Entresto® (**Image I21**) (62–64) and Lisinopril (**Image I8**) (124–126) are two prime examples of registered and prescribed antihypertensive drugs, inhibiting NEP and ACE, respectively. Despite the accumulating evidence on the effectiveness and ease of this approach both in animal models (63–67) and in preliminary proof-of-principal clinical trials, abiding to strict guidelines and approval by the appropriate authorities need to be acquired prior to entering broad clinical practice.

Sacubitril (AHU-377)   **Sacubitrilat (LBQ657)**
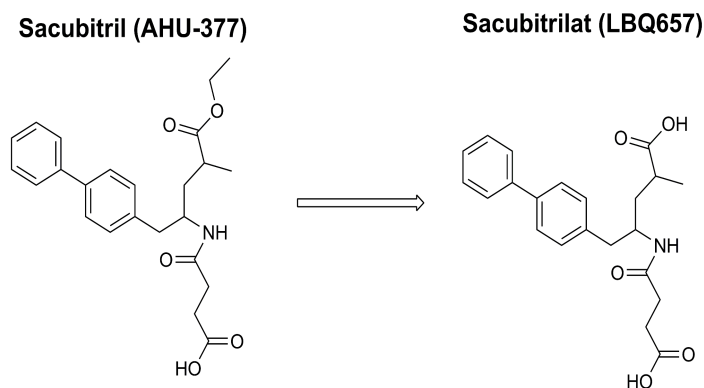
I**mage I21**: Structure of Sacubitril (one of the two active substances of Entresto®) *in vivo* releasing the potent NEP inhibitor sacubitrilat

On the other hand, the structural modification approach is aiming at making the peptide per se more resilient to degradation. It is more time-, cost- and resources-demanding, but it offers the possibility to yield analogs with improved inherent characteristics. There are quite a few examples of structural modifications on the native NT(8-13) motif aiming to increase metabolic stability. One of the modifications resulting in drastic increase of stability is the exchange of Ile^{12} with tert-isoleucine (Tle),

an unnatural amino acid. Other changes that had a lesser impact, are the exchange of Tyr[11] into dimethyl-tyrosine (DMT) or Arg[8/9] into Lys (127–135). Despite the fact that these substitutions resulted in increased stability, they had negative effects on other characteristics of resulting radioligands. For instance, Tle[12] to Ile[12] substitution led to a considerable decrease of radioligand cell uptake (65). On the other hand, Lys[8/9]/Arg[8/9] replacement was associated with unfavorably prolonged retention of the radiotracers in the kidneys (55,57,75,76). Last but not least, DMT[11]/Tyr[11] leads to inferior affinity for NTS$_1$R (136,137). Other modifications were directed at the cleavable peptide bonds, as for example the reduction (e.g. Arg[8]-Arg[9]), or methylation of selected peptide bond(s) or bond substitutions with unnatural non-biodegradable isosteres (triazoles) (138,139). The results from these interventions turned out to negatively affect pharmacokinetics, since they either compromised tumor uptake, or unfavorably led to higher background radioactivity levels, especially in critical organs, like the kidneys. Other worth-mentioning structural modifications involve the C-terminus elongation of the peptide sequence, that in some cases led to increased stability while retaining receptor affinity. On the other hand, the exchange of Leu[13] by unnatural amino acids, such as β-amino acids, or silicon-containing atoms (like trimethylsylil-alanine, TMSA) was attempted as well. It is interesting to note, that TMSA had the unique effect of increasing receptor affinity and internalization rates while further reducing the metabolic stability of resulting radioligands (137,139,140).
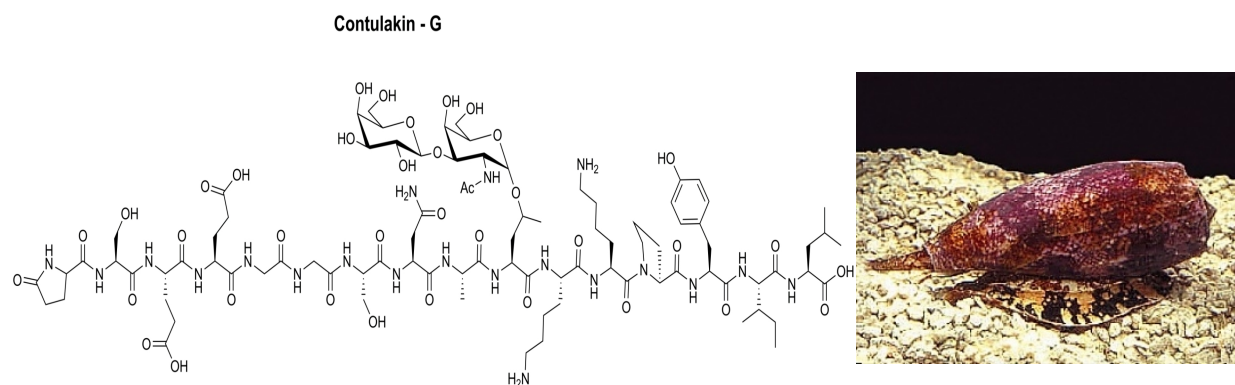
Image I22:Structure of contulakin-G, an invertebrate counterpart of NT (left) isolated from the venom of the predatory cone snail Conus geographus endemic in coral reefs of the Pacific (right)

Moreover, there are examples of metabolically stable NT-like peptides taken from nature, such as contulakin-G, a natural occurring NT-like analog product isolated from *Conus geographus* venom (**Image I22**). This peptide contains a branched segment at position 10 (corresponding to position 7 of human NT) carrying oligosaccharides (141,142). By exploiting the already enhanced stability and bioavailability of contulakin-G and the fact that the introduction of lipid acids is known to increase

stability by binding to albumin in the blood stream (143–145), new lipid acid-containing NT analogs were synthesized (146). These lipid acid-modified analogs exhibited improved bioavailability and affinity for NTS_1R. Alternative substitution, of the oligosaccharides by poly-amine chains also yielded analogs with improved properties. However, their increased blood brain barrier (BBB) penetration represents a drawback for nuclear medicine purposes (147). Furthermore, the presence of primary amine residues in the peptide-chain was shown to be linked with unfavorable kidney uptake (132).

Aim of the present work

The present work has been focused on the design and evaluation of new radiopharmaceuticals for imaging of PC, and especially PDAC. In order to exploit the reported overexpression of NTS_1R in PDAC, new NTS_1R-targeting radiopeptides were designed as molecular diagnostic tools for SPECT and SPECT/CT instrumentation. For this purpose, the hexapeptide fragment at the C-terminus of NT, NT(8-13), was chosen as a template for radiotracer design. By conjugation of the bifunctional acyclic tetraamine N_4 chelator at the N-terminus, labeling with the pre-eminent SPECT radionuclide Tc-99m could be achieved. The choice of the radionuclide was based on the wide availability, good logistics and optimal nuclear characteristics of Tc-99m.

Special emphasis was given on the *in vivo* metabolic stability and optimal pharmacokinetics of resulting radiopeptides. To achieve these goals, two major approaches were explored:

First, *in situ* inhibition of NEP and/or ACE was adopted as a means to improve the metabolic stability and overall performance of "revisited" and novel [^{99m}Tc]Tc-radiotracers. These two enzymes have been reported to degrade NT, NT(8-13) and their analogs. Hence, increased stability and improved tumor uptake was anticipated for NT(8-13)-based radiotracers after their inactivation by administration of suitable inhibitors, such as PA / Entresto® for NEP and Lis for ACE. Entresto® was preferred over PA, because it is a registered anti-hypertensive drug already in clinical use (the same applies for Lis). This fact is expected to facilitate the clinical translation the *in situ* inhibition approach with regards to biosafety regulations and guidelines (63,65,67).

Second, structural changes were introduced on the NT(8-13) motif, aiming to improve the metabolic stability and *in vivo* performance of the new radiotracers as such, or in combination with the peptidase inhibitors. These modifications fall into two categories: (a) Amino-acid substitution and elongation at the C-terminus of the N_4-Gly-NT(8-13) template, (b) Introduction of lateral groups at the ε-amino group after substitution Lys^7/Gly^7, comprising of an albumin binding domain (ABD) and/or a polyethyleneglycol (PEGx) residue.

The first modifications were based on reports claiming increased resistance of related peptides against ACE with little to non-hindrance on NTS_1R binding (148). Accordingly, two new analogs were designed, DT7, whereby the C-terminus of the N_4-Gly-NT(8-13) template was elongated by a D-asparagine residue, after position 13, and DT13, in which Leu^{13} was substituted by (S)-$β^3$hLeu.

The next modifications, aimed to increase metabolic stability and tumor targeting of related radioligands via the introduction side chains, with or without of albumin binding capabilities. However, selecting the position of branching in the N_4-Gly-NT(8-13) template represents a crucial step forward for the success of this approach. Interestingly, relevant information could be retrieved from literature concerning the design of new painkillers based on contulakin-G, an invertebrate counterpart of NT. One of the reported compounds derivatized with a pendant palmitoyl group could retain high affinity for NTS_1R and at the same time displayed high bioavailability. Based on this information, a small library of radiotracers was designed by introducing a palmitoyl group (1st generation – DT8) (142,146) or other side-chains with altered albumin binding capabilities and/or length (DT9, DT10 and DT11)

To efficiently assess the above-described approaches, a few major goals needed to be addressed first:

- Re-evaluation of previously reported analogs (DT1,5,6) (131,132), both *in vitro* and *in vivo*, to reveal potential benefits on metabolic stability and overall performance during *in situ* NEP/ACE inhibition. Furthermore, selection of a reference compound to serve as the standard for evaluating new strategies, experimental models and analogs.

- Establishing a new reliable and convenient cell and animal PC model as a basis to compare all the above-mentioned approaches. New data need to be correlated with the previously reported results obtained from colon adenocarcinoma WiDr cell and tumor models. Four different PC cell lines were tested for that purpose (63,65).

- Synthesis and evaluation of novel radiotracers on the newly established cell and animal PC models of PC.

- Comparison of novel analogs with the reference compound without or after administration of NEP and/or ACE inhibitors.

Materials and Methods

Peptides and reagents

All chemicals were of reagent grade and were used without further purification. NT (pyroGlu-Leu-Tyr-Glu-Asn-Lys-Pro-Arg-Arg-Pro-Tyr-Ile-Leu-OH) was purchased from Bachem (Bubendorf, Switzerland). Entresto® was sourced from a local pharmacy. Lisinopril (Lis, [N2-[(S)-1-carboxy-3-phenylpropyl]-L-lysyl-L-proline) was obtained from Sigma-Aldrich (St. Louis, MO, USA). Phosphoramidon (PA, N-(α-l-rhamnopyranosyl-oxyhydroxyphosphinyl)-L-leucyl-L-tryptophan disodium dihydrate) was provided from PeptaNova GmbH (Sandhausen, Germany). The series of NT(8-13) analogs, code-named as Demotensin X (DTx where X: 1, 5 - 11, 13) were synthesized by PiChem (Graz, Austria).

Radionuclides

- Tc-99m: in the form of $[^{99m}Tc]NaTcO_4$ was acquired after elution of a $[^{99}Mo]Mo/[^{99m}Tc]Tc$-generator (Ultra-Technekow V4 Generator) from Curium Pharma (Petten, The Netherlands)

- I-125: in the form of $[^{125}I]NaI$ in a 0.1 M NaOH solution was acquired carrier-free from Perkin Elmer (Massachusetts, USA).

Radiolabeling and quality control

Lyophilized peptide analogs DTx (x: 1, 5 − 11, 13) dissolved in HPLC-grade water (1 mM, 50 uL aliquots were stored at -20 ºC in Eppendorf protein LoBind vials) were used for labeling.

$[^{99m}Tc]Tc$ labeling

The procedure was performed in an Eppendorf protein LoBind vial containing phosphate buffer (0.5 M, pH 11.5, 50 uL). The addition of $[^{99m}Tc]NaTcO_4$ eluate (420 uL, 370–550 MBq) was followed by sodium citrate (0.1 M, 5 uL), the peptide stock solution (15 uL, 15 nmol) and a freshly prepared $SnCl_2$ solution in ethanol (10 uL, 10 ug). The mixture was left to react for 30 min at room temperature. Then the pH was adjusted to 7 with the addition of HCl (0.1 M).

Quality control of [^{99m}Tc]Tc-radiotracers

For the quality control of the forming radiotracers after labeling both reversed-phase high performance liquid chromatography (RP-HPLC) and instant thin-layer chromatography (iTLC) were used.

For HPLC analyses, a Waters Chromatograph equipped with a 600 E multi-solvent delivery system and coupled to a 2998 photodiode array UV-detector (Waters, Vienna, Austria) and a Gabi gamma detector (Raytest RSM Analytische Instrumente GmbH, Straubenhardt, Germany). Data processing was performed via the Empower Software (Waters, Milford, MA, USA). A Symmetry Shield RP-18 (5 μm, 3.9 mm × 150 mm) column was used; for the elution a flow rate of 1 mL/min was used, applying a linear gradient system, A/B – 100/0 to A/B – 60/40 in 20 min (solvent A: 0.1% aqueous trifluoroacetic acid, TFA; solvent B: acetonitrile, MeCN).

For iTLC analyses, 3 mm strips of Whatman chromatography paper (GE Healthcare, Chicago, IL, USA) were used. They were left to develop up to 10 cm from the application point. For the detection of the reduced hydrolyzed technetium ([^{99m}Tc]TcO$_2$ × nH$_2$O, remaining at the application point) a mixture of ammonium acetate (5 M) and methanol 1:1 (v/v) was used. For the detection of pertechnetate ([^{99m}Tc]TcO$_4^-$, migrating to the solvent front) acetone was used as a mobile phase. Then the strips were cut into pieces and their activity was measured with an automated multi-sample well-type γ-counter with a NaI(Tl) 3'' crystal (Canberra Packard CobraTM Quantum U5003/1, Auto-Gamma(R) 5000-series counting system).

Preparation of [^{125}I]I-Tyr^3-NT

In an Eppendorf protein LoBind vial, containing sodium phosphate buffer (10 mM, pH 7.4), we added 1 nmol NT (1 mM, dissolved in HPLC grade water), [^{125}I]NaI (0.5 nmol, 1 mCi) and chloramine-T (16 nmol). The mixture was left to react for 1 min at room temperature. After the incubation, Na$_2$S$_2$O$_6$ (16 nmol) and bovine serum albumin (BSA, 50 ug) were added to the mixture to stop the reaction.

For the separation of [^{125}I]I-Tyr^3-NT from the mixture RP-HPLC was used, with a two step elution gradient. For the first step a gradient starting at 90% A / 10% B and linearly reaching at 70% A / 30% B over 28 min, while for the second step the ratios reached at 65% A / 35% B over 20 min. The retention times (t$_R$) for the two mono-iodinated compounds were: [^{125}I]I-Tyr^8-NT, 36 min; [^{125}I]I-Tyr^3-

NT, 37 min and the bis-radioiodinated compound, 40-41 min, allowing for collection of the $[^{125}I]I$-Tyr^3-NT product only in excellent purity and at specific activity of ~81.4 GBq / umol.

Cell culture

Five different human cell lines were used in the present thesis: i) the colon adenocarcinoma WiDr cell line and the four PDAC cell lines ii) AsPC-1 (ascite metastasis), iii) MiaPaca-2 (epithelial), iv) PANC-1 (epithelial) and v) CAPAN-1 (epithelial). WiDr cells were purchased from LGC Promochem (Teddington, UK) and the pancreatic cell lines from LGC Standards GmbH (Wesel, Germany).

The cells were expanded and maintained in 75 cm^2 filter capped flasks, at 37 ^{o}C and an atmosphere of 5% CO_2 and 95% humidity in a Heal Force SMART CELL HF-90 incubator. The culture media used were from Gibco BRL, Life technologies (Grand Island, NY, USA) and the supplements from Biochrom KG Seromed (Berlin, Germany). For WiDr cells McCoy's medium was used. AsPC-1 cells were grown in Roswell Park Memorial Institute-1640 medium (RPMI). For the rest of the cell lines Dulbecco's Modified Eagle's Medium (DMEM) was used. All media contained GlutMAX-I and were supplemented with 10% v/v fetal bovine serum (FBS), 100 U/mL penicillin and 100 ug/mL streptomycin.

The cell cultures were reduced at a ratio of 1:3 − 1:5 when their confluence was reaching 80-90% by treatment with a Trypsin/EDTA (0.05% / 0.02% w/v) solution. Trypsin was inactivated with the addition of complete medium. When not in culture, cells were preserved in cryovials in a liquid nitrogen tank, in freezing medium (complete growth medium supplemented with of 10% v/v dimethyl sulfoxide (DMSO)).

Competition binding

Membrane isolation

When cultured cells reached 80-90% confluency, they were scraped from the bottom of the flasks using a cell-scraper. Resuspended cells were then collected in 50 mL tubes and centrifuged at 2000 g for 10 min in a Hettich UNIVERSAL 320 R centrifuge (Tuttlingen, Germany). The supernatant was discarded and the cells were washed with 40 mL of PBS buffer (pH 7.4) and re-centrifuged at 2000 g for 10 min. Then the cells were resuspended in cold (4 ^{o}C) Tris/EDTA buffer (Tris 10 mM, EDTA 0.1

mM, pH 7.4). The cell suspension was homogenized at 4 $^{\circ}$C using a Bioblock Scientific homogeniser over ice. The homogenate was then centrifuged at 5000 g for 20 min at 4 $^{\circ}$C and the supernatant, which contained the cell membranes, was collected. Next, the supernatant was centrifuged at 26000 rpm – 45000 g for 20 min at 4 $^{\circ}$C, on a Beckman Coulter, Optimal L-90K ultracentrifuge equipped with a 50.2TI head. The supernatant was discarded and the pellet was resuspended in cold Tris/EDTA buffer, 100 uL per flask used, divided into aliquotes in 1.5 mL Eppendorf tubes and stored at -80 $^{\circ}$C until used.

Membrane test

- **Binding Buffer**
  - 50 mM HEPES
  - 5.5 mM $MgCl_2$
  - 0.1 mg/mL bacitracin
  - 1% w/v BSA
  - pH 7.4

- **Washing Buffer**
  - 10 mM HEPES
  - 150 mM NaCl
  - pH 7.4

A solution of NT(8-13) (10^{-5} M) was prepared by dissolving a NT(8-13) stock solution (1 mM) in binding buffer (Cold). Also a solution of [^{125}I]I-Tyr^3-NT was prepared by diluting the stock solution in binding buffer aiming for ~40000 cpm per 70 ul (corresponding to a concentration of 214 pM) (HOT). A set of triplicates, was prepared for each membrane concentration by mixing 30 uL of Cold or binding buffer, with 70 uL of HOT in 200 uL of each membrane concentration in binding buffer. All solutions were kept on ice. After 1 h incubation at 22 $^{\circ}$C under constant steering in an Incubator-Orbital Shaker (MPM Instr. Srl, Italy), the reaction was stopped by dilution with ice cold washing buffer. Samples were then aspirated on a 48-sample Brandel Cell Harvester (Adi Hassel Ingenieur Büro, Munich, Germany), through Whatman GF/B filters presoaked in binding buffer. After a couple of washes with cold washing buffer, the filters were dried over vacuum and the parts corresponding to each sample were cut and placed in 5 mL RIA tubes. The radioactivity of the tubes was measured in the γ-counter. The concentration corresponding to a maximum of 10% non-specific binding (with the addition of Cold) over the total binding (with the addition of binding buffer) was chosen as the amount of membranes used in the competition binding assays that followed.

Competition binding assays

A series of dilutions ranging from 10^{-12} – 10^{-5} M of the peptide under evaluation was prepared and kept on ice. A freshly prepared solution of $[^{125}I]I$-Tyr^3-NT (~40000 cpm per 70 uL, 214 pM – HOT) was also kept on ice. In each series of RIA tube, 30 uL of the corresponding concentration of Cold was added with 70 uL of HOT solution and 200 uL of membrane homogenate in binding buffer. The samples were incubated at 22 ^{o}C for 1 h under constant steering. The binding reaction was terminated by addition of washing buffer (4 ^{o}C) and aspiration of the samples on the Brandel Cell Harvester loaded with fiber glass filters presoaked in binding buffer. The activity of the filters was measured on the γ-counter. The inhibition curves were plotted and the half maximal inhibitory concentration (IC_{50}) values were calculated with GraphPad Prism 6 (GraphPad Software, San Diego, CA, USA), applying a nonlinear one-site model. Results for each compound are given as mean ± standard deviation of at least three independent repetitions of the experiment performed in triplicate.

Cell uptake assays

In order to assess the cell-binding and internalization kinetics of the compound under investigation, approximately $1{\times}10^6$ cells were seeded per well of a 6-well plate and incubated overnight. The following day, the cells were washed twice with culture medium supplemented with 1% FBS (internalization medium or IM) at 4 ^{o}C. Then 1200 uL of IM at 37 ^{o}C were added per well, followed by 150 uL of radiolabeled compound solution, corresponding to 250 fmol peptide, and either 150 uL IM (total series) or NT (10^{-5} M in IM, non-specific series). The cells were incubated at 37 ^{o}C.

At specific time points, the plates were removed from the incubator and placed on ice to stop the internalization process. The supernatant was collected in RIA tubes and the cells were washed with 1 mL of phosphate buffer saline (PBS, pH 7.4) supplemented with 0.5% w/v BSA (IPBS) at 4 ^{o}C. The washings were collected and the cells were incubated twice with 600 uL of acid glycine buffer (50 mM glycine, 0.1 M NaCl, pH 2.8) for 5 min each time; the supernatants, corresponding to the membrane bound fraction (MB), were collected. After a wash with 1 mL of ice cold IPBS, the cells were lysed with 600 uL 1 M NaOH and the lysate was collected; this step was repeated once more and the collected lysates combined – internalized fraction. The sample radioactivity was measured on the γ-counter.

Overall, three fractions were collected per well (supernatant, MB and internalized). Each fraction was expressed as a percentage of the initial activity added per well. By subtracting the non-

specific fractions (in the presence of 1 uM NT) from the respective total fractions (whereby only IM was added), the specific MB and internalization fractions could be calculated. Each assay was performed at least three times in triplicate. The results were expressed as mean ± standard deviation.

Albumin binding assays (149–151)

In 6-well plates 1200 uL HBS-BSA (HEPES buffered saline: NaCl 150 mM, HEPES 20 mM, pH 7.4, supplemented with 0.5% w/v BSA) were added, followed by 150 uL radiopeptide solution in HBS (250 fmol peptide) and 150 uL of HBS-BSA or Ibuprofen (22.2 mg/ml) in HBS with V_{final} = 1.5 mL. After incubation for 30 min at 37 ^{o}C, the supernatant was discarded, the wells were treated twice with 600 uL 1 M NaOH and the liquid was collected. The sample radioactivity was measured on the γ-counter and was expressed as percentage of the activity added per well. The difference between the samples after treatment with NaOH for the different peptides provides a qualitative evaluation of their affinity for BSA. All experiments were performed at least three times in triplicate and the results were expressed as mean ± standard deviation.

Animal studies

In vivo stability

For the assessment of the *in vivo* stability of test radioligands healthy Swiss Albino mice (SAMs) were purchased from NCSR "Demokritos" animal house. The animals were housed in appropriate facilities with 12 h day/night cycles and were provided with chow food and drinking water ad libitum.

After an acclimatization period, the animals were divided randomly into groups of three. Mice in the control groups received no treatment, while the other groups were treated with either a NEP-inhibitor, (PA or Entresto$^®$) and /or an ACE-inhibitor (Lis), as shown in the Table below. Radiotracers were administered via the tail vein in a physiological saline solution (200 uL, 3 nmol of peptide). Five minutes after iv injection the animals were euthanized and blood was collected in ice-cold Eppendorf vials containing 20 uL of EDTA solution (0.1 mM).

Blood samples were centrifuged for 10 min at 5000 rpm at 4 ^{o}C and the serum was collected in new tubes and diluted with an equal volume of MeCN. After a brief mixing, the samples were centrifuged at 15000 rpm for 10 min at 4 ^{o}C. The supernatant was transferred into glass vials and the

samples were concentrated to approximately 100 uL using mild heating under a gentle nitrogen gas stream. Then the samples were diluted in 300-350 uL physiological saline and filtered through a Millex GV filter (0.22 μm, 13 mm diameter, Millipore, Milford, CT, USA).

Aliquots of the filtrate were analyzed by radio-HPLC, on a reversed-phase Waters Symmetry Shield RP18 column (5 μm, 3.9 mm × 20 mm). The flow rate was adjusted at 1 mL/min and the ratio A/B for the solvents (pg 47) started at 0% B and increased by 1% per min. The peak corresponding to the intact radiotracer was determined by coinjection of aliquots of the labeling solution; coelution confirmed intact radiopeptide retention times (t_R).

Inhibitor	Amount (ug, *mg)	Route of administration	Time of administration
PA / Lis / PA+Lis	300 / 200 / 300+200	iv	co-administered
Entresto®	12*	per os	30 min in advance

Biodistribution experiments

The severe combined immunodeficiency mice (SCID) used in biodistribution experiments were purchased from the NCSR "Demokritos" animal house. After an acclimatization period, six weeks-old animals were subcutaneously implanted in the right flank with 150 uL suspension of cells in sterile PBS under aseptic conditions. The cell suspensions used for tumor induction per animal were: (i) WiDr: $18×10^6$ cells, (ii) AsPC-1: $5×10^6$ cells, (iii) MiaPaca-2: $3×10^6$ cells. After 3 – 4 weeks well-palpable xenografts developed at the implantation sites in the majority (~90%) of the animals (corresponding to approximately 100 ug tumor mass). During this period, animals were housed in licensed facilities under aseptic conditions, controlled temperature and humidity, 12 h day/night cycles and were provided with sterilized bedding, chow food and drinking water ad libitum.

On the day of the experiment, the animals were divided randomly in groups of four. Each group was assigned a time interval as well as a treatment. In all groups animals received a bolus injection of a physiological saline solution of the radiopeptide (100 uL, 3 pmol) under evaluation via the tail vein.

Control groups received 100 ul physiological saline, while the others received one or a combination of inhibitors, as described above in the *in vivo* stability sergment. In an additional group, animals received an excess of NT (100 ug) along with the corresponding inhibitor(s) and the radiotracer, to assess NTS_1R-specificity of tumor uptake (block-group).

At predetermined time intervals the animals were euthanized and weighted. Their blood, organs and selected tissue samples as well as the implanted tumors were collected, weighted and their radioactivity was measured on the γ-counter together with proper standards of the injected activity. Results were calculated as percentage of injected activity per gram of tissue (%IA/g) and presented as mean ± standard deviation. For statistics, a Two-way ANOVA with Tukey's post hoc analysis was performed using GraphPad Prism 6.

Imaging studies

For SPECT/CT imaging, animals bearing WiDr or AsPC-1 xenografts were used. Each animal received [^{99m}Tc]Tc-DT1 or [^{99m}Tc]Tc-DT10 iv corresponding to ~50 MBq activity and 1.5 nmol of total peptide. The peptidase inhibitors PA+Lis were co-administered iv with the radiotracer, while Entresto$^{®}$ was given po 30 min in advance of radiotracer injection. The animals were euthanized 3 or 4 pi and SPECT/CT images were acquired, in collaboration with BIOEMTECH (Lefkippos Attica Technology Park, Attica, Greece).

Authorization of facilities and protocols

All experiments involving the use of radioactive solutions were performed by trained and authorized personnel behind sufficient shielding, in compliance to European radiation-safety guidelines and under supervision by the Greek Atomic Energy Commission. License number of the authorized laboratories: A/435/17092/2019.

The animals were housed in proper facilities supervised by the local authorities and they complied with the European legislation concerning laboratory animal welfare. Animal facility number: EL 25 BIOexp 021.

The protocols of the experimental procedures concerning animal-use were monitored and licensed by the local bioethics committee and were approved by the Department of Agriculture and Veterinary Service of the Prefecture of Athens, in accordance to the European legislation. The license number for *in vivo* stability protocol was #1609, 24-04-2019, while for the biodistribution protocol was #1610, 24-04-2019.

Results

As previously outlined (Aim, pgs 21 – 22), the aim of the current work was to develop and evaluate [^{99m}Tc]Tc-radiotracers targeting NTS$_1$R as radiopharmaceutical candidates in the diagnostic imaging of PDAC with SPECT or SPECT/CT.

In this perspective two major routes were pursued. The first one concerned the *in vivo* stabilization of previously reported analogs, by *in situ* inhibition of NEP and/or ACE, aiming to improve their biological profile. The second one involved structural modifications on the [Gly^7]NT(8-13) motif to yield new improved analogs. The impact of NEP and/or ACE inhibition on the profile of the new structurally modified analogs was evaluated as well. The results from this extensive study are presented in the following sections.

The first part is dedicated on efforts towards establishing a reference compound as base-line for evaluating the *in situ* stabilization approach and/or the profile of new analogs. It also includes all relevant steps followed for selecting a suitable NTS$_1$R-positive PC cell line and setting up reliable and practically convenient *in vitro* (cell assays) and *in vivo* (tumor bearing mice for biodistribution and imaging studies) models. To that purpose, the previously reported DT1, DT5 and DT6-based radioligands were "revisited" (65,131,132), first using the NTS$_1$R-positive colon adenocarcinoma WiDr cell line and then applying a NTS$_1$R-expressing pancreatic cell line; the latter was chosen after comparing four commercially available ones (63). The second part summarizes the results obtained from the evaluation of newly designed [^{99m}Tc]Tc-NT(8-13) tracers, following two different modification approaches in the peptide sequence. The biological profiles of these analogs were tested in NTS$_1$R-positive pancreatic cancer AsPC-1 cell models in comparison with the radiopeptide selected as reference.

NEP/ACE-inhibition approaches to improve the profile of reported [^{99m}Tc]Tc-DTx (x = 1, 5, 6)

Previous studies have demonstrated a stepwise increase of metabolic stability *in vitro* for the three NT(8-13)-based tracers, shown in Image 6. Going from [^{99m}Tc]Tc-DT1 (N$_4$-Gly-Arg-Arg-Pro-Tyr-Ile-Leu-OH) to [^{99m}Tc]Tc-DT5 (N$_4$-βAla-Arg-Dab-Pro-Tyr-Ile-Leu-OH) the βAla^7/Gly^7 and Dab^9/Arg^9 substitutions led to increased resistance to proteases both in murine plasma and kidney homogenates, which was further enhanced by Tle^{12}/Ile^{12} exchange in [^{99m}Tc]Tc-DT6 (N$_4$-βAla-Arg-Dab-Pro-Tyr-Tle-

Leu-OH). The effects of these modifications on cell-uptake, *in vivo* stability and other important biological features were tested against NEP and/or ACE inhibition strategies, adopted to improve metabolic stability as well as the pharmacokinetic profiles in tumor-bearing mice (131,132).
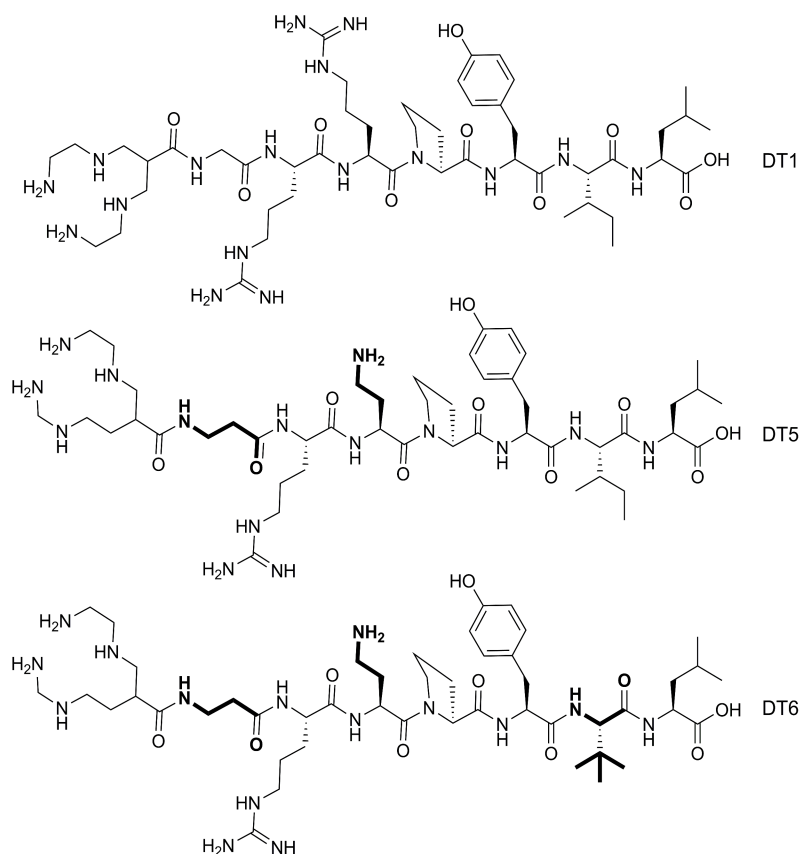
Image 1: Structure of DT1, DT5 ([**βAla^7,Dab^9**]DT1) and DT6 ([**βAla^7,Dab^9,Tle^{12}**]DT1)

Labeling

Labeling of DT1, DT5 and DT6 with Tc-99m was performed after short incubation of the peptides with [^{99m}Tc]TcO$_4^-$ generator eluate and the reducing agent SnCl$_2$ in the presence of citrate anions in alkaline pH; molar activities of 20 – 40 MBq/nmol of peptide were achieved (M+Ms, pgs. 23 – 24). Potential radiochemical impurities that could be present in the final mixture are the uncomplexed [^{99m}Tc]TcO$_4^-$, [^{99m}Tc]Tc-citrate and any forming [^{99m}Tc]TcO$_2$ × nH$_2$O. The first two can be easily detected via radio-HPLC and iTLC, but the reduced polymeric [^{99m}Tc]TcO$_2$ × nH$_2$O sticks to the column and cannot be detected and quantified by HPLC, but instead can be detected by iTLC (M&Ms, pg:47). Quality control of the labeled products by combined iTLC and HPLC confirmed radiochemical yields exceeding 98% and radiochemical purities greater than 99%. No further purification was

performed for the following biological experiments and analysis of all used solutions were made before and after the complition of the experiments (Appendix, **Images A2, A7 & A11**, pgs: 92, 95 & 99).

Cell uptake

We first compared the cell uptake and internalization capabilities of [^{99m}Tc]Tc-DT1, [^{99m}Tc]Tc-DT5 and [^{99m}Tc]Tc-DT6 in WiDr cells, which have served as the evaluation cell line in the past (131,132). However, in these previous reports the internalization and membrane bound fractions were calculated as percentage of the cell associated activity. Consequently, a direct comparison of the cell uptake across the analogs was not feasible and thus, the impact of the structural modifications made could not be properly assessed either. By expressing the membrane bound and internalized fractions as percentage of the total added radioactivity per well in this study, the impact of the structural modifications between [^{99m}Tc]Tc-DT1 and [^{99m}Tc]Tc-DT5 or [^{99m}Tc]Tc-DT6 became clearly visible. As demonstrated in **Image 2** and summarized in **Table 1**, a great difference ($p < 0.0001$) could be shown across analogs after 1 h incubation at 37 ^{o}C in WiDr cells.
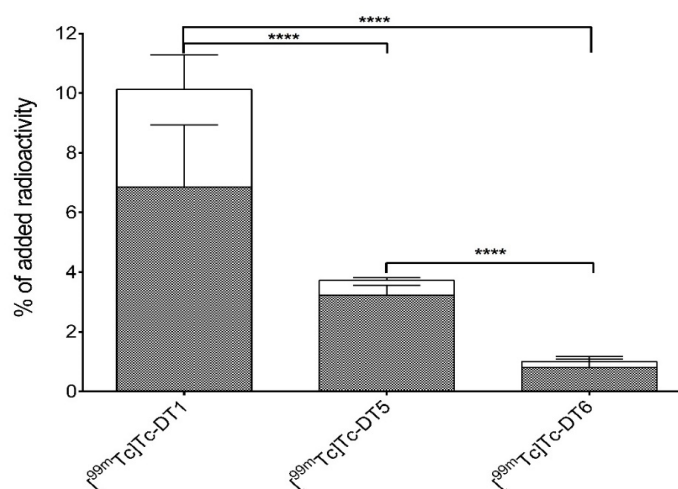
Image 2: Schematic representation of the cell uptake of radiotracers after 1 h incubation at 37 ^{o}C in WiDr cells, the dotted – gray part of the bars corresponds to the internalized, while the white part of the bar corresponds to the membrane bound fractions. Results are expressed as percentage of the total added radioactivity per well (mean ± sd), **** indicate a p value < 0.0001).

Table 1: NTS_1R-specific cell uptake of $[^{99m}Tc]Tc$-DT1, $[^{99m}Tc]Tc$-DT5 and $[^{99m}Tc]Tc$-DT5 in WiDr cells after 1 h incubation at 37 ºC; values are expressed as % of total added activity per well, mean ± sd, with number of wells shown in parentheses

Analog	Internalized (%)	Membrane Bound (%)	Total Uptake (%)
$[^{99m}Tc]$-DT1	6.85 ± 2.09 (42)	3.27 ± 1.16 (42)	10.12 ± 2.29 (42)
$[^{99m}Tc]$-DT5	3.23 ± 0.33 (18)	0.49 ± 0.09 (18)	3.72 ± 0.32 (18)
$[^{99m}Tc]$-DT6	0.81 ± 0.36 (18)	0.19 ± 0.09 (18)	1.00 ± 0.40 (18)

In vivo stability – The impact of NEP/ACE-inhibition

The metabolic stability of the three radiotracers in the bloodstream of mice, was compared at 5 min pi. In addition, the effects of treating the mice with NEP and/or ACE inhibitors (PA and Lis, respectively) were evaluated as well. As we can see in the control groups in **Table 2**, the Tle^{11}-modified $[^{99m}Tc]Tc$-DT6 displayed significantly higher stability in peripheral mice blood compared with the two Ile^{11}-containing $[^{99m}Tc]Tc$-DT1 and $[^{99m}Tc]Tc$-DT5, which were rapidly degraded ($[^{99m}Tc]Tc$-DT1 / $[^{99m}Tc]Tc$-DT5 vs. $[^{99m}Tc]Tc$-DT6 – $p < 0.0001$). For both $[^{99m}Tc]Tc$-DT1 and $[^{99m}Tc]Tc$-DT5 the use of either PA or Lis alone had little to no effect on metabolic stability. In contrast, $[^{99m}Tc]Tc$-DT6 could be fully stabilized by PA alone (control vs. PA – $p <0.001$). Only the combined administration of PA and Lis led to sufficient stabilization of $[^{99m}Tc]Tc$-DT1 and $[^{99m}Tc]Tc$-DT5 (control vs. Lis+PA – $p < 0.001$). These results imply that Ile^{11} to Tle^{11}-modification was effective in stabilizing $[^{99m}Tc]Tc$-DT6 against ACE in mice circulation. Representative radiochromatograms of this study are presented in the Appendix (**Image A11,** pg 98).

Table 2: *In vivo* stability of $[^{99m}Tc]Tc$-DT1, $[^{99m}Tc]Tc$-DT5 and $[^{99m}Tc]Tc$-DT6, in mice blood at 5 min pi; values represent % intact radioligand detected in the blood samples and are given as mean ± sd, with number of repetitions shown in parentheses.

Group	$[^{99m}Tc]Tc$-DT1	$[^{99m}Tc]Tc$-DT5	$[^{99m}Tc]Tc$-DT6
Control	1.8 ± 0.8 (4)	1.2 ± 0.2 (3)	53.7 ± 1.9 (2)
Lis	18.8 ± 2.5 (3)	28.7 ± 3.6 (3)	
PA	28.2 ± 3.5 (3)	15.4 ± 5.1 (2)	89.3 ± 6.7 (2)
Lis+PA	72.3 ± 3.2 (4)	79.0 ± 1.7 (2)	

Biodistribution in WiDr tumor-bearing mice

The biodistribution profiles of [^{99m}Tc]Tc-DT1, [^{99m}Tc]Tc-DT5 and [^{99m}Tc]Tc-DT6 were evaluated in SCID mice bearing WiDr xenografts at 4 h pi. Two animal groups for each radiotracer were used for comparison, a control group that received no treatment and a group that was treated with the combination of PA+Lis. Extensive tables with the biodistribution results (expressed as %IA/g, mean ± sd, n = 4) for each radioligand are listed in the Appendix (**Tables A1, A4 & A5**, pgs: 94, 97 & 99), while representative data is summarized in **Image 3**.

All three compounds demonstrated a fast washout from the background, including the NTS$_1$R-rich intestines. The tumor uptake for the control groups was very low, ranging between 0.2 – 1 %IA/g. Radioactivity cleared mainly via the kidneys and the urinary tract, differing in kidney retention across analogs, being low for [^{99m}Tc]Tc-DT1 (1.80 ± 0.14 %IA/g) and moderate for the other two compounds (8.63 ± 1.60 and 6.09 ± 1.15 %IA/g for [^{99m}Tc]Tc-DT5 and [^{99m}Tc]Tc-DT6, respectively).

After treatment of mice with the PA+Lis combination, tumor values significantly increased. Thus, for [^{99m}Tc]Tc-DT1 it reached 9.60 ± 3.62 %IA/g (p < 0.0001 vs. control) and for [^{99m}Tc]Tc-DT5 increased to 12.29 ± 2.73 %IA/g (p < 0.0001 vs. control). Interestingly, the most stable Tle^{12}-modified analog, [^{99m}Tc]Tc-DT6, reached a tumor uptake of 3.50 ± 0.34 %IA/g only, most probably as a result of its slower internalization in the WiDr cells, observed *in vitro*.

Treatment of mice with the inhibitors resulted in a notable increase of kidney uptake for both [^{99m}Tc]Tc-DT5 and [^{99m}Tc]Tc-DT6, (16.62 ± 1.63 %IA/g and 14.61 ± 3.16 %IA/g, respectively), assigned to the free primary amine group of Dab^9. These results could be visualized for [^{99m}Tc]Tc-DT1 by SPECT/CT (**Image 4**).
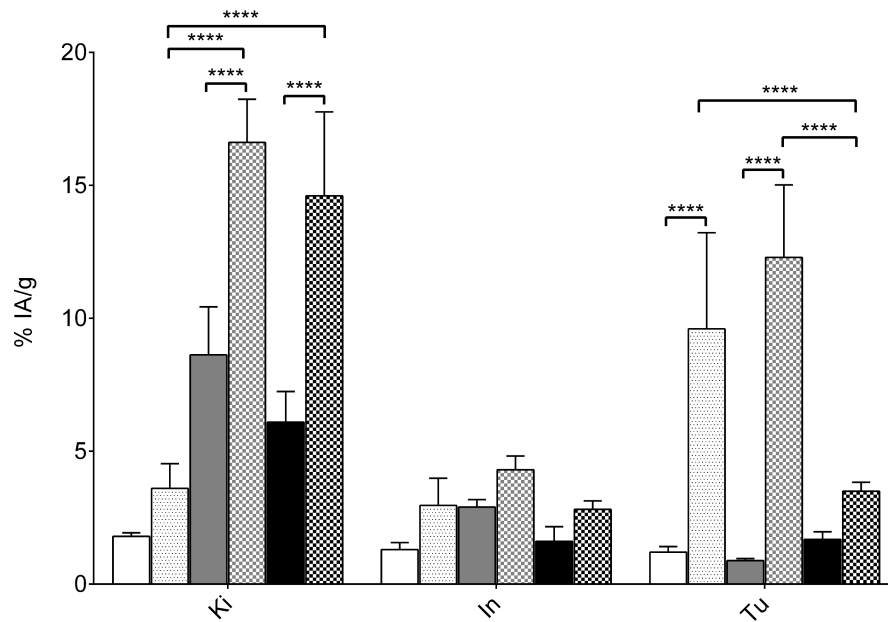
Image 3: Comparative biodistribution of [^{99m}Tc]Tc-DT1, [^{99m}Tc]Tc-DT5 and [^{99m}Tc]Tc-DT6 in SCID mice bearing WiDr xenografts at 4 h pi, selectively included here for Ki: kidneys, In: Intestines and Tu: WiDr tumors; data is provided as %IA/g values and represents the mean ± sd, n = 4. White: [^{99m}Tc]Tc-DT1, white – dotted: [^{99m}Tc]Tc-DT1 + PA + Lis, gray: [^{99m}Tc]Tc-DT5, gray – dotted: [^{99m}Tc]Tc-DT5 + PA + Lis, black: [^{99m}Tc]Tc-DT6, black – dotted: [^{99m}Tc]Tc-DT6 + PA + Lis. Only statistically significant differences across groups are shown (p<0.0001, ****)

Image 4: SPECT/CT image of SCID mice bearing WiDr xenografts at 3 h pi of [^{99m}Tc]Tc-DT1. (Left) control mouse, (Right) mouse after coinjection of [^{99m}Tc]Tc-DT1with a combination of PA + Lis. Red circles indicate xenograft sites.

Summary

The above three bioconjugates had similar sub-nM affinities for NTS_1R (IC_{50}, DT1: 0.14 ± 0.02 nM, DT5: 0.03 ± 0.01 nM and DT6: 0.08 ± 0.02 nM) (131,132,152), as previously reported. However, the newly acquired data from the present study demonstrated that fast cell internalization and *in vivo* metabolic stability of radioligands are equally important prerequisites for effective tumor targeting. It was clearly shown that such parameters were directly affected by the structural interventions performed on the [^{99m}Tc]Tc-DT1 motif.

Specifically, it was shown that double ßAla^7/Gly^7 and Dab^9/Arg^9 replacement failed to improve the *in vivo* stability and led to impaired uptake of [^{99m}Tc]Tc-DT5 in WiDr cells. Additional Tle^{12}/Ile^{12} substitution, although greatly improving the *in vivo* metabolic stability, further compromised the cell uptake of [^{99m}Tc]Tc-DT6, resulting in sub-optimal tumor uptake in mice. Notably, Dab^9/Arg^9 replacement in both [^{99m}Tc]Tc-DT5 and [^{99m}Tc]Tc-DT6 led to unfavorable increase of kidney values, which was associated with the free primary amine of Dab.

In contrast, *in situ* NEP and/or ACE inhibition turned out to be a very effective strategy to improve the *in vivo* stability and the overall pharmacokinetic profile of the radiotracers, especially of the unmodified [^{99m}Tc]Tc-DT1. The latter displayed a superior tumor uptake and faster body clearance among this group of analogs when administered in combination with the NEP-inhibitor PA and the ACE-inhibitor Lis.

Two major hurdles need to be addressed prior to translating these results in the clinic. Firstly, the replacement of the non-registered PA by a clinically approved alternative NEP inhibitor will facilitate the safe application of this concept in patients. For this purpose, the switch to the registered anti-hypertensive drug Entresto® was subsequently adopted in this work. Administered per os the drug releases *in vivo* the potent NEP-inhibitor sacubitrilat. The second hurdle is associated with the cases of angioedema reported during the application of dual NEP and ACE inhibitors in the clinic. To address this challenge, a combination of smart structural interventions and the use of a single inhibitor was explored, as presented in the following chapters (65).

In search of a preclinical NTS$_1$R-positive model for PC

The next objective was to translate the results described above from the colon adenocarcinoma WiDr-based model to a reliable PC model. The latter should be expressing the NTS$_1$R-target in

sufficient density, but at the same time remain practically convenient for both *in vitro* and *in vivo* evaluation of new radiotracers. Further important factors should be also taken into account, such as cell culture doubling times and times required for tumor growth after inoculation of mice. Four different human pancreatic cancer cell lines were selected for evaluation according to the above-set criteria, namely AsPC-1, CAPAN-1, MiaPaca-2 and PANC-1 cells (M+Ms, pg. 48).

Cell uptake

The NTS$_1$R-specific cell uptake of [^{99m}Tc]Tc-DT1 was tested head-to-head in the four PC cell lines, as an indication of their relative NTS$_1$R-expression levels. As detailed in the previous chapter, cell uptake *in vitro* had a great impact on tumor uptake in the animals and was considered to be essential for assessing the impact of structural modifications across radiotracers.

As evident from the cell uptake (**Images 5** and **6**) these values for [^{99m}Tc]Tc-DT1 turned out to be statistically different across cell lines. Specifically, [^{99m}Tc]Tc-DT1 displayed the greatest uptake in AsPC-1 cells, reaching 15.2 ± 2.6 % of added radioactivity, with PANC-1 being next in rank (8.1 ± 2.8 %, $p < 0.0001$), followed by MiaPaca-2 (2.7 ± 0.3 %, $p < 0.0001$) and CAPAN-1 (0.4 ± 0.1 %, $p < 0.0001$) at 1 h incubation, reaching a plateau thereafter. In all cases, the majority of the activity taken up by the cells was located intracellularly, consistent with an NTS$_1$R-agonist profile.

By comparing [^{99m}Tc]Tc-DT1 and [^{99m}Tc]Tc-DT5 in AsPC-1 cells (**Image 7**) the same trend was observed as in WiDr cells, with [^{99m}Tc]Tc-DT5 having significantly lower cell-uptake (8.4 ± 0.8%) compared with [^{99m}Tc]Tc-DT1 (15.2 ± 2.6%, $p < 0.0001$).
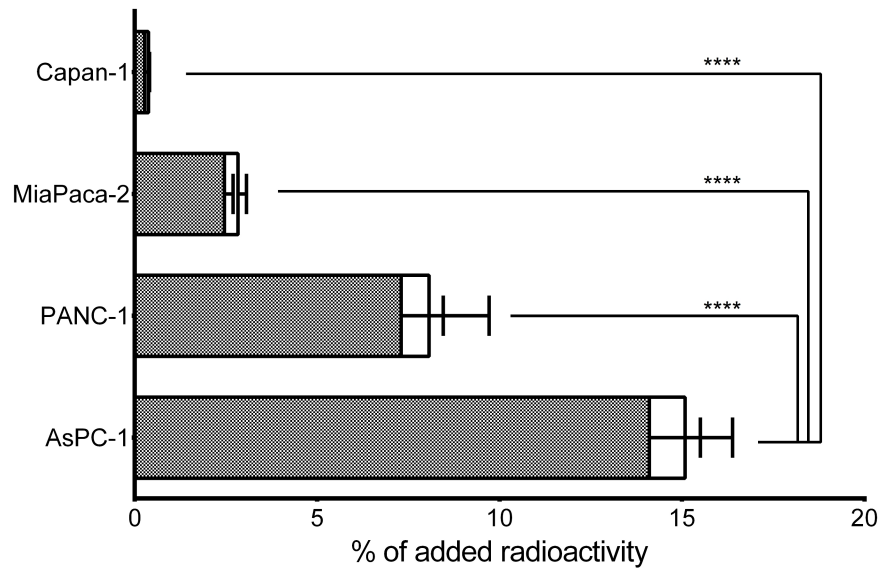
Image 5: Comparative NTS$_1$R-specific cell uptake of [^{99m}Tc]Tc-DT1 after 1 h incubation at 37 ^{o}C in various pancreatic cell lines with values expressed as % of total-added activity per well; the dotted – gray porsion corresponds to internalized, while the white bar corresponds to membrane bound radioactivity (****, p < 0.0001).
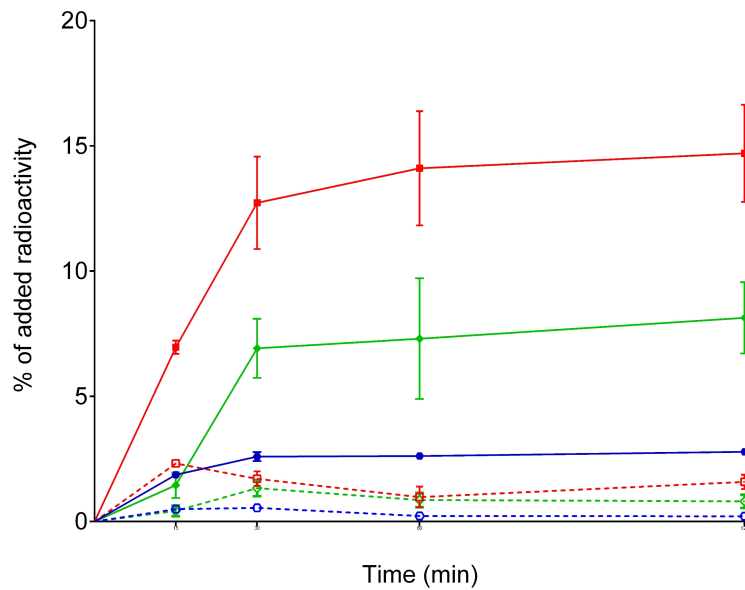
Image 6: Comparative NTS$_1$R-specific time-dependent cell uptake of [^{99m}Tc]Tc-DT1 after incubation at 37 ^{o}C with various pancreatic cell lines, expressed as % of total-added activity per well; solid lines: internalized, dotted lines: membrane bound radioactivity. Red: AsPC-1, green: Panc-1, blue: MiaPaca-2.
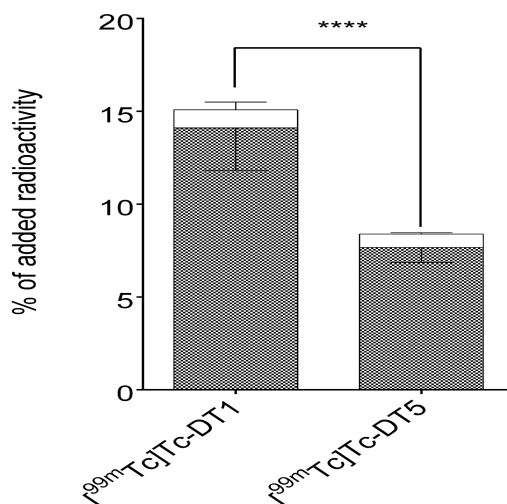
Image 7: Comparison of NTS$_1$R-specific cell uptake of [^{99m}Tc]Tc-DT1 and [^{99m}Tc]Tc-DT5 after 1 h incubation at 37 °C with AsPC-1 cells, with values expressed as % of total-added activity per well; dotted – gray bar section corresponds to internalized, while the white bar section corresponds to membrane bound radioactivity (****, p < 0.0001).

In vivo stability

Aiming to facilitate the clinical translation of the protease-inhibition concept in future, Entresto® replaced the previously used NEP inhibitor PA in all following studies. The registered drug was administered per os in healthy mice 30 min prior to the radioligand injection, alone or with Lis-coinjection. Blood collected 5 min pi was analyzed by HPLC for detecting potential formation of radiometabolites. Results are summarized in **Table 3**, while representative radiochromatograms can be found in the Appendix (**Image A3** pg 93 & **Image A8** pg. 96).

Table 3: *In vivo* stability results of [^{99m}Tc]Tc-DT1 and [^{99m}Tc]Tc-DT5 in healthy mice 5 min pi without or after treatment with Entresto®, Lis, or their combination, expressed as % intact radioligand; values are given as mean ± sd, with number of repetitions shown in parentheses.

Group	[^{99m}Tc]Tc-DT1	[^{99m}Tc]Tc-DT5
Control	1.8 ± 0.8 (4)	1.2 ± 0.2 (3)
Lis	18.8 ± 2.5 (3)	28.7 ± 3.6 (3)
Entresto®	5.5 ± 3.9 (5)	2.0 ± 0.6 (3)
Entresto® + Lis	63.8 ± 7.5 (3)	70.2 ± 4.9 (3)

Despite the fact that both PA and Entresto® were used for NEP inhibition, a statistically significant difference was apparent between the animal groups treated with either. Specifically,

[^{99m}Tc]Tc-DT1 remained 5.5 ± 3.9 % intact in the Entresro® group while in the PA group this value was 28.2 ± 3.5 % (**Table 2**) (p < 0.001). The same trend could be seen for [^{99m}Tc]Tc-DT5 with values at 2.0 ± 0.6 % intact for the Entresto® group and 15.4 ± 5.1 % intact for the PA (p < 0.01). In contrast, the mice groups treated with either the PA+Lis or the Entresto®+Lis combination, showed no difference in the stability of either radiotracer. The observed difference between PA and Entresto can be attributed to the ability of PA in higher concentrations to inhibit ACE as well although in a lesser extent (153). This fact turns out to be significant considering the synergistic role of these proteases in the degradation of NT and its analogs.

Biodistribution

In order to assess the tumorgenicity of AsPC-1 cells in SCID mice, animals were inoculated subcutaneously in their flanks with a AsPC-1 cell suspension and monitored for tumor development. After 3-4 weeks, well palpable tumors were evident at the inoculation site in the majority of animals and the biodistribution profile of [^{99m}Tc]Tc-DT1 was assessed, without or after mice treatment with the Entresto®+Lis combination.

As shown in **Table A2** (pg 94, Appendix) and **Image 8**, a fast washout of the radioligand was evident from the background via the kidneys and the urinary tract. As depicted in **Image 8**, at 4 h pi tumor uptake drastically increased from 1.25 ± 0.14 %IA/g, in controls to 7.05 ± 0.80 %IA/g in the Entresto®+Lis animal group (p < 0.0001). These values are in correlation with those found for the WiDr xenografts both in controls and in mice receiving the PA+Lis combination (1.80 ± 0.14 %IA/g and 12.29 ± 2.73 %IA/g, respectively; **Image 3**). However, AsPC-1 tumor values were consistently lower to those in WiDr tumors, probably implying a lower NTS$_1$R-expression in the AsPC-1 xenografts.

Uptake in the NTS$_1$R-rich mice intestines remained rather low in both groups (control: 0.65 ± 0.04 %IA/g, Entresto®+Lis: 2.13 ± 0.24 %IA/g). Renal uptake on the other hand was not affected by the use of inhibitors (control: 4.18 ± 3.80 %IA/g, Entresto®+Lis: 6.81 ± 1.74 %IA/g; p > 0.05), resulting in an overall improvement of pharmacokinetics during NEP and ACE inhibition and consistent with the improvement observed in WiDr tumor-bearing mice treated with the PA+Lis combination.
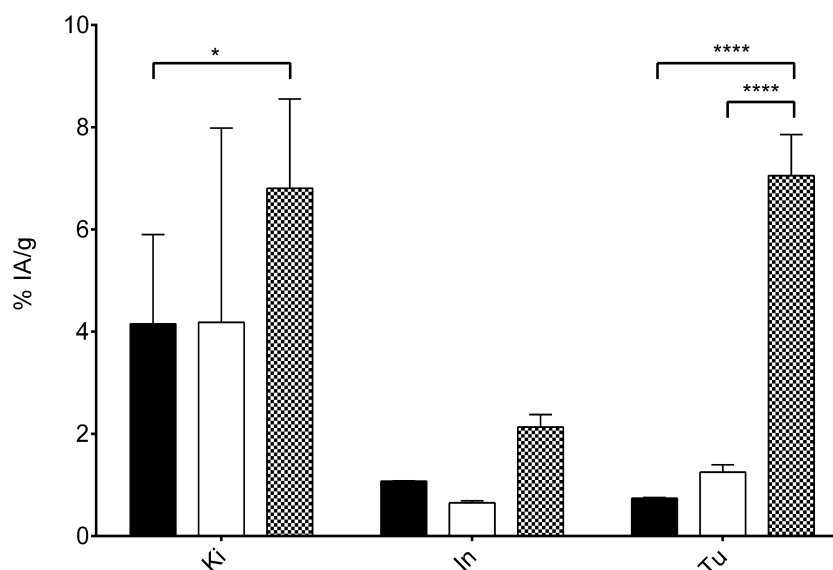
Image 8: Biodistribution of [^{99m}Tc]Tc-DT1 in SCID mice bearing AsPC-1 xenografts at 4 h pi selectively shown for Ki: kidneys, In: Intestines and Tu: AsPC-1 tumors; data is provided as %IA/g and represents mean ± sd, n = 4; black: blocked, white: control, chequered: Entresto®+Lis (*, p < 0.05 ; ****, p < 0.0001)

Summary

The uptake of [^{99m}Tc]Tc-DT1 in AsPC-1 and WiDr cells (*in vitro*) and their uptake in the respective xenografts (*in vivo*) were found to be comparable. In addition, the tumor growth rates of both AsPC-1 and WiDr tumors were within the same time-span, ranging between 3 and 4 weeks. It is therefore evident that the AsPC-1 cell-based model is a reliable and practically convenient PC model for the preclinical evaluation of NTS$_1$R-targeting radioligands.

On the other hand, the use of Entresto® was proven equally efficient with PA for *in situ* inhibition of NEP. The minor differences on the stability of the peptides between the animals administered with PA and Entresto could be attributed to differences across animals, the fluctuation in their body weights, differences in absorption and bioavailability between iv and per os administration, as well as the fact that PA is not absolutely selective for NEP, displaying also partial ACE inhibitory capabilities. Then again, only with the combined use of Entresto®+Lis, a sufficient stability was achieved (63).

Structural interventions – Introducing new [^{99m}Tc]Tc-DTx analogs

The next objective of the current work has been the introduction of novel [^{99m}Tc]Tc-DTx analogs, aiming at improved metabolic stability and enhanced tumor targeting efficacy, either when administered alone or with the aid of a single registered inhibitor. For such purposes, two distinct approaches were adopted. The first concerned the introduction of structural changes at the C-terminus of [^{99m}Tc]Tc-DT1, which served as a template, while the second involved the incorporation of a pendant albumin binding domain (ABD) and/or PEGX group at the ε-amino group of a Lys^7 residue. [^{99m}Tc]Tc-DT1 served as the standard in the evaluation of the new radiotracers, since it displayed high metabolic stability, AsPC-1 tumor targeting efficacy and excellent pharmacokinetics in mice during combined NEP and ACE inhibition.

Elongation / C-terminal modifications as a means to increase *in vivo* stability: [^{99m}Tc]Tc-DTx, x = 7, 13

The first structural changes tested were the elongation of the DT1 by incorporation a D-asparagine (DT7) after position 13 and the exchange of leucine at position 13 by (S)-β^{3}hLeu (DT13) (**Image 9**) (137,140). It is well known that the introduction of D-amino acids in a peptide chain often induces changes in the 3D conformation. Such alterations may lead to steric hindrance in the docking of peptides in the active center of degrading proteases, thereby resulting in metabolic stability improvements. However, these changes may inadvertently affect receptor affinity as well. The D-Asn^{14}-elongation of NT(8-13) analogs was previously shown to be well tolerated by the NTS$_1$R with related analogs retaining high receptor affinity.

Likewise, it is well established that β-amino acids increase the metabolic stability of peptides, since β-amide bonds can hardly be cleaved by proteolytic enzymes (154–156). In fact, only a handful of proteases in nature are capable of degrading peptide bonds containing β-amino acid residues. It was previously shown that β^{3}hLeu^{13}/Leu^{13}-substituted NT(8-13) analogs retained binding affinity for NTS$_1$R, while their stability in blood serum increased *in vitro*, indicating an increased resistance to ACE (137,140).
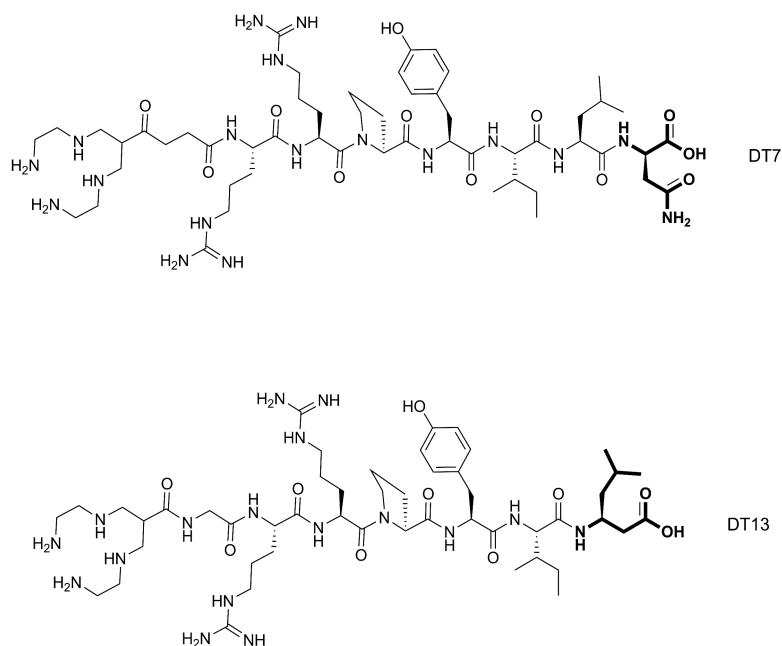
Image 9: Structure of DT7 (N₄-Gly-Arg-Arg-Pro-Tyr-Ile-Leu-**D-Asn**-OH) and DT13 (N₄-Gly-Arg-Arg-Pro-Tyr-Ile-**β³hLeu**-OH)

Labeling

The Tc-99m labeling procedure for DT7 and DT13 was performed, as previously described (pgs. 23 – 24). After a short incubation in ambient temperature with the generator eluate, $SnCl_2$ as a reducing agent in alkaline pH, molecular activities of 20 – 40 MBq/nmol were acquired. The iTLC and HPLC controls indicated yields >98% and radiochemical purity >99% (Appendix, **Images A14 & A28**, pgs 99 & 109).

Binding affinity of DT7 and DT13 for NTS₁R

The IC_{50} values for these analogs were determined by competition binding assays against $[^{125}I]I$-Tyr³-NT on NTS₁R-positive WiDr cell membranes. An IC_{50} of 29.05 ± 4.11 nM (n=4) was determined for DT7, while an IC_{50} of 0.63 ± 0.05 nM (n=3) was calculated for DT13 (representative displacement curves included in **Image 10**). This finding demonstrates that the β³hLeu¹³/Leu¹³ substitution was much better tolerated by the NTS₁R, in comparison with the D-Asn¹⁴-elongation.
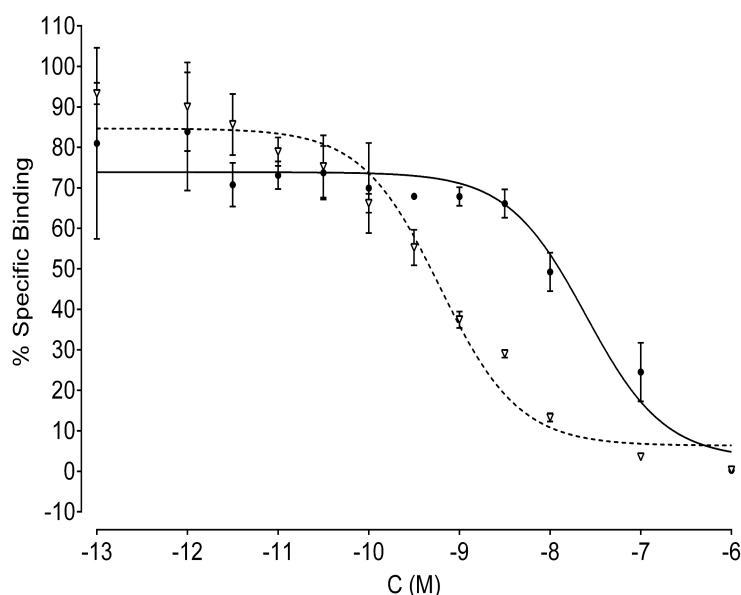
Image 10: Representative curves of [^{125}I]I-Tyr^3-NT displacement from NTS$_1$R sites on WiDr cell membranes by increasing concentrations of DT7 (solid line) or DT13 (dotted line).

Cell uptake of [^{99m}Tc]Tc-DT7 & [^{99m}Tc]Tc-DT13

The cell uptake of both radioligands was tested by 1 h incubation at 37 ^{o}C in AsPC-1 cells. Despite the fair to excellent affinity of the non-metalated analogs for NTS$_1$R, neither of the respective [^{99m}Tc]Tc-radiotracers exceeded a specific cell uptake of 1% of added radioactivity. In fact, [^{99m}Tc]Tc-DT7 achieved only 0.3 ± 0.13 % cell uptake and [^{99m}Tc]Tc-DT13 hardly reached the 0.6 ± 0.20 % value (**Image 11**).
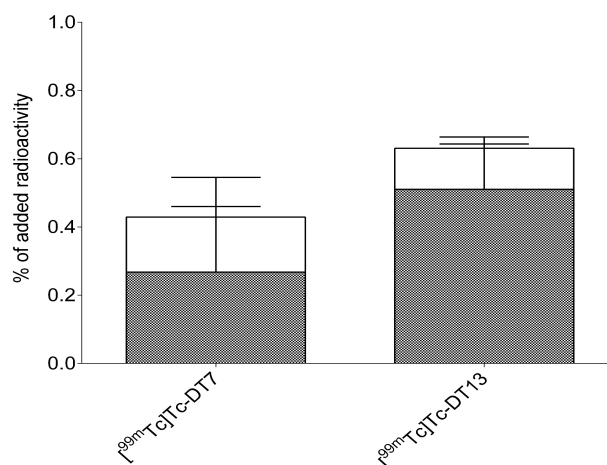
Image 11: Cell uptake of [^{99m}Tc]Tc-DT7 and [^{99m}Tc]Tc-DT13 after 1 h incubation at 37 ^{o}C in AsPC-1 cells; the dotted – gray bars correspond to internalized radioactivity, while white bars correspond to the membrane bound radioactivity.

68

In vivo stability

Both [^{99m}Tc]Tc-DT7 and [^{99m}Tc]Tc-DT13 displayed significantly higher stability (**Table 4**) in mice blood at 5 min pi in comparison with [^{99m}Tc]Tc-DT1 (1.8 ± 0.8 % intact, **Table 3**), with 26.91 ± 0.19 % intact (p<0.001) and 22.03 ± 2.86 % intact (p < 0.05) peptide detected intact, respectively. With Entresto® the percentage of intact radioligand increased to 56.61 ± 7.93% for [^{99m}Tc]Tc-DT7 (p < 0.0001 vs. control) and 62.05 ± 11.36 % intact for [^{99m}Tc]Tc-DT13 (p < 0.0001 vs. control). The use of Entresto®+Lis did not alter these values (60.23 ± 11.82 % intact and 62.80 ± 4.87% intact, respectively). Notably, [^{99m}Tc]Tc-DT1 reached similar levels only after applying the combination of NEP and ACE inhibitors. These results are a strong indication that both [^{99m}Tc]Tc-DT7 and [^{99m}Tc]Tc-DT13 are resistant to ACE, in accordance with findings reported in literature for similarly C-terminal modified NT analogs (137,140).

Table 4: *In vivo* stability of [^{99m}Tc]Tc-DT7 and [^{99m}Tc]Tc-DT13 in healthy mice at 5 min pi, without or after treatment with NEP and/or ACE inhibitors, expressed as % intact radioligand; values are given as mean ± sd, with number of repetitions shown in parentheses.

Group	[^{99m}Tc]Tc-DT7	[^{99m}Tc]Tc-DT13
Control	26.91 ± 1.91 (3)	22.03 ± 2.86 (2)
Lis		26.20 ± 0.83 (2)
Entresto	56.61 ± 7.93 (6)	62.05 ± 11.36 (2)
Entresto+Lis	60.23 ± 11.82 (2)	62.80 ± 4.87 (2)

Summary

Both C-terminal modified peptide analogs displayed an high NTS$_1$R affinity and enhanced degradation resistance against ACE, as expected from previous reports for similar NT(8-13) analogs. Once again, it was evident that high receptor affinities do not directly imply optimal kinetics with regards to cell uptake, as previously reported for [^{99m}Tc]Tc-DT6 (Appendix, **Table A5**, pg 99) (65). Therefore, despite the increased *in vivo* stability and the low IC$_{50}$s, the biodistribution profile of these peptide radioligands was not assessed in animals bearing AsPC-1 xenografts.

Lys[7]-Branching as a means to increase *in vivo* stability, 1st Generation: A fatty acid group – [99mTc]Tc-DT8

Contulakin-G is a 16-mer invertebrate counterpart of mammal NT, carrying a saccharide residue at Thr[10] (**Image I12**), corresponding to Pro[7] in the native NT sequence. Several synthetic analogs of contulakin-G have been developed after replacement of the Thr[10]-attached saccharide by other chemical entities, including a palmitic acid coupled to ε-amino group of a Lys residue (141,142,146). Incorporation of fatty acids on peptides has been reported to result in increased *in vivo* stability, higher bioavailability and prolonged circulation time of resulting analogs (118,143,144). These attractive features have been attributed to binding of palmitic acid to albumin, the most abundant blood protein. Albumin exhibits an approximately 16 h-long half-life in the circulation and a biological half-life of 12-19 days (157,158). It binds fatty acid-modified peptides and slowly releases them in circulation. In this way, it acts as a natural reservoir that increases the residence time of the peptides in the blood stream. It is hypothesized that it may also protect related analogs from degrading peptidases (157–160).

Studies on contulakin-G and related analogs have demonstrated that bulky branches, such as palmitoyl acid at position 10, can be well tolerated by the NTS$_1$R. Hence, it is reasonable to assume that they will be likewise tolerated at the corresponding position 7 of the DT1 motif. Accordingly, DT8 was designed based on the DT1-template after replacement of Gly[7] by Lys[7], and coupling of a palmitoyl residue at the ε-amine (**Image 12**).
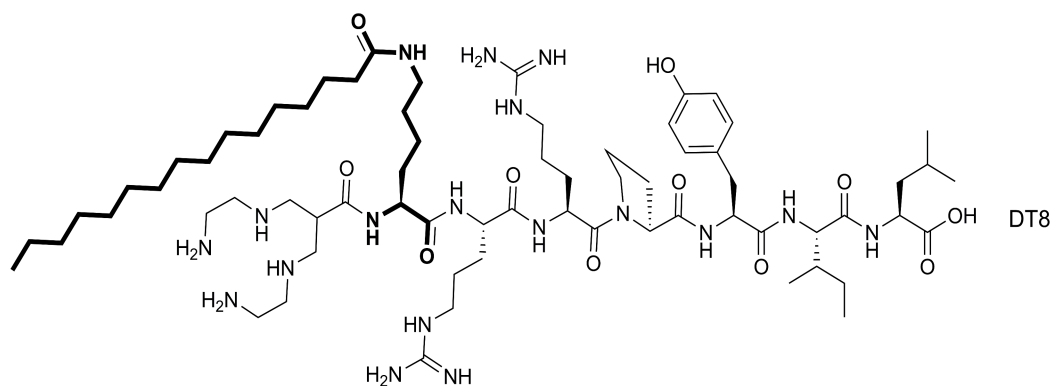
Image 12: Structure of DT8 (N$_4$-**Lys(palmitoyl)**-Arg-Arg-Pro-Tyr-Ile-Leu-OH)

Labeling

The above mentioned labeling protocol was applied for DT8. After labeling, molar activities of 20 – 40 MBq/nmol of peptide were achieved. Quality control labeling yields >98% and radiochemical purity >99% (Appendix, **Image A17**, pg. 101).

Binding affinity of DT8 for NTS$_1$R

Despite the bulkiness of the pendant palmitoyl group, DT8 displayed high affinity for NTS$_1$R. During competition binding assays against [^{125}I]I-Tyr^3-NT, it displayed an IC$_{50}$ of 0.89 ± 0.70 nM (n=4) (**Image 13**). This fact is concordant with the well-tolerated modification at the corresponding position 10 of contulakin-G and position 7 of NT.
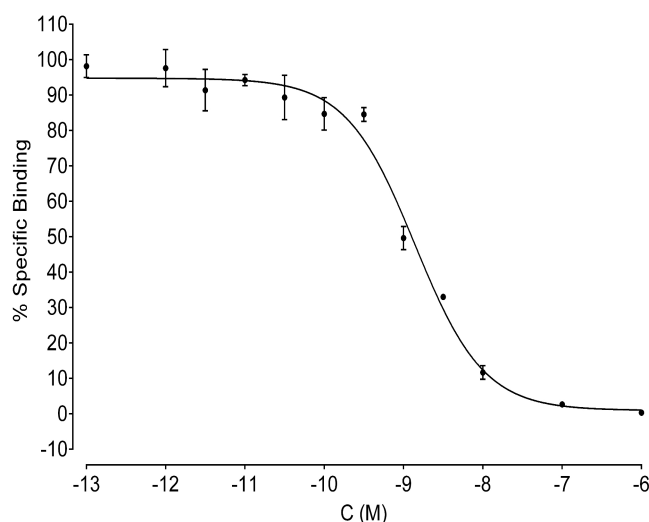
Image 13: Representative curve of [^{125}I]I-Tyr^3-NT displacement from NTS$_1$R on WiDr cell membranes by increasing concentrations of DT8

Cell uptake of [^{99m}Tc]Tc-DT8

Time-dependent cell uptake of [^{99m}Tc]Tc-DT8 was assessed in AsPC-1 cells at 37 ^{o}C, including four time points (15 min, 30 min, 60 min and 120 min). For all time points the majority of cell-associated activity was intracellularly located. Cell uptake reached 16.53 ± 1.12% of added activity at 1 h incubation and it further increased to 21.71 ± 0.91% of added activity at 120 min (**Image 14**). In contrast, [^{99m}Tc]Tc-DT1 reached a plateau after 1 h with cell uptake reaching 15.2 ± 2.6% of added radioactivity.
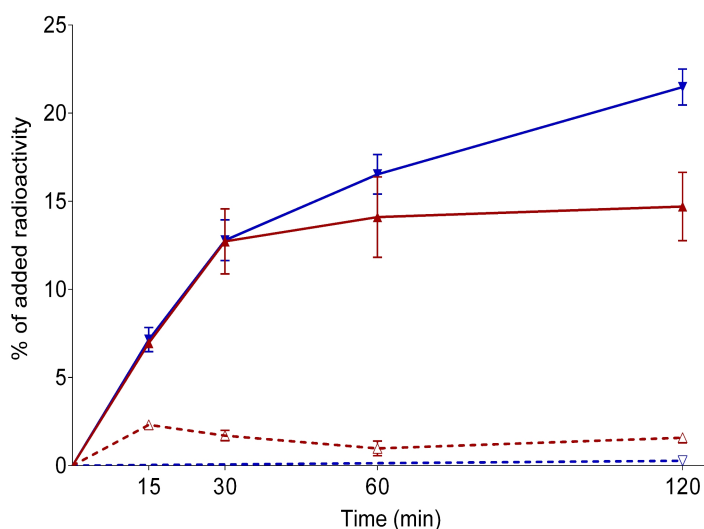
Image 14: Comparative time-dependent cell uptake of [^{99m}Tc]Tc-DT1 (red lines) and [^{99m}Tc]Tc-DT8 (blue lines) during incubation with AsPC-1 cells at 37 °C; solid lines: internalized radioactivity, dotted lines: membrane bound radioactivity.

In vivo stability

As illustrated in **Image 15**, [^{99m}Tc]Tc-DT8 displayed excellent *in vivo* stability, remaining practically intact in mice blood at 5 min pi. The percentage of the intact peptide in the blood of control mice was 98.06 ± 1.18 % (n=3), being indistinguishable from the values acquired from mice treated with either Entresto® (98.06 ± 1.18 %, n=3; p > 0.05) or Lis (98.06 ± 1.18 %, n=3; p>0.05;).
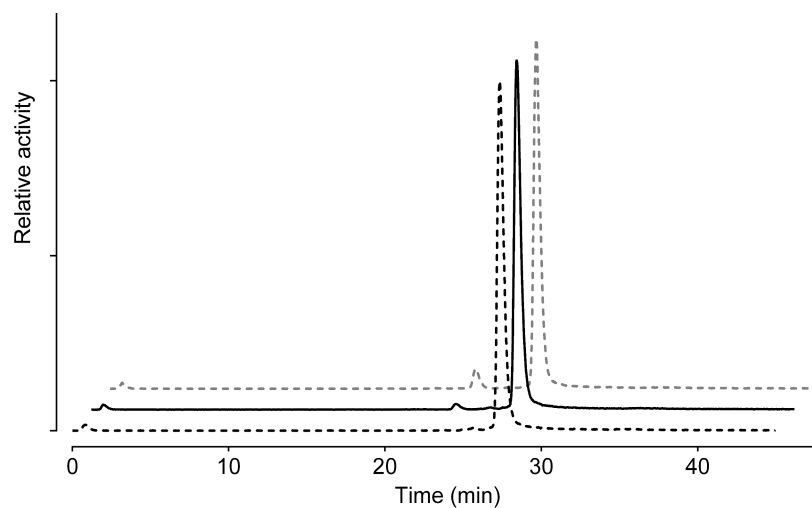
Image 15: Representative radiochromatograms for the *in vivo* stability of [^{99m}Tc]Tc-DT8 in peripheral mice blood at 5 min pi, without or during NEP or ACE inhibition.; black – dotted line: control, black – solid line: treatment with Lis, gray – dotted line: treatment with Entresto®.

Biodistribution

The biodistribution profile [^{99m}Tc]Tc-DT8 was assessed at 4 and 24 h pi; earlier time points were not considered in view of the prolonged blood clearance anticipated for the radiotracer. As shown in **Table A6** (Appendix, pg. 102) and **Image 16**, [^{99m}Tc]Tc-DT8 showed good uptake and fair retention in the implanted AsPC-1 tumors (6.15 ± 0.92 %IA/g at 4 h and 3.32 ± 0.35 %IA/g at 24 h pi).

However, it displayed a very unfavorable pharmacokinetic profile with persistently high background radioactivity levels up to 24 h pi. Thus, kidney values ranged from 9.42 ± 1.18 %IA/g at 4 h to 3.81 ± 0.54% IA/g at 24 h, intestinal uptake reached 13.03 ± 4.6%IA/g at 4 h decreasing to 4.26 ± 0.61%IA/g at 24 h and liver uptake reached as high as 29.56 ± 3.77%IA/g at 4 h to decline to 12.93 ± 1.66 %IA/g at 24 h. The high blood radioactivity levels, originating from the extensive binding of the palmitoyl residue to albumin, in combination with its high lipophilicity, seem to be the main causes for the extremely high radioactivity background.
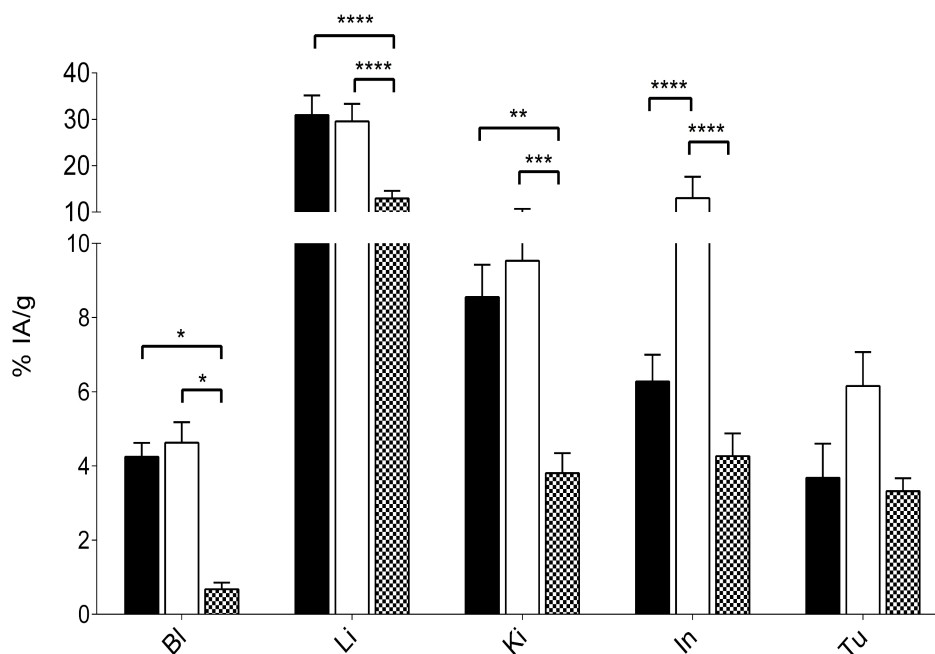
Image 16: Biodistribution data of [^{99m}Tc]Tc-DT8 in SCID mice bearing AsPC-1 xenografts, selectively presented for Bl: blood, Li: liver, Ki: kidneys, In: intestines and. Tu: AsPC-1 tumors; data is provided as %IA/g and represents mean $\pm$ sd, n = 4; black: blocked – 4 h pi, white: control – 4 h pi, dotted: control – 24 h pi (*,$p < 0.05$; **, $p < 0.01$; ***, $p < 0.001$; ****, $p < 0.0001$).

Summary

The palmitoylated [99mTc]Tc-DT8 displayed high cell uptake *in vitro* as well as high proteolytic resistance and prolonged circulation times *in vivo*. Notably, uptake in AsPC-1 tumors at 4 h pi was comparable with that of the [99mTc]Tc-DT1 in mice treated with the Entresto®+Lis combination (6.15 ± 0.92 %IA/g vs. 7.05 ± 0.80 %IA/g, p > 0.05; Appendix, **Tables A2**, pg 94 & **A6**, pg 102). Unfortunately, the unfavorably high background levels following radioligand injection in tumor-bearing mice, compromised these positive results. The observed profile turned out to be drastically different to that of the rapidly clearing [99mTc]Tc-DT1, either when administered alone or with the Entresto®+Lis combination. Extremely elevated liver and intestinal radioactivity levels indicate a high percentage of hepatobiliary excretion for [99mTc]Tc-DT8 as opposed to [99mTc]Tc-DT1, which was predominantly excreted through the kidneys and the urinary tract.

These findings lead to a few important conclusions. First of all, the branching approach at the ε-Lys[7], even in the case of a lengthy chain as in DT8, was well tolerated by the NTS_1R, as originally anticipated. Accordingly, the affinity of DT8 for NTS_1R as well as the *in vitro* uptake of [99mTc]Tc-DT8 in AsPC-1 cells were well preserved compared with [99mTc]Tc-DT1. Furthermore, [99mTc]Tc-DT8 was found to be stable in peripheral mice blood, as initially hypothesized. It remains to be established if this stabilization was related to persistent binding to blood albumin or it was a result of steric interference by the bulky palmitoyl arm, hindering docking of [99mTc]Tc-DT8 to the active center of NEP and/or ACE.

On the other hand, the pharmacokinetic profile of [99mTc]Tc-DT8 turned out to be far from ideal, with a high background and not a totally NTS_1R-dependent tumor uptake (159,161,162). These results can be associated with an unfavorably high affinity of the palmitoyl group for the albumin in the blood stream, combined with its high lipophilicity. Therefore, it is reasonable to assume that the introduction of pendant groups with different lipophilicity, size and albumin binding capabilities compared with the palmitoyl residue may lead to improved radioligands.

2nd Generation: ABD/PEG pendant groups – [⁹⁹ᵐTc]Tc-DTx, x= 9,10,11

Three more Lys⁷-branched analogs were designed based on [⁹⁹ᵐTc]Tc-DT8 findings, by attaching three different pendant groups at the ε-amine of Lys⁷ instead of the palmitic acid.

In DT9, a 4-(4-methylphenyl)butyric acid (MPBA) moiety was coupled (**Image 17**), which is an ABD with a lower affinity to albumin than palmitic acid (163,164). For DT10 a PEG4 (165) linker was introduced between the ε-amine of Lys⁷ and MPBA (**Image 17**), in order to keep the length of the pendant group as close as possible to that of the palmitic acid, while increasing its hydrophilicity over DT8 & DT9. Finally, an ABD was altogether omitted in DT11 and a methyl-PEG5-CH₂-COOH (from here on PEG6) arm was coupled at the ε-amine of Lys⁷ (**Image 17**), in order to distinguish potential stabilization effects arising by steric hindrance of docking of the resulting radioligand to NEP and/or ACE active center(s), not related to albumin binding (165).
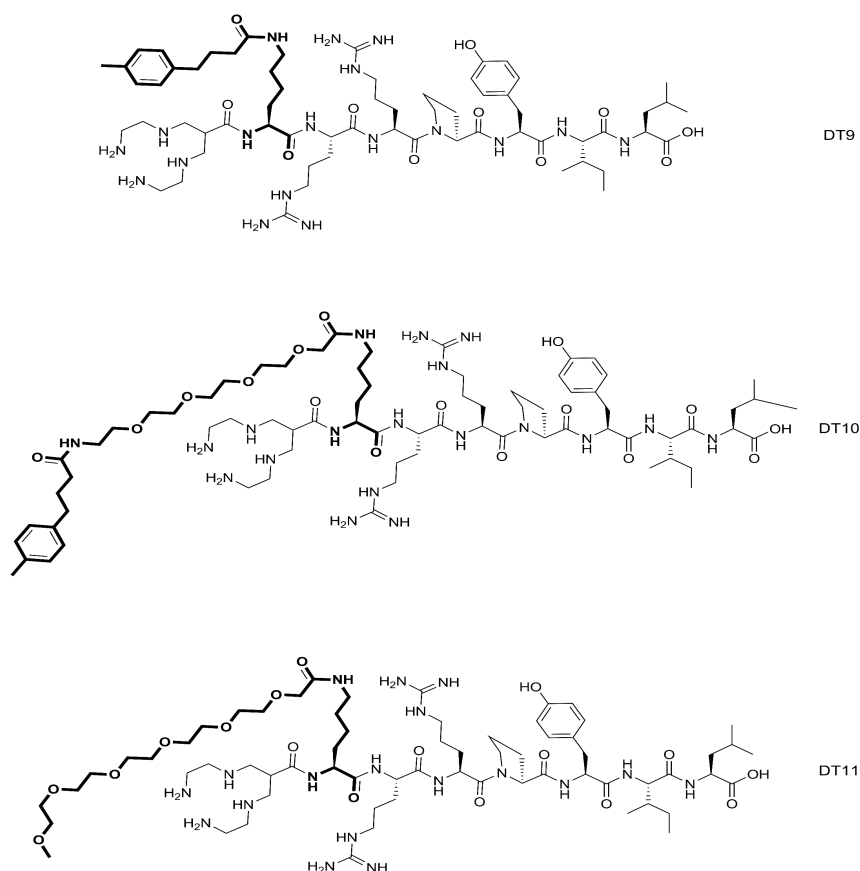
Image 17: Structure of DT9 (N₄-Lys(MPBA)-Arg-Arg-Pro-Tyr-Ile-Leu-OH), DT10 (N₄-Lys(PEG4-MPBA)-Arg-Arg-Pro-Tyr-Ile-Leu-OH) and DT11 (N₄-Lys(CO-CH₂-PEG5-Met)-Arg-Arg-Pro-Tyr-Ile-Leu-OH)

Labeling

Labeling of DT9, DT10 and DT11 with Tc-99m followed the same procedure. Quality control demonstrated, less than 2% radiochemical impurities consisting of [^{99m}Tc]Tc-citrate, [^{99m}Tc]TcO$_4^-$ and [^{99m}Tc]TcO$_2 \times$ nH$_2$O and a radiochemical purity greater than 99% (**Images A20, A23** and **A26** at pgs: 103, 105 and 107, Appendix).

Binding affinities of DTx (x = 9, 10, 11) for NTS$_1$R

As shown from the curves of [^{125}I]I-Tyr^3-NT displacement from NTS$_1$R sites in WiDr cell membranes (**Image 18**), all three new compounds displayed high affinity for NTS$_1$R. Specifically, DT9 exhibited an IC$_{50}$ of 0.06 ± 0.03 nM (n =3), DT10 of 0.08 ± 0.05 nM (n = 3) and DT11 of 0.10 ± 0.03 nM (n = 3).
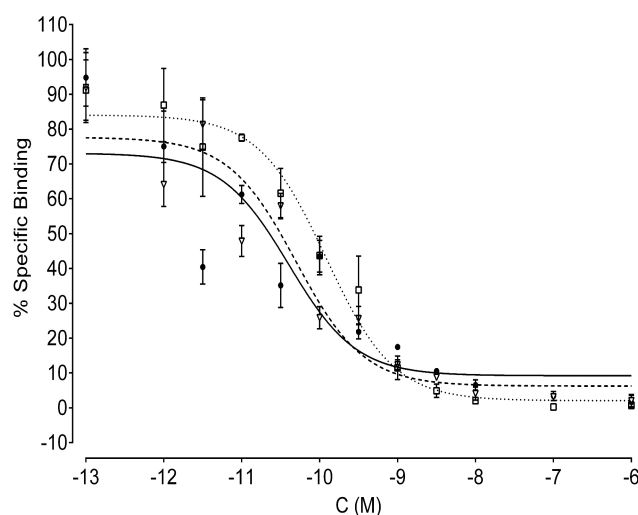
Image 18: Representative displacement curves of [^{125}I]I-Tyr^3-NT from NTS$_1$R sites on WiDr cell membranes by increasing concentrations of: DT9 (solid line), DT10 (dashed line) and DT11 (dotted line).

Cell uptake of [^{99m}Tc]Tc-DTx (x = 9, 10, 11) in AsPC-1 cells

Time-dependent cell uptake curves of the three new Lys^7-modified radioligands and [^{99m}Tc]Tc-DT1 in AsPC-1 cells are included in **Image 19**. A comparable behavior was observed for [^{99m}Tc]Tc-DT1, [^{99m}Tc]Tc-DT9 and [^{99m}Tc]Tc-DT10 (p > 0.05 across analogs), while [^{99m}Tc]Tc-DT11 showed lower uptake (p < 0.0001). After 1 h, all radiotracers reached a plateau and at the 2 h interval the values remained more or less the same (p > 0.5 between 1 and 2 h for all four compounds). The predominant part of the cell associated activity was internalized as consistent with an agonist profile.
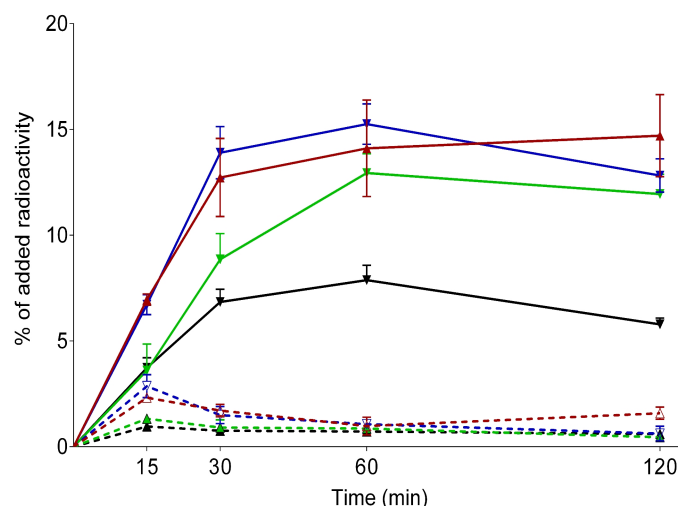
Image 19: Comparative cell-uptake curves over time for [99mTc]Tc-DT1 (red lines), [99mTc]Tc-DT9 (blue lines), [99mTc]Tc-DT10 (green lines) and [99mTc]Tc-DT11 (black lines) during incubation at 37 °C with AsPC-1 cells; solid lines: internalized, dotted lines: membrane bound radioactivity

Albumin binding of [99mTc]Tc-DTx (x = 9, 10, 11)

As shown in **Image 20**, [99mTc]Tc-DT1 had negligible albumin uptake in this assay with 0.98 ± 0.15 %, followed by [99mTc]Tc-DT11 with 3.88 ± 0.50 %, as expected due to the lack of ABD groups in their structure. The two compounds with the ABD-domain at Lys^7, [99mTc]Tc-DT9 and [99mTc]Tc-DT10, displayed clear binding to albumin. Notably, binding to albumin could be significantly reduced by ibuprofen, a compound previously reported for its high albumin affinity (166–168). [99mTc]Tc-DT9 had an albumin binding of 23.42 ± 1.49 %, which dropped to 5.48 ± 0.44 % by ibuprofen. In the case of [99mTc]Tc-DT10 albumin binding reached the highest value of 41.18 ± 2.66 %, declining to 12.81 ± 4.51 % with the addition of ibuprofen. These results indicate that the PEG4 spacer positioned between Lys^7 and MPBA relieved some of the steric restrictions imposed by the peptide backbone of the conjugate to albumin binding.
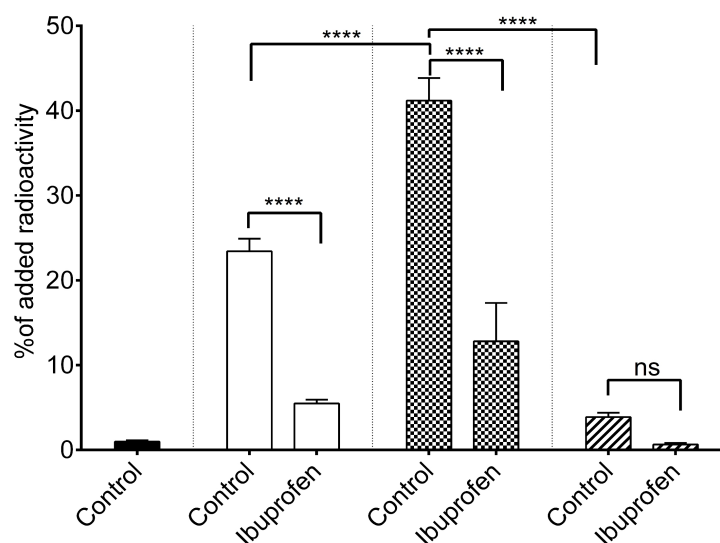
Image 20: Comparative albumin binding of [^{99m}Tc]Tc-DT1 (solid black bars), [^{99m}Tc]Tc-DT9 (white bars), [^{99m}Tc]Tc-DT10 (chequered bars) and [^{99m}Tc]Tc-DT11 (dashed bars) (****, $p < 0.0001$; ns: non-significant, $p > 0.05$)

In vivo stability of [^{99m}Tc]Tc-DTx (x = 9, 10, 11)

The impact of different type side-chains introduced at Lys[7] on the *in vivo* stability of resulting radioligands was studied in mice blood samples collected 5 min pi, as summarized in **Table 5**. [^{99m}Tc]Tc-DT9 turned out to be the most degradation-prone radiotracer with only 5.09 ± 0.89 % detected intact in peripheral mice blood ($p > 0.05$ vs. [^{99m}Tc]Tc-DT1), while [^{99m}Tc]Tc-DT10 showed the highest stability with 56.56 ± 5.19 % found intact ($p < 0.0001$ vs. [^{99m}Tc]Tc-DT1). [^{99m}Tc]Tc-DT11 displayed an intermediate stability with 35.65 ± 5 % remaining intact ($p < 0.0001$ vs. [^{99m}Tc]Tc-DT1). With the use of Entresto®, stability was increased to 5.15 ± 1.58 % ($p > 0.05$ vs. control), 76.98 ± 3.31 ($p < 0.0001$ vs. control) and 58.69 ± 7.17 % ($p < 0.0001$ vs. control) for the three respective radiotracers. In the Lis treated groups, [^{99m}Tc]Tc-DT9 remained up to 37.14 ± 6.49 % intact ($p < 0.0001$ vs. control), [^{99m}Tc]Tc-DT10 increased slightly to 66.89 ± 1.24% ($p > 0.05$ vs. control) and [^{99m}Tc]Tc-DT11 to 42.63 ± 2.79 % ($p > 0.05$ vs. control). Notably, in the groups receiving the combination of inhibitors, all three radioligands demonstrated maximum stability, with the respective values being 68.02 ± 3.01 % ($p < 0.0001$ vs. control), 86.33 ± 1.94 % ($p < 0.0001$ vs. control) and 73.98 ± 4.93 % ($p < 0.0001$ vs. control) intact.

These results, once more confirm the major role of two peptidases, NEP and ACE, in the *in vivo* degradation of [^{99m}Tc]Tc-DT9, [^{99m}Tc]Tc-DT10 and [^{99m}Tc]Tc-DT11. Furthermore, it is evident that two key factors contribute to their partial stabilization in circulation. First, the steric effect of the pendant

78

groups at Lys[7] for the approaching enzymes and second the affinity of those side-chains for albumin. Their combination in [^{99m}Tc]Tc-DT10 could produce the best outcome in terms of stabilization. Interestingly, [^{99m}Tc]Tc-DT10, with the PEG4-MPBA branch, displayed the highest albumin binding (**Image 20**), and was the most stable member in this small library of analogs. It remained equally stable during single treatment with Entresto® with [^{99m}Tc]Tc-DT9 & [^{99m}Tc]Tc-DT11 treated with the NEP/ACE – inhibitor combination (p > 0.05). Another interesting finding is a strong impact of the non-albumin binding PEG6 group on the observed resistance of [^{99m}Tc]Tc-DT11 to ACE (42.63 ± 2.79% intact in the Lis group vs. 35.65 ± 5% intact in controls, p > 0.05). In contrast, the strong stabilization effect of Lis-treatment was evident in the case of the ABD-carrying [^{99m}Tc]Tc-DT9 (37.14 ±6.49 % intact in the Lis group vs. 5.09 ± 0.89 % intact in controls, p < 0.0001), revealing the impact of steric factors in the observed higher stability of [^{99m}Tc]Tc-DT11 against ACE.

Table 5: *In vivo* stability of [^{99m}Tc]Tc-DT9, [^{99m}Tc]Tc-DT10 and [^{99m}Tc]Tc-DT11 in the blood of healthy mice 5 min pi without or after treatment of animals with NEP and/or ACE inhibitor(s); values correspond to percentage of intact radioligand and are the mean ± sd, with number of experiments shown in parentheses.

Group	[^{99m}Tc]Tc-DT9	[^{99m}Tc]Tc-DT10	[^{99m}Tc]Tc-DT11
Control	5.09 ± 0.89 (3)	56.56 ± 5.19 (3)	35.65 ± 5 (3)
Entresto	5.15 ± 1.58 (3)	76.98 ± 3.31 (3)	58.69 ± 7.17 (3)
Lis	37.14 ±6.49 (3)	66.89 ± 1.24 (3)	42.63 ± 2.79 (3)
Entresto®+Lis	68.02 ± 3.01 (3)	86.33 ± 1.94 (3)	73.98 ± 4.93 (3)

Biodistribution of [^{99m}Tc]Tc-DTx (x = 9, 10, 11) in AsPC-1 tumor-bearing mice

The biodistribution profile of the three new radioligands was assessed both at 4 h and 24 h pi taking into account the anticipated prolonged circulation times of [^{99m}Tc]Tc-DT9 and [^{99m}Tc]Tc-DT10 due to their albumin binding capabilities (**Image 20**). It should be noted that for [^{99m}Tc]Tc-DT10 only Entresto® was administered in the animals, based on findings from the stability study. Comparable stabilization levels could be achieved for [^{99m}Tc]Tc-DT9 and [^{99m}Tc]Tc-DT11 only by the combination of inhibitors and therefore, the latter stabilization option was adopted for the two radiotracers. As shown in **Tables A7, A8 & A9** (Appendix, pgs: 104, 106 & 108) and **Image 21**, the three analogs displayed higher uptake in the AsPC-1 tumors at 4 h pi in comparison with [^{99m}Tc]Tc-DT1 in the

control groups ([^{99m}Tc]Tc-DT9 – 2.5 ± 0.6 %IA/g, p < 0.0001; [^{99m}Tc]Tc-DT10 – 4.49 ± 0.37 %IA/g, p < 0.0001, [^{99m}Tc]Tc-DT11 – 3.63 ± 0.42 %IA/g, p < 0.0001). With the administration of the inhibitor(s) those values increased to 5.03 ± 0.47 %IA/g, p < 0.0001; 6.14 ± 0.08 %IA/g, p < 0.0001; and 4.48 ± 1.23 %IA/g, p > 0.05, vs. the corresponding controls. Tumor values substantially declined at 24 h pi for both control and inhibitor(s)-treated groups. For the control groups the values were 0.47 ± 0.06 %IA/g for [^{99m}Tc]Tc-DT9, 1.87 ± 0.07 %IA/g for [^{99m}Tc]Tc-DT10 and 1.74 ± 0.20% IA/g for [^{99m}Tc]Tc-DT11, reaching to 1.71 ± 0.28 %IA/g, 2.96 ± 0.63 %IA/g and 2.47 ± 0.57 %IA/g in the treated groups, respectively. We observe that [^{99m}Tc]Tc-DT10 displayed a superior tumor targeting both in controls and in the single inhibitor-treated animals compared to [^{99m}Tc]Tc-DT9 and [^{99m}Tc]Tc-DT11, even when the latter were treated with both inhibitors.

All three radiopeptides displayed a faster clearance from the background in comparison with [^{99m}Tc]Tc-DT8, both in the control groups and the treated groups. In the 4 h control group [^{99m}Tc]Tc-DT9 displayed, 3.27 ± 0.53 %IA/g liver uptake (p < 0.0001), 5.79 ± 0.63 %IA/g kidney uptake (p < 0.0001) and 2.34 ± 0.39 %IA/g uptake in the intestines (p < 0.0001), while in the inhibitor-treated mice, these values were 2.00 ± 0.21 %IA/g (p < 0.001), 4.38 ± 0.81 %IA/g (p < 0.0001) and 2.49 ± 0.16 % IA/g (p < 0.0001), respectively. [^{99m}Tc]Tc-DT10 displayed lower liver (1.19 ± 0.18 %IA/g – control, p < 0.0001; 1.28 ± 0.08 %IA/g – Entresto®, p < 0.0001) and kidney uptake (3.11 ± 0.32 %IA/g – control, p < 0.0001; 3.57 ± 0.36% IA/g – Entresto®, p < 0.0001), with similar values in intestines (1.89 ± 0.18 %IA/g – control, p < 0.0001; 2.61 ± 0.2% IA/g – Entresto®, p < 0.0001). Last, [^{99m}Tc]Tc-DT11 displayed similar clearance pattern with [^{99m}Tc]Tc-DT10, with the liver (0.26 ± 0.04 %IA/g – control, p > 0.05; 1.04 ± 0.31 %IA/g – Entresto®+Lis, p > 0.05) and intestinal (2.44 ± 0.51 %IA/g – control, p > 0.05; 6.92 ± 2.55 %IA/g – Entresto®+Lis, p > 0.05) uptake found on the same level with [^{99m}Tc]Tc-DT10. In contrast, kidney values in controls at 4 h pi were at 2.44 ± 0.51 %IA/g (p > 0.05), while in the Entresto® +Lis treated group they increased to 6.92 ± 2.55 %IA/g (p < 0.0001), being statistically different from the values of [^{99m}Tc]Tc-DT10 in the Entresto® treated group at 4 h pi. All three compounds were cleared from the background at 24 h pi with the uptake values for liver, kidney and intestines dropping below 1 % IA/g. These results could be visualized by SPECT/CT for [^{99m}Tc]Tc-DT10 (**Image 22**) and for [^{99m}Tc]Tc-DT1 (**Image 23**) at 4 h pi.
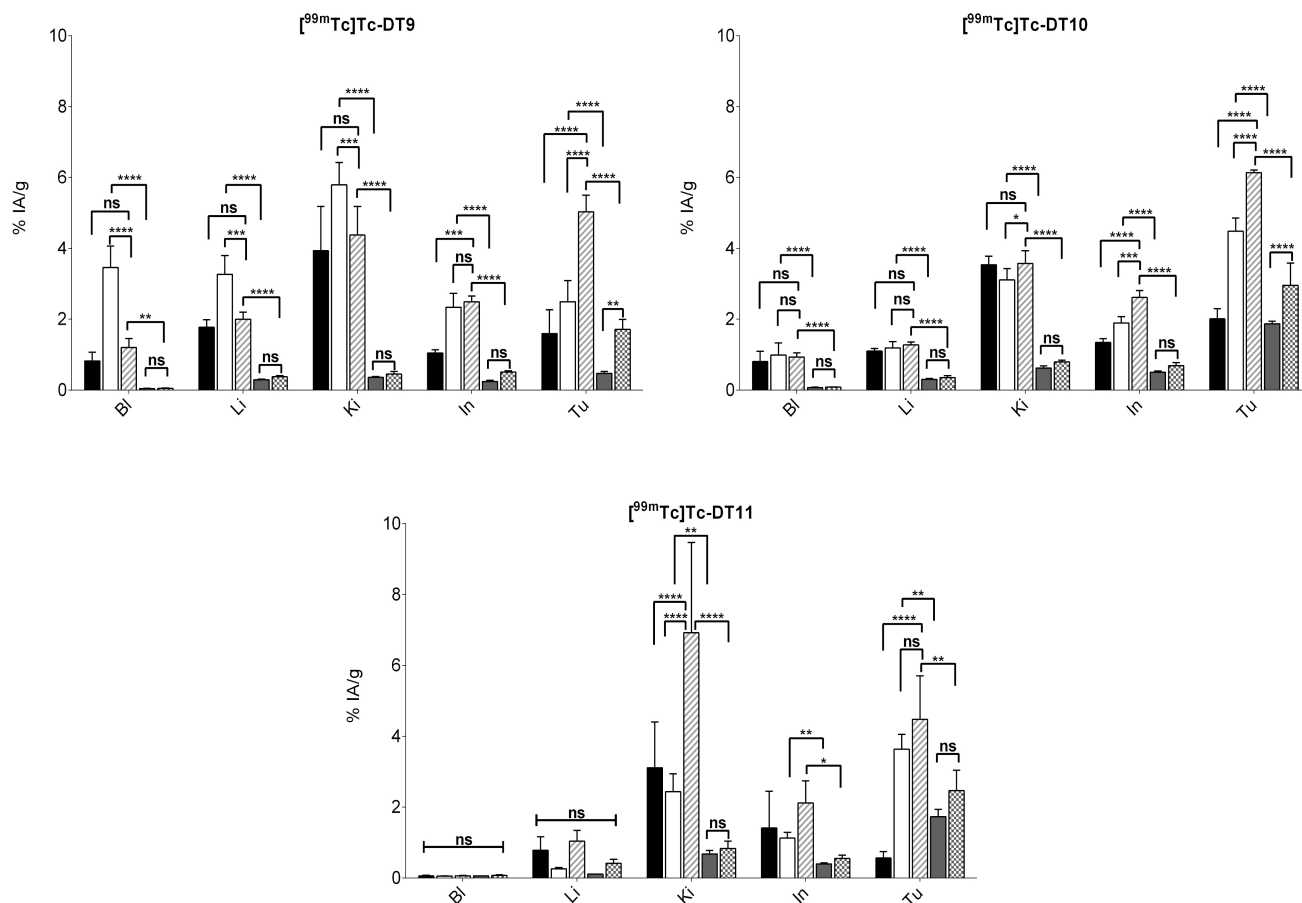
Image 21: Biodistribution of [^{99m}Tc]Tc-DT9 (up-left), [^{99m}Tc]Tc-DT10 (up-right) and [^{99m}Tc]Tc-DT11 (bottom - center) in SCID mice bearing AsPC-1 xenografts, selectively for Bl: blood, Li: liver, Ki: kidneys, In: intestines and. Tu: AsPC-1 tumor; data is expressed as %IA/g and represents the mean ± sd, n = 4. Black bars: blocked 4 h pi, white bars: control 4 h pi, dashed bars: Entresto®+Lis 4 h pi (only Entresto® for [^{99m}Tc]Tc-DT10), gray bars: control 24 h pi, chequered bars: Entresto®+Lis treated 24 h pi (only Entresto® for [^{99m}Tc]Tc-DT10) (ns: non-significant, $p > 0.05$; *, $p < 0.05$; **, $p < 0.01$; ***, $p < 0.001$; ****, $p < 0.0001$).
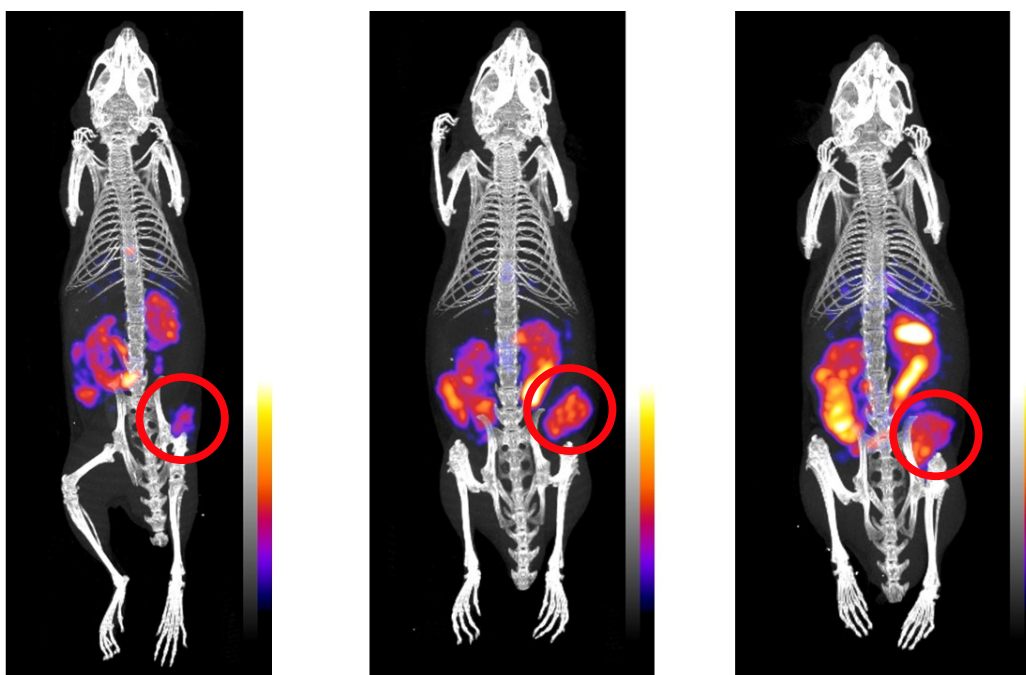
Image 22: SPECT/CT image of [^{99m}Tc]Tc-DT10 in SCID mice bearing AsPC-1 xenografts, 4 h pi. From left to right: block, control and Entresto® treated mouse (block: mouse treated with excess NT and Entresto®). Red circles indicate xenograft sites.
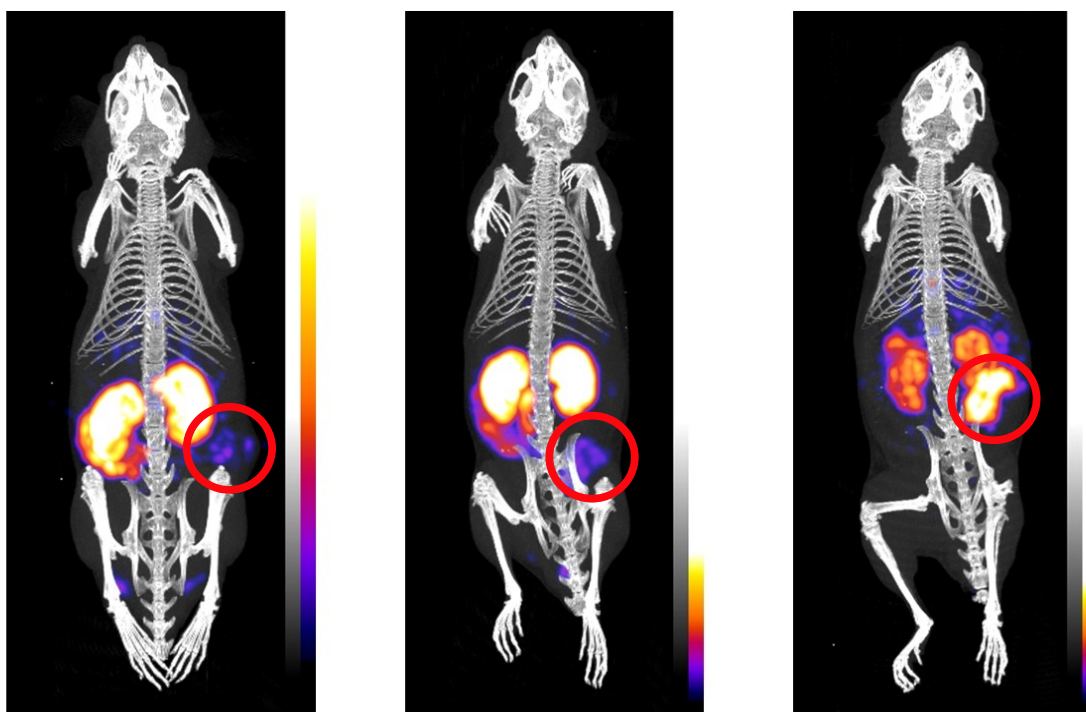
Image 23: SPECT/CT image of [^{99m}Tc]Tc-DT1 in SCID mice bearing AsPC-1 xenografts, 4 h pi. From left to right: block, control and Entresto®+Lis mouse (block: mouse treated with excess NT and Entresto®+Lis). Red circles indicate xenograft sites.

Summary

Three new compounds, each with a different ABD/PEGx pendant group attached to the ε-amine of Lys^7 introduced in the DT1 motif were developed and evaluated. Specifically, DT9 carried the ABD-moiety MPBA. For DT10 a PEG4 spacer was introduced between Lys^7 and MPBA, while in DT11 a non-albumin binding PEG6 group was attached. As reported in the preceding section, such modifications could be well tolerated by the NTS$_1$R, even in the case of bulky substituents (e.g. the palmitoyl-group in [^{99m}Tc]Tc-DT8). Indeed, such compounds (e.g. DT8) were shown to retain high NTS$_1$R affinity and the corresponding [^{99m}Tc]Tc-radioligands (e.g. [^{99m}Tc]Tc-DT8) to show high cell uptake capability in AsPC-1 cells.

At the molecular level, the three new analogs displayed comparable sub-nanomolar affinity for NTS$_1$R, confirming the suitability of position Lys^7 for introduction of bulky-chain groups. In a head-to-head comparison in AsPC-1 cells, [^{99m}Tc]Tc-DT9 and [^{99m}Tc]Tc-DT10 displayed comparable cell uptake with [^{99m}Tc]Tc-DT1, while the PEG6-containing [^{99m}Tc]Tc-DT11 exhibited slightly lower values. Their rank of albumin binding capabilities was as expected. Thus, the non-ABD-carrying [^{99m}Tc]Tc-DT11 showed similar values with the unmodified [^{99m}Tc]Tc-DT1. On the other hand, the MPBA-containing [^{99m}Tc]Tc-DT9 and [^{99m}Tc]Tc-DT10 showed high albumin binding. The presence of the PEG4 linker in [^{99m}Tc]Tc-DT10 resulted in almost twice as high the uptake of [^{99m}Tc]Tc-DT9, probably due to steric factors.

In mice peripheral blood, [^{99m}Tc]Tc-DT9 displayed similar stability with [^{99m}Tc]Tc-DT1, despite its higher binding to albumin, thereby emphasizing the impact of steric factors in the radioligand resistance against NEP and/or ACE. On the other hand, both [^{99m}Tc]Tc-DT10 and [^{99m}Tc]Tc-DT11, showed notably higher stability, which further indicates that both albumin binding and steric hindrance towards the involved peptidases play a synergistic roll in the extent of their *in vivo* degradation. Of particular interest is the fact that in all instances [^{99m}Tc]Tc-DT10 displayed superior stability over the other two radioligands. Notably, [^{99m}Tc]Tc-DT10, after single treatment with Entresto®, reached comparable stability values to [^{99m}Tc]Tc-DT9 or [^{99m}Tc]Tc-DT11, during treatment with Entresto®+Lis.

In mice bearing NTS$_1$R-positive AsPC-1 xenografts, all three compounds displayed higher tumor uptake in comparison with [^{99m}Tc]Tc-DT1 in the control groups, a finding attributed to their increased stability. Notably, [^{99m}Tc]Tc-DT10 outperformed [^{99m}Tc]Tc-DT9 and [^{99m}Tc]Tc-DT11, reaching superior tumor uptake across all groups, even after treatment of animals with inhibitors.

Likewise, [^{99m}Tc]Tc-DT10 by far outperformed [^{99m}Tc]Tc-DT8 in terms of background clearance. Interestingly, [^{99m}Tc]Tc-DT11 demonstrated the fastest blood clearance among the Lys^7 branched analogs, due to little to non-binding to albumin and its higher hydrophilicity.

Discussion

As outlined in the chapter "Aim of the present work" the main objective of the current work was the evaluation of new analogs and strategies in the diagnostic imaging of PC, using SPECT and SPECT/CT modalities. In order to achieve this goal, the over-expression of NTS_1R in the majority of PDAC cases was exploited and Tc-99m labeled radiopeptides based on NT(8-13) and conjugated with an open-chain tetraamine chelator were developed and evaluated.

Two major routes, as well as their combination were explored. Firstly, potential improvements in the performance of previously reported NT(8-13) [99mTc]Tc-radiopeptides were investigated adopting *in situ* inhibition of NEP and/or ACE methods through the administration of selective, potent and reversible peptidase-inhibitors (39,67). Secondly, key structural changes were introduced aiming to improve the *in vivo* stability and overall pharmacokinetics of the new analogs. Such structural changes can be subdivided into two categories: (1) C-terminal modification/elongation (140,148) and (2) branching via the ε-amino group of a Lys[7] residue, carrying the tetraamine chelator at its α-amino group.

Some major objectives had to be tackled in order to efficiently assess the above-mentioned approaches.

- First the *in vitro* and *in vivo* re-evaluation of previously reported analogs was undertaken in order to reveal potential benefits during *in situ* inhibition of NEP and/or ACE. Accordingly, a reference compound/methodology could be selected to serve as a baseline in any further assessments. By a head-to-head comparison of [99mTc]Tc-DT1, [99mTc]Tc-DT5 and [99mTc]Tc-DT6 in colon adenocarcinoma WiDr cells and animal models adopting NEP/ACE inhibition modes (NEP-inhibitor PA, or the ACE-inhibitor Lis, a registered antihypertensive drug), some conclusions could be drawn:

- The substitutions introduced into the motive of DT1 thus resulting DT5 ([βAla[7],Dab[9]]DT1) and DT6 ([βAla[7],Dab[9],Tle[12]]DT1), especially the Tle[12]/Ile[12] replacement, were successful in improving the radioligand *in vivo* stability in mice peripheral blood. However, these modifications were at the cost of cell uptake *in vitro*, eventually resulting in poor tumor uptake *in vivo* (in mice bearing WiDr xenografts).

- The free primary amine of Dab resulted in unfavorably high kidney uptake and retention of [^{99m}Tc]Tc-DT5 and [^{99m}Tc]Tc-DT6. On the other hand, all animal groups which received [^{99m}Tc]Tc-DT1 displayed a much faster clearance from the background with significant lower kidney values in comparison with the two Dab^9-modified radiotracers.

- The unmodified [^{99m}Tc]Tc-DT1 displayed the highest cell uptake *in vitro*. Nevertheless, the corresponding tumor values were low *in vivo*, at least in the control groups. This finding is attributed to its fast degradation by both NEP and ACE, resulting in only 1.8 ± 0.8 % radiotracer remaining intact 5 min pi in healthy mice. After treatment of the animals with the combination of PA+Lis stability drastically increased to 72.3 ± 3.2 % in peripheral mice blood and tumor values went up to 9.60 ± 3.62 %IA/g at 4 h pi in tumor beraing mice, the highest observed values amongst all analogs and groups tested herein.

- *In situ* inhibition of NEP and/or ACE may represent a valid strategy to improve the pharmacokinetic profile of already reported biodegradable radiotracers based on NT(8-13).

According to the above, [^{99m}Tc]Tc-DT1 was chosen as the reference compound under NEP and ACE inhibition during the *in vivo* assessments for the rest of this work (65).

For the establishment of a convenient and reliable cell and animal model to assess new strategies and compounds for PC, four different PC cell lines were initially tested *in vitro*. The cell uptake rate for all four was directly compared with that of [^{99m}Tc]Tc-DT1 (63). It was demonstrated that the highest cell-uptake values were reached in AsPC-1 cells (15.2 ± 2.6 %), which were comparable to those in WiDr cells (10.12 ± 2.29). The radiotracer showed stepwise declining values in PANC-1, MiaPaca-2 and CAPAN-1 cells. Tested for tumorigenicity in SCID mice, AsPC-1 cells were found to produce well-palpable tumors in a time span of 3-4 weeks post implantation, a period comparable with the one required for WiDr tumor induction. During biodistribution of [^{99m}Tc]Tc-DT1 in SCID mice bearing AsPC-1 xenografts, the radiotracer displayed a similar profile to the one shown in WiDr tumor-bearing mice. Uptake in AsPC-1 tumors (7.05 ± 0.80 %IA/g) under combined NEP and ACE inhibition, in Entresto$^®$+Lis treated mice, were comparable (although slightly inferior) to the uptake in WiDr tumors in mice treated with PA+Lis (9.60 ± 3.62 %IA/g). Hence, AsPC-1 cells turned out to be a convenient and reliable NTS$_1$R-positive cell model of PC. Moreover, the switch from PA to the registered antihypertensive drug Entresto$^®$ was shown to be successful in NEP-inhibition, in support of the clinical translation of the *in situ* NEP and/or ACE inhibition approach (63,65,67). It should be noted

however that cases of angioedema have been reported in patients receiving dual NEP/ACE-inhibitors (121).

In the next steps, new [^{99m}Tc]Tc-DT1 mimics were developed adopting two sets of structural changes and evaluated in AsPC-1 cell and animal models vs. [^{99m}Tc]Tc-DT1, without or during NEP and/or ACE inhibition with Entresto® and Lis, repectively.

First, the C-terminal modification was pursued via either C-terminal elongation of the peptide chain by D-Asn at position 14 (DT7), or the β^{3}hLeu^{13}/Leu^{13} substitution (DT13) (140,148). As expected from similar analogs, these modifications were well tolerated by NTS$_1$R with both analogs retaining high receptor affinities (DT7: IC$_{50}$= 29.05 ± 4.11 nM; DT13: IC$_{50}$= 0.63 ± 0.05 nM). Furthermore, the respective [^{99m}Tc]Tc-radiotracers turned out to be more stable against ACE, although only the combination of Entresto®+Lis led to their full stabilization. Unfortunately, these changes compromised the uptake of both [^{99m}Tc]Tc-DT7 and [^{99m}Tc]Tc-DT13 in AsPC-1 cells, with uptake values not exceeding 1 % of added radioactivity. Hence, the biodistribution profile of neither radiotracer was tested in mice bearing AsPC-1 xenografts, since low *in vitro* cell uptake was previously shown to be associated with low tumor values *in vivo*.

The next structural intervention approach, involved analogs having different pendant groups attached to the ε-amino group of Lys that substitute the Gly^7 in the DT1 motif. The first such group was a palmitoyl side chain (DT8), mimicking analogs related to contulakin–G which showed increased degradation resistance and bioavailability (141,142,146). In accordance to this hypothesis, DT8 displayed an excellent receptor affinity (IC$_{50}$= 0.89 ± 0.70 nM) and the resulting [^{99m}Tc]Tc-radiotracer a cell uptake (16.53 ± 1.12% at 1 h) exceeding that of [^{99m}Tc]Tc-DT1 (15.2 ± 2.6 % at 1 h) in AsPC-1 cells. *In vivo* [^{99m}Tc]Tc-DT8 was stable in peripheral mice blood and achieved high uptake and retention in AsPC-1 tumors in mice (6.15 ± 0.92 %IA/g at 4 h and 3.32 ± 0.35 %IA/g at 24 h pi). However, [^{99m}Tc]Tc-DT8 displayed unfavorably high background radioactivity levels. Very high values were found in kidneys, liver and intestines, while the tumor uptake per se was not fully NTS$_1$R-specific (159,161,162) (**Table A6**, pg. 102, Appendix). Palmitic acid is certainly very lipophilic and has a very high binding affinity for albumin, the most abundant protein in blood (159,160). As a result, [^{99m}Tc]Tc-DT8 exhibited prolonged residence in mice circulation with the radioactivity slowly sequestered from blood following the albumin-excretion route.

Three new radiotracers were eventually developed carrying ABD or non-ABD pendant groups on Lys^7. Two analogs contained MPBA(163,164) either directly (DT9), or via a PEG4-linker (DT10). MPBA was chosen as an ABD moiety with a significantly lower affinity for albumin in comparison with palmitic acid. The non-ABD pendant group attached to Lys^7 was PEG6 (DT11), to closer imitate the length of palmitic acid in DT8, but not its excessive lipophilicity or albumin biding capacity. In this way, steric parameters in the interaction of the resulting radiotracer with the active center of NEP or ACE became more evident. All three analogs, despite the bulky side-chains at Lys^7, retained very high affinity for NTS_1R (DT9: IC_{50}= 0.06 ± 0.03 nM; DT10: IC_{50}= 0.08 ± 0.05 nM; DT11: IC_{50}= 0.10 ± 0.03 nM). The respective [^{99m}Tc]Tc-DT9 and [^{99m}Tc]Tc-DT10 radioligands were taken up in AsPC-1 cells equally well with [^{99m}Tc]Tc-DT1, with [^{99m}Tc]DT11 however showing somewhat lower uptake (**Image 21**, pg 53, Results). The latter finding is in agreement with previous reports on the negative effect of increasing PEG-chain length on the cell uptake of PEG-carrying radiotracers (169–172) Concerning albumin binding capabilities, [^{99m}Tc]Tc-DT9 and [^{99m}Tc]Tc-DT10 displayed the highest binding to albumin (23.42 ± 1.49 % and 41.18 ± 2.66 %, respectively). This binding could be significantly reduced with the addition of ibuprofen, a widely used pain-killer with high albumin affinity (166–168). In contrast, [^{99m}Tc]Tc-DT11 showed much lower binding to albumin (3.88 ± 0.50 %), which was found closer to the binding of [^{99m}Tc]Tc-DT1 (0.98 ± 0.15 %), a finding expected for compounds lacking ABD residues.

During *in vivo* stability measurements, [^{99m}Tc]Tc-DT9 showed little to no-resistance to either NEP or ACE (5.09 ± 0.89 % intact at 5 min pi), unlike [^{99m}Tc]DT10 and [^{99m}Tc]DT11 which displayed drastically higher stability ([^{99m}Tc]Tc-DT10: 56.56 ± 5.19 % intact; [^{99m}Tc]Tc-DT11: 35.65 ± 5 % intact). All three radiotracers though reached their maximum stability with the combination of Entresto®+Lis (68.02 ± 3.01 % intact, 86.33 ± 1.94 % intact and 73.98 ± 4.93 % intact, respectively). Interestingly, [^{99m}Tc]Tc-DT10 during Entresto® treatment (66.89 ± 1.24 %) achieved stability levels similar to [^{99m}Tc]Tc-DT9 or [^{99m}Tc]Tc-DT11 during treatment with the Entresto®+Lis combination. The biodistribution profile of all three radiopeptides was subsequently investigated in SCID mice bearing AsPC-1 xenografts to relate *in vitro* data and *in vivo* stability results with tumor uptake and pharmacokinetics. Tumor uptake in control groups of all radiotracers were superior to [^{99m}Tc]Tc-DT1, with [^{99m}Tc]Tc-DT10 achieving the highest uptake in the AsPC-1 tumors (4.49 ± 0.37 %IA/g at 4 h pi). They all showed a faster clearance from the background in comparison with [^{99m}Tc]Tc-DT8. In particular, they displayed a similar background pattern with [^{99m}Tc]Tc-DT1. Interestingly, [^{99m}Tc]Tc-

DT10 even during treatment with Entresto® or [99mTc]Tc-DT9 and [99mTc]Tc-DT11 during treatment with the Entresto®+Lis, demonstrated equally rapid clearance from the background. Moreover, it became evident that [99mTc]Tc-DT10 outperformed all other radiotracers tested in the present work, in terms of AsPC-1 tumor targeting capabilities and background clearance while reaching its maximum efficacy during treatment with Entresto®. This result, is significant by setting any concerns about angioedema at rest, concerns associated with the occurrence of angiodema after application of dual NEP/ACE inhibitors in human (121).

It is necessary at this point to make a comparison between [99mTc]Tc-DT10 and other reported NTS$_1$R-targeting radiotracers. First in line for comparison is [99mTc]Tc-NT-XI ((NαHis)Ac-Lys-(ψCH$_2$-NH)-Arg-Pro-Tyr-Tle-Leu) (**Image D1**) , a doubly stabilized NT(8-13) analog, with a plasma half-life of 21 days *in vitro,* which underwent pilot clinical trials in a small number of PDAC patients (129). Despite a high affinity for NTS$_1$R (K$_D$= 0.5 ± 0.3 nM) in HT-29 cell membranes, its biodistribution profile was far from optimal, with high kidney retention (10.1 ± 2.6 %IA/g at 3 h pi, 6.2 ± 0.7 %IA/g at 24 h pi) and rather low tumor uptake (1.7 ± 1.0 %IA/g at 3 h pi and 1.4 ± 0.2 %IA/g at 24 h pi) in female CD1 nude mice with HT-29 xenografts. After changing the chelator to DTPA (**Image D1**) and labeling with In-111, the affinity dropped (K$_i$= 8.11 ± 1.03 nM) and the kidney and tumor values dropped as well in the same animal model (3.90 ± 0.59 %IA/g and 0.52 ± 0.23 %IA/g, respectively, at 1 h pi) (173).
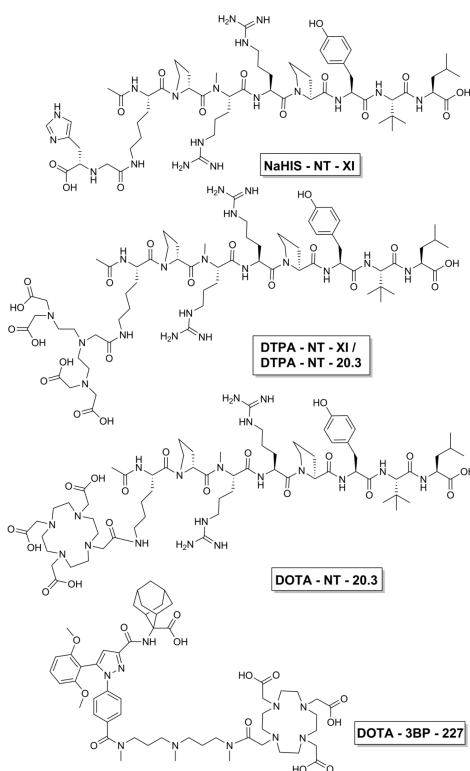
Image D1. Structures of NαHIS-NT-XI, DTPA-NT-XI (DTPA-NT-20.3), DOTA-NT-20.3 and DOTA-3BP-227

Another NT(6-13)-based radiotracer, $[^{111}In]$In-DTPA-NT-20.3 (Ac-Lys(DTPA)-Pro-Arg-Nme-Arg-Pro-Tyr-Tle-Leu) (**Image D1**) (173), clearly displayed a higher affinity for NTS_1R in comparison with the above two analogs (2.24 ± 0.21 nM). The radiopeptide was found to remain 26.5% (26 – 27%) intact at 15 min pi in BALB/c mice. During biodistribution in CD1 nude mice bearing HT-29 xenografts, values reported for tumors were up to 4.85 ± 0.25 %IA/g at 3 h pi in the best case or 2.0 ± 0.4 %IA/g in another report, dropping to 0.86 ± 0.07 %IA/g at 24 h pi. Kidney values were 2.38 ± 0.21 IA/g or 7 ± 2 %IA/g at 3 h pi, dropping to 1.9 ± 0.3 %IA/g at 24 h pi. By switching the chelator to DOTA (**Image D1**) (174), the $[^{nat}In]$In-tagged DOTA-analog displayed fair NTS_1R-affinity in assays with living HT-29 cells (IC_{50} = 15 ± 1 nM). The respective $[^{111}In]$In-DOTA-radiotracer injected in BALB/c mice remained 22 ± 1 % intact in circulation at 15 min pi. Tumor and kidney values were at 2.5 ± 0.2 %IA/g and 4.9 ± 0.4 %IA/g, respectively, at 3 h pi declining to 1.9 ± 0.2 %IA/g and 5.2 ± 0.5 %IA/g, respectively, at 24 h pi, in female CD1 nude mice bearing HT-29 xenografts.

Very recently NTS_1R-direceted radioligands based on small organic NTS_1R-antagonists have been emerging as theranostic radiopharmaceutical candidates of human PC. Such is 3BP-227 (**Image D1**), with $[^{177}Lu]$Lu-3BP-227 already in clinical trials for metastatic PDAC therapy (175,176). The biodistribution profile of $[^{111}In]$In-3BP-227 was preclinically assessed in female nude mice bearing HT-

29 tumors. Tumor values reached 7.49 ± 2.94 %IA/g at 3 h pi dropping to 2.32 ± 1.28 %IA/g at 24 h pi, while kidney values were 2.49 ± 0.42 %IA/g at 3 h pi and declining as low as 1.37 ± 0.67 %IA/g at 24 h pi (177).

A few important points have to be taken into account before drawing solid conclusions from the comparison of the above reported data against the findings of the present work: first, the phenotype differences across different strains and genders of mice and second the varying NTS_1R-expression levels across cell lines and tumors thereof. In the present study, [99mTc]Tc-DT1 displayed higher uptake in WiDr tumors *in vivo* during combined NEP+ACE inhibition than in the AsPC-1 implants. It should be noted that WiDr cells derive from HT-29 cells (178) and accordingly, [99mTc]Tc-DT10 could show higher uptake in HT-29 tumors anyway. In view of that, it could be concluded that [99mTc]Tc-DT10 outperformed any of the aforementioned peptide radiotracers in their NTS_1R-positive tumor targeting capabilities, while showing lower kidney retention even during treatment with Entresto® (129,173,174). In comparison with [111In]In-3BP-227 (177), [99mTc]Tc-DT10 displayed similar tumor uptake at 4 h pi after treatment of the mice with Entresto®, while at 24 h pi similar values were observed with [99mTc]Tc-DT10, even in the control group. When comparing the kidney retention of the two radiotracers, similar renal values could be observed at 3 and 4 h pi, respectively. During treatment with Entresto®, renal values for [99mTc]Tc-DT10 were slightly higher, while at 24 h pi [111In]In-3BP-227 displayed higher retention than [99mTc]Tc-DT10 in both control and Entresto®-treated groups. Despite the similar performance of [111In]In-3BP-227 and [99mTc]Tc-DT10, the latter has some attributes that render it more appealing for broader clinical use, such as: the high availability of Tc-99m via commercial Mo-99/Tc-99m generators, the faster and cheaper synthesis of a peptide-conjugate vs. a small organic molecule conjugate as well as the lower chances of a peptide analog for off-targeting. Some could nevertheless raise the argument of the higher inherent biosafety of antagonists over agonists, but all the clinical data acquired thus far for NT(8-13)-based radiotracers have shown their excellent tolerability and safety after administration to patients (152,175,179,180).

Appendix

Data for [⁹⁹ᵐTc]Tc-DT1

Labeling & QC

Image A1: Representative chromatogram of DT1 - quality control (QC) after labeling; photometric trace at UV 220 nm.

Image A2: Representative radiochromatogram of [⁹⁹ᵐTc]Tc-DT1 - QC after labeling; gamma trace

In vivo stability

Image A3: Representative radiochromatograms for the *in vivo* stability of [^{99m}Tc]Tc-DT1: blood samples from healthy mice at 5 min pi. Dashed – black line: control, solid – black line: PA, dashed – gray: Lis, solid – gray line: PA+Lis.

Image A4: Representative radiochromatograms for the *in vivo* stability of [^{99m}Tc]Tc-DT1: blood samples from healthy mice 5 min pi. Dashed – black line: control, solid – black line: Entresto®, dashed – gray: Lis, solid – gray line: Entresto®+Lis.

Biodistribution tables

Table A1: Biodistribution results of [^{99m}Tc]Tc-DT1 in male SCID mice bearing WiDr xenografts at 4 h pi. Results are expressed as %IA/g and represent the mean values ± sd (n = 4). The animals in Block were administered with an excess of NT and the combination of PA + Lis.

Tissue	Control	PA	Lis	PA + Lis	Block
Blood	0.15 ± 0.01	0.12 ± 0.03	0.10 ± 0.01	0.13 ± 0.06	0.07 ± 0.02
Liver	0.42 ± 0.02	0.47 ± 0.05	0.39 ± 0.05	0.58 ± 0.12	0.42 ± 0.02
Heart	0.08 ± 0.00	0.10 ± 0.02	0.08 ± 0.02	0.10 ± 0.02	0.05 ± 0.01
Kidneys	1.80 ± 0.14	2.26 ± 0.30	2.24 ± 0.34	3.61 ± 0.93	2.89 ± 0.56
Stomach	1.89 ± 0.26	1.39 ± 0.12	1.18 ± 0.22	1.39 ± 0.73	0.90 ± 0.25
Intestines	1.30 ± 0.26	2.91 ± 0.30	1.72 ± 0.29	2.96 ± 1.02	0.43 ± 0.14
Spleen	0.26 ± 0.06	0.56 ± 0.13	0.32 ± 0.07	1.01 ± 0.30	0.43 ± 0.14
Muscle	0.03 ± 0.01	0.05 ± 0.03	0.03 ± 0.01	0.07 ± 0.06	0.26 ± 0.02
Lungs	0.23 ± 0.01	0.42 ± 0.06	0.19 ±0.02	0.67 ± 0.08	0.23 ± 0.10
Pancreas	0.08 ± 0.01	0.10 ± 0.02	0.06 ± 0.01	0.12 ± 0.02	0.04 ± 0.01
Tumor	1.20 ± 0.21	4.58 ± 0.47	1.60 ± 0.47	9.60 ± 3.62	0.23 ± 0.09

Table A2: Biodistribution results of [^{99m}Tc]Tc-DT1 in male SCID mice bearing AsPC-1 xenografts at 4 and 24 h pi. Results are expressed as %IA/g and represent mean values ± sd (n = 4). EL stands for Entresto®+Lis. The animals in Block were administered with an excess of NT and the combination of Entresto®+Lis.

Tissue	4 h	4 h +EL	24 h	24 h + EL	4 h Block
Blood	0.07 ± 0.01	0.08 ± 0.02	0.08 ± 0.07	0.07 ± 0.01	0.09 ± 0.01
Liver	0.44 ± 0.05	0.67 ± 0.06	0.17 ± 0.01	0.4 ±0.07	0.055 ± 0.06
Heart	0.08 ± 0.01	0.11 ± 0.02	0.08 ± 0.05	0.14 ± 0.04	0.18 ± 0.11
Kidneys	4.18 ± 3.80	6.81 ± 1.74	0.58 ± 0.1	1.46 ± 0.07	4.15 ± 1.75
Stomach	0.48 ± 0.26	0.57 ± 0.14	0.44 ± 0.46	0.28 ± 0.02	2.75 ± 1.63
Intestines	0.65 ± 0.04	2.13 ± 0.24	0.34 ±0.08	1.04 ± 0.09	1.07 ± 0.01
Spleen	0.22 ± 0.05	0.58 ± 0.35	0.25 ± 0.21	0.55 ± 0.21	0.31 ± 0.07
Muscle	0.03 ± 0.01	0.06 ± 0.03	0.06 ± 0.05	0.06 ± 0.02	0.07 ± 0.06
Lungs	0.18 ± 0.03	0.62 ± 0.35	0.12 ± 0.08	0.31 ± 0.03	0.41 ± 0.07
Pancreas	0.05 ± 0.01	0.10 ± 0.01	0.08 ± 0.07	0.10 ± 0.01	0.08 ± 0.00
Tumor	1.25 ± 0.14	7.05 ± 0.80	0.71 ± 0.1	2.43 ± 0.37	0.74 ± 0.01

Table A3: Biodistribution results of [^{99m}Tc]Tc-DT1 in male SCID mice bearing MiaPaca-2 xenografts at 4 h pi during treatment with the Entresto®+Lis combination. Results are expressed as %IA/g and represent mean values ± sd (n = 4).

Tissue	4 h + EL
Blood	0.06 ± 0.01
Liver	0.57 ± 0.04
Heart	0.08 ± 0.02
Kidneys	5.86 ± 0.14
Stomach	0.37 ± 0.05
Intestines	2.43 ± 0.6
Spleen	0.49 ±0.03
Muscle	0.03 ± 0.01
Lungs	0.43 ± 0.04
Pancreas	0.1 ± 0.02
Tumor	1.97 ± 0.25

Data for [^{99m}Tc]Tc-DT5

Labeling & QC

Image A6: Representative chromatogram of DT5 - QC after labeling; photometric trace at UV 220 nm.

Image A7: Representative radiochromatogram of [^{99m}Tc]Tc-DT5 - QC after labeling; radiometric trace.

In vivo stability

Image A8: Representative radiochromatograms for the *in vivo* stability of [^{99m}Tc]Tc-DT5: blood samples from healthy mice 5 min pi. Dashed – black line: control, solid – black line: PA, dashed – gray: Lis, solid – gray line: PA+Lis.

Image A9: Representative radiochromatograms for the *in vivo* stability of [^{99m}Tc]Tc-DT5: blood samples from healthy mice 5 min pi. Dashed – black line: control, solid – black line: Entresto®, dashed – gray: Lis, solid – gray line: Entresto®+Lis.

96

Biodistribution tables

Table A4: Biodistribution results of [^{99m}Tc]Tc-DT5 in male SCID mice bearing WiDr xenografts at 4 h pi. Reuslts are expressed as %IA/g and represent mean values ± sd (n = 4). The animals in Block were treated with excess NT and the PA + Lis combination

Tissue	Control	PA + Lis	Block
Blood	0.45 ± 0.16	0.41 ± 0.12	
Liver	0.90 ± 0.20	1.12 ± 0.27	
Heart	0.16 ± 0.04	0.22 ± 0.05	
Kidneys	8.63 ± 1.8	16.62 ± 1.63	
Stomach	2.00 ± 0.35	2.02 ± 0.37	
Intestines	2.90 ± 0.28	4.30 ± 0.52	0.42 ± 0.01
Spleen	0.31 ± 0.09	0.86 ± 0.07	
Muscle	0.07 ± 0.02	0.11 ± 0.16	
Lungs	0.43 ± 0.10	1.10 ± 0.16	
Pancreas	0.16 ± 0.04	0.29 ± 0.03	
Tumor	0.88 ± 0.08	12.29 ± 2.73	0.13 ± 0.01

Data for [^{99m}Tc]Tc-DT6

Labeling & QC

Image A10: Representative chromatogram of DT6 - QC after labeling; photometric trace at UV 220 nm.

Image A11: Representative radiochromatogram of [^{99m}Tc]Tc-DT6 - QC after labeling; radiometric trace.

In vivo stability

Image A12: Representative radiochromatograms for the *in vivo* stability of [^{99m}Tc]Tc-DT6: blood samples from healthy mice 5 min pi. Dashed – black line: control, solid – black line: PA

Biodistribution tables

Table A5: Biodistribution results of [^{99m}Tc]Tc-DT6 in male SCID mice bearing WiDr xenografts at 4 h pi. Results are expressed as %IA/g and represent mean values ± sd (n = 4). The animals in Block were treated with excess NT and the PA + Lis combination.

Tissue	Control	PA	Lis	PA + Lis	Block
Blood	0.10 ± 0.06	0.10 ± 0.03	0.08 ± 0.03	0.09 ± 0.00	0.11 ± 0.09
Liver	0.34 ± 0.07	0.42 ± 0.05	0.28 ± 0.01	0.45 ± 0.07	0.36 ± 0.06
Heart	0.08 ± 0.02	0.12 ± 0.03	0.07 ± 0.02	0.10 ± 0.02	0.09 ± 0.04
Kidneys	6.09 ± 1.15	11.14 ± 3.87	6.24 ± 1.56	14.61 ± 3.16	10.83 ± 3.26
Stomach	0.44 ± 0.11	0.87 ± 0.22	0.62 ± 0.22	0.89 ± 0.16	0.93 ± 0.30
Intestines	1.61 ± 0.55	2.52 ±0.40	1.46 ± 0.32	2.81 ± 0.32	0.46 ± 0.21
Spleen	0.64 ± 0.14	1.71 ± 0.26	0.75 ± 0.09	1.84 ± 0.28	0.48 ± 0.16
Muscle	0.04 ± 0.03	0.05 ± 0.02	0.03 ± 0.01	0.09 ± 0.06	0.03 ± 0.01
Lungs	0.22 ± 0.06	1.26 ± 0.15	0.19 ± 0.03	1.27 ± 0.02	0.54 ± 0.07
Pancreas	0.10 ± 0.04	0.14 ± 0.02	0.07 ± 0.01	0.16 ± 0.02	0.07 ± 0.04
Tumor	1.68 ± 0.28	3.89 ± 0.71	2.15 ± 0.43	3.50 ± 0.34	0.38 ± 0.15

Data for [^{99m}Tc]Tc-DT7

Labeling & QC

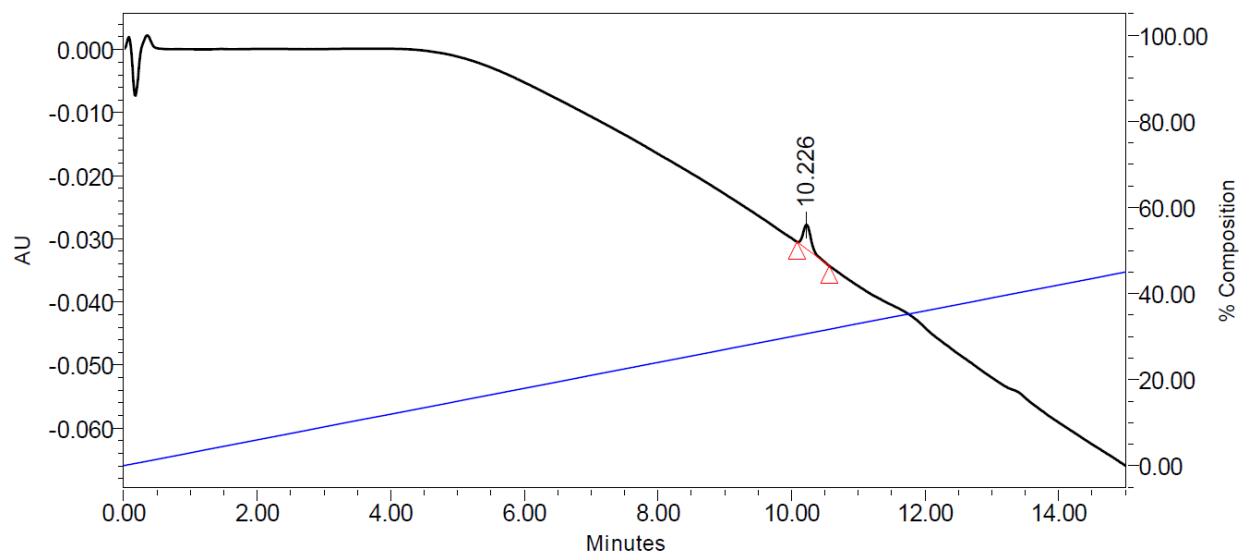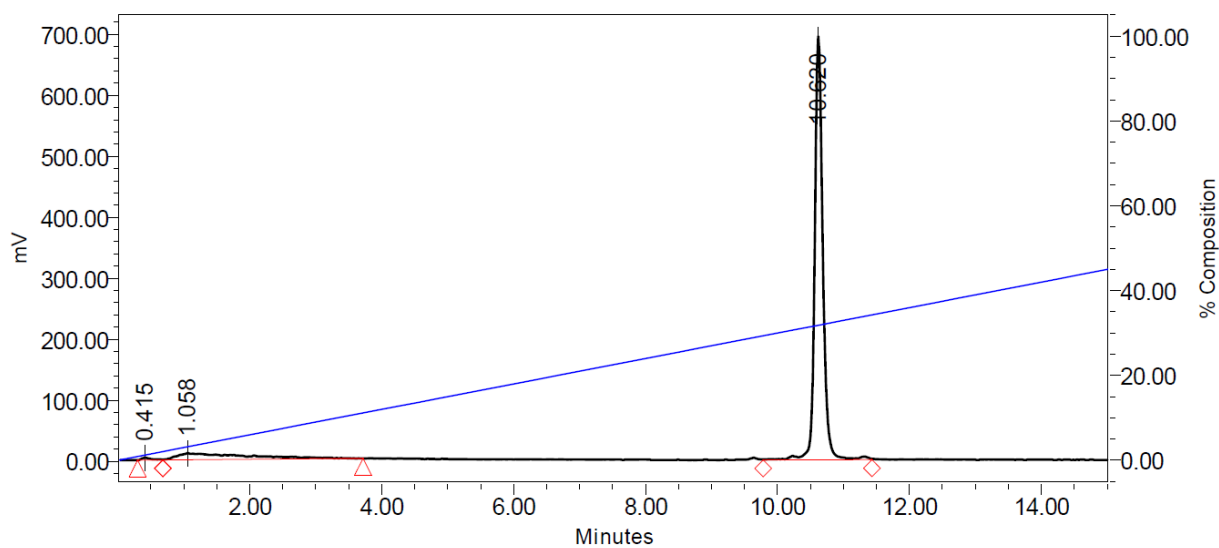**Image A13**: Representative chromatogram of DT7 - QC after labeling; photometric trace at UV 220 nm.

Image A14: Representative radiochromatogram of [^{99m}Tc]Tc-DT7 - QC after labeling; radiometric trace.

In vivo stability

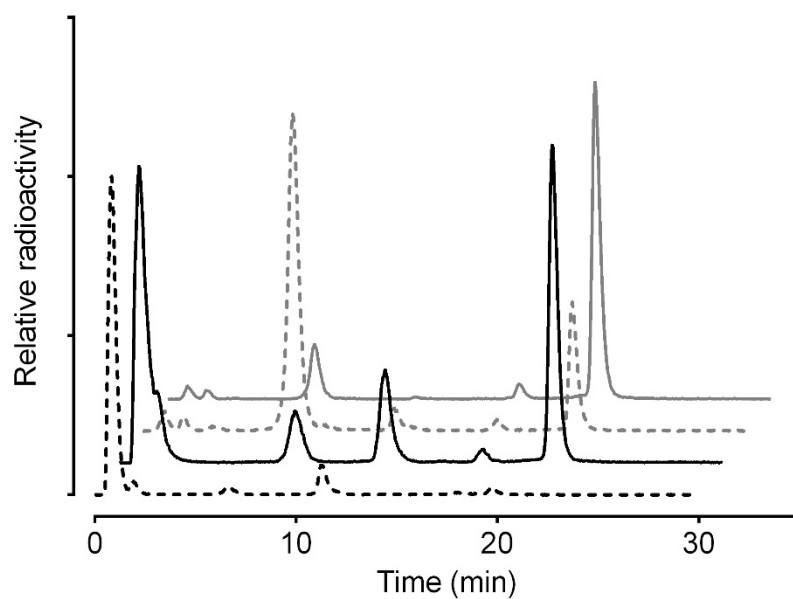**Image A15**: Representative radiochromatograms for the *in vivo* stability of [^{99m}Tc]Tc-DT7: blood samples from healthy mice 5 min pi. Dashed – black line: control, solid – black line: Entresto®, dashed – gray: Entresto®+Lis.

Data for [^{99m}Tc]Tc-DT8

Labeling & QC
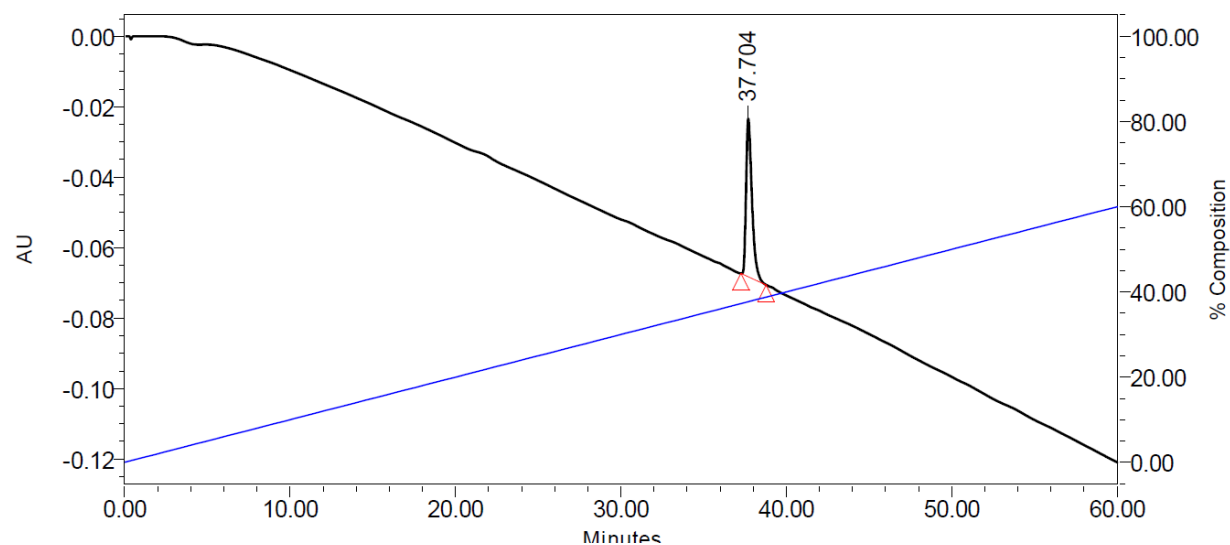
Image A16: Representative chromatogram of DT8 - QC after labeling; photometric trace at UV 220 nm.
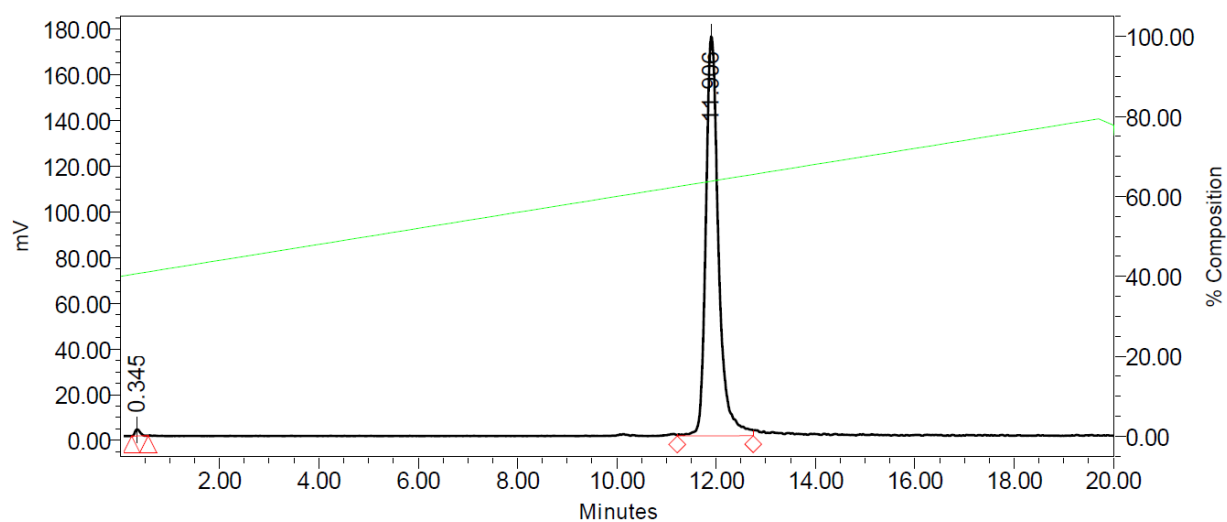
Image A17: Representative radiochromatogram of [^{99m}Tc]Tc-DT8 - QC after labeling; radiometric trace.
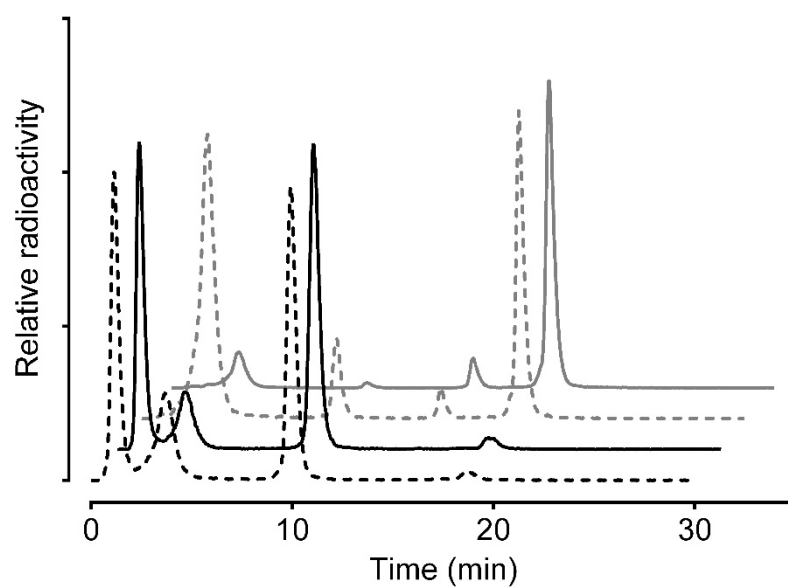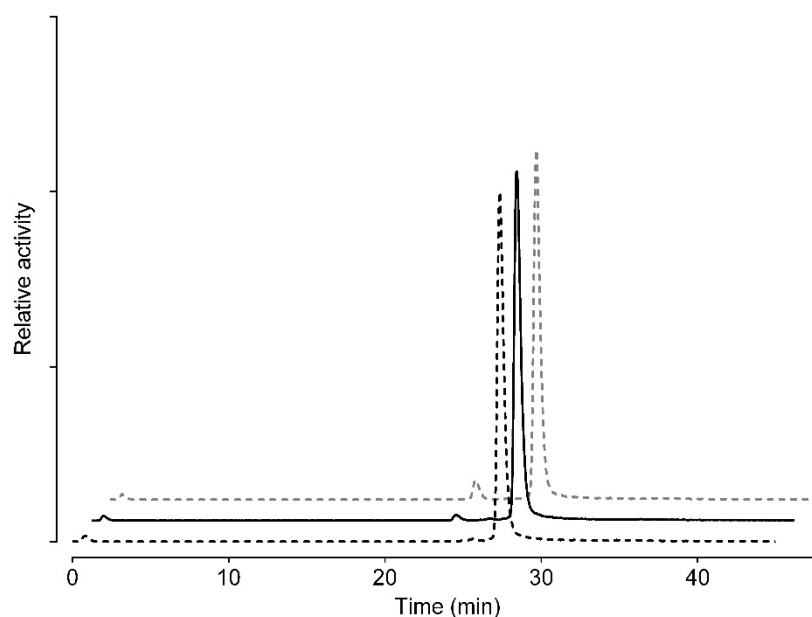
In vivo stability

Image A18: Representative radiochromatograms for the *in vivo* stability of [^{99m}Tc]Tc-DT8: blood samples from healthy mice 5 min pi. Dashed – black line: control, solid – black line: Entresto$^®$, dashed – gray: Entresto$^®$+Lis.

Biodistribution tables

Table A6: Biodistribution results of [^{99m}Tc]Tc-DT8 in male SCID mice bearing AsPC-1 xenografts at 4 and 24 h pi. Results are expressed as %IA/g and represent mean values ± sd (n = 4). The animals in Block were treated with excess NT and the Entresto$^®$+Lis combination. EL: Entresto$^®$+Lis.

Tissue	4 h	4 h + EL	24 h	24 h +EL	4 h Block
Blood	4.63 ± 0.55	4.32 ± 0.42	0.68 ± 0.18	0.70 ± 0.06	4.25 ± 0.37
Liver	29.56 ± 3.77	28.42 ± 2.48	12.93 ± 1.66	16.96 ± 0.94	30.93 ± 4.25
Heart	3.12 ± 0.43	2.85 ± 2.48	0.64 ± 0.11	0.71 ± 0.06	2.79 ± 0.47
Kidneys	9.53 ± 1.18	9.15 ± 0.62	3.81 ± 0.54	4.63 ± 0.15	8.56 ± 0.87
Stomach	3.09 ± 1.06	2.27 ± 0.38	1.73 ± 0.50	1.56 ± 0.31	2.06 ± 0.47
Intestines	13.02 ± 4.60	7.90 ± 0.88	4.26 ± 0.61	5.37 ± 1.61	6.27 ± 0.72
Spleen	6.82 ± 1.11	5.47 ± 0.47	3.42 ± 0.54	4.47 ± 0.83	6.18 ± 1.37
Muscle	0.93 ± 0.13	0.81 ± 0.04	0.22 ± 0.02	0.24 ± 0.01	0.82 ± 0.11
Lungs	8.80 ± 1.42	7.61 ± 0.64	3.42 ± 0.67	3.62 ± 0.94	8.46 ± 1.26
Pancreas	2.10 ± 0.30	1.85 ± 0.18	0.75 ± 0.17	0.80 ± 0.07	1.84 ± 0.41
Brain	0.20 ± 0.04	0.18 ± 0.02	0.14 ± 0.03	0.16 ± 0.01	0.14 ± 0.01
Tumor	6.15 ± 0.92	5.24 ± 0.27	3.32 ± 0.35	2.84 ± 0.43	3.68 ± 0.92

Data for [⁹⁹ᵐTc]Tc-DT9

Labeling & QC
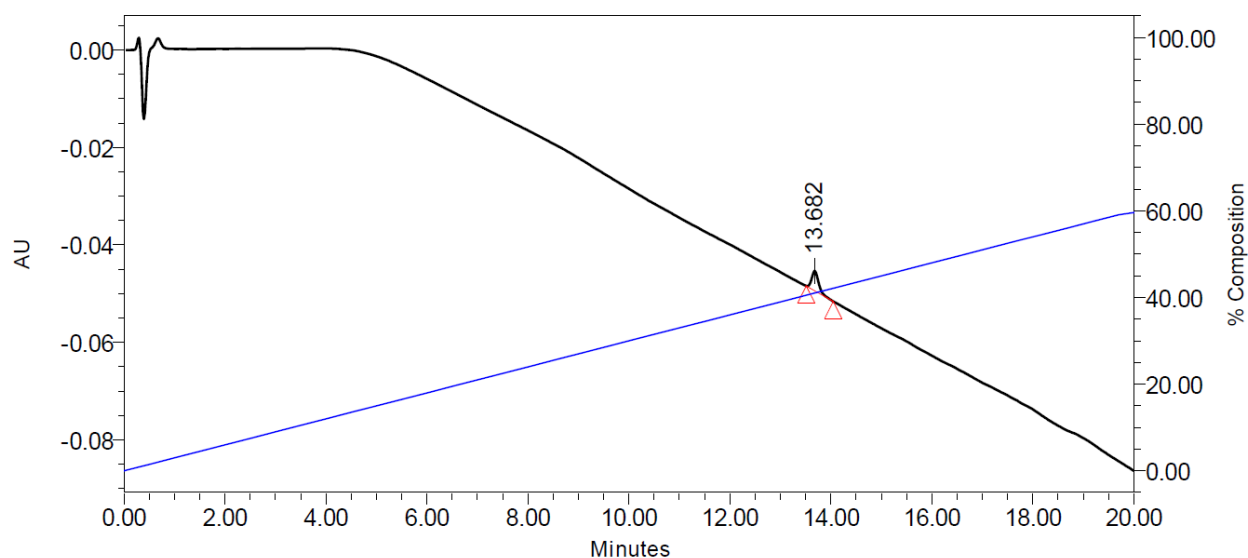
Image A19: Representative chromatogram of DT9 - QC after labeling; photometric trace at UV 220 nm.
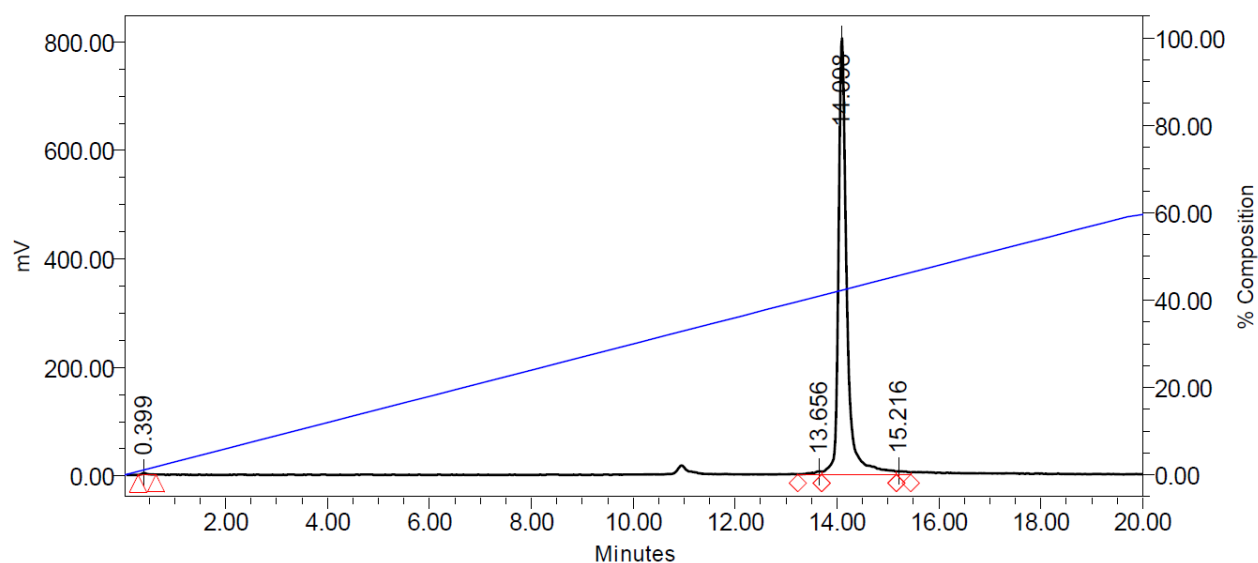
Image A20: Representative radiochromatogram of [⁹⁹ᵐTc]Tc-DT9 - QC after labeling; photometric trace at UV 220 nm.

In vivo stability
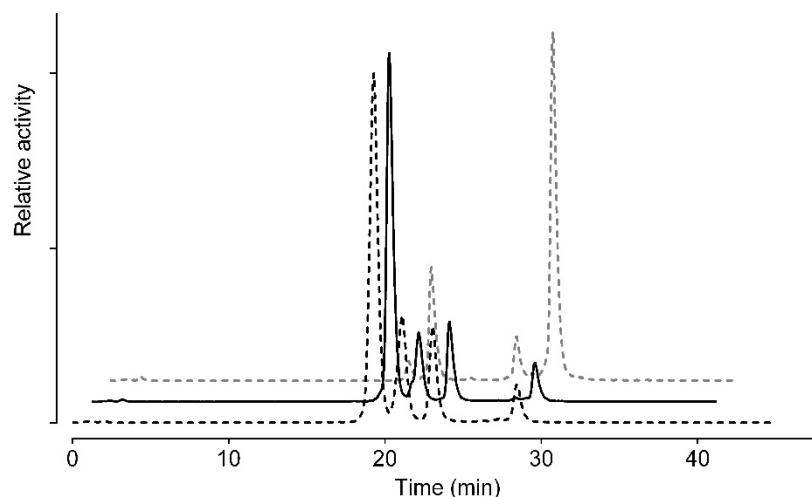
Image A21: Representative chromatograms for the *in vivo* stability of [^{99m}Tc]Tc-DT9: blood samples from healthy mice 5 min pi. Dashed – black line: control, solid – black line: Entresto®, dashed – gray: Entresto®+Lis.

Biodistribution table

Table A7: Biodistribution results of [^{99m}Tc]Tc-DT9 in male SCID mice bearing AsPC-1 xenografts both at 4 and 24 h pi. Results are expressed as %IA/g and represent mean values ± sd (n = 4). The animals in Block were treated with excess NT and the Entresto®+Lis combination, EL: Entresto®+Lis

Tissue	4 h	4 h + EL	24 h	24 h +EL	4 h Block
Blood	3.46 ± 0.60	1.20 ± 0.26	0.04 ± 0.01	0.05 ± 0.01	0.82 ± 0.25
Liver	3.27 ± 0.53	2.00 ± 0.20	0.29 ± 0.02	0.38 ± 0.04	1.77 ± 0.21
Heart	1.12 ± 0.31	0.43 ±0.07	0.04 ± 0.01	0.04 ± 0.01	0.28 ± 0.06
Kidneys	5.79 ± 0.63	4.38 ± 0.81	0.36 ± 0.03	0.45 ± 0.07	3.93 ± 1.25
Stomach	1.03 ± 0.29	0.90 ± 0.34	0.17 ± 0.04	0.11 ± 0.03	0.43 ± 0.12
Intestines	2.34 ± 0.39	2.49 ± 0.16	0.24 ± 0.04	0.51 ± 0.04	1.04 ± 0.10
Spleen	0.65 ± 0.11	1.10 ± 0.22	0.10 ± 0.02	0.26 ± 0.03	0.66 ± 0.08
Muscle	0.37 ±0.05	0.16 ± 0.04	0.01 ± 0.01	0.02 ± 0.01	0.13 ± 0.04
Lungs	2.15 ± 0.25	1.30 ± 0.48	0.16 ± 0.03	0.18 ± 0.04	0.84 ± 0.17
Pancreas	0.51 ± 0.11	0.30 ± 0.16	0.02 ± 0.00	0.03 ± 0.01	0.20 ± 0.03
Tumor	2.49 ± 0.60	5.03 ± 0.47	0.47 ± 0.06	1.71 ± 0.28	1.60 ± 0.67

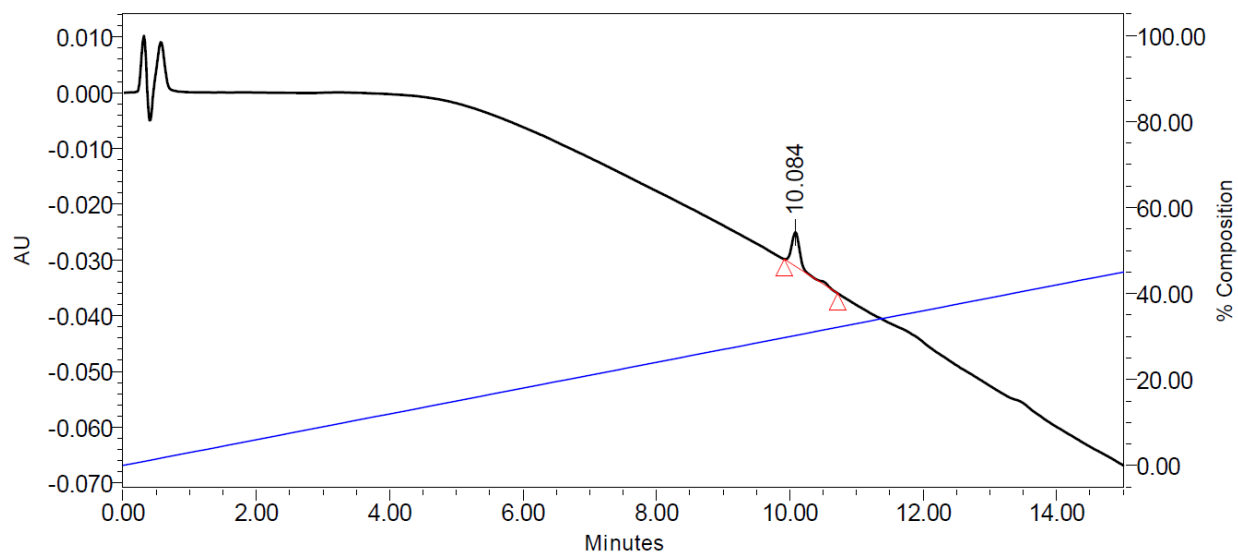# Data for [99mTc]Tc-DT10

Labeling & QC
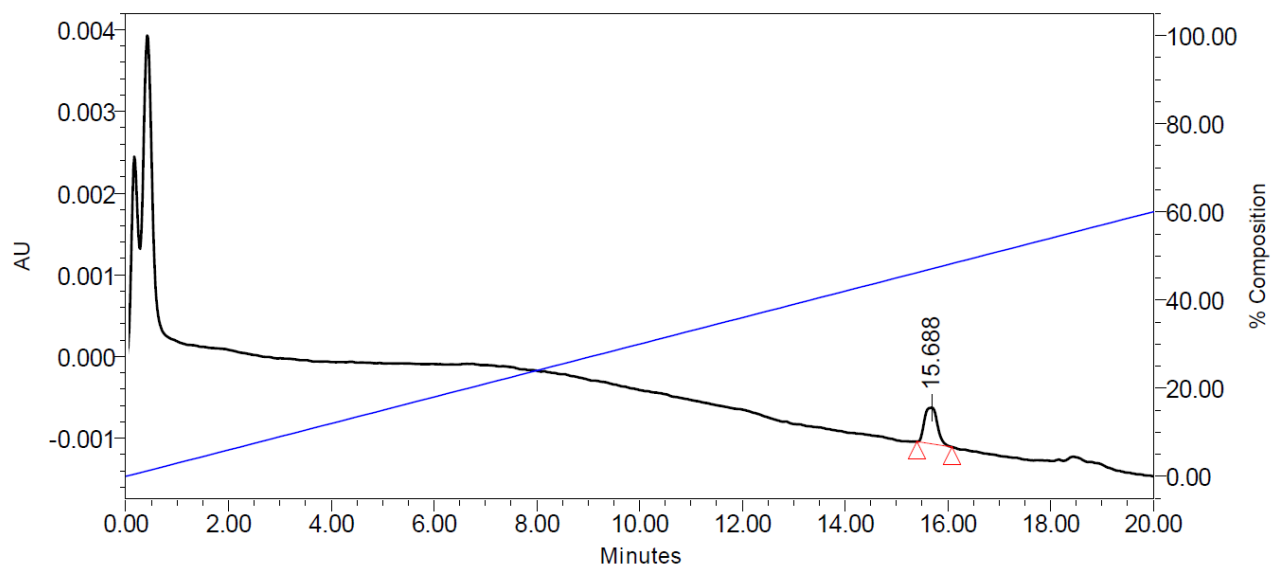
Image A22: Representative chromatogram of DT10 - QC after labeling; photometric trace at UV 220 nm.
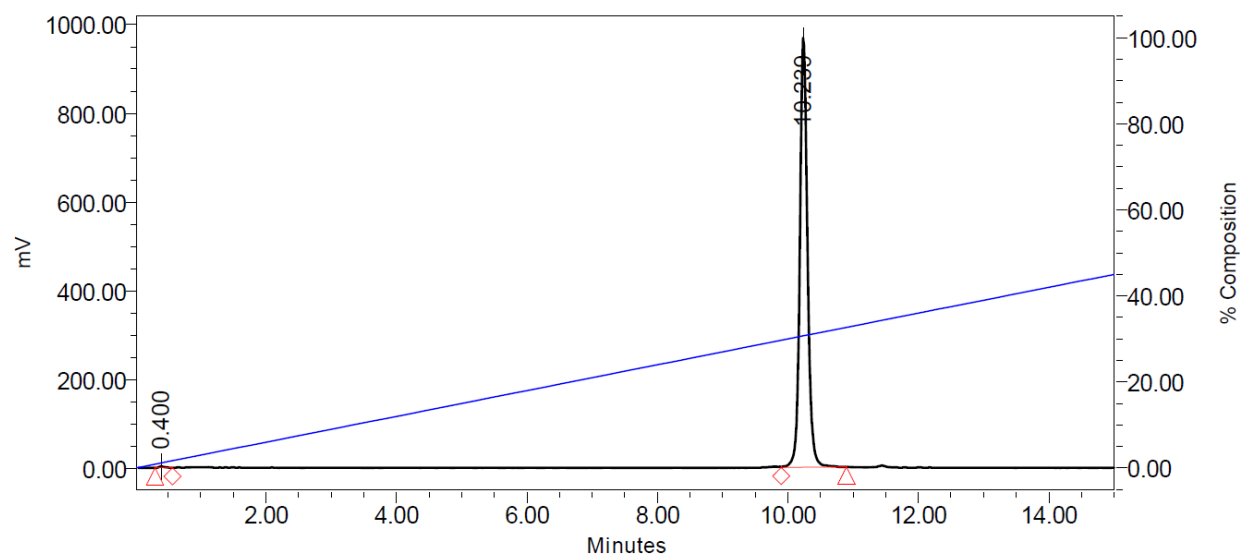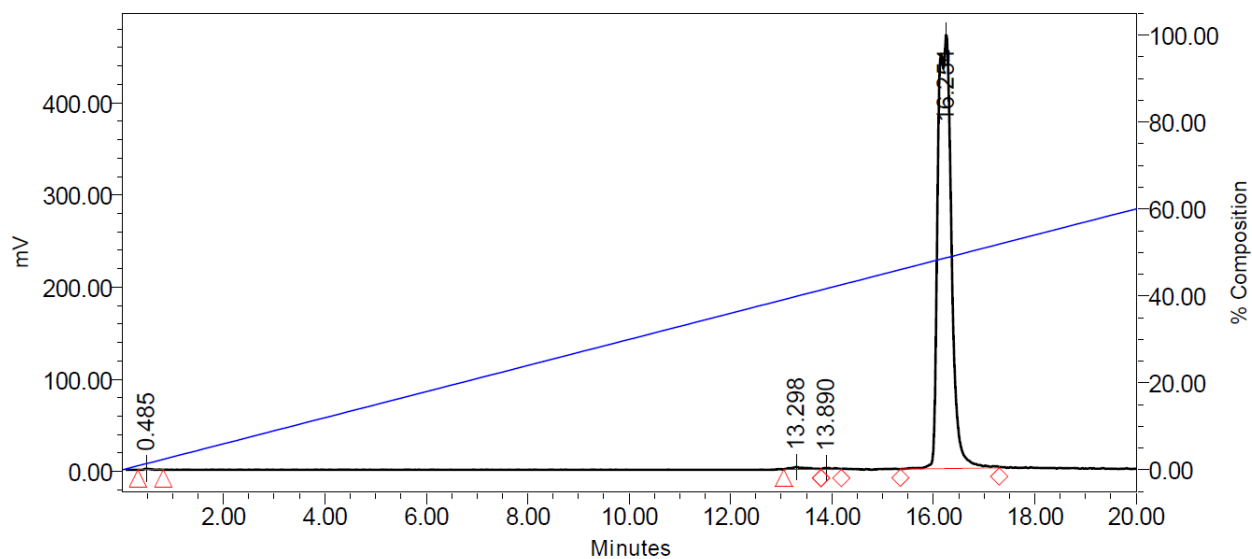

Image A23: Representative radiochromatogram of [99mTc]Tc-DT10 - QC after labeling; radiometric trace.
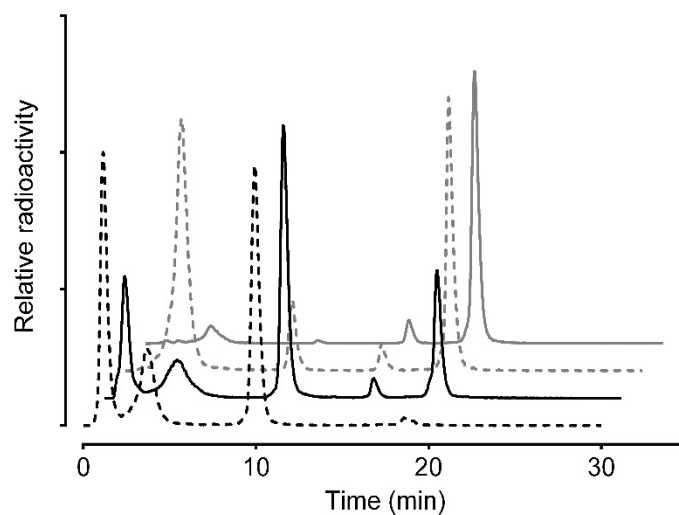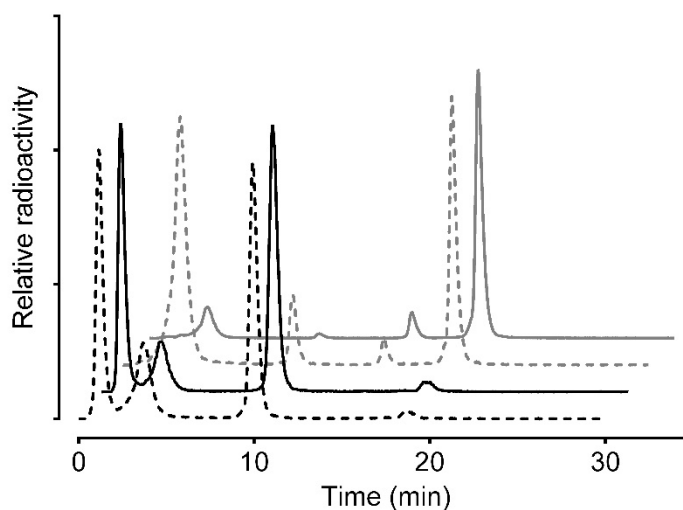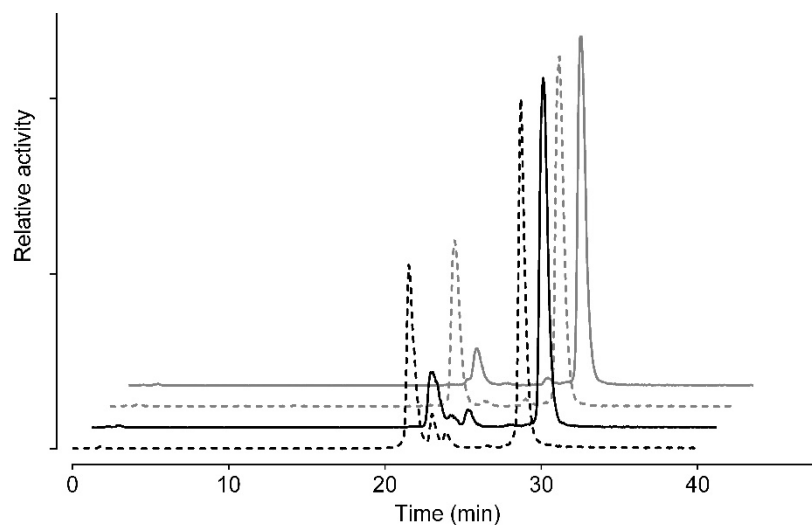
In vivo stability

Image A24: Representative radiochromatograms for the *in vivo* stability of [^{99m}Tc]Tc-DT10: blood samples from healthy mice 5 min pi. Dashed – black line: control, solid – black line: Entresto®, dashed – gray: Lis, solid – gray line: Entresto®+Lis

Biodistribution table

Table A8: Biodistribution results of [^{99m}Tc]Tc-DT10 in male SCID mice bearing AsPC-1 xenografts at 4 and 24 h pi. Data is expressed as %IA/g and represent mean values ± sd (n = 4).The animals in Block were treated with excess NT and the Entresto®+Lis combination, EL: Entresto®+Lis.

Tissue	4 h	4 h + Entresto®	24 h	24 h +Entresto®	4 h Block
Blood	0.99 ± 0.35	0.93 ± 0.12	0.07 ± 0.01	0.08 ± 0.01	0.081 ± 0.29
Liver	1.19 ± 0.18	1.27 ± 0.08	0.31 ± 0.02	0.35 ± 0.05	0.31 ± 0.02
Heart	0.39 ± 0.10	0.34 ± 0.06	0.04 ± 0.01	0.08 ± 0.02	0.04 ± 0.01
Kidneys	3.11 ± 0.32	3.57 ± 0.36	0.62 ± 0.06	0.80 ± 0.05	0.62 ± 0.06
Stomach	0.71 ± 0.09	0.63 ± 0.13	0.19 ± 0.02	0.16 ± 0.04	0.19 ± 0.02
Intestines	1.89 ± 0.18	2.61 ± 0.20	0.50 ± 0.04	0.69 ± 0.09	0.50 ± 0.04
Spleen	0.85 ± 0.06	1.37 ± 0.18	0.44 ± 0.14	0.60 ± 0.09	0.44 ± 0.14
Muscle	0.14 ± 0.04	0.17 ± 0.01	0.03 ± 0.01	0.04 ± 0.00	0.03 ± 0.01
Lungs	0.86 ± 0.21	1.23 ± 0.15	0.18 ± 0.03	0.34 ± 0.06	0.18 ± 0.03
Pancreas	0.25 ± 0.04	0.33 ± 0.06	0.07 ± 0.02	0.08 ± 0.02	0.07 ± 0.02
Tumor	4.48 ± 0.37	6.14 ± 0.08	1.87 ± 0.07	2.96 ± 0.63	1.87 ± 0.07

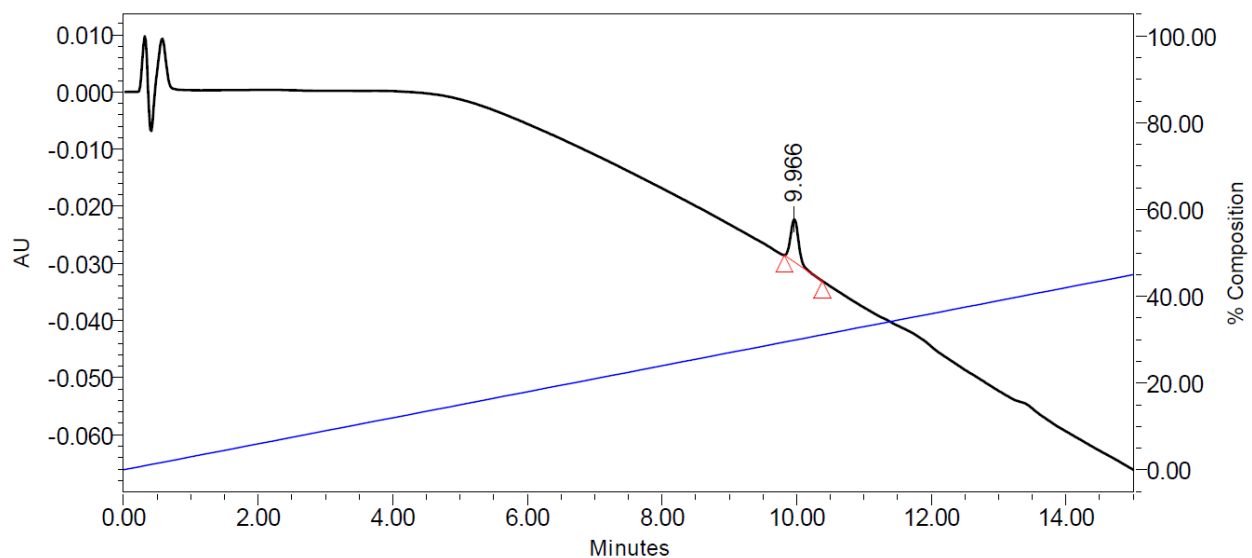# Data for [^{99m}Tc]Tc-DT11

Labeling & QC
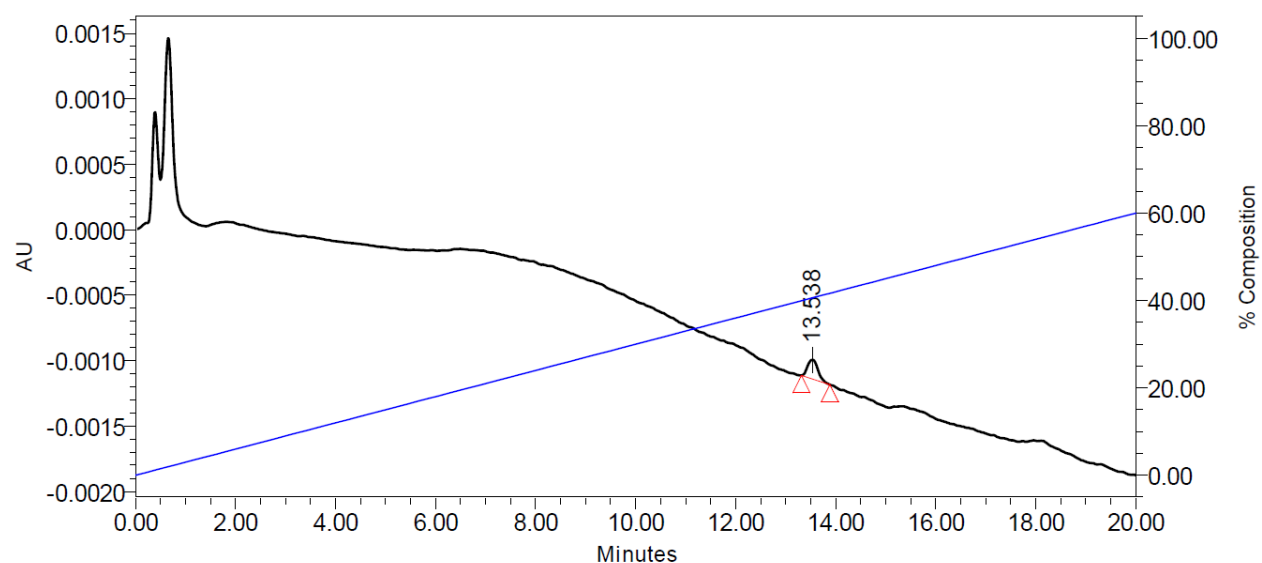
Image A25: Representative chromatogram of DT11 QC after labeling; photometric trace at UV 220 nm.
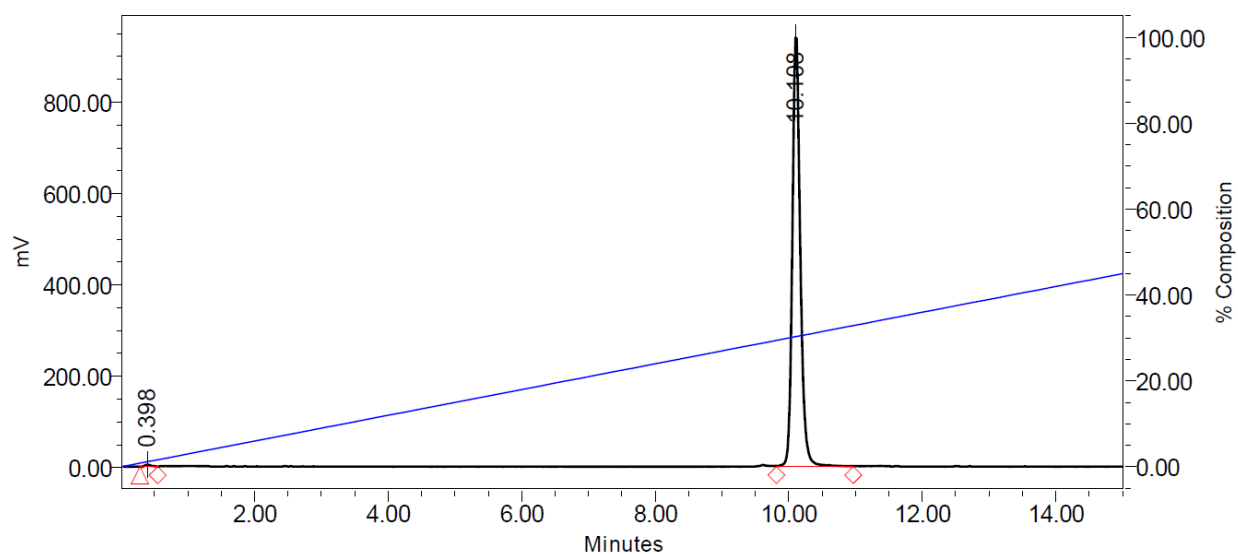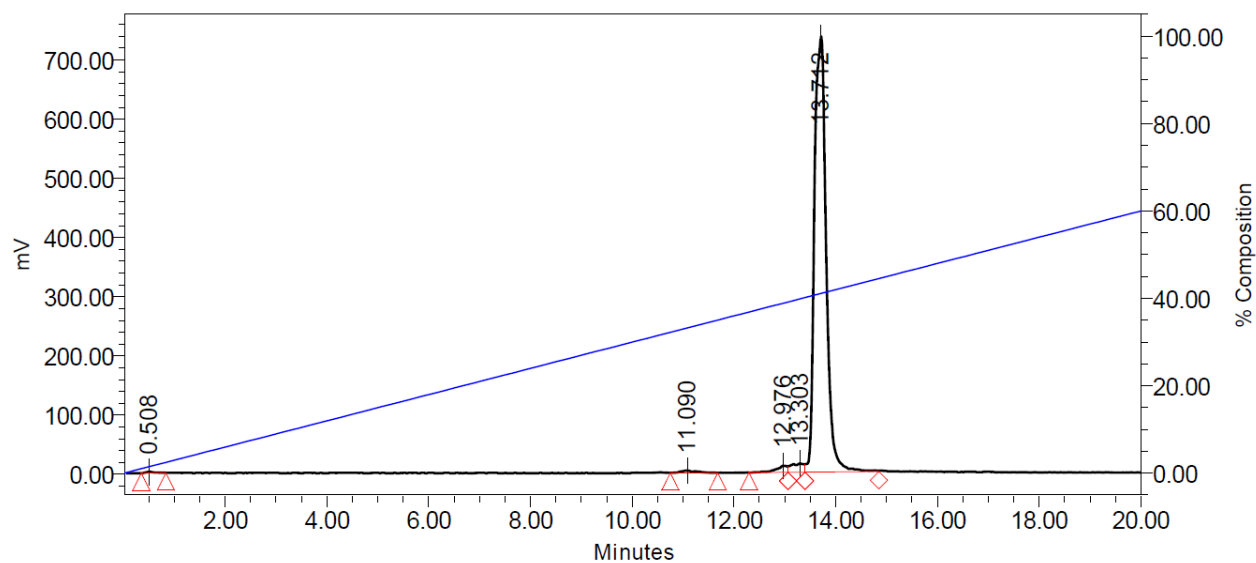

Image A26: Representative radiochromatogram of [^{99m}Tc]Tc-DT11 - QC after labeling; radiometric trace.
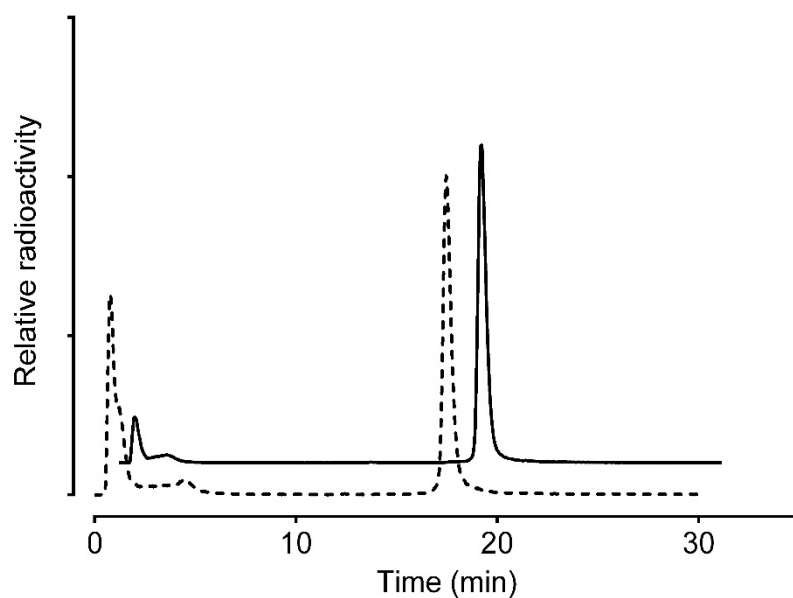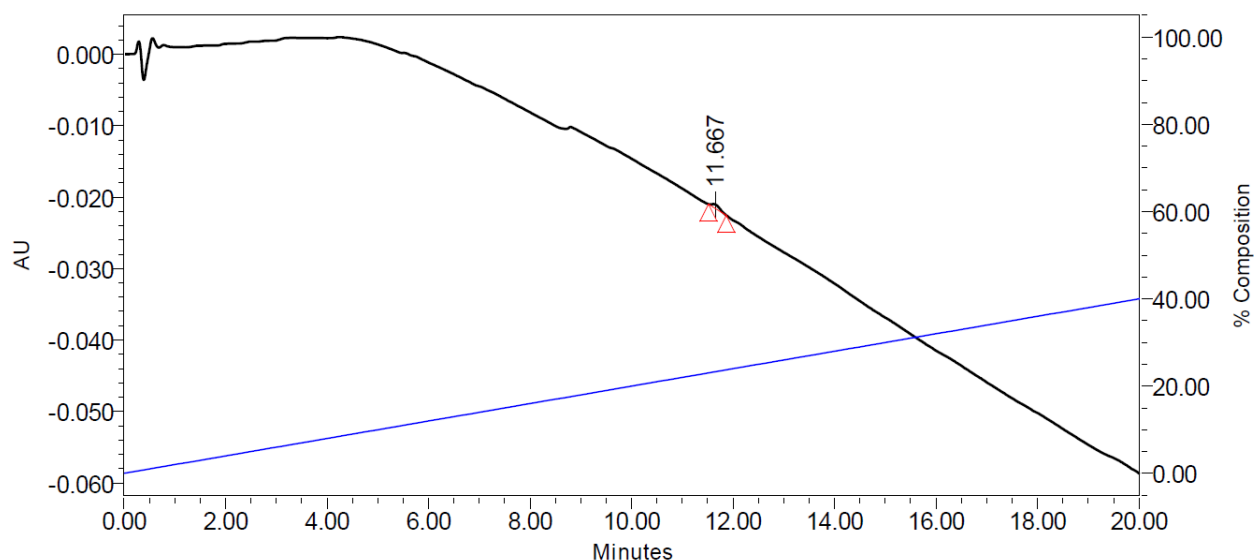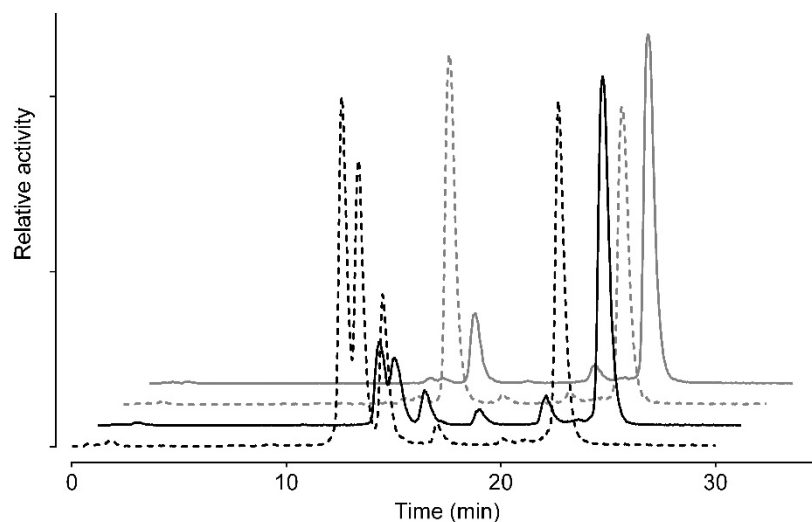
In vivo stability

Image A27: Representative radiochromatograms for the *in vivo* stability of [^{99m}Tc]Tc-DT11: blood samples from healthy mice 5 min pi. Dashed – black line: control, solid – black line: Entresto®, dashed – gray: Lis, solid – gray line: Entresto®+Lis

Biodistribution tables

Table A9: Biodistribution results of [^{99m}Tc]Tc-DT11 in male SCID mice bearing AsPC-1 xenografts at 4 and 24 h pi. Results are expressed as %IA/g and represent mean values ± sd (n = 4).The animals in Block were treated with excess NT and the Entresto®+Lis combination, EL: Entresto®+Lis.

Tissue	4 h	4 h + EL	24 h	24 h +EL	4 h Block
Blood	0.05 ± 0.01	0.06 ± 0.01	0.05 ± 0.01	0.07 ± 0.02	0.06 ± 0.02
Liver	0.26 ± 0.04	1.04 ± 0.31	0.11 ± 0.00	0.41 ± 0.11	0.79 ± 0.38
Heart	0.05 ± 0.01	0.09 ± 0.02	0.05 ± 0.04	0.06 ± 0.02	0.05 ± 0.02
Kidneys	2.43 ± 0.51	6.92 ± 2.55	0.68 ± 0.10	0.83 ± 0.20	3.11 ± 1.29
Stomach	0.19 ± 0.05	0.36 ± 0.06	0.08 ± 0.01	0.14 ± 0.07	0.28 ± 0.17
Intestines	1.12 ± 0.17	2.12 ± 0.62	0.40 ± 0.03	0.55 ± 0.09	1.41 ± 1.04
Spleen	0.28 ± 0.02	2.23 ± 0.81	0.20 ± 0.03	0.97 ± 0.30	1.01 ± 0.68
Muscle	0.03 ± 0.00	0.06 ± 0.02	0.03 ± 0.01	0.04 ± 0.01	0.02 ± 0.02
Lungs	0.12 ± 0.00	0.65 ± 0.15	0.08 ± 0.01	0.26 ± 0.02	0.35 ± 0.12
Pancreas	0.06 ± 0.00	0.12 ± 0.02	0.05 ± 0.01	0.06 ± 0.01	0.08 ± 0.04
Tumor	3.63 ± 0.42	4.48 ± 1.23	1.74 ± 0.20	2.47 ± 0.57	0.56 ± 0.18

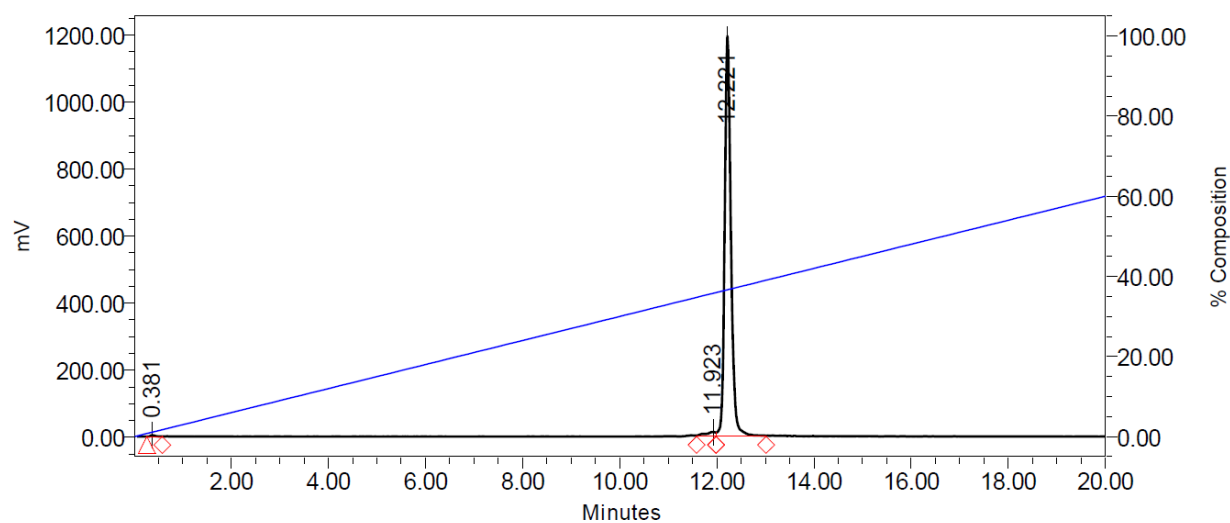# Data for [^{99m}Tc]Tc-DT13

Labeling & QC
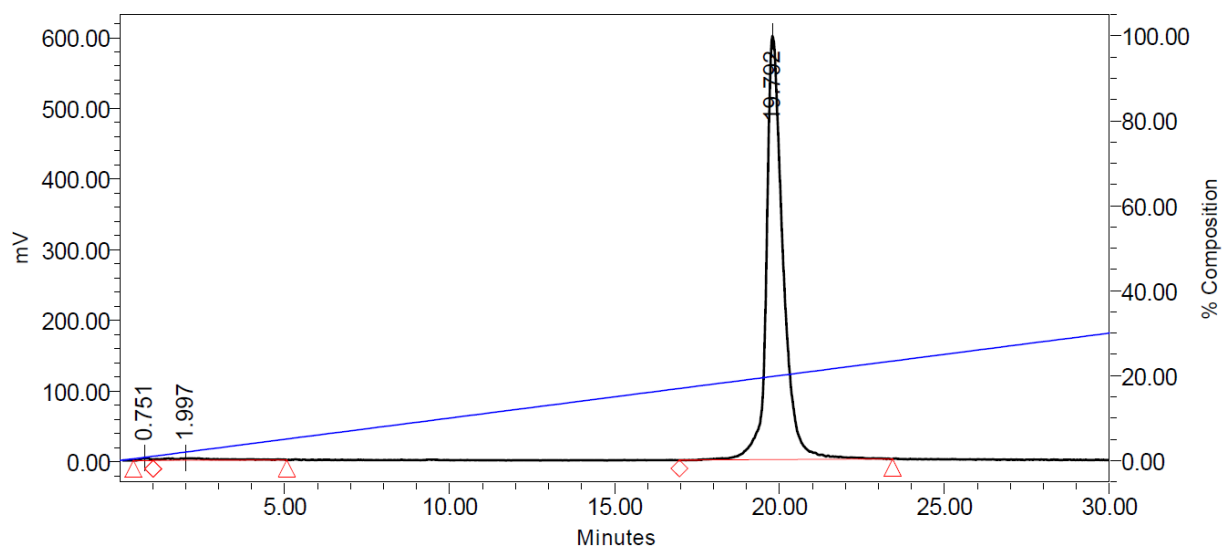
Image A28: Representative radiochromatogram of [^{99m}Tc]Tc-DT13 - QC after labeling; radiometric trace.
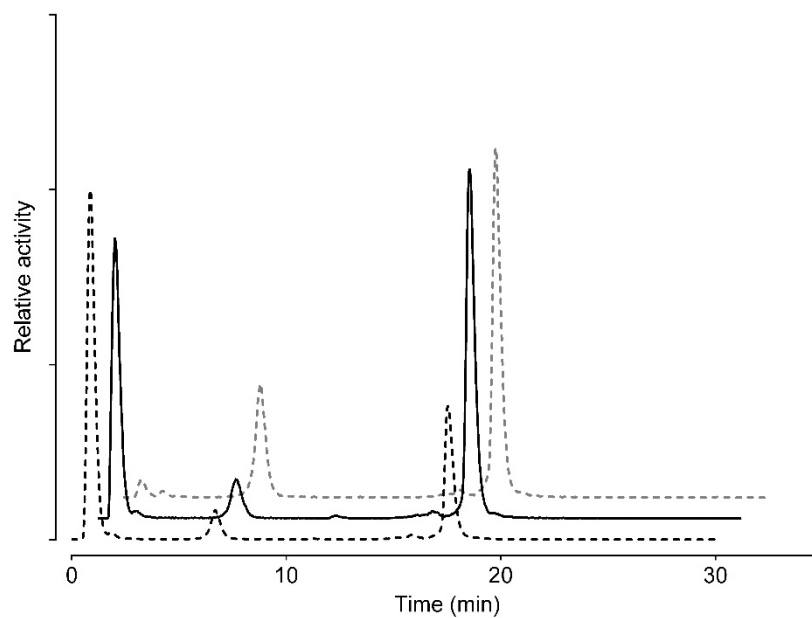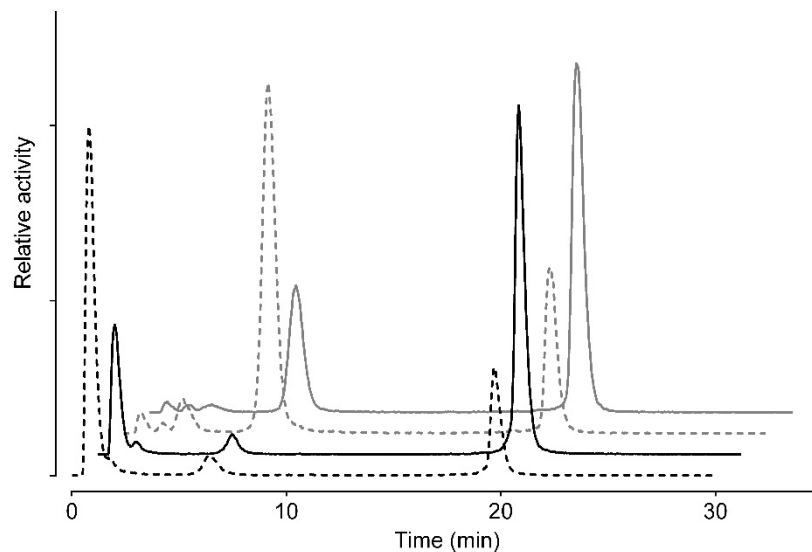
In vivo stability

Image A29: Representative radiochromatograms for the *in vivo* stability of [^{99m}Tc]Tc-DT13: blood samples from healthy mice 5 min pi. Dashed – black line: control, solid – black line: Entresto®, dashed – gray: Lis, solid – gray line: Entresto®+Lis.

References

1.   Leung PS. Overview of the Pancreas. In 2010. p. 3–12. Available from:
        http://link.springer.com/10.1007/978-90-481-9060-7_1

2.   Leung PS. Physiology of the Pancreas. In 2010. p. 13–27. Available from:
        http://link.springer.com/10.1007/978-90-481-9060-7_2

3.   Atkinson MA, Campbell-Thompson M, Kusmartseva I, Kaestner KH. Organisation of the
        human pancreas in health and in diabetes. Diabetologia [Internet]. 2020 Oct 7;63(10):1966–73.
        Available from: https://link.springer.com/10.1007/s00125-020-05203-7

4.   Leung PS. Common Pancreatic Disease. In 2010. p. 29–51. Available from:
        http://link.springer.com/10.1007/978-90-481-9060-7_3

5.   Tonini V, Zanni M. Pancreatic cancer in 2021: What you need to know to win. World J
        Gastroenterol [Internet]. 2021 Sep 21;27(35):5851–89. Available from:
        https://www.wjgnet.com/1007-9327/full/v27/i35/5851.htm

6.   Bray F, Ferlay J, Soerjomataram I, Siegel RL, Torre LA, Jemal A. Global cancer statistics 2018:
        GLOBOCAN estimates of incidence and mortality worldwide for 36 cancers in 185 countries.
        CA Cancer J Clin [Internet]. 2018 Nov;68(6):394–424. Available from:
        http://doi.wiley.com/10.3322/caac.21492

7.   Siegel RL, Miller KD, Fuchs HE, Jemal A. Cancer Statistics, 2021. CA Cancer J Clin [Internet].
        2021 Jan 12;71(1):7–33. Available from: https://onlinelibrary.wiley.com/doi/10.3322/caac.21654

8.   Fass L. Imaging and cancer: A review. Mol Oncol [Internet]. 2008 Aug;2(2):115–52. Available
        from: http://doi.wiley.com/10.1016/j.molonc.2008.04.001

9.   Cyran CC, Paprottka PM, Eisenblätter M, Clevert DA, Rist C, Nikolaou K, et al. Visualization,
        imaging and new preclinical diagnostics in radiation oncology. Radiat Oncol [Internet]. 2014
        Dec 3;9(1):3. Available from: https://ro-journal.biomedcentral.com/articles/10.1186/1748-717X-
        9-3

10.   Fritzberg AR, Kasina S, Eshima D, Johnson DL. Synthesis and biological evaluation of
        technetium-99m MAG3 as a hippuran replacement. J Nucl Med [Internet]. 1986 Jan;27(1):111–
        6. Available from: http://www.ncbi.nlm.nih.gov/pubmed/2934521

11.   Leonard JP, Nowotnik DP, Neirinckx RD. Technetium-99m-d,1-HM-PAO: A new
   radiopharmaceutical for imaging regional brain perfusion using SPECT - a comparison with
        iodine-123 HIPDM. J Nucl Med [Internet]. 1986 Dec;27(12):1819–23. Available from:
        http://www.ncbi.nlm.nih.gov/pubmed/3491188

12. A. Nock B, Maina T. Tetraamine-Coupled Peptides and Resulting 99mTc-Radioligands: An Effective Route for Receptor-Targeted Diagnostic Imaging of Human Tumors. Curr Top Med Chem [Internet]. 2013 Mar 1;12(23):2655–67. Available from: http://www.eurekaselect.com/openurl/content.php?genre=article&issn=1568-0266&volume=12&issue=23&spage=2655

13. Maina T, Thakur M. SPECT Radiochemistry. In: Molecular Imaging: Principles and Practice [Internet]. Elsevier; 2021. p. 479–92. Available from: https://linkinghub.elsevier.com/retrieve/pii/B9780128163863000235

14. Fani M, Maecke HR. Radiopharmaceutical development of radiolabelled peptides. Eur J Nucl Med Mol Imaging [Internet]. 2012 Feb 3;39(SUPPL.1):11–30. Available from: http://link.springer.com/10.1007/s00259-011-2001-z

15. Tan SY, Grimes S. Paul Ehrlich (1854-1915): man with the magic bullet. Singapore Med J [Internet]. 2010 Nov;51(11):842–3. Available from: http://www.ncbi.nlm.nih.gov/pubmed/21140107

16. Marinova M, Alamdar R, Ahmadzadehfar H, Essler M, Attenberger U, Mücke M, et al. Improving quality of life in patients with metastatic prostate cancer following one cycle of 177Lu-PSMA-617 radioligand therapy: A pilot study. NuklearMedizin [Internet]. 2020 Dec 21;59(6):409–14. Available from: http://www.thieme-connect.de/DOI/DOI?10.1055/a-1234-5891

17. Sun M, Niaz MO, Nelson A, Skafida M, Niaz MJ. Review of 177Lu-PSMA-617 in Patients With Metastatic Castration-Resistant Prostate Cancer. Cureus [Internet]. 2020 Jun 30; Available from: https://www.cureus.com/articles/34538-review-of-177lu-psma-617-in-patients-with-metastatic-castration-resistant-prostate-cancer

18. Benesová M, Schäfer M, Bauder-Wüst U, Afshar-Oromieh A, Kratochwil C, Mier W, et al. Preclinical evaluation of a tailor-made DOTA-conjugated PSMA inhibitor with optimized linker moiety for imaging and endoradiotherapy of prostate cancer. J Nucl Med [Internet]. 2015 Jun;56(6):914–20. Available from: http://jnm.snmjournals.org/lookup/doi/10.2967/jnumed.114.147413

19. Sonni I, Felker ER, Lenis AT, Sisk AE, Bahri S, Allen-Auerbach M, et al. Head-to-head comparison of 68Ga-PSMA-11 PET/CT and mpMRI with histopathology gold-standard in the detection, intra-prostatic localization and local extension of primary prostate cancer: results from a prospective single-center imaging trial. J Nucl Med [Internet]. 2022 Jun;63(6):847–54. Available from: http://jnm.snmjournals.org/lookup/doi/10.2967/jnumed.121.262398

20. Hope TA, Eiber M, Armstrong WR, Juarez R, Murthy V, Lawhn-Heath C, et al. Diagnostic Accuracy of 68Ga-PSMA-11 PET for Pelvic Nodal Metastasis Detection Prior to Radical Prostatectomy and Pelvic Lymph Node Dissection: A Multicenter Prospective Phase 3 Imaging

Trial. JAMA Oncol [Internet]. 2021 Nov 1;7(11):1635–42. Available from: https://jamanetwork.com/journals/jamaoncology/fullarticle/2783766

21.   Calais J, Zhu S, Hirmas N, Eiber M, Hadaschik B, Stuschke M, et al. Phase 3 multicenter randomized trial of PSMA PET/CT prior to definitive radiation therapy for unfavorable intermediate-risk or high-risk prostate cancer [PSMA dRT]: study protocol. BMC Cancer [Internet]. 2021 Dec 7;21(1):512. Available from: https://bmccancer.biomedcentral.com/articles/10.1186/s12885-021-08026-w

22.   Slovin SF. Targeting novel antigens for prostate cancer treatment: Focus on prostate-specific membrane antigen. Expert Opin Ther Targets [Internet]. 2005 Jun 10;9(3):561–70. Available from: http://www.tandfonline.com/doi/full/10.1517/14728222.9.3.561

23.   Bouchelouche K, Choyke PL, Capala J. Prostate specific membrane antigen- a target for imaging and therapy with radionuclides. Discov Med [Internet]. 2010 Jan;9(44):55–61. Available from: http://www.ncbi.nlm.nih.gov/pubmed/20102687

24.   Holloway CMB, Scollard DA, Caldwell CB, Ehrlich L, Kahn HJ, Reilly RM. Phase I trial of intraoperative detection of tumor margins in patients with HER2-positive carcinoma of the breast following administration of 111In-DTPA-trastuzumab Fab fragments. Nucl Med Biol [Internet]. 2013 Jul;40(5):630–7. Available from: https://linkinghub.elsevier.com/retrieve/pii/S096980511300053X

25.   Lodish M, Dagalakis U, Chen CC, Sinaii N, Whitcomb P, Aikin A, et al. 111In-octreotide scintigraphy for identification of metastatic medullary thyroid carcinoma in children and adolescents. J Clin Endocrinol Metab [Internet]. 2012 Feb;97(2):E207–12. Available from: https://academic.oup.com/jcem/article-lookup/doi/10.1210/jc.2011-2766

26.   Gruber L, Jiménez-Franco LD, Decristoforo C, Uprimny C, Glatting G, Hohenberger P, et al. MITIGATE-NeoBOMB1, a Phase I/IIa study to evaluate safety, pharmacokinetics, and preliminary imaging of 68Ga-NeoBOMB1, a gastrin-releasing peptide receptor antagonist, in GIST patients. J Nucl Med [Internet]. 2020 Dec;61(12):1749–55. Available from: http://jnm.snmjournals.org/lookup/doi/10.2967/jnumed.119.238808

27.   Reubi JC. Peptide receptors as molecular targets for cancer diagnosis and therapy. Endocr Rev [Internet]. 2003 Aug 1;24(4):389–427. Available from: https://academic.oup.com/edrv/article/24/4/389/2424257

28.   Mona CE, Benz MR, Hikmat F, Grogan TR, Lückerath K, Razmaria A, et al. Correlation of 68 Ga-FAPi-46 PET biodistribution with FAP expression by immunohistochemistry in patients with solid cancers: a prospective translational exploratory study . J Nucl Med [Internet]. 2021 Jul;63(7):jnumed.121.262426. Available from: http://jnm.snmjournals.org/lookup/doi/10.2967/jnumed.121.262426

29. Zhu H, Liu Q, Xu H, Mo M, Wang Z, Lu K, et al. Dose escalation based on 18F-FDG PET/CT response in definitive chemoradiotherapy of locally advanced esophageal squamous cell carcinoma: a phase III, open-label, randomized, controlled trial (ESO-Shanghai 12). Radiat Oncol [Internet]. 2022 Dec 29;17(1):134. Available from: https://ro-journal.biomedcentral.com/articles/10.1186/s13014-022-02099-y

30. Daliri EB-M, Lee BH, Oh DH. Current trends and perspectives of bioactive peptides. Crit Rev Food Sci Nutr [Internet]. 2018 Sep 2;58(13):2273–84. Available from: https://www.tandfonline.com/doi/full/10.1080/10408398.2017.1319795

31. Vlieghe P, Lisowski V, Martinez J, Khrestchatisky M. Synthetic therapeutic peptides: science and market. Drug Discov Today [Internet]. 2010 Jan;15(1–2):40–56. Available from: https://linkinghub.elsevier.com/retrieve/pii/S1359644609003705

32. Fredriksson R, Lagerström MC, Lundin LG, Schiöth HB. The G-protein-coupled receptors in the human genome form five main families. Phylogenetic analysis, paralogon groups, and fingerprints. Mol Pharmacol [Internet]. 2003 Jun;63(6):1256–72. Available from: http://molpharm.aspetjournals.org/lookup/doi/10.1124/mol.63.6.1256

33. Nieto Gutierrez A, McDonald PH. GPCRs: Emerging anti-cancer drug targets. Cell Signal [Internet]. 2018 Jan;41:65–74. Available from: https://linkinghub.elsevier.com/retrieve/pii/S0898656817302395

34. Heldin CH, Lu B, Evans R, Gutkind JS. Signals and receptors. Cold Spring Harb Perspect Biol [Internet]. 2016 Apr 1;8(4):a005900. Available from: http://cshperspectives.cshlp.org/lookup/doi/10.1101/cshperspect.a005900

35. Holik HA, Ibrahim FM, Elaine AA, Putra BD, Achmad A, Kartamihardja AHS. The Chemical Scaffold of Theranostic Radiopharmaceuticals: Radionuclide, Bifunctional Chelator, and Pharmacokinetics Modifying Linker. Molecules [Internet]. 2022 May 10;27(10):3062. Available from: https://www.mdpi.com/1420-3049/27/10/3062

36. Lin A, Giuliano CJ, Palladino A, John KM, Abramowicz C, Yuan M Lou, et al. Off-target toxicity is a common mechanism of action of cancer drugs undergoing clinical trials. Sci Transl Med [Internet]. 2019 Sep 11;11(509). Available from: https://www.science.org/doi/10.1126/scitranslmed.aaw8412

37. Rao MS, Gupta R, Liguori MJ, Hu M, Huang X, Mantena SR, et al. Novel Computational Approach to Predict Off-Target Interactions for Small Molecules. Front Big Data [Internet]. 2019 Jul 17;2. Available from: https://www.frontiersin.org/article/10.3389/fdata.2019.00025/full

38. A. Nock B, Maina T. Tetraamine-Coupled Peptides and Resulting 99mTc-Radioligands: An Effective Route for Receptor-Targeted Diagnostic Imaging of Human Tumors. Curr Top Med Chem [Internet]. 2013 Mar 1;12(23):2655–67. Available from:

http://www.eurekaselect.com/openurl/content.php?genre=article&issn=1568-0266&volume=12&issue=23&spage=2655

39. Nock BA, Maina T, Krenning EP, de Jong M. "To Serve and Protect": Enzyme Inhibitors as Radiopeptide Escorts Promote Tumor Targeting. J Nucl Med [Internet]. 2014 Jan;55(1):121–7. Available from: http://jnm.snmjournals.org/lookup/doi/10.2967/jnumed.113.129411

40. SKEGGS LT, KAHN JR, SHUMWAY NP. The preparation and function of the hypertensin-converting enzyme. J Exp Med [Internet]. 1956 Mar 1;103(3):295–9. Available from: https://rupress.org/jem/article/103/3/295/2211/THE-PREPARATION-AND-FUNCTION-OF-THE

41. Bernstein KE, Martin BM, Edwards AS, Bernstein EA. Mouse angiotensin-converting enzyme is a protein composed of two homologous domains. J Biol Chem [Internet]. 1989 Jul 15;264(20):11945–51. Available from: http://www.ncbi.nlm.nih.gov/pubmed/2545691

42. Soubrier F, Alhenc-Gelas F, Hubert C, Allegrini J, John M, Tregear G, et al. Two putative active centers in human angiotensin I-converting enzyme revealed by molecular cloning. Proc Natl Acad Sci U S A [Internet]. 1988 Dec;85(24):9386–90. Available from: https://pnas.org/doi/full/10.1073/pnas.85.24.9386

43. Vallee BL, Auld DS. Active-site zinc ligands and activated H2O of zinc enzymes. Proc Natl Acad Sci U S A [Internet]. 1990 Jan;87(1):220–4. Available from: https://pnas.org/doi/full/10.1073/pnas.87.1.220

44. Oparil S, Haber E. The Renin-Angiotensin System. N Engl J Med [Internet]. 1974 Aug 22;291(8):389–401. Available from: http://www.nejm.org/doi/abs/10.1056/NEJM197408222910805

45. Oparil S, Haber E. The Renin-Angiotensin System. N Engl J Med [Internet]. 1974 Aug 29;291(9):446–57. Available from: http://www.nejm.org/doi/abs/10.1056/NEJM197408292910905

46. Bruneval P, Hinglais N, Alhenc-Gelas F, Tricottet V, Corvol P, Menard J, et al. Angiotensin I converting enzyme in human intestine and kidney - Ultrastructural immunohistochemical localization. Histochemistry [Internet]. 1986;85(1):73–80. Available from: http://link.springer.com/10.1007/BF00508656

47. Defendini R, Zimmerman EA, Weare JA, Alhenc-Gelas F, Erdös EG. Angiotensin-converting enzyme in epithelial and neuroepithelial cells. Neuroendocrinology [Internet]. 1983;37(1):32–40. Available from: https://www.karger.com/Article/FullText/123512

48. Das M, Hartley JL, Soffers RL. Serum angiotensin converting enzyme. Isolation and relationship to the pulmonary enzyme. J Biol Chem [Internet]. 1977 Feb 25;252(4):1316–9. Available from: http://www.ncbi.nlm.nih.gov/pubmed/190228

49. El-Dorry HA, MacGregor JS, Soffer RL. Dipeptidyl carboxypeptidase from seminal fluid resembles the pulmonary rather than the testicular isoenzyme. Biochem Biophys Res Commun [Internet]. 1983 Sep;115(3):1096–100. Available from: https://linkinghub.elsevier.com/retrieve/pii/S0006291X83800485

50. Yasui T, Alhenc-Gelas F, Corvol P, Menard J. Angiotensin I-converting enzyme in amniotic fluid. J Lab Clin Med [Internet]. 1984 Nov;104(5):741–51. Available from: http://www.ncbi.nlm.nih.gov/pubmed/6092499

51. Schweisfurth H, Schioberg-Schiegnitz S. Assay and biochemical characterization of angiotensin-I-converting enzyme in cerebrospinal fluid. Enzyme [Internet]. 1984;32(1):12–9. Available from: https://www.karger.com/Article/FullText/469445

52. Roques BP. Zinc metallopeptidases: Active site structure and design of selective and mixed inhibitors: New approaches in the search for analgesics and anti-hypertensives. Biochem Soc Trans [Internet]. 1993 Aug 1;21(3):678–85. Available from: https://portlandpress.com/biochemsoctrans/article/21/3/678/83100/Zinc-metallopeptidases-Active-site-structure-and

53. Kerr MA, Kenny AJ. The purification and specificity of a neutral endopeptidase from rabbit kidney brush border. Biochem J [Internet]. 1974 Mar 1;137(3):477–88. Available from: https://portlandpress.com/biochemj/article/137/3/477/8800/The-purification-and-specificity-of-a-neutral

54. Kerr MA, Kenny AJ. The molecular weight and properties of a neutral metallo endopeptidase from rabbit kidney brush border. Biochem J [Internet]. 1974 Mar 1;137(3):489–95. Available from: https://portlandpress.com/biochemj/article/137/3/489/8767/The-molecular-weight-and-properties-of-a-neutral

55. Kenny AJ, Fulcher IS, McGill KA, Kershaw D. Proteins of the kidney microvillar membrane. Reconstitution of endopeptidase in liposomes shows that it is a short-stalked protein. Biochem J [Internet]. 1983 Jun 1;211(3):755–62. Available from: https://portlandpress.com/biochemj/article/211/3/755/15036/Proteins-of-the-kidney-microvillar-membrane

56. Relton JM, Gee NS, Matsas R, Turner AJ, Kenny AJ. Purification of endopeptidase-24.11 ('enkephalinase') from pig brain by immunoadsorbent chromatography. Biochem J [Internet]. 1983 Dec 1;215(3):519–23. Available from: https://portlandpress.com/biochemj/article/215/3/519/15483/Purification-of-endopeptidase-24-11-enkephalinase

57. Matsas R, Kenny AJ, Turner AJ. The metabolism of neuropeptides. The hydrolysis of peptides, including enkephalins, tachykinins and their analogues, by endopeptidase-24.11. Biochem J [Internet]. 1984 Oct 15;223(2):433–40. Available from:

https://portlandpress.com/biochemj/article/223/2/433/18941/The-metabolism-of-neuropeptides-The-hydrolysis-of

58. Roques BP, Noble F, Daugé V, Fournié-Zaluski MC, Beaumont A. Neutral endopeptidase 24.11: structure, inhibition, and experimental and clinical pharmacology. Pharmacol Rev [Internet]. 1993 Mar;45(1):87–146. Available from: http://www.ncbi.nlm.nih.gov/pubmed/8475170

59. Tiraboschi G, Jullian N, Thery V, Antonczak S, Fournie-Zaluski MC, Roques BP. A three-dimensional construction of the active site (region 507-749) of human neutral endopeptidase (EC.3.4.24.11). Protein Eng [Internet]. 1999 Feb;12(2):141–9. Available from: https://academic.oup.com/peds/article-lookup/doi/10.1093/protein/12.2.141

60. Rogues BP, Beaumont A. Neutral endopeptidase-24.11 inhibitors: from analgesics to antihypertensives? Trends Pharmacol Sci [Internet]. 1990 Jun;11(6):245–9. Available from: https://linkinghub.elsevier.com/retrieve/pii/0165614790902524

61. Howell S, Murray H, Scott CS, Turner AJ, Kenny AJ. A highly sensitive e.l.i.s.a. for endopeptidase-24.11, the common acute-lymphoblastic-leukaemia antigen (CALLA, CD-10), applicable to material of porcine and human origin. Biochem J [Internet]. 1991 Sep 1;278(2):417–21. Available from: https://portlandpress.com/biochemj/article/278/2/417/27252/A-highly-sensitive-e-l-i-s-a-for-endopeptidase-24

62. Turner AJ, Elwyn Isaac R, Coates D. The neprilysin (NEP) family of zinc metalloendopeptidases: Genomics and function. BioEssays [Internet]. 2001 Feb 13;23(3):261–9. Available from: https://onlinelibrary.wiley.com/doi/10.1002/1521-1878(200103)23:3%3C261::AID-BIES1036%3E3.0.CO;2-K

63. Kanellopoulos P, Nock BA, Krenning EP, Maina T. Optimizing the Profile of [99mTc]Tc–NT(7–13) Tracers in Pancreatic Cancer Models by Means of Protease Inhibitors. Int J Mol Sci [Internet]. 2020 Oct 26;21(21):7926. Available from: https://www.mdpi.com/1422-0067/21/21/7926

64. Kaloudi A, Lymperis E, Kanellopoulos P, Waser B, de Jong M, Krenning E, et al. Localization of 99mTc-GRP Analogs in GRPR-Expressing Tumors: Effects of Peptide Length and Neprilysin Inhibition on Biological Responses. Pharmaceuticals [Internet]. 2019 Mar 20;12(1):42. Available from: https://www.mdpi.com/1424-8247/12/1/42

65. Kanellopoulos P, Kaloudi A, Jong M de, Krenning EP, Nock BA, Maina T. Key-Protease Inhibition Regimens Promote Tumor Targeting of Neurotensin Radioligands. Pharmaceutics [Internet]. 2020 Jun 9;12(6). Available from: http://www.ncbi.nlm.nih.gov/pubmed/32526874

66. Nock BA, Kaloudi A, Kanellopoulos P, Janota B, Bromińska B, Iżycki D, et al. [99mTc]Tc-DB15 in GRPR-Targeted Tumor Imaging with SPECT: From Preclinical Evaluation to the First

Clinical Outcomes. Cancers (Basel) [Internet]. 2021 Oct 12;13(20):5093. Available from: https://www.mdpi.com/2072-6694/13/20/5093

67. Kanellopoulos P, Kaloudi A, Rouchota M, Loudos G, de Jong M, Krenning EP, et al. One Step Closer to Clinical Translation: Enhanced Tumor Targeting of [99mTc]Tc-DB4 and [111In]In-SG4 in Mice Treated with Entresto. Pharmaceutics [Internet]. 2020 Nov 26;12(12):1145. Available from: https://www.mdpi.com/1999-4923/12/12/1145

68. Eder AC, Schäfer M, Schmidt J, Bauder-Wüst U, Roscher M, Leotta K, et al. Rational linker design to accelerate excretion and reduce background uptake of peptidomimetic PSMA-targeting hybrid molecules. J Nucl Med [Internet]. 2021 Oct;62(10):1461–7. Available from: http://jnm.snmjournals.org/lookup/doi/10.2967/jnumed.120.248443

69. Guillou A, Earley DF, Klingler S, Nisli E, Nüesch LJ, Fay R, et al. The Influence of a Polyethylene Glycol Linker on the Metabolism and Pharmacokinetics of a 89Zr-Radiolabeled Antibody. Bioconjug Chem [Internet]. 2021 Jul 21;32(7):1263–75. Available from: https://pubs.acs.org/doi/10.1021/acs.bioconjchem.1c00172

70. Tedeschini T, Campara B, Grigoletto A, Bellini M, Salvalaio M, Matsuno Y, et al. Polyethylene glycol-based linkers as hydrophilicity reservoir for antibody-drug conjugates. J Control Release [Internet]. 2021 Sep;337:431–47. Available from: https://linkinghub.elsevier.com/retrieve/pii/S0168365921003849

71. Price EW, Orvig C. Matching chelators to radiometals for radiopharmaceuticals. Chem Soc Rev [Internet]. 2014;43(1):260–90. Available from: http://xlink.rsc.org/?DOI=C3CS60304K

72. Sun Y, Anderson CJ, Pajeau TS, Reichert DE, Hancock RD, Motekaitis RJ, et al. Indium(III) and gallium(III) complexes of bis(aminoethanethiol) ligands with different denticities: Stabilities, molecular modeling, and in vivo behavior. J Med Chem [Internet]. 1996 Jan 1;39(2):458–70. Available from: https://pubs.acs.org/doi/10.1021/jm9505977

73. Watanabe S, Hashimoto K, Ishioka NS. Lutetium-177 complexation of DOTA and DTPA in the presence of competing metals. J Radioanal Nucl Chem [Internet]. 2015 Feb 19;303(2):1519–21. Available from: http://link.springer.com/10.1007/s10967-014-3590-3

74. Bakker WH, Albert R, Bruns C, Breeman WAP, Hofland LJ, Marbach P, et al. [111In-DTPA-D-Phe1]-octreotide, a potential radiopharmaceutical for imaging of somatostatin receptor-positive tumors: synthesis, radiolabeling and in vitro validation. Life Sci [Internet]. 1991 Jan;49(22):1583–91. Available from: https://linkinghub.elsevier.com/retrieve/pii/002432059190052D

75. Garrison JC, Rold TL, Sieckman GL, Naz F, Sublett S V., Figueroa SD, et al. Evaluation of the pharmacokinetic effects of various linking group using the 111In-DOTA-X-BBN(7-14)NH2

structural paradigm in a prostate cancer model. Bioconjug Chem [Internet]. 2008 Sep 17;19(9):1803–12. Available from: https://pubs.acs.org/doi/10.1021/bc8001375

76.   Shannon RD. Revised effective ionic radii and systematic studies of interatomic distances in halides and chalcogenides. Acta Crystallogr Sect A [Internet]. 1976 Sep 1;32(5):751–67. Available from: http://scripts.iucr.org/cgi-bin/paper?S0567739476001551

77.   Lahnif H, Grus T, Pektor S, Greifenstein L, Schreckenberger M, Rösch F. Hybrid chelator-based PSMA radiopharmaceuticals: Translational approach. Molecules [Internet]. 2021 Oct 20;26(21):6332. Available from: https://www.mdpi.com/1420-3049/26/21/6332

78.   Maina T, Bergsma H, Kulkarni HR, Mueller D, Charalambidis D, Krenning EP, et al. Preclinical and first clinical experience with the gastrin-releasing peptide receptor-antagonist [68Ga]SB3 and PET/CT. Eur J Nucl Med Mol Imaging [Internet]. 2016 May 2;43(5):964–73. Available from: https://link.springer.com/10.1007/s00259-015-3232-1

79.   Lymperis E, Kaloudi A, Sallegger W, Bakker IL, Krenning EP, De Jong M, et al. Radiometal-Dependent Biological Profile of the Radiolabeled Gastrin-Releasing Peptide Receptor Antagonist SB3 in Cancer Theranostics: Metabolic and Biodistribution Patterns Defined by Neprilysin. Bioconjug Chem [Internet]. 2018 May 16;29(5):1774–84. Available from: https://pubs.acs.org/doi/10.1021/acs.bioconjchem.8b00225

80.   Kostelnik TI, Orvig C. Radioactive Main Group and Rare Earth Metals for Imaging and Therapy. Chem Rev [Internet]. 2019 Jan 23;119(2):902–56. Available from: https://pubs.acs.org/doi/10.1021/acs.chemrev.8b00294

81.   Cutler CS, Hennkens HM, Sisay N, Huclier-Markai S, Jurisson SS. Radiometals for Combined Imaging and Therapy. Chem Rev [Internet]. 2013 Feb 13;113(2):858–83. Available from: https://pubs.acs.org/doi/10.1021/cr3003104

82.   Notni J, Wester H-J. Re-thinking the role of radiometal isotopes: Towards a future concept for theranostic radiopharmaceuticals. J Label Compd Radiopharm [Internet]. 2018 Mar;61(3):141–53. Available from: https://onlinelibrary.wiley.com/doi/10.1002/jlcr.3582

83.   Wadas TJ, Wong EH, Weisman GR, Anderson CJ. Coordinating Radiometals of Copper, Gallium, Indium, Yttrium, and Zirconium for PET and SPECT Imaging of Disease. Chem Rev [Internet]. 2010 May 12;110(5):2858–902. Available from: https://pubs.acs.org/doi/10.1021/cr900325h

84.   R. Dilworth J, J. Parrott S. The biomedical chemistry of technetium and rhenium. Chem Soc Rev [Internet]. 1998;27(1):43. Available from: http://xlink.rsc.org/?DOI=a827043z

85.   Schwochau K. Technetium Radiopharmaceuticals—Fundamentals, Synthesis, Structure, and Development. Angew Chemie Int Ed English [Internet]. 1994 Dec 5;33(22):2258–67. Available from: https://onlinelibrary.wiley.com/doi/10.1002/anie.199422581

86. BAKER RJ. Preparation and properties of 99Tcm-exametazime using stannous ion augmentation of fractionated cold kits. Nucl Med Commun [Internet]. 1999 Mar;20(3):287–94. Available from: http://journals.lww.com/00006231-199903000-00013

87. Hungnes IN, Al-Salemee F, Gawne PJ, Eykyn T, Atkinson RA, Terry SYA, et al. One-step, kit-based radiopharmaceuticals for molecular SPECT imaging: A versatile diphosphine chelator for 99mTc radiolabelling of peptides. Dalt Trans [Internet]. 2021;50(44):16156–65. Available from: http://xlink.rsc.org/?DOI=D1DT03177E

88. Deutsch E, Heineman WR, Zodda JP, Gilbert TW, Williams CC. Preparation of "no-carrier-added" technetium-99m complexes: Determination of the total technetium content of generator eluents. Int J Appl Radiat Isot [Internet]. 1982 Oct;33(10):843–8. Available from: https://linkinghub.elsevier.com/retrieve/pii/0020708X82901260

89. SCHWOCHAU K. The Present Status of Technetium Chemistry. ract [Internet]. 1983 Jun 1;32(1–3):139–52. Available from: https://www.degruyter.com/document/doi/10.1524/ract.1983.32.13.139/html

90. Liu S, Edwards DS. 99m Tc-Labeled Small Peptides as Diagnostic Radiopharmaceuticals. Chem Rev [Internet]. 1999 Sep 8;99(9):2235–68. Available from: https://pubs.acs.org/doi/10.1021/cr980436l

91. Volkert WA, Troutner DE, Holmes RA. Labeling of amine ligands with 99mTc in aqueous solutions by ligand exchange. Int J Appl Radiat Isot [Internet]. 1982 Oct;33(10):891–6. Available from: https://linkinghub.elsevier.com/retrieve/pii/0020708X82901338

92. Bläuenstein P, Pfeiffer G, Schubiger PA, Anderegg G, Zollinger K, May K, et al. Chemical and biological properties of a cationic Tc-tetraamine complex. Int J Appl Radiat Isot [Internet]. 1985 Apr;36(4):315–7. Available from: https://linkinghub.elsevier.com/retrieve/pii/0020708X85900936

93. Herzog KM, Deutsch E, Deutsch K, Silberstein EB, Sarangarajan R, Cacini W. Synthesis and renal excretion of technetium-99m-labeled organic cations. J Nucl Med [Internet]. 1992 Dec;33(12):2190–5. Available from: http://www.ncbi.nlm.nih.gov/pubmed/1460514

94. Koźmiński P, Halik PK, Chesori R, Gniazdowska E. Common Shortcomings in Study on Radiopharmaceutical Design Research: A Case Study of 99mTc-Labelled Methotrexate. Molecules [Internet]. 2021 Sep 27;26(19):5862. Available from: https://www.mdpi.com/1420-3049/26/19/5862

95. Bormans G, Cleynhens B, Adriaens P, Vanbilloen H, De Roo M, Verbruggen A. Investigation of the labelling characteristics of 99mTc-mercaptoacetyltriglycine. Nucl Med Biol [Internet]. 1995 Apr;22(3):339–49. Available from: https://linkinghub.elsevier.com/retrieve/pii/096980519590920H

96. Straub M, Leresche M, Pilloud C, Devynck F, Stritt N, Hesselmann R. A new two-strip TLC method for the quality control of technetium-99m mercaptoacetyl-triglycine (99mTc-MAG3). EJNMMI Radiopharm Chem [Internet]. 2018 Dec 14;3(1):5. Available from: https://ejnmmipharmchem.springeropen.com/articles/10.1186/s41181-018-0040-5

97. Singhi AD, Koay EJ, Chari ST, Maitra A. Early Detection of Pancreatic Cancer: Opportunities and Challenges. Gastroenterology [Internet]. 2019 May;156(7):2024–40. Available from: https://linkinghub.elsevier.com/retrieve/pii/S0016508519303580

98. Pu Y, Wang C, Zhao S, Xie R, Zhao L, Li K, et al. The clinical application of 18F-FDG PET/CT in pancreatic cancer: a narrative review. Transl Cancer Res [Internet]. 2021 Jul;10(7):3560–75. Available from: https://tcr.amegroups.com/article/view/53150/html

99. Refardt J, Hofland J, Kwadwo A, Nicolas GP, Rottenburger C, Fani M, et al. Theranostics in neuroendocrine tumors: an overview of current approaches and future challenges. Rev Endocr Metab Disord [Internet]. 2021 Sep 3;22(3):581–94. Available from: https://link.springer.com/10.1007/s11154-020-09552-x

100. Reubi JC, Waser B, Friess H, Buchler M, Laissue J. Neurotensin receptors: a new marker for human ductal pancreatic adenocarcinoma. Gut [Internet]. 1998 Apr 1;42(4):546–50. Available from: https://gut.bmj.com/lookup/doi/10.1136/gut.42.4.546

101. Wang L, Friess H, Zhu Z, Graber H, Zimmermann A, Korc M, et al. Neurotensin receptor-1 mRNA analysis in normal pancreas and pancreatic disease. Clin Cancer Res [Internet]. 2000 Feb;6(2):566–71. Available from: http://www.ncbi.nlm.nih.gov/pubmed/10690540

102. Körner M, Waser B, Strobel O, Büchler M, Reubi JC. Neurotensin receptors in pancreatic ductal carcinomas. EJNMMI Res [Internet]. 2015 Dec 24;5(1):17. Available from: https://ejnmmires.springeropen.com/articles/10.1186/s13550-015-0094-2

103. Gilbert JA, Richelson E. Neurotensin stimulates formation of cyclic GMP in murine neuroblastoma clone N1E-115. Eur J Pharmacol [Internet]. 1984 Mar;99(2–3):245–6. Available from: https://linkinghub.elsevier.com/retrieve/pii/0014299984902486

104. Gilbert JA, Moses CJ, Pfenning MA, Richelson E. Neurotensin and its analogs—Correlation of specific binding with stimulation of cyclic GMP formation in neuroblastoma clone N1E-115. Biochem Pharmacol [Internet]. 1986 Feb;35(3):391–7. Available from: https://linkinghub.elsevier.com/retrieve/pii/0006295286902108

105. Vincent J-P. Neurotensin receptors: Binding properties, transduction pathways, and structure. Cell Mol Neurobiol [Internet]. 1995 Oct;15(5):501–12. Available from: http://link.springer.com/10.1007/BF02071313

106. Vincent J-P, Mazella J, Kitabgi P. Neurotensin and neurotensin receptors. Trends Pharmacol Sci [Internet]. 1999 Jul;20(7):302–9. Available from:

https://linkinghub.elsevier.com/retrieve/pii/S0165614799013577

107.   Mazella J, Vincent J-P. Functional roles of the NTS2 and NTS3 receptors. Peptides [Internet]. 2006 Oct;27(10):2469–75. Available from: https://linkinghub.elsevier.com/retrieve/pii/S019697810600297X

108.   Pelaprat D. Interactions between neurotensin receptors and G proteins. Peptides [Internet]. 2006 Oct;27(10):2476–87. Available from: https://linkinghub.elsevier.com/retrieve/pii/S0196978106002981

109.   Navarro V, Martin S, Sarret P, Nielsen MS, Petersen CM, Vincent J-P, et al. Pharmacological properties of the mouse neurotensin receptor 3. Maintenance of cell surface receptor during internalization of neurotensin. FEBS Lett [Internet]. 2001 Apr 20;495(1–2):100–5. Available from: http://doi.wiley.com/10.1016/S0014-5793%2801%2902367-5

110.   Mazella J. Sortilin/neurotensin receptor-3: a new tool to investigate neurotensin signaling and cellular trafficking? Cell Signal [Internet]. 2001 Jan;13(1):1–6. Available from: https://linkinghub.elsevier.com/retrieve/pii/S0898656800001303

111.   Paschoalin T, Carmona AK, Rodrigues EG, Oliveira V, Monteiro HP, Juliano MA, et al. Characterization of thimet oligopeptidase and neurolysin activities in B16F10-Nex2 tumor cells and their involvement in angiogenesis and tumor growth. Mol Cancer [Internet]. 2007 Dec 9;6(1):44. Available from: https://molecular-cancer.biomedcentral.com/articles/10.1186/1476-4598-6-44

112.   Berti DA, Morano C, Russo LC, Castro LM, Cunha FM, Zhang X, et al. Analysis of Intracellular Substrates and Products of Thimet Oligopeptidase in Human Embryonic Kidney 293 Cells. J Biol Chem [Internet]. 2009 May;284(21):14105–16. Available from: https://linkinghub.elsevier.com/retrieve/pii/S0021925820581192

113.   Skidgel RA, Engelbrecht S, Johnson AR, Erdös EG. Hydrolysis of substance P and neurotensin by converting enzyme and neutral endopeptidase. Peptides [Internet]. 1984 Jul;5(4):769–76. Available from: https://linkinghub.elsevier.com/retrieve/pii/0196978184900202

114.   Schindler L, Bernhardt G, Keller M. Modifications at Arg and Ile Give Neurotensin(8–13) Derivatives with High Stability and Retained NTS 1 Receptor Affinity. ACS Med Chem Lett [Internet]. 2019 Jun 13;10(6):960–5. Available from: https://pubs.acs.org/doi/10.1021/acsmedchemlett.9b00122

115.   Checler F, Vincent J-P, Kitabgi P. Degradation of Neurotensin by Rat Brain Synaptic Membranes: Involvement of a Thermolysin-Like Metalloendopeptidase (Enkephalinase), Angiotensin-Converting Enzyme, and Other Unidentified Peptidases. J Neurochem [Internet]. 1983 Aug;41(2):375–84. Available from: https://onlinelibrary.wiley.com/doi/10.1111/j.1471-4159.1983.tb04753.x

116. Kitabgi P, Dubuc I, Nouel D, Costentin J, Cuber J-C, Fulcrand H, et al. Effects of thiorphan, bestatin and a novel metallopeptidase inhibitor JMV 390-1 on the recovery of neurotensin and neuromedin N released from mouse hypothalamus. Neurosci Lett [Internet]. 1992 Aug;142(2):200–4. Available from: https://linkinghub.elsevier.com/retrieve/pii/030439409290373F

117. KITABGI P, NADAI F, ROVÈRE C, BIDARD J-N. Biosynthesis, Maturation, Release, and Degradation of Neurotensin and Neuromedin N. Ann N Y Acad Sci [Internet]. 1992 Oct;668(1 The Neurobiol):30–42. Available from: https://onlinelibrary.wiley.com/doi/10.1111/j.1749-6632.1992.tb27337.x

118. Yao J-F, Yang H, Zhao Y-Z, Xue M. Metabolism of Peptide Drugs and Strategies to Improve their Metabolic Stability. Curr Drug Metab [Internet]. 2018 Oct 2;19(11):892–901. Available from: http://www.eurekaselect.com/163325/article

119. Werle M, Föger F. Peroral peptide delivery: Peptidase inhibition as a key concept for commercial drug products. Bioorg Med Chem [Internet]. 2018 Jun;26(10):2906–13. Available from: https://linkinghub.elsevier.com/retrieve/pii/S0968089617308726

120. Heran BS, Wong MM, Heran IK, Wright JM. Blood pressure lowering efficacy of angiotensin converting enzyme (ACE) inhibitors for primary hypertension. Cochrane Database Syst Rev [Internet]. 2008 Oct 8; Available from: https://doi.wiley.com/10.1002/14651858.CD003823.pub2

121. Cuculi F, Erne P. Combined neutral endopeptidase inhibitors. Expert Opin Investig Drugs [Internet]. 2011 Apr 15;20(4):457–63. Available from: https://www.tandfonline.com/doi/full/10.1517/13543784.2011.556617

122. Li EC, Heran BS, Wright JM. Angiotensin converting enzyme (ACE) inhibitors versus angiotensin receptor blockers for primary hypertension. Cochrane Database Syst Rev [Internet]. 2014 Aug 22; Available from: https://doi.wiley.com/10.1002/14651858.CD009096.pub2

123. Abboud A, Januzzi JL. Reverse Cardiac Remodeling and ARNI Therapy. Curr Heart Fail Rep [Internet]. 2021 Apr 22;18(2):71–83. Available from: http://link.springer.com/10.1007/s11897-021-00501-6

124. Messerli FH, Kaesser UR. Lisinopril in the treatment of hypertension. J Hum Hypertens [Internet]. 1989 Jun;3 Suppl 1:17–21. Available from: http://www.ncbi.nlm.nih.gov/pubmed/2550640

125. Simpson K, Jarvis B. Lisinopril. Drugs [Internet]. 2000 May;59(5):1149–67. Available from: http://link.springer.com/10.2165/00003495-200059050-00012

126. Tsai T, Kroehl ME, Smith SM, Thompson AM, Dai IY, Trinkley KE. Efficacy and safety of twice- vs once-daily dosing of lisinopril for hypertension. J Clin Hypertens [Internet]. 2017 Sep;19(9):868–73. Available from: https://onlinelibrary.wiley.com/doi/10.1111/jch.13011

127. Cusack B, McCormick DJ, Pang Y-P, Souder T, Garcia R, Fauq A, et al. Pharmacological and Biochemical Profiles of Unique Neurotensin 8-13 Analogs Exhibiting Species Selectivity, Stereoselectivity, and Superagonism. J Biol Chem [Internet]. 1995 Aug;270(31):18359–66. Available from: https://linkinghub.elsevier.com/retrieve/pii/S0021925817463150

128. García-Garayoa E, Bläuenstein P, Bruehlmeier M, Blanc A, Iterbeke K, Conrath P, et al. Preclinical evaluation of a new, stabilized neurotensin(8--13) pseudopeptide radiolabeled with (99m)tc. J Nucl Med [Internet]. 2002 Mar;43(3):374–83. Available from: http://www.ncbi.nlm.nih.gov/pubmed/11884498

129. Bruehlmeier M, Garayoa EG, Blanc A, Holzer B, Gergely S, Tourwé D, et al. Stabilization of neurotensin analogues: effect on peptide catabolism, biodistribution and tumor binding. Nucl Med Biol [Internet]. 2002 Apr;29(3):321–7. Available from: https://linkinghub.elsevier.com/retrieve/pii/S0969805101003043

130. Maes V, Garcia-Garayoa E, Bläuenstein P, Tourwé D. Novel 99m Tc-Labeled Neurotensin Analogues with Optimized Biodistribution Properties. J Med Chem [Internet]. 2006 Mar 1;49(5):1833–6. Available from: https://pubs.acs.org/doi/10.1021/jm051172f

131. Nock BA, Nikolopoulou A, Reubi J-C, Maes V, Conrath P, Tourwé D, et al. Toward Stable N 4 - Modified Neurotensins for NTS1-Receptor-Targeted Tumor Imaging with 99m Tc. J Med Chem [Internet]. 2006 Jul 1;49(15):4767–76. Available from: https://pubs.acs.org/doi/10.1021/jm060415g

132. Maina T, Nikolopoulou A, Stathopoulou E, Galanis AS, Cordopatis P, Nock BA. [99mTc]Demotensin 5 and 6 in the NTS1-R-targeted imaging of tumours: synthesis and preclinical results. Eur J Nucl Med Mol Imaging [Internet]. 2007 Oct 17;34(11):1804–14. Available from: http://link.springer.com/10.1007/s00259-007-0489-z

133. HEYL DL, SEFLER NM, HE JX, SAWYER TK, WUSTROW DJ, AKUNNE HC, et al. Structure-activity and conformational studies of a series of modified C-terminal hexapeptide neurotensin analogues. Int J Pept Protein Res [Internet]. 2009 Jan 12;44(3):233–8. Available from: https://onlinelibrary.wiley.com/doi/10.1111/j.1399-3011.1994.tb00165.x

134. COUDER J, TOURWÉ D, BINST G, SCHUURKENS J, LEYSEN JE. Synthesis and biological activities of ψ(CH2NH) pseudopeptide analogues of the C-terminal hexapeptide of neurotensin. Int J Pept Protein Res [Internet]. 2009 Jan 12;41(2):181–4. Available from: https://onlinelibrary.wiley.com/doi/10.1111/j.1399-3011.1993.tb00129.x

135. Doulut S, Rodriguez M, Lugrin D, Vecchini F, Kitabgi P, Aumelas A, et al. Reduced peptide bond pseudopeptide analogues of neurotensin. Pept Res [Internet]. 5(1):30–8. Available from: http://www.ncbi.nlm.nih.gov/pubmed/1623301

136. Eiselt E, Gonzalez S, Martin C, Chartier M, Betti C, Longpré J-M, et al. Neurotensin Analogues Containing Cyclic Surrogates of Tyrosine at Position 11 Improve NTS2 Selectivity Leading to Analgesia without Hypotension and Hypothermia. ACS Chem Neurosci [Internet]. 2019 Nov 20;10(11):4535–44. Available from: https://pubs.acs.org/doi/10.1021/acschemneuro.9b00390

137. Previti S, Vivancos M, Rémond E, Beaulieu S, Longpré J-M, Ballet S, et al. Insightful Backbone Modifications Preventing Proteolytic Degradation of Neurotensin Analogs Improve NTS1-Induced Protective Hypothermia. Front Chem [Internet]. 2020 Jun 5;8. Available from: https://www.frontiersin.org/article/10.3389/fchem.2020.00406/full

138. Mascarin A, Valverde IE, Vomstein S, Mindt TL. 1,2,3-Triazole Stabilized Neurotensin-Based Radiopeptidomimetics for Improved Tumor Targeting. Bioconjug Chem [Internet]. 2015 Oct 21;26(10):2143–52. Available from: https://pubs.acs.org/doi/10.1021/acs.bioconjchem.5b00444

139. Mascarin A, Valverde IE, Mindt TL. Structure-Activity Relationship Studies of Amino Acid Substitutions in Radiolabeled Neurotensin Conjugates. ChemMedChem [Internet]. 2016 Jan;11(1):102–7. Available from: https://onlinelibrary.wiley.com/doi/10.1002/cmdc.201500468

140. Sparr C, Purkayastha N, Yoshinari T, Seebach D, Maschauer S, Prante O, et al. Syntheses, Receptor Bindings, in vitro and in vivo Stabilities and Biodistributions of DOTA-Neurotensin(8-13) Derivatives Containing β -Amino Acid Residues - A Lesson about the Importance of Animal Experiments. Chem Biodivers [Internet]. 2013 Dec;10(12):2101–21. Available from: https://onlinelibrary.wiley.com/doi/10.1002/cbdv.201300331

141. Craig AG, Norberg T, Griffin D, Hoeger C, Akhtar M, Schmidt K, et al. Contulakin-G, an O-Glycosylated Invertebrate Neurotensin. J Biol Chem [Internet]. 1999 May;274(20):13752–9. Available from: https://linkinghub.elsevier.com/retrieve/pii/S002192581973230X

142. Westerlind U, Norberg T. Chemical synthesis of analogs of the glycopeptide contulakin-G, an analgetically active conopeptide from Conus geographus. Carbohydr Res [Internet]. 2006 Jan;341(1):9–18. Available from: https://linkinghub.elsevier.com/retrieve/pii/S0008621505005203

143. Zaman R, Islam RA, Ibnat N, Othman I, Zaini A, Lee CY, et al. Current strategies in extending half-lives of therapeutic proteins. J Control Release [Internet]. 2019 May;301:176–89. Available from: https://linkinghub.elsevier.com/retrieve/pii/S0168365919300914

144. AlQahtani AD, O'Connor D, Domling A, Goda SK. Strategies for the production of long-acting therapeutics and efficient drug delivery for cancer treatment. Biomed Pharmacother [Internet]. 2019 May;113:108750. Available from: https://linkinghub.elsevier.com/retrieve/pii/S0753332219301623

145. Zhang L, Bulaj G. Converting Peptides into Drug Leads by Lipidation. Curr Med Chem [Internet]. 2012 Mar 1;19(11):1602–18. Available from:

http://www.eurekaselect.com/openurl/content.php?genre=article&issn=0929-8673&volume=19&issue=11&spage=1602

146. Lee H-K, Zhang L, Smith MD, Walewska A, Vellore NA, Baron R, et al. A marine analgesic peptide, Contulakin-G, and neurotensin are distinct agonists for neurotensin receptors: uncovering structural determinants of desensitization properties. Front Pharmacol [Internet]. 2015 Feb 10;6. Available from: http://journal.frontiersin.org/Article/10.3389/fphar.2015.00011/abstract

147. Zhang L, Lee H-K, Pruess TH, White HS, Bulaj G. Synthesis and Applications of Polyamine Amino Acid Residues: Improving the Bioactivity of an Analgesic Neuropeptide, Neurotensin. J Med Chem [Internet]. 2009 Mar 26;52(6):1514–7. Available from: https://pubs.acs.org/doi/10.1021/jm801481y

148. Einsiedel J, Hübner H, Hervet M, Härterich S, Koschatzky S, Gmeiner P. Peptide backbone modifications on the C-terminal hexapeptide of neurotensin. Bioorg Med Chem Lett [Internet]. 2008 Mar;18(6):2013–8. Available from: https://linkinghub.elsevier.com/retrieve/pii/S0960894X08001376

149. Stevens PW, Hansberry MR, Kelso DM. Assessment of Adsorption and Adhesion of Proteins to Polystyrene Microwells by Sequential Enzyme-Linked-Immunosorbent Assay Analysis. Anal Biochem [Internet]. 1995 Mar;225(2):197–205. Available from: https://linkinghub.elsevier.com/retrieve/pii/S000326978571144X

150. Vlasova IM, Saletsky AM. Study of the denaturation of human serum albumin by sodium dodecyl sulfate using the intrinsic fluorescence of albumin. J Appl Spectrosc [Internet]. 2009 Jul 16;76(4):536–41. Available from: http://link.springer.com/10.1007/s10812-009-9227-6

151. Liu S, Bilal M, Rizwan K, Gul I, Rasheed T, Iqbal HMN. Smart chemistry of enzyme immobilization using various support matrices – A review. Int J Biol Macromol [Internet]. 2021 Nov;190:396–408. Available from: https://linkinghub.elsevier.com/retrieve/pii/S0141813021019188

152. Gabriel M, Decristoforo C, Wöll E, Eisterer W, Nock B, Maina T, et al. Demotensin VI: Biodistribution and initial clinical results in tumor patients of a pilot/phase i study. Cancer Biother Radiopharm [Internet]. 2011 Oct;26(5):557–63. Available from: http://www.liebertpub.com/doi/10.1089/cbr.2010.0952

153. Kukkola PJ, Savage P, Sakane Y, Berry JC, Bilci NA, Ghai RD, et al. Differential structure-activity relationships of phosphoramidon analogues for inhibition of three metalloproteases: endothelin-converting enzyme, neutral endopeptidase, and angiotensin-converting enzyme. J Cardiovasc Pharmacol [Internet]. 1995;26 Suppl 3:S65-8. Available from: http://www.ncbi.nlm.nih.gov/pubmed/8587470

154. Frackenpohl J, Arvidsson PI, Schreiber J V., Seebach D. The Outstanding Biological Stability ofβ- andγ-Peptides toward Proteolytic Enzymes: An In Vitro Investigation with Fifteen Peptidases. ChemBioChem [Internet]. 2001 Jun 1;2(6):445–55. Available from: https://onlinelibrary.wiley.com/doi/10.1002/1439-7633(20010601)2:6%3C445::AID-CBIC445%3E3.0.CO;2-R

155. Steer D, Lew R, Perlmutter P, Smith A, Aguilar M-I. β-Amino Acids: Versatile Peptidomimetics. Curr Med Chem [Internet]. 2002 Apr 1;9(8):811–22. Available from: http://www.eurekaselect.com/openurl/content.php?genre=article&issn=0929-8673&volume=9&issue=8&spage=811

156. De Pol S, Zorn C, Klein CD, Zerbe O, Reiser O. Surprisingly Stable Helical Conformations inα/β-Peptides by Incorporation ofcis-β-Aminocyclopropane Carboxylic Acids. Angew Chemie Int Ed [Internet]. 2004 Jan 16;43(4):511–4. Available from: https://onlinelibrary.wiley.com/doi/10.1002/anie.200352267

157. Sleep D. Albumin and its application in drug delivery. Expert Opin Drug Deliv [Internet]. 2015 May 4;12(5):793–812. Available from: http://www.tandfonline.com/doi/full/10.1517/17425247.2015.993313

158. Elsadek B, Kratz F. Impact of albumin on drug delivery — New applications on the horizon. J Control Release [Internet]. 2012 Jan;157(1):4–28. Available from: https://linkinghub.elsevier.com/retrieve/pii/S0168365911008546

159. van der Vusse GJ. Albumin as Fatty Acid Transporter. Drug Metab Pharmacokinet [Internet]. 2009;24(4):300–7. Available from: http://linkinghub.elsevier.com/retrieve/pii/S1347436715301154

160. Zorzi A, Middendorp SJ, Wilbs J, Deyle K, Heinis C. Acylated heptapeptide binds albumin with high affinity and application as tag furnishes long-acting peptides. Nat Commun [Internet]. 2017 Dec 17;8(1):16092. Available from: http://www.nature.com/articles/ncomms16092

161. Wang J, Ueno H, Masuko T, Hashimoto Y. Binding of Serum Albumin on Tumor Cells and Characterization of the Albumin Binding Protein. J Biochem [Internet]. 1994 May;115(5):898–903. Available from: https://academic.oup.com/jb/article/759690/Binding

162. Stremmel W, Pohl J, Ring A, Herrmann T. A new concept of cellular uptake and intracellular trafficking of long-chain fatty acids. Lipids [Internet]. 2001 Sep;36(9):981–9. Available from: http://doi.wiley.com/10.1007/s11745-001-0809-2

163. Dumelin CE, Trüssel S, Buller F, Trachsel E, Bootz F, Zhang Y, et al. A Portable Albumin Binder from a DNA-Encoded Chemical Library. Angew Chemie Int Ed [Internet]. 2008 Apr 14;47(17):3196–201. Available from: https://onlinelibrary.wiley.com/doi/10.1002/anie.200704936

164. Müller C, Struthers H, Winiger C, Zhernosekov K, Schibli R. DOTA Conjugate with an Albumin-Binding Entity Enables the First Folic Acid–Targeted 177 Lu-Radionuclide Tumor Therapy in Mice. J Nucl Med [Internet]. 2013 Jan;54(1):124–31. Available from: http://jnm.snmjournals.org/lookup/doi/10.2967/jnumed.112.107235

165. Zhang X, Wang H, Ma Z, Wu B. Effects of pharmaceutical PEGylation on drug metabolism and its clinical concerns. Expert Opin Drug Metab Toxicol [Internet]. 2014 Dec 30;10(12):1691–702. Available from: http://www.tandfonline.com/doi/full/10.1517/17425255.2014.967679

166. Montero MT, Estelrich J, Valls O. Binding of non-steroidal anti-inflammatory drugs to human serum albumin. Int J Pharm [Internet]. 1990 Jul;62(1):21–5. Available from: https://linkinghub.elsevier.com/retrieve/pii/0378517390900272

167. Itoh T, Saura Y, Tsuda Y, Yamada H. Stereoselectivity and enantiomer-enantiomer interactions in the binding of ibuprofen to human serum albumin. Chirality [Internet]. 1997;9(7):643–9. Available from: https://onlinelibrary.wiley.com/doi/10.1002/(SICI)1520-636X(1997)9:7%3C643::AID-CHIR1%3E3.0.CO;2-8

168. Deberle LM, Benešová M, Umbricht CA, Borgna F, Büchler M, Zhernosekov K, et al. Development of a new class of PSMA radioligands comprising ibuprofen as an albumin-binding entity. Theranostics [Internet]. 2020;10(4):1678–93. Available from: http://www.thno.org/v10p1678.htm

169. Abiraj K, Mansi R, Tamma M-L, Fani M, Forrer F, Nicolas G, et al. Bombesin Antagonist–Based Radioligands for Translational Nuclear Imaging of Gastrin-Releasing Peptide Receptor–Positive Tumors. J Nucl Med [Internet]. 2011 Dec;52(12):1970–8. Available from: http://jnm.snmjournals.org/lookup/doi/10.2967/jnumed.111.094375

170. Jamous M, Tamma ML, Gourni E, Waser B, Reubi JC, Maecke HR, et al. PEG spacers of different length influence the biological profile of bombesin-based radiolabeled antagonists. Nucl Med Biol [Internet]. 2014 Jul;41(6):464–70. Available from: https://linkinghub.elsevier.com/retrieve/pii/S0969805114000894

171. Varasteh Z, Rosenström U, Velikyan I, Mitran B, Altai M, Honarvar H, et al. The Effect of Mini-PEG-Based Spacer Length on Binding and Pharmacokinetic Properties of a 68Ga-Labeled NOTA-Conjugated Antagonistic Analog of Bombesin. Molecules [Internet]. 2014 Jul 17;19(7):10455–72. Available from: http://www.mdpi.com/1420-3049/19/7/10455

172. Kanellopoulos P, Lymperis E, Kaloudi A, de Jong M, Krenning EP, Nock BA, et al. [99mTc]Tc-DB1 Mimics with Different-Length PEG Spacers: Preclinical Comparison in GRPR-Positive Models. Molecules [Internet]. 2020 Jul 28;25(15):3418. Available from: https://www.mdpi.com/1420-3049/25/15/3418

173. Alshoukr F, Rosant C, Maes V, Abdelhak J, Raguin O, Burg S, et al. Novel Neurotensin Analogues for Radioisotope Targeting to Neurotensin Receptor-Positive Tumors. Bioconjug Chem [Internet]. 2009 Aug 19;20(8):1602–10. Available from: https://pubs.acs.org/doi/10.1021/bc900151z

174. Alshoukr F, Prignon A, Brans L, Jallane A, Mendes S, Talbot J-N, et al. Novel DOTA-Neurotensin Analogues for 111 In Scintigraphy and 68 Ga PET Imaging of Neurotensin Receptor-Positive Tumors. Bioconjug Chem [Internet]. 2011 Jul 20;22(7):1374–85. Available from: https://pubs.acs.org/doi/10.1021/bc200078p

175. Baum RP, Singh A, Schuchardt C, Kulkarni HR, Klette I, Wiessalla S, et al. 177 Lu-3BP-227 for Neurotensin Receptor 1–Targeted Therapy of Metastatic Pancreatic Adenocarcinoma: First Clinical Results. J Nucl Med [Internet]. 2018 May;59(5):809–14. Available from: http://jnm.snmjournals.org/lookup/doi/10.2967/jnumed.117.193847

176. Schulz J, Rohracker M, Stiebler M, Goldschmidt J, Stöber F, Noriega M, et al. Proof of Therapeutic Efficacy of a 177 Lu-Labeled Neurotensin Receptor 1 Antagonist in a Colon Carcinoma Xenograft Model. J Nucl Med [Internet]. 2017 Jun;58(6):936–41. Available from: http://jnm.snmjournals.org/lookup/doi/10.2967/jnumed.116.185140

177. Schulz J, Rohracker M, Stiebler M, Goldschmidt J, Grosser OS, Osterkamp F, et al. Comparative Evaluation of the Biodistribution Profiles of a Series of Nonpeptidic Neurotensin Receptor-1 Antagonists Reveals a Promising Candidate for Theranostic Applications. J Nucl Med [Internet]. 2016 Jul;57(7):1120–3. Available from: http://jnm.snmjournals.org/lookup/doi/10.2967/jnumed.115.170530

178. Chen TR, Drabkowski D, Hay RJ, Macy M, Peterson W. WiDr is a derivative of another colon adenocarcinoma cell line, HT-29. Cancer Genet Cytogenet [Internet]. 1987 Jul;27(1):125–34. Available from: https://linkinghub.elsevier.com/retrieve/pii/0165460887902676

179. Buchegger F, Bonvin F, Kosinski M, Schaffland AO, Prior J, Reubi JC, et al. Radiolabeled neurotensin analog, 99mTc-NT-XI, evaluated in ductal pancreatic adenocarcinoma patients. J Nucl Med [Internet]. 2003 Oct;44(10):1649–54. Available from: http://www.ncbi.nlm.nih.gov/pubmed/14530481

180. Hodolic M, Wu W-Y, Zhao Z, Yu F, Virgolini I, Wang F. Safety and tolerability of 68Ga-NT-20.3, a radiopharmaceutical for targeting neurotensin receptors, in patients with pancreatic ductal adenocarcinoma: the first in-human use. Eur J Nucl Med Mol Imaging [Internet]. 2021 Apr 2;48(4):1229–34. Available from: https://link.springer.com/10.1007/s00259-020-05045-w

Curriculum Vitae

Panagiotis Kanellopoulos

Date of birth: 1-10-1990

+30 2106503891

+30 6978213303

kanelospan@gmail.com

Working experience:

25/07/2018 - : Postgraduate associate, program: "**Radiolabeled Vectors in Nuclear Oncology" (E-12224)**, **NCSR "Demokritos"**, project director: Maina–Nock Theodosia

06/08/2014-16/02/2015: **QC/QA for the small soap idustry** "Saponaria", Papapetrou Gavala 89, Heraklion, Crete, Greece

Studies:

18/04/2019- : **PhD candidate, School of Medicine, University of Crete,** supervisor: Prof. Liapakis George. Lab of thesis elaboration: Molecular Radiopharmacy, INRASTES, NCSR "Demokritos", Supervisor, Research Director: Maina–Nock Theodosia

May-June 2019: Educational seminar «6th international Lab Animal Course Crete 2019 FELASA accredited»

2014-16: **MSc "Neuroscience",** School of Medicine, University of Crete

2008-14: **Bachelor degree in Chemistry**, Department of Chemistry, University of Crete

Scholarships – Awards:

09-12/2021: **Scholarship** as an exchange PhD student from Theranostics group, BMC, Uppsala University

Teaching/Training Experience:

2019-2021: Laboratory training of BSc and MSc students from the same institute or abroad on procedures and protocols on molecular radiopharmacy. (e.g: students from M.Sc. Oncology: From Oncogenesis to Therapy, School of Medicine, University of Crete, National Hellenic Research Foundation)

<u>Foreign Languages:</u>

English: **Level 1 Certificate of English, University of Cambridge**

<u>Thesis:</u>

2016:   Master Thesis, title: **Subcloning the type 2 CRF receptor gene and pharmacological characterization of receptor.** Lab: Molecular Pharmacology, Supervisor: Prof. Liapakis George

2013:   Bachelor Thesis**,** title: **Can the acquired drug resistance, of the protozoan parasite Leishmania, be maintained after passage in macrophages of the human cell line THP-1.** Lab: Laboratory of Clinical Bacteriology Parasitology Zoonoses and Geographical Medicine. Supervisor: Antoniou Maria, Professor in charge: Katerinopoulos HE

<u>Other activities:</u>

2003-2008: Classical guitar, up to intermediate level

1999-2003: Participating in a local basketball team

Publications in Peer-Review Scientific Journals: 11; Presentations in Scientific Meetings: 16

List of Publications

Publications in Peer-Review Scientific Journals (11)

1. Nock BA, **Kanellopoulos P**, Chepurny OG, Rouchota M, Loudos G, Holz GG, Krenning EP, Maina T. Nonpeptidic Z360-Analogs Tagged with Trivalent Radiometals as Anti-CCK$_2$R Cancer Theranostic Agents: A Preclinical Study. Pharmaceutics. 2022 Mar 18;14(3):666. doi: 10.3390/pharmaceutics14030666. PMID: 35336041; PMCID: PMC8954547.

2. Nock BA, Kaloudi A, **Kanellopoulos P**, Janota B, Bromińska B, Iżycki D, Mikołajczak R, Czepczynski R, Maina T. [^{99m}Tc]Tc-DB15 in GRPR-Targeted Tumor Imaging with SPECT: From Preclinical Evaluation to the First Clinical Outcomes. Cancers (Basel). **2021** Oct 12;13(20):5093. doi: 10.3390/cancers13205093. PMID: 34680243; PMCID: PMC8533986.

3. **Kanellopoulos P**, Kaloudi A, Rouchota M, Loudos G, de Jong M, Krenning EP, Nock BA, Maina T. One Step Closer to Clinical Translation: Enhanced Tumor Targeting of [^{99m}Tc]Tc-DB4 and [^{111}In]In-SG4 in Mice Treated with Entresto. *Pharmaceutics*. **2020**;26;12(12):1145. doi: 10.3390/pharmaceutics12121145.

4. **Kanellopoulos P,** Nock BA, Krenning EP, Maina T. Optimizing the Profile of [^{99m}Tc]Tc-NT(7-13) Tracers in Pancreatic Cancer Models by Means of Protease Inhibitors. *Int J Mol Sci*. **2020**;26;21(21):7926. doi: 10.3390/ijms21217926.

5. **Kanellopoulos P**, Lymperis E, Kaloudi A, de Jong M, Krenning EP, Nock BA, Maina T. [^{99m}Tc]Tc-DB1 Mimics with Different-Length PEG Spacers: Preclinical Comparison in GRPR-Positive Models. *Molecules* **2020**;25(15):3418. doi: 10.3390/molecules25153418.

6. Kaloudi A, **Kanellopoulos P**, Radolf T, Chepurny OG, Rouchota M, Loudos G, Andreae F, Holz GG, Nock BA, Maina T. [^{99m}Tc]Tc-DGA1, a Promising CCK$_2$R-Antagonist-Based Tracer for Tumor Diagnosis with Single-Photon Emission Computed Tomography. *Mol Pharm.* **2020**;17(8):3116-3128. doi: 10.1021/acs.molpharmaceut.0c00605.

7. **Kanellopoulos P**, Kaloudi A, Jong M, Krenning EP, Nock BA, Maina T. Key-Protease Inhibition Regimens Promote Tumor Targeting of Neurotensin Radioligands. *Pharmaceutics*. **2020**;12(6):528. doi: 10.3390/pharmaceutics12060528.

8. Lymperis E, Kaloudi A, **Kanellopoulos P**, Krenning EP, de Jong M, Maina T, Nock BA. Comparative evaluation of the new GRPR-antagonist ^{111}In-SB9 and ^{111}In-AMBA in prostate cancer models: Implications of *in vivo* stability. *J Labelled Comp Radiopharm*. **2019**;62(10):646-655. doi: 10.1002/jlcr.3733.

9. Kaloudi A, Lymperis E, **Kanellopoulos P**, Waser B, de Jong M, Krenning EP, Reubi JC, Nock BA, Maina T. Localization of ^{99m}Tc-GRP Analogs in GRPR-Expressing Tumors: Effects of Peptide Length and Neprilysin Inhibition on Biological Responses. *Pharmaceuticals*. **2019**;12(1):42. doi: 10.3390/ph12010042.

10. Lymperis E, Kaloudi A, **Kanellopoulos P**, de Jong M, Krenning EP, Nock BA, Maina T. Comparing Gly[11]/dAla[11]-Replacement vs. the in-Situ Neprilysin-Inhibition Approach on the Tumor-targeting Efficacy of the ^{111}In-SB3/^{111}In-SB4 Radiotracer Pair. *Molecules*. **2019**;24(6):1015. doi: 10.3390/molecules24061015.

11. **Kanellopoulos P**, Dokianakis E, Tsirigotakis N, Koutala E, Antoniou M. Assessment of the infectivity potential of Leishmania infantum, using flow cytometry. *Exp Parasitol*. **2014**;145:29-33. doi: 10.1016/j.exppara.2014.07.005.

Presentations in Scientific Meetings (16)

1. **Kanellopoulos P**, Karageorgos V, Gelain A, Spyridaki K, Villa S. and Liapakis G., 2016, Pharmacological properties of novel GnRH analogues, *9th Panhellenic Symposium of the Hellenic Association of Basic and Clinical Pharmacology*. Thessaloniki, 20-22 May, 2016.

2. Maina T, Kaloudi A, **Kanellopoulos P**, Chepurney O, Holz GG, Nock BA. [99mTc]DGA1, a novel radiotracer based on a CCK_2R-antagonist for diagnostic imaging of human cancer: First comparisons with [99mTc]DG2. *WCA-2019*, Valencia, Spain, May 8-9, 2019.

3. **Kanellopoulos P**, Kaloudi A, Nock BA, Krenning EP, Maina T. Structural intervention vs. protease-inhibition methods to improve NTS1R-tumor uptake of neurotensin radiotracers: A preclinical comparison of 99mTc-DT1 and 99mTc-DT6. *WCA-2019*, Valencia, Spain, May 8-9, 2019.

4. **Kanellopoulos P**, Kaloudi A, de Jong M, Krenning EP, Nock BA, Maina T. One step closer to clinical translation: Notably enhanced localization of [111In]SG4 in CCK_2R-positive xenografts in mice treated with Entresto®. *Annual Congress of the EANM*, October 12–16, 2019, Barcelona, Spain; *Eur. J. Nucl. Med. Mol. Imaging*. 46 (Suppl. 1): OP-706, S269-S270; 2019.

5. **Kanellopoulos P**, Kaloudi A, de Jong M, Krenning EP, Maina T, Nock BA. Entresto®-treated mice show superior targeting of PC-3 xenografts vs. controls after injection of the SPECT tracer [99mTc]DB4. *Annual Congress of the EANM*, October 12–16, 2019, Barcelona, Spain; *Eur. J. Nucl. Med. Mol. Imaging*. 46 (Suppl. 1): EP-0699, S704-S705; 2019.

6. **Kanellopoulos P**, Kaloudi A, Giannoutsos I, de Jong M, Krenning EP, Nock BA, Maina T. [99mTc]Demobesin analogs with different length PEG spacers: Effects on biological responses in GRPR-positive cells and animal models. *Cyprus Society of Nuclear Medicine Anniversary Congress*, November 6–10, 2019, Limassol, Cyprus; *World J Nucl Med*. 18(Suppl. 1): 103, S2;2019.

7. **Kanellopoulos P**, Kaloudi A, Krenning EP, Nock BA, Maina T. Preclinical comparison of 99mTc-DT1 and 99mTc-DT6: The impact of cell internalization and *in vivo* stability on radiotracer uptake in NTS1-positive WiDr xenografts in mice. *Cyprus Society of Nuclear Medicine*

Anniversary Congress, November 6–10, 2019, Limassol, Cyprus (**poster award**); *World J Nucl Med.* 18(Suppl. 1): 104, S2-S3;2019.

8. **Kanellopoulos P**, Krenning EP, Nock BA, Maina T. Exchange of Ile^{12} by Tle^{12} in NT(8-13) based radiotracers: Effects on internalization, stability and tumor uptake. *15th Annual Meeting of the European Society for Molecular Imaging – ESMI, European Molecular Imaging Meeting - EMIM 2020*, 25 - 28 August 2020 HELEXPO, Thessaloniki, Greece.

9. **Kanellopoulos P**, Lymperis E, Kaloudi A, de Jong M, Krenning EP, Nock BA, Maina T. Effects of different-length PEG spacers on the biological responses of ^{99m}Tc-DB1 mimics in GRPR-positive preclinical models. *15th Annual Meeting of the European Society for Molecular Imaging – ESMI, European Molecular Imaging Meeting - EMIM 2020*, 25 - 28 August 2020 HELEXPO, Thessaloniki, Greece.

10. Maina T, **Kanellopoulos P**, Krenning EP, Nock BA. Recent breakthroughs in GRPR-targeted cancer theranostics - The role of radiopeptide analogs. *World Cancer Actions (WCA-2020)*, Oct 12 - 13, 2020, Brussels, Belgium. (Accepted for Oral Presentation).

11. **Kanellopoulos P**, Nock BA, Krenning EP, Maina T. Pancreatic cancer & NTS1R, revisiting an old molecular target with the aid of clinically established peptidase-inhibitor(s). *World Cancer Actions (WCA-2020)*, Oct 12 - 13, 2020, Brussels, Belgium. (Accepted for Oral Presentation)

12. **Kanellopoulos P**, Nock BA, Krenning EP, Maina T. The effect on *in situ* inhibition of NEP and/or ACE on tumor targeting of a technetium-99m labeled biodegradable neurotensin(7-13) based radiotracer. 15th International Conference on Radiopharmaceutical Therapy (ICRT), December 5-6, 2020, virtual congress.

13. **Kanellopoulos P**, Nock BA, Krenning EP, Maina T. Metabolic stability and tumor uptake improvements via an ABD-arm in [99mTc]Tc-DT10: First preclinical experiences in pancreatic cancer models. TERACHEM 2022, September 14-17, 2022, Bressanone, Italy (accepted abstract).

14. **Kanellopoulos P**, Nock BA, Baum RP, Roesch F, Maina T. First experiences with the SST$_2$R-antagonist [^{68}Ga]Ga-DATA-LM4 for PET imaging of tumors – Preclinical comparison with [^{68}Ga]Ga-DOTA-LM3. TERACHEM 2022, September 14-17, 2022, Bressanone, Italy (accepted for oral presentation).

15. Abouzayed A, Gorislav A, **Kanellopoulos P**, Tolmachev V, Maina T, Nock BA, Orlova A. Development of a stabilized GRPR antagonist for targeted cancer theranostics.TERACHEM 2022, September 14-17, 2022, Bressanone, Italy (accepted abstract).

16. Abouzayed A, Gorislav A, **Kanellopoulos P**, Tolmachev V, Maina T, Nock BA, Orlova A. Preclinical characterization of a stabilized GRPR antagonist for targeted cancer theranostics. *Annual Congress of the EANM*, October 15–19, 2022, Barcelona, Spain (accepted for oral precentation)

Publication – reprints

Article

Key-Protease Inhibition Regimens Promote Tumor Targeting of Neurotensin Radioligands

Panagiotis Kanellopoulos [1,2] **, Aikaterini Kaloudi** [1] **, Marion de Jong** [3] **, Eric P. Krenning** [4] **, Berthold A. Nock** [1] **and Theodosia Maina** [1,*]

1 Molecular Radiopharmacy, INRASTES, NCSR "Demokritos", 15341 Athens, Greece; kanelospan@gmail.com (P.K.); katerinakaloudi@yahoo.gr (A.K.); nock_berthold.a@hotmail.com (B.A.N.)
2 Molecular Pharmacology, School of Medicine, University of Crete, 70013 Heraklion, Greece
3 Department of Radiology & Nuclear Medicine Erasmus MC, 3015 CN Rotterdam, The Netherlands; m.hendriks-dejong@erasmusmc.nl
4 Cyclotron Rotterdam BV, Erasmus MC, 3015 CE Rotterdam, The Netherlands; erickrenning@gmail.com
* Correspondence: maina_thea@hotmail.com; Tel.: +30-210-650-3908

check for updates

Abstract: Neurotensin subtype 1 receptors (NTS1R) represent attractive molecular targets for directing radiolabeled neurotensin (NT) analogs to tumor lesions for diagnostic and therapeutic purposes. This approach has been largely undermined by the rapid in vivo degradation of linear NT-based radioligands. Herein, we aim to increase the tumor targeting of three ^{99m}Tc-labeled NT analogs by the in-situ inhibition of two key proteases involved in their catabolism. DT1 ([N_4-Gly^7]NT(7-13)), DT5 ([N_4-βAla^7,Dab^9]NT(7-13)), and DT6 ([N_4-βAla^7,Dab^9,Tle^{12}]]NT(7-13)) were labeled with ^{99m}Tc. Their profiles were investigated in NTS1R-positive colon adenocarcinoma WiDr cells and mice treated or not with the neprilysin (NEP)-inhibitor phosphoramidon (PA) and/or the angiotensin converting enzyme (ACE)-inhibitor lisinopril (Lis). Structural modifications led to the partial stabilization of ^{99m}Tc-DT6 in peripheral mice blood (55.1 ± 3.9% intact), whereas ^{99m}Tc-DT1 and ^{99m}Tc-DT5 were totally degraded within 5 min. Coinjection of PA and/or Lis significantly stabilized all three analogs, leading to a remarkable enhancement of tumor uptake for ^{99m}Tc-DT1 and ^{99m}Tc-DT5, but was less effective in the case of poorly internalizing ^{99m}Tc-DT6. In conclusion, NEP and/or ACE inhibition represents a powerful tool to improve tumor targeting and the overall pharmacokinetics of NT-based radioligands, and warrants further validation in the field of NTS1R-targeted tumor imaging and therapy.

Keywords: neurotensin; neurotensin subtype 1 receptor; ^{99m}Tc-radiotracer; tumor targeting; protease-inhibition; neprilysin-inhibitor; angiotensin-converting enzyme-inhibitor

1. Introduction

Recent advances in nuclear medicine include personalized treatment of cancer patients, whereby molecular probes are administered to deliver diagnostic or therapeutic radionuclides to cancer cells with high specificity. For example, peptide analogs may be used as carriers of gamma (^{99m}Tc, ^{111}In) or positron emitters (^{68}Ga, ^{64}Cu) for diagnostic single photon emission computed tomography (SPECT) or positron emission tomography (PET) imaging to identify patients eligible for radionuclide therapy. Therapy per se is then operated by the peptide analog carrying the respective therapeutic radionuclide (a beta, ^{177}Lu, ^{90}Y, Auger electron, ^{111}In, or an alpha emitter, ^{225}Ac) to upload cytotoxic radiation doses selectively to tumor lesions [1–5]. The rationale of this integrated "theranostic" approach relies on the overexpression of the target biomolecule in cancer cells while healthy surrounding tissues remain devoid of target expression [6].

Accordingly, the neurotensin subtype 1 receptor (NTS1R) [7,8] has been regarded as an attractive molecular target for such purposes owing to its high density expression in many human cancers [9,10]. Thus, high NTS1R expression has been documented in pancreatic ductal adenocarcinoma [11–13], Ewing's sarcoma [14], colon carcinoma [15], prostate [16] and breast cancer [17], as well as other cancer types [18]. This finding offers the opportunity to develop theranostic NTS1R-directed radioligands based on the native tridecapeptide neurotensin (NT) for oncological applications. In recent years, many such analogs have been developed, whereby the C-terminal hexapeptide NT(8-13) representing the shortest fragment retaining full binding affinity for the NTS1R [19], served as motif. Several metal-chelators were coupled to its N-terminus, either directly or via different linkers, to accommodate a variety of clinical relevant radiometals [20–29].

Preclinical evaluation of resulting radiotracers revealed their propensity to proteolytic degradation, impairing their tumor targeting in animal models. Further NTS1R-directed radiotracers were designed by structural changes in the NT(8-13) motif, such as key-amino acid substitutions and/or manipulation of peptide bonds, like reduction, methylation or introduction of triazoles, aiming to metabolic stability improvements [30–34]. It should be noted however that radioligand stability was assessed mainly by the in vitro incubation of analogs in mice or human serum and not in vivo. Furthermore, these structural interventions often led to suboptimal pharmacokinetics, especially with regards to unfavorable increases of kidney uptake. Eventually, three NTS1R-radioligands were selected for clinical validation, but the overall results in patients turned out to be disappointing presumably as a result of fast in vivo catabolism [35–37].

Three cleavage sites have been identified in NT and NT(8-13), including the Arg^8-Arg^9 bond, the Pro^{10}-Tyr^{11} bond and the Tyr^{11}-Ile^{12} bond. A number of proteases have been shown to participate in the fast in-vivo catabolism of these peptides and their analogs. Thus, the angiotensin converting enzyme (ACE) is involved in the rapid cleavage of the Tyr^{11}-Ile^{12} bond, whereas neprilysin (NEP) cleaves both the Pro^{10}-Tyr^{11} and the Tyr^{11}-Ile^{12} bonds [38–42]. It should be noted that NEP is an ectoenzyme present in high densities in many body tissues including vasculature epithelial cells [43,44]. Given that in plasma and serum NEP is practically absent, its impact on NTS1R-radioligand stability cannot be reliably assessed by in vitro incubation studies in the abovementioned biological fluids but should rather be conducted in vivo [33].

We have recently proposed a new strategy to improve the metabolic stability and hence the tumor targeting of radioligands from several peptide families via in situ inhibition of key-proteases involved in their catabolism. Protease-inhibition may be achieved by the co-administration of selected inhibitors together with the biodegradable radiopeptide and has led to marked enhancement of tumor uptake in animal models and most importantly also in human [45–49].

We have decided to explore the efficacy of this promising strategy for the first time in the field of NTS1R-radiopeptides. For this purpose, herein, we compare the biological profile of three acyclic tetraamine-coupled NT(7-13) analogs suitable for labeling with the SPECT radionuclide ^{99m}Tc (Figure 1), namely DT1 ([N_4-Gly^7]NT(7-13)), DT5 ([N_4-βAla^7,Dab^9]NT(7-13)), and DT6 ([N_4-βAla^7,Dab^9,Tle^{12}]]NT(7-13)). Although the synthesis and biological data for these analogs in NTS1R-expressing cells and animal models were previously reported [23,24], in the present study, we mainly focus on the impact of in situ NEP and/or ACE inhibition on the in vivo stability and pharmacokinetic profile of these structurally related analogs. Protease inhibition has been achieved by treatment of mice with the NEP-inhibitor phosphoramidon (PA) [50] and/or the ACE inhibitor lisinopril (Lis) [51]. Findings from this study are discussed in relation to structural modifications of the NT(8-13) motif.
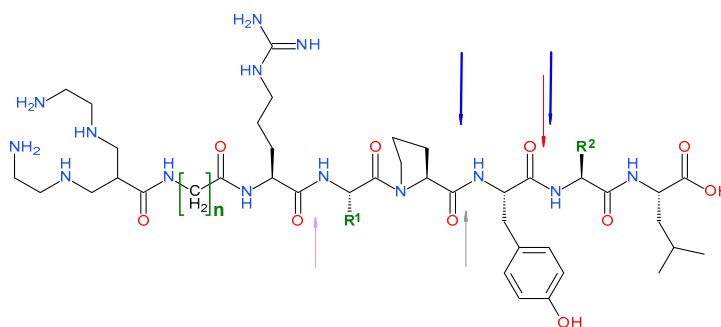
Figure 1. Structure of DT1 (n = 1, Gly; R^1 = $(CH_2)_3$-NH-C=NH-NH$_2$, Arg; R^2 = $CH(CH_3)CH_2CH_3$, Ile); DT5 (n = 2, βAla; R^1 = $(CH_2)_2$-NH$_2$, Dab; R^2 = $CH(CH_3)CH_2CH_3$, Ile) and DT6 (n = 2, βAla; R^1 = $(CH_2)_2$-NH$_2$, Dab; R^2 = $C(CH_3)_3$, Tle); arrows indicate peptidase cleavage sites, violet: EC 3.4.24.15, gray: EC 3.4.24.16, blue: NEP and red: ACE.

2. Materials and Methods

2.1. Peptide Analogs – Protease Inhibitors

The DT1 (N$_4$-Gly-Arg-Arg-Pro-Tyr-Ile-Leu-OH, N$_4$ = 6-(carboxy)-1,4,8,11-tetraazaundecane), DT5 (N$_4$-βAla-Arg-Dab-Pro-Tyr-Ile-Leu-OH) and DT6 (N$_4$-βAla-Arg-Dab-Pro-Tyr-Tle-Leu-OH) peptide conjugates (Figure 1) synthesized on the solid support as previously reported [23,24] were provided by PiChem (Graz, Austria). Neurotensin (NT = Pyr-Leu-Tyr-Glu-Asn-Lys-Pro-Arg-Arg-Pro-Tyr-Ile-Leu-OH) was purchased from Bachem (Bubendorf, Switzerland). The NEP-inhibitor PA (phosphoramidon disodium dehydrate, *N*-(α-rhamnopyranosyloxy-hydroxyphosphinyl)-L-leucyl-L -tryptophan × 2Na × 2H$_2$O) was obtained from PeptaNova GmbH (Sandhausen, Germany) and the ACE-inhibitor Lis (lisinopril dehydrate, ((S)1–1-[N2-(1-carboxy-3-phenylpropyl)-lysyl-proline dehydrate, MK 521) from Sigma–Aldrich (St. Louis, MO, USA).

Preparation and Quality Control of ^{99m}Tc-DT1, ^{99m}Tc-DT5 and ^{99m}Tc-DT6

Each of lyophilized DT1, DT5 or DT6 was dissolved in HPLC-grade H$_2$O (2 mg/mL) and 50 µL aliquots thereof were stored in Eppendorf Protein LoBind tubes at −20 °C. Labeling with ^{99m}Tc was conducted in an Eppendorf vial, wherein the following solutions were consecutively added: i) 0.5 M phosphate buffer pH 11.5 (50 µL), ii) 0.1 M sodium citrate (5 µL), iii) [^{99m}Tc]NaTcO$_4$ generator eluate (415 mL, 300–500 MBq; Ultra-Technekow™ V4 Generator, Curium Pharma), iv) peptide conjugate stock solution (15 µL, 15 nmol) and v) freshly made SnCl$_2$ solution in EtOH (30 µg, 15 µL). After reaction for 30 min at ambient temperature, the pH was brought to ~7 by adding 1 M HCl (10 µL).

Reversed-phase HPLC was performed on a Waters Chromatograph based on a 600E multisolvent delivery system coupled to a Waters 2998 photodiode array detector and a Gabi gamma-detector (Raytest, RSM Analytische Instrumente GmbH, Straubenhardt, Germany). Data processing and chromatography were controlled by the Empower Software (Waters, Vienna, Austria). For quality control aliquots of the radiolabeling solution a Symmetry Shield RP18 cartridge column (5 µm, 3.9 × 20 mm, Waters) was used for analyses. Solutes were eluted with 0.1% TFA/MeCN applying a linear gradient starting from 0% MeCN and a 2% increase per min at 1 mL/min flow rate (system 1). TLC analysis was additionally performed on Whatman 3 mm chromatography paper strips (GE Healthcare, Chicago, IL, USA), developed up to 10 cm from the origin with 5 M ammonium acetate/MeOH 1/1 (*v*/*v*) for ^{99m}TcO$_2$ × *n*H$_2$O, or acetone for ^{99m}TcO$_4$$^-$ detection [23,24]. The radiochemical labeling yield exceeded 98% and the radiochemical purity was >99%. Samples of ^{99m}Tc-DT1, ^{99m}Tc-DT5 and ^{99m}Tc-DT6 were tested before and after the end of biological experiments.

All manipulations with beta and gamma emitting radionuclides and their solutions were performed by trained and authorized personnel behind suitable shielding in licensed laboratories in compliance

to European radiation-safety guidelines and supervised by the Greek Atomic Energy Commission (license # A/435/17092/2019).

2.2. In Vitro Assays

2.2.1. Cell Lines and Culture

Human colorectal adenocarcinoma WiDr cells (LGC Promochem, Teddington, UK) expressing the human NTS1R [52] were cultured in McCoy's GLUTAMAX-I (Gibco BRL, Life Technologies, Grand Island, NY, USA) supplemented by 10% (*v/v*) fetal bovine serum (FBS), 100 U/mL penicillin and 100 µg/mL streptomycin (all from Biochrom KG Seromed, Berlin, Germany). Cells were kept in a controlled humidified atmosphere containing 5% CO_2 at 37 °C. Passages were performed every 4–5 days using a trypsin/EDTA (0.05%/0.02% *w/v*) solution.

2.2.2. Internalization Assay in WiDr Cells

The overall cell association–internalization of ^{99m}Tc-DT1, ^{99m}Tc-DT5 and ^{99m}Tc-DT6 was assessed in confluent WiDr cells. Briefly, the cells were seeded in six-well plates (~1×10^6 cells per well) 24 h before the experiment. Each of ^{99m}Tc-DT1, ^{99m}Tc-DT5 and ^{99m}Tc-DT6 (approximately 150,000 cpm, 250 fmol total peptide in 150 µL of 0.5% BSA/PBS) was added alone (total) or in the presence of 1 µM NT (non-specific). Cells were incubated at 37 °C for 1 h and incubation was interrupted by placing the plates on ice, removing the supernatants and rapid rinsing with ice-cold 0.5% BSA/PBS. Cells were then treated 2×5 min with acid wash buffer (2×0.6 mL, 50 mM glycine buffer, pH 2.8, 0.1 M NaCl) at room temperature and supernatants were collected (membrane-bound fraction). After rinsing with 1 mL chilled 0.5% BSA/PBS, cells were lyzed by treatment with 1 N NaOH (2×0.6 mL) and lysates were collected (internalized fraction). Sample radioactivity was measured in the γ-counter (an automated well-type gamma counter with a NaI(Tl) 3'' crystal, Canberra Packard Auto-Gamma 5000 series instrument) and total cell-associated (internalized + membrane bound) radioactivity was determined vs. total added activity. Results represent the average values ± sd of 3 experiments in triplicate.

2.3. Animal Studies

All animal studies were performed in compliance to European guidelines in supervised and licensed facilities (EL 25 BIO 021), whereas the study protocols were approved by the Department of Agriculture and Veterinary Service of the Prefecture of Athens (protocol numbers # 1609 for the stability studies and # 1610 for biodistribution and imaging studies).

2.3.1. In Vivo Stability Tests

For stability experiments, healthy male Swiss albino mice (30 ± 5 g, NCSR "Demokritos" Animal House Facility) were used. Each radioligand, ^{99m}Tc-DT1, ^{99m}Tc-DT5, or ^{99m}Tc-DT6, was injected as a 100 µL bolus (50–60 MBq, 3 nmol total peptide in vehicle: saline/EtOH 9/1 *v/v*) in the tail vein together with vehicle (100 µL; control) or with i) a phosphoramidon (PA)-solution (100 µL injection solution containing 300 µg PA), ii) a Lis solution (100 µL injection solution containing 200 µg Lis), or iii) a solution of both inhibitors (100 µL injection solution containing 300 µg PA plus 200 µg Lis). Animals were euthanized and blood (0.5–1 mL) was directly withdrawn from the heart and transferred in a pre-chilled EDTA-containing Eppendorf tube on ice. Blood samples were centrifuged for 10 min at 2000× *g*/4 °C and plasma was collected. After addition of an equal volume of ice-cold MeCN the mixture was centrifuged for 10 min at 15,000× *g* and 4 °C. The supernatant was concentrated under a N_2-flux at 40 °C to 0.05–0.1 mL, diluted with saline (0.4 mL), filtered through a 0.22 µm Millex GV filter (Millipore, Milford, MA, USA) and analyzed by RP-HPLC. The Symmetry Shield RP18 (5 µm, 3.9 mm × 20 mm) column was eluted at a flow rate of 1.0 mL/min applying a linear gradient starting with 0% B at 0 min and reaching to 30% B in 30 min; A = 0.1 % TFA in water and

B = MeCN (system 2). The t_R of the intact radiopeptide was determined by coinjection with the respective ^{99m}Tc-DT1, ^{99m}Tc-DT5, or ^{99m}Tc-DT6 reference in the HPLC.

2.3.2. Induction of WiDr Xenografts in Mice

A suspension containing freshly harvested human WiDr cells (≈150 µL of a ≈1.8 × 10^7 cells) was subcutaneously injected in the flanks of male severe combined immune deficiency (SCID) mice (20 ± 3 g, six weeks of age at the day of arrival, NCSR "Demokritos" Animal House Facility). The animals were kept under aseptic conditions and 3 weeks later developed well-palpable tumors (100–300 mg) at the inoculation sites.

2.3.3. Biodistribution of ^{99m}Tc-Radiotracers in WiDr Xenograft-Bearing SCID Mice

For the biodistribution study, animals in groups of 4 received via the tail vein a 100 µL bolus of ^{99m}Tc-DT1, ^{99m}Tc-DT5 or ^{99m}Tc-DT6 (180–230 kBq, corresponding to 10 pmol total peptide) co-injected either with injection solution (100 µL; control) or i) a PA-solution (^{99m}Tc-DT1 and ^{99m}Tc-DT6), or ii) a Lis-solution (^{99m}Tc-DT1 and ^{99m}Tc-DT6), iii) a PA plus Lis-solution (^{99m}Tc-DT1, ^{99m}Tc-DT5 and ^{99m}Tc-DT6), or iv) an excess NT (100 µL injection solution containing 100 µg NT for in vivo NTS1R-blockade along with PA+Lis); ^{99m}Tc-DT1, or ^{99m}Tc-DT6). Animals were euthanized at 4 h post-injection (pi) and dissected. Samples of blood, tumors, and organs of interest were collected, weighed, and measured for radioactivity in the gamma counter. Intestines and stomach were not emptied of their contents. Data was calculated as percent injected dose per gram tissue (%ID/g) with the aid of standard solutions and represent mean values ± sd, *n* = 4.

2.3.4. Statistical Analysis

For statistical analysis of biological results, the two-way ANOVA with multiple comparisons was used applying Tukey's post hoc analysis (GraphPad Prism Software, San Diego, CA, USA). *P* values of <0.05 were considered to be statistically significant. For cell-association experiments, the one-way ANOVA with Tukey's post hoc analysis was used instead.

2.3.5. SPECT/CT Imaging of ^{99m}Tc-DT1 in WiDr Xenograft-Bearing SCID Mice

For SPECT/CT imaging, three mice bearing WiDr xenografts were injected in the tail vein with a bolus containing ^{99m}Tc-DT1 (100 µL, ≈50 MBq, 1.5 nmol total peptide, in vehicle) together with vehicle (100 µL; controls) or with a PA+Lis solution or with a PA+Lis solution in gelofusin (100 µL; Gelo) and were euthanized at 3 h pi. Tomographic SPECT/CT imaging was performed with the y-CUBE/x-CUBE systems (Molecubes, Belgium). The SPECT system is based on monolithic NaI detectors attached to SiPMs, with a 0.6 mm intrinsic resolution. The CT system is based on a structured CMOS detector of CsI with pixels of 75 µm and operates between 35 and 80 kVp, 10–500 µA tube current, with a 33 µm fixed focal spot size. SPECT scans were acquired over 3 h pi, with a 30 min duration protocol based on the injected activity and each SPECT scan was succeeded by a CT scan, following a general purpose protocol under 50 kVp, for co-registration purposes. SPECT images were reconstructed by the MLEM reconstruction method with a 250 µm voxel size and 500 iterations. CT images were reconstructed by using the ISRA reconstruction method with a 100 µm voxel size. Images were exported and post-processed on VivoQuant software, version 4.0 (Invicro, Boston, MA, USA). A smoothing median filter (0.6 mm, spherical window) was applied to the images and bladder was removed for consistency purposes.

3. Results

3.1. Peptides and Radioligands

Labeling of DT1, DT5 and DT6 with ^{99m}Tc typically proceeded by brief peptide-conjugate incubation with ^{99m}TcO$_4^-$ generator eluate, SnCl$_2$ as reducing agent and citrate anions as transfer

ligand in alkaline pH at ambient temperature and molecular activities of 20–40 MBq ^{99m}Tc/nmol peptide. Quality control of the radiolabeled products combined HPLC and TLC analysis. The total radiochemical impurities, comprising ^{99m}TcO$_4^-$, [^{99m}Tc]citrate and ^{99m}TcO$_2 \times n$H$_2$O, did not exceed 2%, while a single radiopeptide species was detected by RP-HPLC. In view of >98% labeling yields and >99% radiochemical purity of the resultant ^{99m}Tc-DT1, ^{99m}Tc-DT5 or ^{99m}Tc-DT6, the radioligands were used without further purification in all subsequent experiments.

3.2. In Vitro Assays

Comparative Internalization of ^{99m}Tc-DT1, ^{99m}Tc-DT5 or ^{99m}Tc-DT6 in WiDr Cells

During 1 h incubation at 37°C, ^{99m}Tc-DT1, ^{99m}Tc-DT5 or ^{99m}Tc-DT6 were taken up by WiDr cells via an NTS1R-mediated process, as shown by the lack of uptake observed in the presence of excess NT (results not shown). In all cases, the bulk of cell-bound radioactivity was found in the internalized fraction, as consistent with a radioagonist profile. The radioligand rank of cell uptake/internalization was ^{99m}Tc-DT1 (10.1 ± 2.3%/6.9 ± 2.1%) >> ^{99m}Tc-DT5 (3.7 ± 0.3%/3.2 ± 0.3%) > ^{99m}Tc-DT6 (1.0 ± 0.4%/0.8 ± 0.4%), revealing the negative effect of structurally modifying ^{99m}Tc-DT1 on cell uptake (Figure 2).
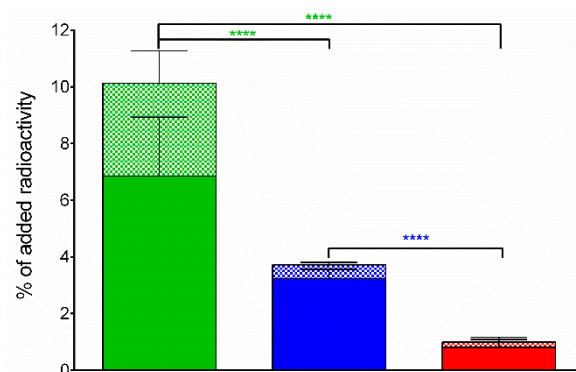
Figure 2. NTS1R-specific cell uptake of ^{99m}Tc-DT1 (green bars), ^{99m}Tc-D5 (blue bars) and ^{99m}Tc-DT6 (red bars) in WiDr cells during 1 h incubation at 37 °C (solid bars: internalized fraction; checkered bars: membrane bound fraction). Results represent average values ± sd (n = 3, in triplicate); non-specific values were obtained in the presence of 1 µM NT and were subtracted from totals to provide specific values; the study was conducted with WiDr cells as confluent monolayers. Statistical analysis is shown for whole-cell association with **** representing $P < 0.0001$.

3.3. In Vivo Comparison of ^{99m}Tc-DT1, ^{99m}Tc-DT5 or ^{99m}Tc-DT6

3.3.1. Stability of ^{99m}Tc-DT1, ^{99m}Tc-DT5 and ^{99m}Tc-DT6 in Mice

The radiotracers exhibited distinct resistance to degrading proteases after injection in mice. As revealed by HPLC analysis of blood samples collected at 5 min pi ^{99m}Tc-DT1 and ^{99m}Tc-DT5 were found equally fast degraded (1.8 ± 0.8% and 1.3 ± 0.2% intact; $P > 0.05$) whereas the Tle^{12}-analog ^{99m}Tc-DT6 displayed significantly higher stability (55.1 ± 3.9% intact; $P < 0.0001$) (Table 1; representative radiochromatograms are shown in Figure 3).

Table 1. Stabilities of ^{99m}Tc-DT1, ^{99m}Tc-DT5 and ^{99m}Tc-DT6 in peripheral mouse blood 5 min pi.

	^{99m}Tc-DT1	^{99m}Tc-DT5	^{99m}Tc-DT6
Control	1.8 ± 0.8 ($n = 4$)	1.3 ± 0.2 ($n = 2$)	55.1 ± 3.9 ($n = 2$)
PA	26.4 ± 2.2 ($n = 2$)	15.4 ± 5.1 ($n = 2$)	89.3 ± 6.7 ($n = 4$)
Lis	18.8 ± 2.5 ($n = 3$)	28.8 ± 5.2 ($n = 2$)	-
PA+Lis	72.3 ± 3.2 ($n = 4$)	79.0 ± 1.7 ($n = 2$)	-

Data represents the mean percentage of intact radioligand ± sd; *n* of experiments are shown in parentheses.

It should be noted that coinjection of the NEP-inhibitor PA enhanced the in vivo stability of all three radioligands, implicating NEP in their degradation. PA was particularly effective in stabilizing ^{99m}Tc-DT6 in mice blood, showing NEP as the major degrading protease of the radiotracer.
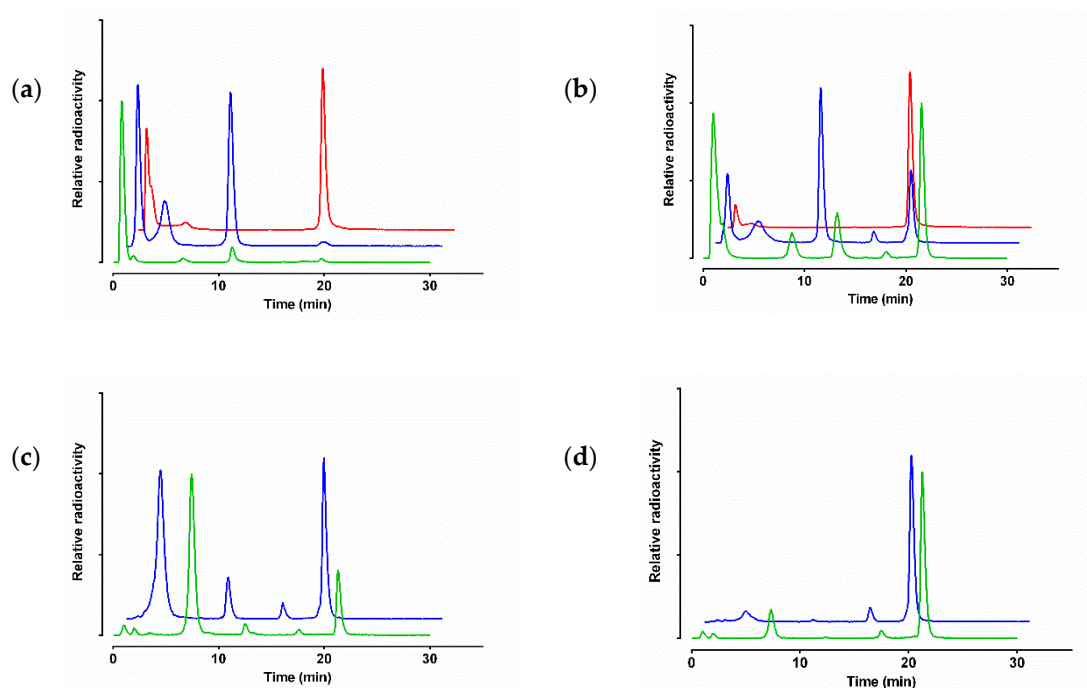
Figure 3. Representative radiochromatograms of HPLC analysis of mouse blood samples collected 5 min pi of ^{99m}Tc-DT1 (green line), ^{99m}Tc-DT5 (blue line) or ^{99m}Tc-DT6 (red line) administered (**a**) without, or (**b**) with PA-, or (**c**) with Lis-, or (**d**) with PA+Lis-coinjection (HPLC system 2); percentages of intact radioligand are summarized in Table 1.

On the other hand, coinjection of the ACE-inhibitor Lis enhanced the in vivo stability of ^{99m}Tc-DT1 and ^{99m}Tc-DT5, revealing the role of this second protease in their in vivo degradation. It is interesting to note that treatment of mice with both protease-inhibitors resulted in a further rigorous enhancement of metabolic stability in peripheral mice blood (72.3 ± 3.2% and 79.0 ± 6.7% intact, respectively; $P < 0.0001$).

3.3.2. Biodistribution of ^{99m}Tc-DT1, ^{99m}Tc-DT5 and ^{99m}Tc-DT6 in WiDr Xenograft-Bearing Mice

The biodistribution of ^{99m}Tc-DT1, ^{99m}Tc-DT5 and ^{99m}Tc-DT6 was studied at 4 h pi in SCID mice bearing subcutaneous WiDr tumors expressing the human NTS1R. Cumulative biodistribution results for ^{99m}Tc-DT1, ^{99m}Tc-DT5 and ^{99m}Tc-DT6 are summarized in Tables 2–4, respectively, and are expressed as mean %ID/g ± sd, $n = 4$. All three radiotracers washed rapidly from the blood and the body of mice predominantly via the kidneys and the urinary system in the control animal groups. However, the Dab^9-modified analogs ^{99m}Tc-DT5 (8.63 ± 1.8%ID/g; $P < 0.001$) and ^{99m}Tc-DT6 (6.09 ± 1.15%ID/g; $P < 0.01$) showed significantly higher renal retention compared to ^{99m}Tc-DT1 (1.80 ± 0.14%ID/g).

Uptake in the intestines was comparable across radioligands ($P > 0.05$) and could be partially blocked by excess NT, given that intestines were not emptied of their contents and NTS1R are expressed in the intestinal walls [53]. Likewise, uptake in the implanted tumors was comparable across analogs ($P > 0.05$).

Treatment of mice with PA and Lis resulted in remarkable enhancement of tumor uptake of ^{99m}Tc-DT1 (from 1.20 ± 0.21%ID/g to 9.60 ± 3.62%ID/g; $P < 0.0001$) and ^{99m}Tc-DT5 (from 0.88 ± 0.08%ID/g to 12.29 ± 2.73%ID/g; $P < 0.0001$) and only to a lesser, but not in statistically significant extent in the case of ^{99m}Tc-DT6 (from 1.68 ± 0.28%ID/g to 3.50 ± 0.34%ID/g; $P > 0.05$). This enhancement is compromised for both ^{99m}Tc-DT5 and ^{99m}Tc-DT6 by a further unfavorable increase of the already elevated renal accumulation. It is interesting to observe that for ^{99m}Tc-DT6 the PA alone suffices to achieve the highest tumor uptake (PA and PA+Lis tumor values $P > 0.05$), while both inhibitors are required for maximum in vivo stabilization and highest tumor values for ^{99m}Tc-DT1 and ^{99m}Tc-DT5.

Table 2. Biodistribution data for ^{99m}Tc-DT1, expressed as %ID/g mean $\pm$ sd, $n = 4$, in WiDr xenograft-bearing SCID mice at 4 h pi without or with coinjection of PA, Lis, or PA+Lis.

Tissue	^{99m}Tc-DT1 – 4 h pi				
	Block [1]	Controls	4 h PA [2]	Lis [3]	PA+Lis [4]
Blood	0.07 ± 0.02	0.15 ± 0.01	0.12 ± 0.03	0.10 ± 0.01	0.13 ± 0.06
Liver	0.42 ± 0.02	0.42 ± 0.02	0.47 ± 0.05	0.39 ± 0.05	0.58 ± 0.12
Heart	0.05 ± 0.01	0.08 ± 0.00	0.10 ± 0.02	0.08 ± 0.02	0.10 ± 0.02
Kidneys	2.89 ± 0.56	1.80 ± 0.14	2.26 ± 0.30	2.24 ± 0.34	3.61 ± 0.93
Stomach	0.90 ± 0.25	1.89 ± 0.26	1.39 ± 0.12	1.18 ± 0.22	1.39 ± 0.73
Intestines	0.43 ± 0.14	1.30 ± 0.26	2.91 ± 0.30	1.72 ± 0.29	2.96 ± 1.02
Spleen	0.26 ± 0.02	0.26 ± 0.06	0.56 ± 0.13	0.32 ± 0.07	1.01 ± 0.30
Muscle	0.02 ± 0.02	0.03 ± 0.01	0.05 ± 0.03	0.03 ± 0.01	0.07 ± 0.06
Lungs	0.23 ± 0.10	0.20 ± 0.03	0.42 ± 0.06	0.19 ± 0.02	0.67 ± 0.08
Pancreas	0.04 ± 0.01	0.08 ± 0.01	0.10 ± 0.02	0.06 ± 0.01	0.12 ± 0.02
Tumor	0.23 ± 0.09	1.20 ± 0.21	4.58 ± 0.47	1.60 ± 0.47	9.60 ± 3.62

All animals were injected with 180–230 kBq/10 pmol peptide; [1] Block mice group with animals co-injected with 100 µg NT for in vivo NTS1R-blockade along with PA+Lis; [2] PA mice group with animals co-injected with 300 µg PA to in situ inhibit NEP; [3] Lis mice group with animals co-injected with 200 µg Lis to in situ inhibit ACE; [4] PA+Lis mice group with animals co-injected with 300 µg PA and 200 µg Lis to in situ inhibit both NEP and ACE.

Table 3. Biodistribution data for ^{99m}Tc-DT5, expressed as %ID/g mean $\pm$ sd, $n = 4$, in WiDr xenograft-bearing SCID mice at 4 h pi without or with coinjection of PA+Lis.

Tissue	^{99m}Tc-DT5 – 4 h pi		
	Block [1,2]	Controls	PA+Lis [3]
Blood		0.45 ± 0.16	0.41 ± 0.12
Liver		0.90 ± 0.20	1.12 ± 0.27
Heart		0.16 ± 0.04	0.22 ± 0.05
Kidneys		8.63 ± 1.80	16.62 ± 1.63
Stomach		2.00 ± 0.35	2.02 ± 0.37
Intestines	0.42 ± 0.01	2.90 ± 0.28	4.30 ± 0.52
Spleen		0.31 ± 0.09	0.86 ± 0.07
Muscle		0.07 ± 0.02	0.11 ± 0.02
Lungs		0.43 ± 0.10	1.10 ± 0.16
Pancreas		0.16 ± 0.04	0.29 ± 0.03
Tumor	0.13 ± 0.01	0.88 ± 0.08	12.29 ± 2.73

All animals were injected with 180–230 kBq/10 pmol peptide; [1] Block mice group with animals co- injected with 100 µg NT for in vivo NTS1R-blockade; [2] values adopted from [23]; [3] PA+Lis mice group with animals co-injected with 300 µg PA and 200 µg Lis to in situ inhibit both NEP and ACE.

Table 4. Biodistribution data for ^{99m}Tc-DT6, expressed as %ID/g mean ± sd, *n* = 4, in WiDr xenograft-bearing SCID mice at 4 h pi without or with coinjection of PA, Lis, or PA+Lis.

Tissue	^{99m}Tc-DT6 – 4 h pi				
	Block [1]	Controls	4 h PA [2]	Lis [3]	PA+Lis [4]
Blood	0.11 ± 0.09	0.10 ± 0.06	0.10 ± 0.03	0.08 ± 0.03	0.09 ± 0.00
Liver	0.36 ± 0.06	0.34 ± 0.07	0.42 ± 0.05	0.28 ± 0.01	0.45 ± 0.07
Heart	0.09 ± 0.04	0.08 ± 0.02	0.12 ± 0.03	0.07 ± 0.02	0.10 ± 0.02
Kidneys	10.83 ± 3.26	6.09 ± 1.15	11.14 ± 3.87	6.24 ± 1.56	14.61 ± 3.16
Stomach	0.93 ± 0.30	0.44 ± 0.11	0.87 ± 0.22	0.62 ± 0.22	0.89 ± 0.16
Intestines	0.46 ± 0.21	1.61 ± 0.55	2.52 ± 0.40	1.46 ± 0.32	2.81 ± 0.32
Spleen	0.48 ± 0.16	0.64 ± 0.14	1.71 ± 0.26	0.75 ± 0.09	1.84 ± 0.28
Muscle	0.03 ± 0.01	0.04 ± 0.03	0.05 ± 0.02	0.03 ± 0.01	0.09 ± 0.06
Lungs	0.54 ± 0.07	0.22 ± 0.06	1.26 ± 0.15	0.19 ± 0.03	1.27 ± 0.02
Pancreas	0.07 ± 0.04	0.10 ± 0.04	0.14 ± 0.02	0.07 ± 0.01	0.16 ± 0.02
Tumor	0.38 ± 0.15	1.68 ± 0.28	3.89 ± 0.71	2.15 ± 0.43	3.50 ± 0.34

All animals were injected with 180–230 kBq/10 pmol peptide; [1] Block mice group with animals co-injected with 100 μg NT for in vivo NTS1R-blockade along with PA+Lis; [2] PA mice group with animals co-injected with 300 μg PA to in situ inhibit NEP; [3] Lis mice group with animals co-injected with 200 μg Lis to in situ inhibit ACE; [4] PA+Lis mice group with animals co-injected with 300 μg PA and 200 μg Lis to in situ inhibit both NEP and ACE.

Comparative biodistribution results for ^{99m}Tc-DT1, ^{99m}Tc-DT5, and ^{99m}Tc-DT6 in mice kidneys, intestines and WiDr tumor 4 h after radioligand administration without or with coinjection of PA+Lis are selectively depicted in Figure 4. The favorable increase in the tumor uptake of ^{99m}Tc-DT1 is not compromised by a high increase of renal accumulation during PA+Lis treatment, as seen for the Dab[9]-modified ^{99m}Tc-DT5. On the other hand, ^{99m}Tc-DT6, despite its high in vivo stabilization by this regimen, fails to reach similar levels of tumor uptake, most probably due to its poor in vitro internalization capability. At the same time, renal accumulation has unfavorably increased.
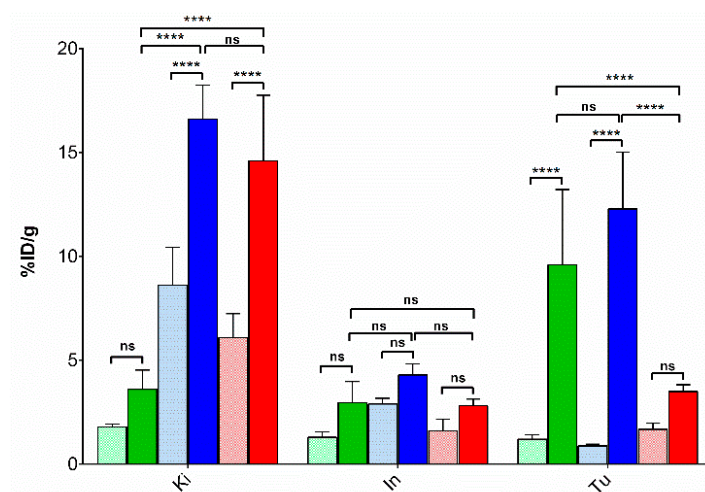
Figure 4. Comparative uptake for ^{99m}Tc-DT1 (green bars), ^{99m}Tc-DT5 (blue bars) or ^{99m}Tc-DT6 (red bars) in kidneys, intestines and WiDr-xenografts at 4 h pi of radioligand administration without (paler bars), or with PA+Lis-coinjection (darker bars) in male SCID mice; results are given as mean %ID/g values ± sd, *n* = 4. Statistical analysis results are also incorporated in the diagram, with **** representing $P < 0.0001$ and ns (non-significant) $P > 0.05$.

3.3.3. SPECT/CT of ^{99m}Tc-DT1 in WiDr Xenograft-Bearing Mice

Mice SPECT/CT images obtained 3 h after injection of ^{99m}Tc-DT1 are presented on Figure 5. Significant accumulation was achieved in the NTS1R-expressing WiDr xenografts and the kidneys. Clear differences in renal and tumor accumulation could be observed between control (Figure 5a),

PA+Lis treated (Figure 5b) and animals coinjected with PA+Lis in the kidney protecting agent, gelofusine (Figure 5c).
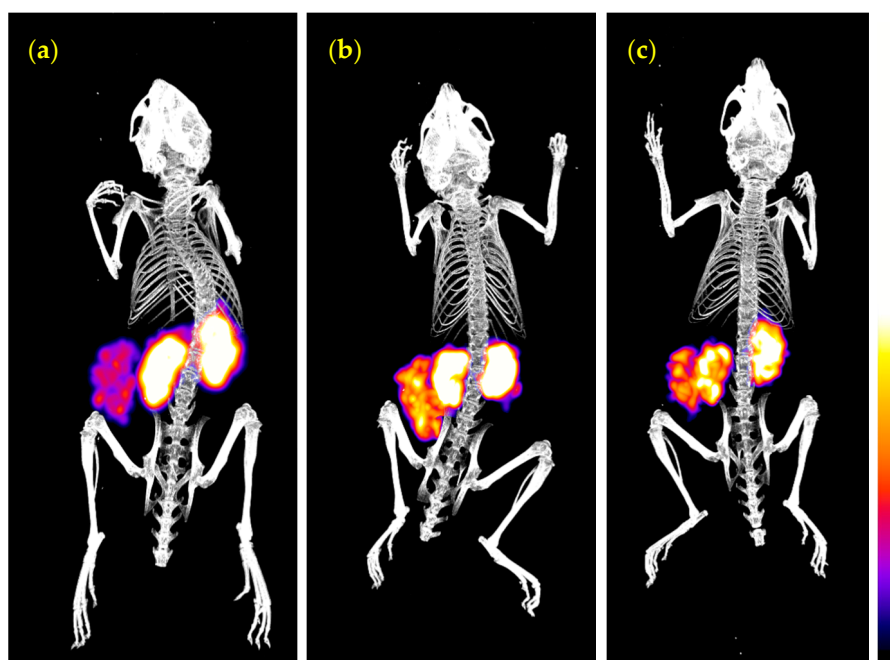
Figure 5. Static whole body SPECT/CT images of three SCID mice bearing WiDr tumors 3 h after injection of ^{99m}Tc-DT1 (**a**) alone, or (**b**) with coinjection of PA+Lis, or (**c**) with coinjection PA+Lis in gelofusine. Intense uptake is seen on kidneys and tumor. In (**a**) high uptake is observed in the kidneys and in (**b**) a notable increase in the tumor uptake has resulted after treatment of mice with PA+Lis. Kidneys and tumor present a very similar uptake in (**c**), with the renal uptake being markedly reduced compared with (**b**) due to gelofusine coinjection. The color bar indicates the difference in accumulated activity (purple being the lowest and white the highest level of accumulation).

4. Discussion

Radiolabeled analogs of neurotensin and especially its C-terminal hexapeptide fragment, NT(8-13), have been proposed for diagnostic imaging and radionuclide therapy of human tumors with high NTS1R expression. In search of metabolically robust analogs, a variety of structural modifications have been introduced on the linear peptide NT(8-13) motif and their impact on metabolic stability, tumor targeting, and overall pharmacokinetics have been assessed during structure–activity relationships studies [9,10,18,19,30,34]. The degradation of NT, NT(8-13), and their analogs has been studied in the past, revealing three major cleavage sites on the peptide backbone: i) Arg^8-Arg^9, ii) Pro^{10}-Tyr^{11} and iii) Tyr^{11}-Ile^{12}. Amongst the peptidases participating in the rapid in vivo catabolism of these analogs, NEP (cleaving the Pro^{10}-Tyr^{11} and the Tyr^{11}-Ile^{12} bonds) and ACE (cleaving the Tyr^{11}-Ile^{12} bond) play a major role. Two additional metallopeptidases, EC 3.4.24.15 (thiolsensitive metallo oligopeptidase, thimet-oligopeptidase, TOP) hydrolyzing the Arg^8-Arg^9 bond and EC 3.4.24.16 (neurolysin) hydrolyzing the Pro^{10}-Tyr^{11} bond (Figure 1), are also implicated in the degradation of NT, NT(8-13) and their analogs [30,31,33,34,38,40–42]. However, the latter two enzymes are predominantly located within the cells and hence are less expected to have any considerable impact on the stability of circulating NT-derived radiopeptides after iv administration and on their way to tumor sites [54,55].

Thus far, most efforts toward metabolically stable NT-analogs and their radioligands have been focused on the two Arg^8-Arg^9 and Tyr^{11}-Ile^{12} bonds. Stabilization of the Arg^8-Arg^9 bond has been attempted by a replacement of either Arg by DArg, Lys, or Dab as well as by a reduction or methylation of the bond. Further stabilization of the Tyr^{11}-Ile^{12} site could be achieved by substitution of Ile^{12} by Tle^{12} [30,31,33,34,41]. The effects of the above modifications on the pharmacokinetic profile of resulting

radioligands have not been fully understood. This may be attributed to the methods commonly applied for metabolic stability determination, comprising almost exclusively in vitro radioligand incubation in tissue homogenates and/or serum/plasma [30,33,34]. In the first case, homogenization will disrupt cell membranes and otherwise intracellularly compartmentalized enzymes will be released. As a result, radioligands will be exposed to enzymes which they would not actually encounter after injection in the living organism. On the other hand, during in vitro incubation of radiopeptides in serum or plasma, the action of ectoenzymes anchored on epithelial cells of the vasculature and other tissues of the body, e.g., NEP [42–44], is totally overseen [33,45].

We have previously developed a series of NT(8-13)-based analogs carrying an open chain tetraamine chelator for stable binding of ^{99m}Tc [23,24]. During incubation of resulting ^{99m}Tc-radioligands in mice plasma, we have also observed increasing stabilization effects by Arg^9/Dab^9 and Ile^{12}/Tle^{12} replacements. However, responses on overall pharmacokinetics in tumor-bearing mice were less straightforward. For example, renal accumulation unfavorably increased without any remarkable gain in tumor targeting for ^{99m}Tc-DT6, as would be expected by the high metabolic in vitro stability determined for this doubly substituted, Arg^9/Dab^9 and Ile^{12}/Tle^{12}, analog. Similar sub-optimal tumor-targeting results were subsequently obtained in a pilot study with ^{99m}Tc-DT6 in a small number of cancer patients [36].

Aiming to better understand the above intriguing findings, we herein compare the biological profiles of such previously reported NT-radiopeptides under a new light. We achieve this mainly by taking into account results from recent studies relating in vivo metabolic fate and tumor targeting capabilities of a series of biodegradable radiopeptides [45–49]. These studies have revealed the central, but hitherto unrecognized, role of NEP in the rapid catabolism of many radiopeptides from different peptide families, including somatostatin, bombesin and gastrin, in peripheral blood, compromising their sufficient delivery to tumor sites. Most interestingly, by administration of suitable NEP-inhibitors it was possible to induce stabilization of these radiopeptides in circulation, thereby enhancing tumor localization with clear benefits envisaged for diagnosis and therapy. In the present study, we report for the first time, outcomes after applying this methodology in the field of NT-radiopeptides. For this purpose, we selected ^{99m}Tc-DT1 (^{99m}Tc-[N$_4$-Gly^7]NT(7-13)), ^{99m}Tc-DT5 (^{99m}Tc-[N$_4$-βAla^7,Dab^9]NT(7-13)) and ^{99m}Tc-DT6 (^{99m}Tc-[N$_4$-βAla^7,Dab^9,Tle^{12}]]NT(7-13)) as examples (Figure 1).

Surprisingly, we observed gradual loss of cell uptake/internalization from ^{99m}Tc-DT1 to ^{99m}Tc-DT5 (single Arg^9/Dab^9-replacement) to ^{99m}Tc-DT6 (double Arg^9/Dab^9 and Ile^{12}/Tle^{12} replacement) in NTS1R-expressing WiDr cells, revealing a negative effect of above modifications on the interaction of resulting radioligands with the NTS1R at the cellular level. This result has been previously missed and was unexpected considering the comparable affinities of these analogs for the NTS1R [23,24].

On the other hand, only the double-modified ^{99m}Tc-DT6 showed a significantly higher metabolic stability in peripheral mice blood at 5 min pi (55.1 ± 3.9% intact) compared with either ^{99m}Tc-DT1 or ^{99m}Tc-DT5 that were degraded within this period (1.8 ± 0.8% and 1.3 ± 0.2% intact, respectively; *P* < 0.0001). This finding demonstrates that single Arg^9/Dab^9 replacement had no impact on the stability of the circulating radioligand. It further shows that both ^{99m}Tc-DT5 and ^{99m}Tc-DT6 are more rapidly degraded in vivo compared to their in vitro degradation in mouse plasma [23]. To investigate the involvement of NEP or ACE in the rapid in vivo catabolism of all three radioligands, we have treated mice with the NEP-inhibitor PA, the ACE-inhibitor Lis, or a combination of the two, and analyzed the blood of mice collected 5 min afterwards with HPLC. As summarized in Table 1, PA co-injection led to maximum stabilization of double-modified ^{99m}Tc-DT6 (89.3 ± 6.7% intact; *P* < 0.0001). Considering the high in vitro stability of ^{99m}Tc-DT6 in mice plasma, whereby NEP is absent and ACE is present, this result implies that NEP plays the major role in the in vivo degradation of the Ile^{12}/Tle^{12}-modified radioligand. In contrast, ^{99m}Tc-DT1 or ^{99m}Tc-DT5 were only partially stabilized by either PA or Lis and only their combination led to maximum stabilization in peripheral mouse blood (72.3 ± 3.2% intact

and 79.0 ± 1.7% intact, respectively; $P < 0.0001$). This result suggests a combined role for ACE and NEP in the in vivo degradation of NT-radioligands non-substituted at Ile^{12} [33,38–40].

It is interesting to observe how the abovementioned structural modifications, affecting both internalization/cell-uptake of the three radioligands and their in vivo stability, translate in NTS1R-specific tumor localization and overall pharmacokinetics in WiDr tumor-bearing mice. As shown in Tables 2–4 and Figure 4, there's no significant difference in the localization of ^{99m}Tc-DT1, ^{99m}Tc-DT5 or ^{99m}Tc-DT6 in the implanted tumors ($P > 0.05$). Thus, effects induced by structural changes compensated each other, eventually resulting in similar outcomes with regards to tumor uptake. In contrast, renal uptake is found significantly increased in both Arg^9/Dab^9-modified ^{99m}Tc-DT5 (8.63 ± 1.80%ID/g; $P < 0.0001$) and ^{99m}Tc-DT6 (6.09 ± 1.15%ID/g; $P < 0.01$) compared with ^{99m}Tc-DT1 (1.80 ± 0.14%ID/g), revealing the unfavorable impact of the pendant $-NH_2$ of Dab^9 on kidney accumulation. Similar observations have been previously reported for other Lys^8- or Lys^9-modified NT-radioligands likewise carrying pendant $-NH_2$ groups [23,24,34].

Of particular interest is the impact of in situ NEP- and ACE-inhibition on the biodistribution of these radioligands. After combined treatment of mice with PA and Lis, tumor localization significantly increased for both ^{99m}Tc-DT1 (9.60 ± 3.62%ID/g; $P < 0.0001$) and ^{99m}Tc-DT5 (12.29 ± 2.73%ID/g; $P < 0.0001$) compared with untreated controls, highlighting the significance of in vivo stability for the efficient delivery of intact radiopeptides to tumor sites, as previously documented [45–48]. Surprisingly, the increase observed in the tumor uptake of ^{99m}Tc-DT6 was much lower (3.50 ± 0.34%ID/g; $P > 0.05$) indicating the pronounced negative impact of the poor internalization/cell uptake of this Ile^{12}/Tle^{12}-modified radiotracer on tumor uptake. On the other hand, renal accumulation was found to be increased for all analogs after PA+Lis treatment, but in the case of the two Arg^9/Dab^9-modified radioligands, renal values were significantly much higher compared with ^{99m}Tc-DT1 (^{99m}Tc-DT5: 16.62 ± 1.63%ID/g; $P < 0.0001$ and ^{99m}Tc-DT6: 14.61 ± 3.16%ID/g; $P < 0.0001$ vs. ^{99m}Tc-DT1: 3.61 ± 0.93%ID/g; $P > 0.05$). In view of the above, the most favorable pharmacokinetics amongst this series of NT-radiotracers are displayed by ^{99m}Tc-DT1 during treatment of mice with the PA+Lis combination. In contrast, the structural interventions in ^{99m}Tc-DT5 (high kidney accumulation) and ^{99m}Tc-DT6 (poor cell association/internalization and consequent low tumor uptake), despite their stabilization effect, led to unfavorable overall pharmacokinetics.

5. Conclusions

The impact of in-situ NEP and ACE inhibition on tumor targeting and pharmacokinetics of NT-based radioligands has been assessed for the first time employing three structurally related analogs, namely ^{99m}Tc-DT1 (^{99m}Tc-[N_4-Gly^7]NT(7-13)), ^{99m}Tc-DT5 (^{99m}Tc-[N_4-βAla^7,Dab^9]NT(7-13)), and ^{99m}Tc-DT6 (^{99m}Tc-[N_4-βAla^7,Dab^9,Tle^{12}]]NT(7-13)), as examples. Structural interventions led to sub-optimal outcomes, with Arg^9/Dab^9-replacement leading to unfavorable renal accumulation (^{99m}Tc-DT5 and ^{99m}Tc-DT6) and further Ile^{12}/Tle^{12}-substitution compromising cell uptake/internalization (^{99m}Tc-DT6). Notably, ^{99m}Tc-DT1, retaining high cell-binding/internalization capability and effectively stabilized in vivo by PA+Lis coinjection, achieved markedly enhanced tumor localization while preserving lower kidney values. These findings verify previous reports on the improved pharmacokinetic profile of other radiopeptides from different families in animal models and very recently in patients during key-protease inhibition. Hence, they highlight the need for further validation of this promising concept in the field of neurotensin radioligands in cancer theranostics. It should be noted that registered NEP and or ACE inhibitors have been used for years and can theoretically be applied in oncology. The first results of using such an over-the-counter NEP-inhibitor drug (racecadotril) in combination with biodegradable radiolabeled gastrin in medullary thyroid cancer patients have been recently reported [49] and strongly support the clinical applicability of this concept.

6. Patents

Theodosia Maina, Berthold A. Nock, Marion de Jong Enhanced in vivo targeting of radiolabelled peptides with the means of enzyme inhibitors. EP2729183B1; 05.09.2018 Bulletin 2018/36.

Author Contributions: Conceptualization, B.A.N. and T.M.; methodology, B.A.N. and T.M.; validation, B.A.N., P.K., T.M. and M.d.J.; formal analysis, P.K.; investigation, P.K., A.K., B.A.N. and T.M.; resources, E.P.K.; writing—original draft preparation, T.M.; writing—review and editing, all authors; visualization, P.K., A.K., B.A.N. and T.M.; supervision, B.A.N., P.K., T.M, M.d.J. and E.P.K.; project administration, T.M.; funding acquisition, E.P.K. All authors have read and agreed to the published version of the manuscript.

Conflicts of Interest: The authors declare no conflict of interest.

References

1. Baum, R.P.; Kulkarni, H.R. Theranostics: From molecular imaging using Ga-68 labeled tracers and PET/CT to personalized radionuclide therapy—The Bad Berka experience. *Theranostics* **2012**, *2*, 437–447. [CrossRef] [PubMed]

2. de Jong, M.; Breeman, W.A.; Kwekkeboom, D.J.; Valkema, R.; Krenning, E.P. Tumor imaging and therapy using radiolabeled somatostatin analogues. *Acc. Chem. Res.* **2009**, *42*, 873–880. [CrossRef] [PubMed]

3. Zhang, J.; Singh, A.; Kulkarni, H.R.; Schuchardt, C.; Müller, D.; Wester, H.J.; Maina, T.; Rosch, F.; van der Meulen, N.P.; Müller, C.; et al. From bench to bedside-the Bad Berka experience with first-in-human studies. *Semin. Nucl. Med.* **2019**, *49*, 422–437. [CrossRef] [PubMed]

4. Cutler, C.S.; Hennkens, H.M.; Sisay, N.; Huclier-Markai, S.; Jurisson, S.S. Radiometals for combined imaging and therapy. *Chem. Rev.* **2013**, *113*, 858–883. [CrossRef]

5. Kostelnik, T.I.; Orvig, C. Radioactive main group and rare earth metals for imaging and therapy. *Chem. Rev.* **2019**, *119*, 902–956. [CrossRef] [PubMed]

6. Reubi, J.C. Peptide receptors as molecular targets for cancer diagnosis and therapy. *Endocr. Rev.* **2003**, *24*, 389–427. [CrossRef]

7. Vincent, J.P.; Mazella, J.; Kitabgi, P. Neurotensin and neurotensin receptors. *Trends Pharmacol. Sci.* **1999**, *20*, 302–309. [CrossRef]

8. Kitabgi, P. Functional domains of the subtype 1 neurotensin receptor (NTS1). *Peptides* **2006**, *27*, 2461–2468. [CrossRef]

9. Kitabgi, P. Targeting neurotensin receptors with agonists and antagonists for therapeutic purposes. *Curr. Opin. Drug Discov. Dev.* **2002**, *5*, 764–776.

10. Evers, B.M. Neurotensin and growth of normal and neoplastic tissues. *Peptides* **2006**, *27*, 2424–2433. [CrossRef]

11. Reubi, J.C.; Waser, B.; Friess, H.; Büchler, M.; Laissue, J. Neurotensin receptors: A new marker for human ductal pancreatic adenocarcinoma. *Gut* **1998**, *42*, 546–550. [CrossRef] [PubMed]

12. Ishizuka, J.; Townsend, C.M., Jr.; Thompson, J.C. Neurotensin regulates growth of human pancreatic cancer. *Ann. Surg.* **1993**, *217*, 439–445. [CrossRef] [PubMed]

13. Ehlers, R.A.; Kim, S.; Zhang, Y.; Ethridge, R.T.; Murrilo, C.; Hellmich, M.R.; Evans, D.B.; Townsend, C.M., Jr.; Mark Evers, B. Gut peptide receptor expression in human pancreatic cancers. *Ann. Surg.* **2000**, *231*, 838–848. [CrossRef] [PubMed]

14. Reubi, J.C.; Waser, B.; Schaer, J.C.; Laissue, J.A. Neurotensin receptors in human neoplasms: High incidence in Ewing's sarcomas. *Int. J. Cancer* **1999**, *82*, 213–218. [CrossRef]

15. Gui, X.; Guzman, G.; Dobner, P.R.; Kadkol, S.S. Increased neurotensin receptor-1 expression during progression of colonic adenocarcinoma. *Peptides* **2008**, *29*, 1609–1615. [CrossRef]

16. Morgat, C.; Chastel, A.; Molinie, V.; Schollhammer, R.; Macgrogan, G.; Velasco, V.; Malavaud, B.; Fernandez, P.; Hindie, E. Neurotensin receptor-1 expression in human prostate cancer: A pilot study on primary tumors and lymph node metastases. *Int. J. Mol. Sci.* **2019**, *20*, 1721. [CrossRef]

17. Souaze, F.; Dupouy, S.; Viardot-Foucault, V.; Bruyneel, E.; Attoub, S.; Gespach, C.; Gompel, A.; Forgez, P. Expression of neurotensin and NT1 receptor in human breast cancer: A potential role in tumor progression. *Cancer Res.* **2006**, *66*, 6243–6249. [CrossRef]

18. Nikolaou, S.; Qiu, S.; Fiorentino, F.; Simillis, C.; Rasheed, S.; Tekkis, P.; Kontovounisios, C. The role of neurotensin and its receptors in non-gastrointestinal cancers: A review. *Cell Commun. Signal.* **2020**, *18*, 68. [CrossRef]

19. Granier, C.; van Rietschoten, J.; Kitabgi, P.; Poustis, C.; Freychet, P. Synthesis and characterization of neurotensin analogues for structure/activity relationship studies. Acetyl-neurotensin-(8–13) is the shortest analogue with full binding and pharmacological activities. *Eur. J. Biochem.* **1982**, *124*, 117–124. [CrossRef]

20. García-Garayoa, E.; Allemann-Tannahill, L.; Blauenstein, P.; Willmann, M.; Carrel-Remy, N.; Tourwé, D.; Iterbeke, K.; Conrath, P.; Schubiger, P.A. In vitro and in vivo evaluation of new radiolabeled neurotensin(8-13) analogues with high affinity for nt1 receptors. *Nucl. Med. Biol.* **2001**, *28*, 75–84. [CrossRef]

21. Maes, V.; García-Garayoa, E.; Blauenstein, P.; Tourwé, D. Novel [99mTc]-labeled neurotensin analogues with optimized biodistribution properties. *J. Med. Chem.* **2006**, *49*, 1833–1836. [CrossRef] [PubMed]

22. Alshoukr, F.; Rosant, C.; Maes, V.; Abdelhak, J.; Raguin, O.; Burg, S.; Sarda, L.; Barbet, J.; Tourwé, D.; Pelaprat, D.; et al. Novel neurotensin analogues for radioisotope targeting to neurotensin receptor-positive tumors. *Bioconjug. Chem.* **2009**, *20*, 1602–1610. [CrossRef] [PubMed]

23. Maina, T.; Nikolopoulou, A.; Stathopoulou, E.; Galanis, A.S.; Cordopatis, P.; Nock, B.A. [99mTc]demotensin 5 and 6 in the NTS1-R-targeted imaging of tumours: Synthesis and preclinical results. *Eur. J. Nucl. Med. Mol. Imaging* **2007**, *34*, 1804–1814. [CrossRef]

24. Nock, B.A.; Nikolopoulou, A.; Reubi, J.C.; Maes, V.; Conrath, P.; Tourwé, D.; Maina, T. Toward stable N_4-modified neurotensins for NTS1-receptor-targeted tumor imaging with [99mTc]. *J. Med. Chem.* **2006**, *49*, 4767–4776. [CrossRef] [PubMed]

25. de Visser, M.; Janssen, P.J.; Srinivasan, A.; Reubi, J.C.; Waser, B.; Erion, J.L.; Schmidt, M.A.; Krenning, E.P.; de Jong, M. Stabilised [111In]-labelled DTPA- and DOTA-conjugated neurotensin analogues for imaging and therapy of exocrine pancreatic cancer. *Eur. J. Nucl. Med. Mol. Imaging* **2003**, *30*, 1134–1139. [CrossRef]

26. Achilefu, S.; Srinivasan, A.; Schmidt, M.A.; Jimenez, H.N.; Bugaj, J.E.; Erion, J.L. Novel bioactive and stable neurotensin peptide analogues capable of delivering radiopharmaceuticals and molecular beacons to tumors. *J. Med. Chem.* **2003**, *46*, 3403–3411. [CrossRef] [PubMed]

27. Mascarin, A.; Valverde, I.E.; Mindt, T.L. Structure-activity relationship studies of amino acid substitutions in radiolabeled neurotensin conjugates. *ChemMedChem* **2016**, *11*, 102–107. [CrossRef]

28. Jia, Y.; Shi, W.; Zhou, Z.; Wagh, N.K.; Fan, W.; Brusnahan, S.K.; Garrison, J.C. Evaluation of DOTA-chelated neurotensin analogs with spacer-enhanced biological performance for neurotensin-receptor-1-positive tumor targeting. *Nucl. Med. Biol.* **2015**, *42*, 816–823. [CrossRef]

29. Alshoukr, F.; Prignon, A.; Brans, L.; Jallane, A.; Mendes, S.; Talbot, J.N.; Tourwé, D.; Barbet, J.; Gruaz-Guyon, A. Novel DOTA-neurotensin analogues for [111In] scintigraphy and [68Ga] PET imaging of neurotensin receptor-positive tumors. *Bioconjug. Chem.* **2011**, *22*, 1374–1385. [CrossRef]

30. Schubiger, P.A.; Allemann-Tannahill, L.; Egli, A.; Schibli, R.; Alberto, R.; Carrel-Remy, N.; Willmann, M.; Blauenstein, P.; Tourwé, D. Catabolism of neurotensins. Implications for the design of radiolabeling strategies of peptides. *Q. J. Nucl. Med.* **1999**, *43*, 155–158.

31. Couder, J.; Tourwé, D.; Van Binst, G.; Schuurkens, J.; Leysen, J.E. Synthesis and biological activities of *psi* (CH_2NH) pseudopeptide analogues of the C-terminal hexapeptide of neurotensin. *Int. J. Pept. Protein Res.* **1993**, *41*, 181–184. [CrossRef] [PubMed]

32. Mascarin, A.; Valverde, I.E.; Vomstein, S.; Mindt, T.L. 1,2,3-triazole stabilized neurotensin-based radiopeptidomimetics for improved tumor targeting. *Bioconjug. Chem.* **2015**, *26*, 2143–2152. [CrossRef] [PubMed]

33. Sparr, C.; Purkayastha, N.; Yoshinari, T.; Seebach, D.; Maschauer, S.; Prante, O.; Hubner, H.; Gmeiner, P.; Kolesinska, B.; Cescato, R.; et al. Syntheses, receptor bindings, in vitro and in vivo stabilities and biodistributions of DOTA-neurotensin(8-13) derivatives containing beta-amino acid residues—A lesson about the importance of animal experiments. *Chem. Biodivers.* **2013**, *10*, 2101–2121. [CrossRef] [PubMed]

34. Maschauer, S.; Prante, O. Radiopharmaceuticals for imaging and endoradiotherapy of neurotensin receptor-positive tumors. *J. Label. Compd. Radiopharm.* **2018**, *61*, 309–325. [CrossRef]

35. Fröberg, A.C.; van Eijck, C.H.; Verdijsseldonck, M.C.; Melis, M.; Bakker, H.; Krenning, E.P. Use of neurotensin analogue In-111-DTPA-neurotensin (IN-111-MP2530) in diagnosis of pancreatic adenocarcinoma. *Eur. J. Nucl. Med. Mol. Imaging* **2004**, *31*, S392. [CrossRef]

36. Gabriel, M.; Decristoforo, C.; Woll, E.; Eisterer, W.; Nock, B.; Maina, T.; Moncayo, R.; Virgolini, I. [99mTc]demotensin VI: Biodistribution and initial clinical results in tumor patients of a pilot/phase I study. *Cancer Biother. Radiopharm.* **2011**, *26*, 557–563. [CrossRef]

37. Buchegger, F.; Bonvin, F.; Kosinski, M.; Schaffland, A.O.; Prior, J.; Reubi, J.C.; Blauenstein, P.; Tourwé, D.; Garcia Garayoa, E.; Bischof Delaloye, A. Radiolabeled neurotensin analog, 99mTc-NT-XI, evaluated in ductal pancreatic adenocarcinoma patients. *J. Nucl. Med.* **2003**, *44*, 1649–1654.

38. Kitabgi, P.; De Nadai, F.; Rovere, C.; Bidard, J.N. Biosynthesis, maturation, release, and degradation of neurotensin and neuromedin N. *Ann. N. Y. Acad. Sci.* **1992**, *668*, 30–42. [CrossRef]

39. Kitabgi, P.; Dubuc, I.; Nouel, D.; Costentin, J.; Cuber, J.C.; Fulcrand, H.; Doulut, S.; Rodriguez, M.; Martinez, J. Effects of thiorphan, bestatin and a novel metallopeptidase inhibitor JMV 390-1 on the recovery of neurotensin and neuromedin N released from mouse hypothalamus. *Neurosci. Lett.* **1992**, *142*, 200–204. [CrossRef]

40. Checler, F.; Vincent, J.P.; Kitabgi, P. Degradation of neurotensin by rat brain synaptic membranes: Involvement of a thermolysin-like metalloendopeptidase (enkephalinase), angiotensin-converting enzyme, and other unidentified peptidases. *J. Neurochem.* **1983**, *41*, 375–384. [CrossRef]

41. Schindler, L.; Bernhardt, G.; Keller, M. Modifications at Arg and Ile give neurotensin(8-13) derivatives with high stability and retained NTS1 receptor affinity. *ACS Med. Chem. Lett.* **2019**, *10*, 960–965. [CrossRef] [PubMed]

42. Skidgel, R.A.; Engelbrecht, S.; Johnson, A.R.; Erdös, E.G. Hydrolysis of substance P and neurotensin by converting enzyme and neutral endopeptidase. *Peptides* **1984**, *5*, 769–776. [CrossRef]

43. Roques, B.P.; Noble, F.; Dauge, V.; Fournie-Zaluski, M.C.; Beaumont, A. Neutral endopeptidase 24.11: Structure, inhibition, and experimental and clinical pharmacology. *Pharmacol. Rev.* **1993**, *45*, 87–146.

44. Roques, B.P. Zinc metallopeptidases: Active site structure and design of selective and mixed inhibitors: New approaches in the search for analgesics and anti-hypertensives. *Biochem. Soc. Trans.* **1993**, *21*, 678–685. [CrossRef] [PubMed]

45. Nock, B.A.; Maina, T.; Krenning, E.P.; de Jong, M. "To serve and protect": Enzyme inhibitors as radiopeptide escorts promote tumor targeting. *J. Nucl. Med.* **2014**, *55*, 121–127. [CrossRef]

46. Lymperis, E.; Kaloudi, A.; Sallegger, W.; Bakker, I.L.; Krenning, E.P.; de Jong, M.; Maina, T.; Nock, B.A. Radiometal-dependent biological profile of the radiolabeled gastrin-releasing peptide receptor antagonist SB3 in cancer theranostics: Metabolic and biodistribution patterns defined by neprilysin. *Bioconjug. Chem.* **2018**, *29*, 1774–1784. [CrossRef]

47. Chatalic, K.L.; Konijnenberg, M.; Nonnekens, J.; de Blois, E.; Hoeben, S.; de Ridder, C.; Brunel, L.; Fehrentz, J.A.; Martinez, J.; van Gent, D.C.; et al. In vivo stabilization of a gastrin-releasing peptide receptor antagonist enhances PET imaging and radionuclide therapy of prostate cancer in preclinical studies. *Theranostics* **2016**, *6*, 104–117. [CrossRef]

48. Kaloudi, A.; Nock, B.A.; Lymperis, E.; Krenning, E.P.; de Jong, M.; Maina, T. 99mTc-labeled gastrins of varying peptide chain length: Distinct impact of NEP/ACE-inhibition on stability and tumor uptake in mice. *Nucl. Med. Biol.* **2016**, *43*, 347–354. [CrossRef]

49. Valkema, R.; Froberg, A.; Maina, T.; Nock, B.; de Blois, E.; Melis, M.; Konijnenberg, M.; Koolen, S.; Peeters, R.; de Herder, W.; et al. Clinical translation of the pepprotect concept: Improved detection of cancer and metastases, applied in medullary thyroid cancer patients with [111In]In-MG1 scanning during neprilysin inhibition. *Eur. J. Nucl. Med. Mol. Imaging* **2019**, *46*, S701–S702.

50. Suda, H.; Aoyagi, T.; Takeuchi, T.; Umezawa, H. Letter: A thermolysin inhibitor produced by actinomycetes: Phosphoramidon. *J. Antibiot. (Tokyo)* **1973**, *26*, 621–623. [CrossRef]

51. Millar, J.A.; Derkx, F.H.; McLean, K.; Reid, J.L. Pharmacodynamics of converting enzyme inhibition: The cardiovascular, endocrine and autonomic effects of MK421 (enalapril) and MK521. *Br. J. Clin. Pharmacol.* **1982**, *14*, 347–355. [CrossRef]

52. Maoret, J.J.; Pospai, D.; Rouyer-Fessard, C.; Couvineau, A.; Laboisse, C.; Voisin, T.; Laburthe, M. Neurotensin receptor and its MRNA are expressed in many human colon cancer cell lines but not in normal colonic epithelium: Binding studies and RT-PCR experiments. *Biochem. Biophys. Res. Commun.* **1994**, *203*, 465–471. [CrossRef] [PubMed]

53. Reubi, J.C.; Waser, B.; Schmassmann, A.; Laissue, J.A. Receptor autoradiographic evaluation of cholecystokinin, neurotensin, somatostatin and vasoactive intestinal peptide receptors in gastro-intestinal adenocarcinoma samples: Where are they really located? *Int. J. Cancer* **1999**, *81*, 376–386. [CrossRef]

54. Paschoalin, T.; Carmona, A.K.; Rodrigues, E.G.; Oliveira, V.; Monteiro, H.P.; Juliano, M.A.; Juliano, L.; Travassos, L.R. Characterization of thimet oligopeptidase and neurolysin activities in B16F10-NEX2 tumor cells and their involvement in angiogenesis and tumor growth. *Mol. Cancer* **2007**, *6*, 44. [CrossRef] [PubMed]

55. Berti, D.A.; Morano, C.; Russo, L.C.; Castro, L.M.; Cunha, F.M.; Zhang, X.; Sironi, J.; Klitzke, C.F.; Ferro, E.S.; Fricker, L.D. Analysis of intracellular substrates and products of thimet oligopeptidase in human embryonic kidney 293 cells. *J. Biol. Chem.* **2009**, *284*, 14105–14116. [CrossRef]

Article

Optimizing the Profile of [99mTc]Tc–NT(7–13) Tracers in Pancreatic Cancer Models by Means of Protease Inhibitors

Panagiotis Kanellopoulos [1,2,*], Berthold A. Nock [1] , Eric P. Krenning [3] and Theodosia Maina [1,*]

[1] Molecular Radiopharmacy, INRASTES, NCSR "Demokritos", 15341 Athens, Greece; nock_berthold.a@hotmail.com
[2] Molecular Pharmacology, School of Medicine, University of Crete, Heraklion, 70013 Crete, Greece
[3] Cyclotron Rotterdam BV, Erasmus MC, 3015 CE Rotterdam, The Netherlands; erickrenning@gmail.com
[*] Correspondence: kanelospan@gmail.com (P.K.); maina_thea@hotmail.com (T.M.); Tel.: +30-210-650-3891 (P.K.); +30-210-650-3908 (T.M.)

check for updates

Abstract: Background: The overexpression of neurotensin subtype 1 receptors (NTS1Rs) in human tumors may be elegantly exploited for directing neurotensin (NT)-based radionuclide carriers specifically to cancer sites for theranostic purposes. We have recently shown that [99mTc]Tc–DT1 ([99mTc]Tc–[N_4–Gly^7]NT(7–13)) and [99mTc]Tc–DT5 ([99mTc]Tc–[N_4–βAla^7,Dab^9]NT(7–13)) show notably improved uptake in human colon adenocarcinoma WiDr xenografts in mice treated with neprilysin (NEP) inhibitors and/or angiotensin-converting enzyme (ACE) inhibitors compared with untreated controls. Aiming toward translation of this promising approach in NTS1R-positive pancreatic ductal adenocarcinoma (PDAC) patients, we now report on the impact of registered NEP/ACE inhibitors on the performance of [99mTc]Tc–DT1 and [99mTc]Tc–DT5 in pancreatic cancer models. Methods: The cellular uptake of [99mTc]Tc–DT1 and [99mTc]Tc–DT5 was tested in a panel of pancreatic cell lines, and their stability was assessed in mice treated or not treated with Entresto, lisinopril, or their combinations. Biodistribution was conducted in severe combined immunodeficiency (SCID) mice bearing pancreatic AsPC-1 xenografts. Results: The Entresto + lisinopril combination maximized the metabolic stability of the fast-internalizing [99mTc]Tc–DT1 in mice, resulting in notably enhanced tumor uptake (7.05 ± 0.80% injected activity (IA)/g vs. 1.25 ± 0.80% IA/g in non-treated controls at 4 h post-injection; $p < 0.0001$). Conclusions: This study has shown the feasibility of optimizing the uptake of [99mTc]Tc–DT1 in pancreatic cancer models with the aid of clinically established NEP/ACE inhibitors, in favor of clinical translation prospects.

1. Introduction

The neurotensin subtype 1 receptor (NTS1R) has been regarded as a valid biomolecular target in cancer theranostics, owing to its high-density expression in a variety of human tumors, such as pancreatic ductal adenocarcinoma (PDAC), colon carcinoma, Ewing's sarcoma, or prostate and breast cancer [1–12]. This overexpression can be elegantly exploited to direct NTS1R-seeking radionuclide carriers to tumor sites [13,14]. Typically, radiolabeled analogs of the C-terminal hexapeptide fragment of neurotensin (NT = Pyr–Leu–Tyr–Glu–Asn–Lys–Pro–Arg–Arg–Pro–Tyr–Ile–Leu–OH), NT(8–13), have been considered for such purposes [15–24]. For stable binding of metal radionuclides, a suitable

chelator needs to be covalently attached to the N-terminus of the peptide chain, directly or via a linker [25].

Accordingly, NT conjugates can be properly designed to carry a gamma emitting radiometal ($[^{99m}Tc]$Tc, $[^{111}In]$In) for single-photon emission computed tomography (SPECT), or a positron emitter ($[^{68}Ga]$Ga, $[^{64}Cu]$Cu) for positron emission tomography (PET). SPECT or PET imaging of tumor sites allows for the diagnosis, staging, and assessment of disease spread, and indicates patients eligible for radionuclide therapy. During radionuclide therapy, the respective therapeutic radiometal (beta emitter: $[^{177}Lu]$Lu, $[^{90}Y]$Y; Auger electron emitter: $[^{111}In]$In; alpha emitter: $[^{225}Ac]$Ac) will be delivered to NTS1R-positive cancer sites applying the same carrier molecule. The success of the aforementioned theranostic concept has already been established in the clinic for radiolabeled somatostatin analogs used in the management of patients with somatostatin receptor-positive neuroendocrine tumors (NETs) [14,26,27]. Radiolabeled, prostate-specific membrane antigen (PSMA) inhibitors recently introduced against prostate cancer represent another successful paradigm of theranostics in nuclear oncology [14,27].

We have previously developed a small library of NT(7–13) analogs, coupled to an acyclic tetraamine chelator at the N-terminus for stable binding of the eminent SPECT radionuclide $[^{99m}Tc]$Tc. The preclinical evaluation of this series of compounds was carried out in human colon adenocarcinoma HT29 and WiDr cells expressing the NTS1R [28,29]. During translation of the best-performing radiotracer, $[^{99m}Tc]$Tc–DT6 ($[^{99m}Tc]$Tc–$[N_4–\beta Ala^7,Dab^9,Tle]$NT(7–13); N_4 = 6–(carboxy)–1,4,8,11–tetraazaundecane), in a small number of patients, poor NTS1R targeting of tumor lesions and very fast washout of radioactivity via the kidneys into urine was observed [30]. This disappointing result was attributed to rapid in vivo catabolism of the linear peptide chain. In fact, several proteases have been reported to swiftly degrade NT and its analogs. Thus, angiotensin-converting enzyme (ACE) has been shown to rapidly cleave the $Tyr^{11}–Ile^{12}$ bond, whereas neprilysin (NEP) quickly hydrolyzes both the $Pro^{10}–Tyr^{11}$ and the $Tyr^{11}–Ile^{12}$ bonds [31–36]. Two additional metallopeptidases, EC 3.4.24.15 (thiolsensitive metallo-oligopeptidase, thimet-oligopeptidase (TOP)) cleaving the $Arg^8–Arg^9$ bond and EC 3.4.24.16 (neurolysin) hydrolyzing the $Pro^{10}–Tyr^{11}$ bond, may further contribute in the degradation of NT and its analogs [37,38]. However, these proteases are located within cells, and hence are less expected to encounter circulating NT radioligands and disturb their delivery to tumor sites.

In a recent study, we were able to demonstrate the involvement of ACE and NEP in the in vivo degradation of $[^{99m}Tc]$Tc–DT1 ($[^{99m}Tc]$Tc–$[N_4–Gly^7]$NT(7–13)) and $[^{99m}Tc]$Tc–DT5 ($[^{99m}Tc]$Tc–$[N_4–\beta Ala^7,Dab^9]$NT(7–13)) [39]. Furthermore, we showed that co-injection of the NEP inhibitor phosphoramidon (PA) [40] and the ACE inhibitor lisinopril (Lis) [41] resulted in significant stabilization of these radiotracers in peripheral mouse blood. Consequently, the uptake of both $[^{99m}Tc]$Tc–DT1 and $[^{99m}Tc]$Tc–DT5 in human NTS1R-positive colon adenocarcinoma tumors in mice was significantly enhanced [39]. Following this rationale, we are now interested in translating these positive findings into pancreatic cancer models. It should be noted that 95% of all pancreatic cancers are actually PDAC, one of the most devastating cancer types, with a five-year survival not exceeding 10%. A major problem in the management of PDAC is that the disease remains practically asymptomatic, and has already disseminated by the time of diagnosis. Treatment may be comprised of surgical resection followed by chemo/radiotherapy, but outcomes are rather limited, with most patients dying soon after diagnosis and the average survival not surpassing 28 months [42]. It is therefore imperative to make available effective theranostic tools to combat PDAC, including radiolabeled NTS1R-directed probes.

In the present study, we first evaluated the uptake of $[^{99m}Tc]$Tc–DT1 in a series of commercially available pancreatic cell lines, namely AsPC-1, PANC-1, MiaCapa-2, and Capan-1. We were interested in identifying the cell line by combining high radioligand uptake, indicative of high NTS1R expression, with practical convenience of handling, including acceptable doubling times during culture, as well as easy development of experimental tumors in severe combined immunodeficiency (SCID) mice available

in our facilities. The cell uptake of [99mTc]Tc–DT1 and [99mTc]Tc–DT5 was compared in the AsPC-1 cell line of choice. The metabolic stability of the two radioligands was compared in healthy mice without or during treatment with two approved and registered drugs, Entresto [43,44] or Lis, or their combination. Entresto pills for oral use contain a pro-form of the potent NEP inhibitor sacubitril released in vivo (Figure S1, Supplementary Materials), while Lis is a potent ACE inhibitor [41]. The impact of these treatments on the radioligand tumor uptake was studied in SCID mice bearing AsPC-1 xenografts, in order to assess the translational prospects of this methodology in PDAC patients.

2. Results

2.1. Radiolabelling and Quality Control

Radiolabelling of DT1 and DT5 with [99mTc]Tc was accomplished by 30 min incubation at room temperature in alkaline aqueous medium containing citrate anions and $SnCl_2$ as a reductant. Quality control of the radiolabelled products included high-performance liquid chromatography (HPLC) and instant thin-layer chromatography (ITLC) analysis, and revealed less than 2% total radiochemical impurities ([99mTc]TcO$_4$$^-$, [99mTc]Tc citrate, and [99mTc]TcO$_2$ × nH$_2$O). A single radiopeptide species was obtained at molecular activities of 20–40 MBq [99mTc]Tc/nmol peptide; representative radiochromatograms are included in Figure 1. Based on these findings, [99mTc]Tc–DT1 and [99mTc]Tc–DT5 were used without further purification in all subsequent biological assays.
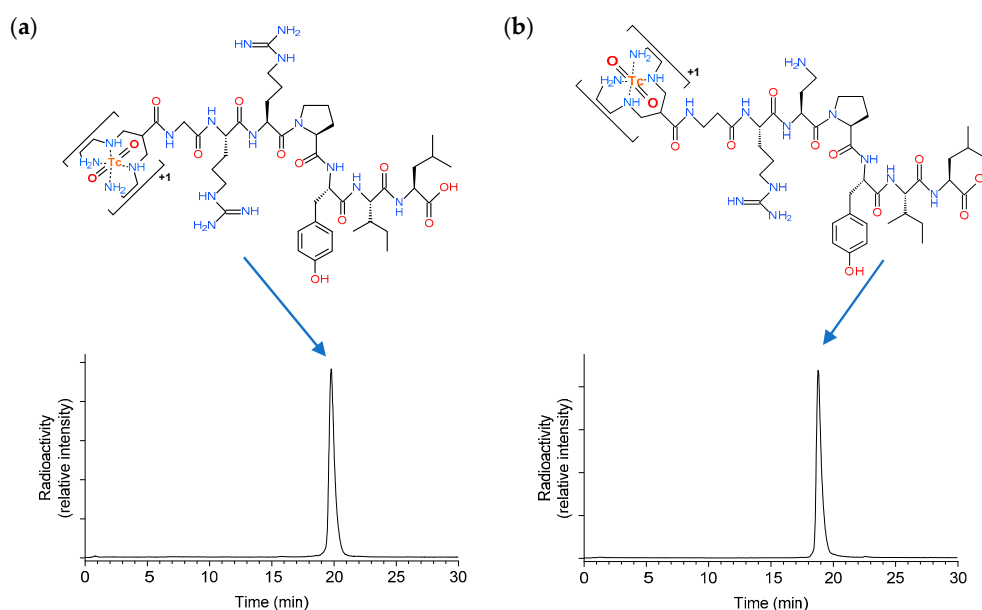

Figure 1. Representative radiochromatograms of high-performance liquid chromatography (HPLC) analysis of the radiolabeling mixture of (**a**) [99mTc]Tc–DT1 and (**b**) [99mTc]Tc–DT5 with the respective radioligand structures indicated.

2.2. Cell Uptake Studies

Comparative Cell Uptake of [99mTc]Tc–DT1 in AsPC-1, PANC-1, MiaCapa-2, and Capan-1 Cells

During 1 h incubation at 37 °C, [99mTc]Tc–DT1 displayed distinct NTS1R-mediated uptake across the AsPC-1, PANC-1, MiaCapa-2, and Capan-1 cell lines, as summarized in Figure 2a. The rank of specific cell uptake of [99mTc]Tc–DT1 was AsPC-1 (15.2% ± 2.6%) > PANC-1 (8.1% ± 2.8%; $p < 0.0001$ vs. AsPC-1) > MiaCapa-2 (2.7% ± 0.3%; $p <0.0001$ vs. PANC-1) > Capan-1 (0.4% ± 0.1%; $p < 0.0001$ vs. PANC-1, $p > 0.05$ vs. MiaCapa-2). In all cases, the bulk of cell-bound radioactivity was found in the internalized fraction, as consistent with a radioagonist profile. Cell uptake was banned in the presence of excess NT, implying an NTS1R-mediated process (Table S1; Supplementary Materials).
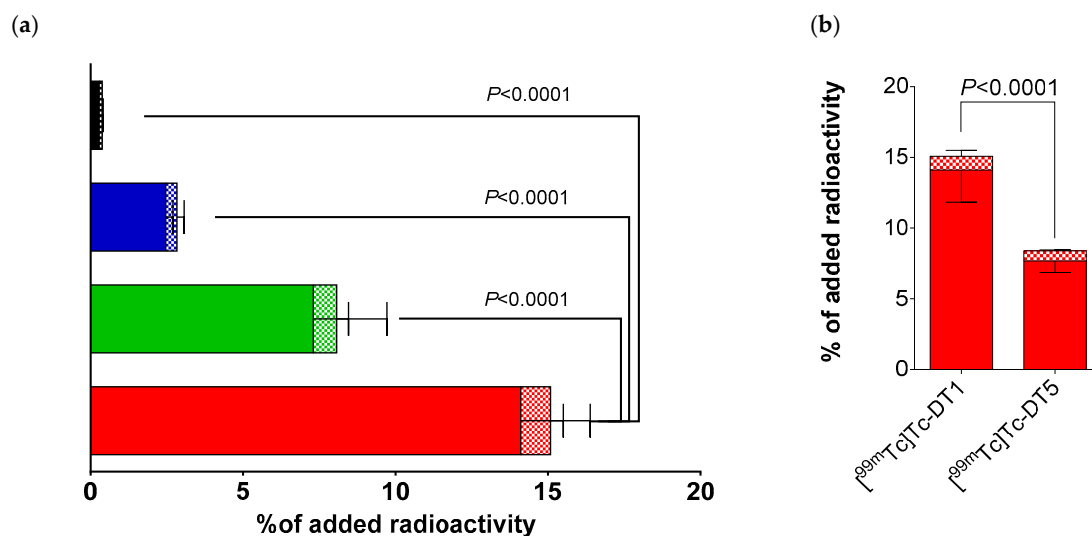
Figure 2. (**a**) Neurotensin subtype 1 receptor (NTS1R)-specific cell uptake of [^{99m}Tc]Tc–DT1 in AsPC-1 (red column), PANC-1 (green column), MiaCapa-2 (blue column), and Capan-1 (black column) cells during 1 h incubation at 37 °C. (**b**) Comparison of NTS1R-specific uptake of [^{99m}Tc]Tc–DT1 and [^{99m}Tc]Tc–DT5 in AsPC-1 cells during 1 h incubation at 37 °C; solid bars: internalized fraction; checkered bars: membrane-bound fraction. Results represent average values ± SD (*n* = 3, in triplicate); non-specific values were obtained in the presence of 1 μM neurotensin (NT), and were subtracted from totals to provide specific values. The study was conducted with cells as confluent monolayers.

When comparing [^{99m}Tc]Tc–DT1 and [^{99m}Tc]Tc–DT5 for their NTS1R-uptake in AsPC-1 cells at 1 h incubation at 37 °C, [^{99m}Tc]Tc–DT1 displayed significantly higher values (15.2% ± 2.6% vs. 8.4% ± 0.8%; *p* < 0.0001), as depicted in Figure 2b.

Time-dependent cell uptake curves for [^{99m}Tc]Tc–DT1 in AsPC-1, PANC-1, and MiaCapa-2 cells are included in Figure 3, but not for Capan-1, cells due to their poor overall uptake during the 1 h incubation. We observed the same trend of [^{99m}Tc]Tc–DT1 uptake across cell lines at all time intervals. Likewise, the bulk of radioactivity was found in the internalized fraction, with a lesser amount bound on the cell membrane.
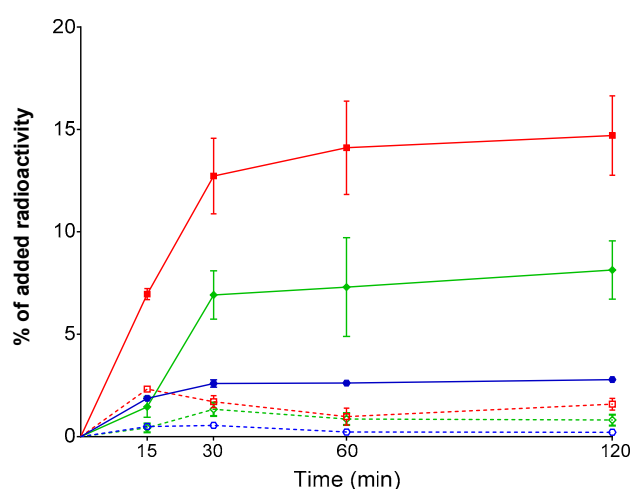
Figure 3. Time-dependent, NTS1R-specific cell uptake curves of [^{99m}Tc]Tc–DT1 in AsPC -1 (red lines), PANC-1 (green lines), and MiaCapa-2 (blue lines) cells at 37 °C (solid lines: internalized fraction; dotted lines: membrane-bound fraction). Results represent average values ± SD (*n* = 3, in triplicate); non-specific values were obtained in the presence of 1 μM NT, and were subtracted from totals to provide specific values. The study was conducted with cells as confluent monolayers.

2.3. In Vivo Studies

2.3.1. Comparative Stability of [^{99m}Tc]Tc–DT1 and [^{99m}Tc]Tc–DT5 in Mice: The Impact of Protease Inhibitors

The radiotracers exhibited poor resistance to degrading proteases after intravenous injection in mice. As revealed by HPLC analysis of blood samples collected at 5 min post-injection (pi), [^{99m}Tc]Tc–DT1 and [^{99m}Tc]Tc–DT5 degraded equally fast (1.8 ± 0.8% and 1.2 ± 0.2% intact; $p > 0.05$), although the pattern of forming radiometabolites was different for each compound (Table 1; Figure 4).

Table 1. Stabilities of [^{99m}Tc]Tc–DT1 and [^{99m}Tc]Tc–DT5 in peripheral mouse blood 5 min post-injection (pi) in untreated controls and in animals treated with Entresto, lisinopril (Lis), or their combination.

	Control	Entresto	Lis	Entresto+Lis
[^{99m}Tc]Tc–DT1	1.8 ± 0.8 (*n* = 4)	5.5 ± 3.9 (*n* = 5)	18.8 ± 2.5 (*n* = 3)	63.8 ± 7.5 (*n* = 3)
[^{99m}Tc]Tc–DT5	1.2 ± 0.2 (*n* = 3)	2.0 ± 0.6 (*n* = 3)	28.7 ± 3.6 (*n* = 3)	70.2 ± 4.9 (*n* = 3)

Data represents the mean percentage of intact radioligand ± SD; *n* of experiments are shown in parentheses.
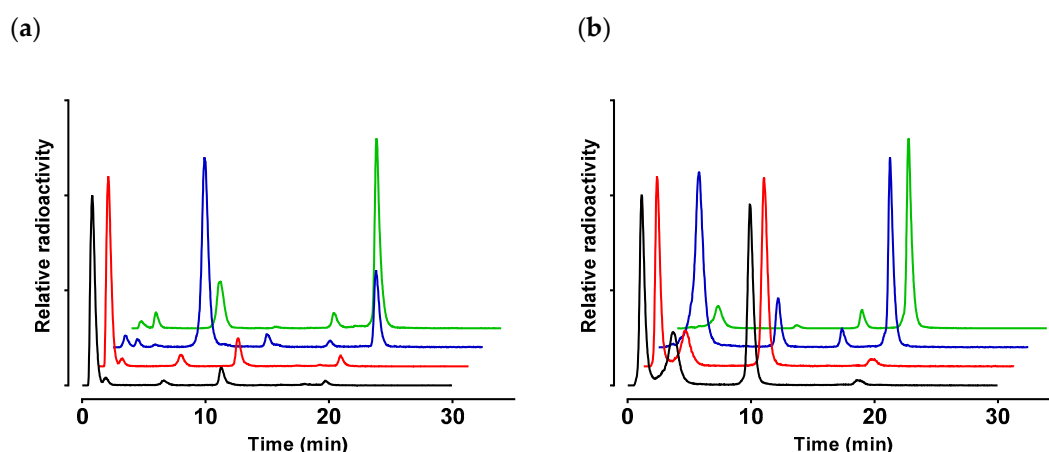
(**a**)   (**b**)

Figure 4. Representative radiochromatograms of HPLC analysis of mouse blood samples collected 5 min pi with (**a**) [^{99m}Tc]Tc–DT1 and (**b**) [^{99m}Tc]Tc–DT5; black line graphs correspond to samples from untreated controls, red line graphs to samples from animals receiving per os Entresto 30 min prior to radioligand injection, blue line graphs to samples from animals with Lis co-injected together with the radioligand, and green line graphs to samples from animals receiving Entresto 30 min prior to radioligand co-injection with Lis (HPLC system 2); percentages of intact radioligand are summarized in Table 1.

Treatment of mice with clinically established NEP and ACE inhibitors, as well as their combination, exerted profound effects not only on the overall metabolic stability of [^{99m}Tc]Tc–DT1 and [^{99m}Tc]Tc–DT5, but also on the pattern of radiometabolites found in mice blood at 5 min pi. Thus, treatment of mice with Entresto taken orally 30 min prior to radiotracer injection had hardly any effect on stability ($p > 0.05$ vs. controls for both radioligands). Conversely, co-injection of Lis significantly increased the overall stability of both radiotracers ([^{99m}Tc]Tc–DT1 to 18.8 ± 2.5% intact, $p < 0.0001$ vs. controls; [^{99m}Tc]Tc–DT5 to 28.7 ± 3.6% intact, $p < 0.0001$ vs. controls). Interestingly, a combination of these treatments resulted in further significant increases of metabolic stabilities of the two radiotracers ([^{99m}Tc]Tc–DT1 to 63.8 ± 7.5% intact, $p < 0.0001$ vs. Lis-treated mice; [^{99m}Tc]Tc–DT5 to 70.2 ± 4.9% intact, $p < 0.0001$ vs. Lis-treated mice).

These results imply cooperation of the two proteases, ACE and NEP, in the fast in vivo catabolism of [^{99m}Tc]Tc–DT1 and [^{99m}Tc]Tc–DT5. Furthermore, they indicate that ACE acts faster, given that

Entresto alone provides no considerable improvement of stability of either radiotracer, and is only effective during concomitant in situ inhibition of ACE by Lis.

2.3.2. Biodistribution of [^{99m}Tc]Tc–DT1 in AsPC-1 Tumor-Bearing SCID Mice: The Impact of Protease Inhibitors

The effect of in situ NEP + ACE inhibition on the biodistribution of [^{99m}Tc]Tc–DT1 in SCID mice bearing AsPC-1 xenografts at 4 h pi is summarized in Table 2; data is expressed as percent of injected activity per gram tissue (% IA/g) and represents mean values ± SD. The [^{99m}Tc]Tc–DT5 was not included in this study, in view of its inferior uptake by AsPC-1 cells compared with [^{99m}Tc]Tc–DT1 (Figure 2b). In addition, it displayed high renal values in mice during a previous study, most probably as a result of the pendant δ-amine of Dab^9 in the peptide chain [39].

Table 2. Biodistribution data for [^{99m}Tc]Tc–DT1, expressed as % IA/g mean ± SD in AsPC-1 xenograft-bearing SCID mice at 4 h pi, without or after treatment with Entresto + Lis.

	[^{99m}Tc]Tc–DT1: 4 h pi				
	Controls [1]		**Entresto + Lis** [2]		**Block** [3]
Blood	0.07 ± 0.01		0.08 ± 0.02		0.09 ± 0.01
Liver	0.44 ± 0.05		0.67 ± 0.06		0.55 ± 0.06
Heart	0.08 ± 0.01		0.11 ± 0.02		0.18 ± 0.11
Kidneys	4.18 ± 3.80	⊢ *p* < 0.0001 ⊣	6.81 ± 1.74	⊢ *p* < 0.001 ⊣	4.15 ± 1.75
Stomach	0.48 ± 0.26		0.57 ± 0.14		2.75 ± 1.63
Intestines	0.65 ± 0.04		2.13 ± 0.24		1.07 ± 0.01
Spleen	0.22 ± 0.05		0.58 ± 0.35		0.31 ± 0.07
Muscle	0.03 ± 0.01		0.06 ± 0.03		0.07 ± 0.06
Lungs	0.18 ± 0.03		0.62 ± 0.35		0.41 ± 0.07
Pancreas	0.05 ± 0.01		0.10 ± 0.01		0.08 ± 0.00
Tumor	1.25 ± 0.14	⊢ *p* < 0.0001 ⊣	7.05 ± 0.80	⊢ *p* < 0.0001 ⊣	0.74 ± 0.01

All animals were injected with 185 kBq/10 pmol peptide; [1] Control mice group (*n* = 4) with untreated animals; [2] Entresto + Lis mice group (*n* = 4) with animals receiving 12 mg Entresto per os 30 min prior to radiotracer co-injection, together with 200 μg Lis to in situ to inhibit NEP and ACE, respectively. [3] Block mice group (*n* = 3), with animals co-injected with 100 μg NT for in vivo NTS1R blockade, in addition to being treated with the Entresto + Lis combination.

We observe that the radioactivity in the blood and the body of mice has substantially cleared at 4 h pi. Uptake in the AsPC-1 xenografts is clearly visible, albeit low (1.25 ± 0.14% IA/g), while a higher radioactivity level is retained in the kidneys (4.18 ± 3.80% IA/g). Treatment of mice with the Entresto + Lis combination led to notable increase of the [^{99m}Tc]Tc–DT1 uptake in the AsPC-1 tumors (to 7.05 ± 0.80% IA/g; *p* < 0.0001 vs. controls) without affecting background radioactivity levels, except for the kidneys. Although some minor increase is observed in the kidneys, the increase in the tumors is higher during treatment, resulting in Tu/Ki ratios > 1. The observed high uptake of [^{99m}Tc]Tc–DT1 in the AsPC-1 tumors during Entresto + Lis treatment was shown to be NTS1R-mediated, given that it was banned by co-injection of excess NT in mice treated with the same inhibitor regimen (drop to 0.74 ± 0.01% IA/g; *p* < 0.0001 vs. Entresto + Lis treated mice).

The uptake of [^{99m}Tc]Tc–DT1 at 4 h pi in MiaCapa-1 xenografts in SCID mice treated with the Entresto + Lis combination (Table S2; Supplementary Materials) was much lower compared with AsPC-1 tumors in the respective Entresto + Lis group (1.97% ± 0.23% IA/g vs. 7.05% ± 0.80% IA/g; *p* < 0.0001), in line with findings from in vitro cell uptake/internalization assays.

3. Discussion

The limited success in the application of NTS1R-directed NT(8-13)-derived radiopeptides in cancer theranostics [30,45,46] has been related to the rapid cleavage of the NT backbone by peptidases. For example, ACE has been reported to hydrolyze the Tyr^{11}–Ile^{12} bond [31,32], and its action was

very soon recognized during metabolic stability determination assays [24]. Typically, this kind of experiments involves in vitro incubation of radioligands in mouse/human plasma, followed by chromatographic analysis of incubate samples to detect generated radiometabolites. Consequently, efforts toward ACE-resistant NTS1R-radioligands were directed to stabilize the Tyr^{11}–Ile^{12} bond, primarily via Tle^{12}/Ile^{12}–replacement [22,24,29].

Following this rationale, we have developed the Tle^{12}/Ile^{12}–modified [^{99m}Tc]Tc–DT6, displaying high receptor affinity (IC_{50} = 0.08 ± 0.02 nM) and high stability in mice plasma (>90% intact in mice plasma 2 h incubates) [29]. Unexpectedly, however, [^{99m}Tc]Tc–DT6 failed to target NTS1R-expressing tumor lesions in a subsequent "proof-of-principle" study in patients [30]. Aiming to elucidate these findings, we further studied the cell binding capabilities and in vivo stability of the radiotracer. We observed that the Tle^{12}/Ile^{12} substitution led to poor binding/internalization of [^{99m}Tc]Tc–DT6 in WiDr cells compared with non-Ile^{12}-substituted radioligands (e.g., 1.0 ± 0.4% specific cell binding vs. 10.1 ± 2.3% of [^{99m}Tc]Tc–DT1 at 1 h incubation; p < 0.0001) [39]. Furthermore, the in vivo stability of [^{99m}Tc]Tc–DT6 was found to be surprisingly lower than expected from in vitro assays (only 55.1 ± 3.9% of the radiotracer detected intact in peripheral mice blood at 5 min pi). The combination of these two unfavorable features seems to have led to the sub-optimal performance of [^{99m}Tc]Tc–DT6 in patients.

Earlier reports have implicated NEP (next to ACE) in the in vivo catabolism of NT, rapidly hydrolyzing both the Tle^{12}–Ile^{12} and the Pro^{10}–Tyr^{11} bonds of the peptide chain [31,32,35]. NEP is an ecto-enzyme with a broad substrate repertoire, and is omnipresent on vasculature walls and major tissues/organs of the body in high local concentrations, where it remains anchored on the membrane of epithelial cells [47,48]. Consequently, during stability assessment of peptide radioligands by in vitro assays in plasma incubates, the fast degrading action of NEP documented in vivo has been altogether missed. We have shown that NEP can quickly break down a wide range of radiopeptides entering the circulation, thereby compromising their supply and accumulation on tumor models in mice. Next, we were able to drastically interfere with this chain of disadvantageous events with the aid of NEP inhibitors. Through in situ inhibition of NEP, we could induce marked enhancement of tumor uptake of numerous biodegradable radiopeptides [49,50].

In the present study, we were interested in exploring the efficacy of [^{99m}Tc]Tc–DT1 to target NTS1R–positive pancreatic cancer during NEP and ACE inhibition in mice models. We have selected [^{99m}Tc]Tc–DT1 as the radioligand because it displayed maximum internalization/cell-binding amongst a series of related NT(7–13)-based radiotracers in colon adenocarcinoma WiDr cells [39]. As a first task, we have investigated the cell-binding/internalization of [^{99m}Tc]Tc–DT1 in a panel of human pancreatic cancer cell lines, in order to determine the cell line of choice to use in our preclinical models. As shown in Figure 2, clear differences could be established in the cell uptake/internalization of [^{99m}Tc]Tc-DT1 across AsPC-1, PANC-1, MiaCapa-2, and Capan-1 cells, with highest values associated with AsPC-1 cells at 1 h incubation. It is interesting to note that our findings were in line with previously reported NTS1R expression at the gene and protein levels across these cell lines [51]. Next, a time-dependent internalization study was carried out, whereby [^{99m}Tc]Tc–DT1 displayed again significantly higher values in AsPC-1 cells compared with all other cell lines (Figure 3). Subsequently, we compared the cell uptake/internalization of [^{99m}Tc]Tc–DT1 and a second, non-Tle^{12}/Ile^{12}-modified reference, [^{99m}Tc]Tc–DT5. In agreement with findings from WiDr cells [39], [^{99m}Tc]Tc–DT1 showed significantly higher values than [^{99m}Tc]Tc–DT5 in AspC-1 cells (Figure 2b).

Our second goal was to stabilize [^{99m}Tc]Tc–DT1, and the second reference [^{99m}Tc]Tc–DT5, in mice circulation by in situ ACE and/or NEP inhibition, using clinically established inhibitors. Through co-injection with the NEP inhibitor PA or the ACE-inhibitor Lis, we could previously induce significant stabilization of these radioligands in peripheral mice blood [39]. PA is not a clinically approved drug [40], and consequently time- and cost-intensive studies are required for approval of its use in a "proof-of-concept" study in PDAC patients. For such purposes, we have instead selected Entresto, a registered anti-hypertensive drug containing sacubitril (AHU377) [43,44]. The latter is actually the pro-drug, releasing the potent and specific NEP inhibitor sacubitrilat (LBQ657) in vivo upon

ester-hydrolysis by native esterases (Figure S1). We have orally administered single 12 mg/200 mL doses of Entresto (24/26 sacubitril/valsartan) pills per animal (*vide infra*) 30 min prior to radioligand injection to accomplish maximum NEP inhibition. As summarized in Table 1, both [99mTc]Tc–DT1 and [99mTc]Tc–DT5 were found to be >63% intact in peripheral mice blood during concomitant NEP- and ACE-inhibition, vs. the <2% intact found in non-treated controls. Entresto alone had only a very minor effect on stability, in contrast to Lis, which led to partial stabilization of the two analogs. However, Entresto had significant impact on further stabilizing the radiotracers when mice received Lis as well. This finding is consistent with the assumption that ACE acts faster on the two analogs, and upon ACE inhibition, NEP is given time to act. These stabilization effects validate Entresto as a viable candidate for clinical testing of this concept.

The third and final goal of the present study was to evaluate the biodistribution of [99mTc]Tc–DT1 in pancreatic mice models without or during treatment with the Entresto + Lis combination. Based on cell uptake results, we selected AsPC-1 cells for tumor induction in mice. As summarized in Table 2, Entresto + Lis treatment resulted in marked increase of [99mTc]Tc–DT1 uptake in the AsPC-1 xenografts at 4 h pi (7.05% ± 0.80% IA/g vs. 1.25% ± 0.14% IA/g in controls; $p < 0.0001$), which was shown to be NTS1R-mediated. Uptake in all other organs remained low, except for the kidneys. However, in the Entresto + Lis treated mice, the tumor-to-kidneys ratio was clearly superior. To our knowledge, these are the highest uptake values reported for AsPC-1 xenografts in mice for radiolabeled NT-radiotracers. For example, [68Ga]Ga–DOTA–NT–20.3 (Ac–Lys(1,4,7,10-tetraazacyclododecane–1,4,7,10-tetraacetic acid)–Pro–Me–Arg–Arg–Pro–Tyr–Tle–Leu–OH) reached 5.28% ± 0.93% IA/g uptake at 1 h pi, with about the same values found in the kidneys [52]. In another example, the bi-modal tracer [68Ga]Ga–NODAGA–Lys(Cy5**)–AEEAc–[Me–Arg8,Tle12]NT(7–13) (NODAGA: 1,4,7-triazacyclononane,1-glutaric acid-4,7-acetic acid; Cy5**: tetrasulfonated cyanine 5.0; AEEAc: 8-amino-3,6-dioxaoctanoic acid) reached 2.56% ± 0.97% IA/g at 1 h in the same model, with quite elevated kidney values though (20% IA/g) [53]. However, such comparisons should be made with caution, in view of potential differences in protocols applied across labs.

The aforementioned positive results obtained with the Entresto + Lis combination in AsPC-1 xenografts confirm previous observations in mice bearing WiDr tumors and treated with PA + Lis [39]. Undoubtedly, perspectives for clinical translation of this promising methodology in PDAC patients rely on the availability of clinically established NEP and ACE inhibitors, such as Entresto [43,44] and Lis [41] used in the present study. It should be noted that application of the NEP inhibition approach has been recently shown to improve the diagnostic sensitivity of radiolabeled gastrin in medullary thyroid cancer patients. In this first "proof-of-concept" study, patients received per os the registered and widely used anti-diarrhea drug racecadotril [54]. The latter is a pro-drug releasing the potent NEP-inhibitor thiorphan in the blood after in vivo ester-hydrolysis by native esterases [48]. Therefore, further studies are warranted to explore the applicability of this concept in PDAC patients as well.

4. Materials and Methods

4.1. Chemicals and Radionuclides

All chemicals were reagent grade, and were used as such without further purification. The peptide conjugates DT1 and DT5 were synthesized on the solid support and obtained from PiChem (Graz, Austria). NT was purchased from Bachem (Bubendorf, Switzerland). Entresto was obtained from a local pharmacy, and Lis was purchased from Sigma-Aldrich (St. Louis, MO, USA).

Technetium-99m in the form of [99mTc]NaTcO4 was collected by elution of a [99Mo]Mo/[99mTc]Tc generator (Ultra-Technekow V4 Generator, Curium Pharma, Petten, The Netherlands).

4.1.1. Radiolabeling

The lyophilized peptide analogs were dissolved in water to a final concentration of 1 mM, and 50 μL aliquots were stored at −20 °C. Labelling with [^{99m}Tc]Tc was performed in an Eppendorf vial containing 0.5 M phosphate buffer (pH 11.5; 50 μL). The [^{99m}Tc]NaTcO$_4$ eluate (420 μL, 370–550 MBq) was added to the vial, followed by 0.1 M sodium citrate (5 μL), the peptide stock solution (15 μL, 15 nmol), and a freshly prepared SnCl$_2$ solution in ethanol (10 μL, 10 μg). The mixture was left to react for 30 min at room temperature, and the pH was neutralized with the addition of 0.1 M HCl.

4.1.2. Quality Control

Quality control was comprised of radioanalytical, high-performance liquid chromatography (HPLC) and instant thin-layer chromatography (ITLC). HPLC analyses were performed on a Waters Chromatograph coupled to a 996-photodiode array UV detector (Waters, Vienna, Austria) and a Gabi gamma detector (Raytest RSM Analytische Instrumente GmbH, Straubenhardt, Germany). Data processing and chromatography were controlled with Empower Software (Waters, Milford, MA, USA). For analyses, a Symmetry Shield RP-18 (5 μm, 3.9 mm × 150 mm) cartridge column (Waters, Eschborn, Germany) was eluted at 1 mL/min flow rate with a linear gradient system, system 1, starting from 0% B and advancing to 40% B within 20 min (solvent A = 0.1% aqueous trifluoroacetic acid (TFA) and B = acetonitrile (MeCN)). ITLC analyses were performed on Whatman 3 mm chromatography paper strips (GE Healthcare, Chicago, IL, United States), developed up to 10 cm from the origin, with 5 M ammonium acetate/MeOH 1:1 (*v/v*) for the detection of reduced, hydrolyzed technetium ([^{99m}Tc]TcO$_2$ × nH$_2$O) or acetone for the detection of [^{99m}Tc]TcO$_4^-$.

All manipulations with beta- and gamma-emitting radionuclides and their solutions were performed by trained and authorized personnel behind suitable shielding in licensed laboratories, in compliance with European radiation safety guidelines, and were supervised by the Greek Atomic Energy Commission (license #A/435/17092/2019).

4.2. *In Vitro Assays*

4.2.1. Cell Lines and Culture

The human pancreatic adenocarcinoma AsPC-1, PANC-1, MiaCapa-2, and Capan-1 cell lines were obtained from LGC Standards GmbH (Wesel, Germany). All culture reagents were purchased from Gibco BRL, Life Technologies (Grand Island, NY, USA) or from Biochrom KG Seromed (Berlin, Germany). Cells were grown in Roswell Park Memorial Institute-1640 Medium (RPMI-1640; AsPC-1 cells) or Dulbecco's Modified Eagle's Medium (DMEM; PANC-1, MiaCapa-2, and Capan-1 cells) with GlutaMAX-I, supplemented with 10% (*v/v*) fetal bovine serum (FBS), 100 U/mL penicillin, and 100 μg/mL streptomycin, and kept in a controlled humidified air containing 5% CO$_2$ at 37 °C. Splitting of cells with a ratio of 1:3 to 1:5 was performed when approaching confluency, using a trypsin/EDTA (0.05%/0.02% *w/v*) solution.

4.2.2. Internalization of [^{99m}Tc]Tc Radiotracers in AsPC-1, PANC-1, MiaCapa-2, and Capan-1 Cells

For internalization assays, AsPC-1, PANC-1, MiaCapa-2, and Capan-1 cells were seeded in six-well plates (≈1 × 10^6 cells per well) the day before the experiment. Cells were rinsed twice with ice-cold internalization medium (IM; culture medium supplemented by 1% (*v/v*) FBS), and then fresh IM was added (1.2 mL) at 37 °C, followed by test radiopeptide (250 fmol total peptide in 150 μL IPBS (0.5% *w/v* BSA–PBS,) 100,000–200,000 cpm). Non-specific internalization was determined by a parallel triplicate series containing 1 μM NT. After incubation at 37 °C, the plates were placed on ice, the medium was collected, and the plates were washed with IPBS (1 mL). Membrane-bound fractions were collected by incubating the cells 2 × 5 min in acid-wash solution (2 × 600 μL; 50 mM glycine buffer pH 2.8, 0.1 M NaCl) at room temperature. After rinsing the cells with IPBS (1 mL), internalized fractions were collected by lysing the cells with 1 M NaOH (2 × 600 μL). Sample radioactivity was measured

on the gamma counter, and the percentage of specific internalized and membrane-bound fractions were calculated with Microsoft Excel (after subtracting the non-specific from the overall internalized and membrane-bound counts). Results represent the specific mean internalized ± SD of total added radioactivity per well from three experiments performed in triplicate. Furthermore, the internalization and cell uptake of [^{99m}Tc]Tc-DT1 and [^{99m}Tc]Tc-DT5 were compared head-to-head during 1 h incubation in AsPC-1 cells at 37 °C, following the above-described procedure.

In another set of experiments, the internalization/cell uptake of [^{99m}Tc]Tc–DT1 was assessed overtime in AsPC-1, PANC-1, and MiaCapa-2 by incubation at 37 °C. During this study, the same protocol was followed again, but four different incubation times were applied: 15 min, 30 min, 1 h, and 2 h; Capan-1 cells were not included in this assay, due to the poor internalization/cell uptake of [^{99m}Tc]Tc–DT1 shown in the first set of experiments at 1 h.

4.3. Animal Studies

4.3.1. Metabolic Studies in Mice

A bolus containing [^{99m}Tc]Tc–DT1 and [^{99m}Tc]Tc–DT5 (100 μL, 50–60 MBq, 3 nmol of total peptide in vehicle: saline/EtOH = 9:1 *v/v*) was injected in the tail vein of healthy male Swiss albino mice, together with the vehicle (100 μL; control group) or Lis (100 μL of vehicle containing 200 μg Lis; Lis group). In another set of animals, mice received a single Entresto dose by gavage 30 min prior to injection of the radiotracer, together with the vehicle (100 μL; Entresto group) or Lis (100 μL of vehicle containing 200 μg Lis; Entresto + Lis group). For animal treatment, Entresto (24/26 sacubitril/valsartan) pills were ground to a fine powder in a mortar, divided, and suspended in tab water to individual 12 mg/200 mL doses per animal. Animals were euthanized 5 min pi, and blood was collected and immediately placed in pre-chilled polypropylene vials containing EDTA on ice. Samples were centrifuged at 2000× *g* at 4 °C for 10 min, then the plasma was collected and mixed with an equal volume of MeCN and centrifuged again for 10 min at 15,000× *g* at 4 °C. The supernatant was collected and concentrated to a small volume under a gentle N$_2$ flux at 40 °C, diluted with physiological saline (400 μL) and filtered through a Millex GV filter (0.22 μm). Suitable aliquots of the filtrate were analyzed by RP-HPLC on a Symmetry Shield RP18 (5 μm, 3.9 mm × 20 mm) column (Waters, Germany), eluted at a flow rate of 1 mL/min and adopting gradient system 2: 100% A/0% B to 70% A/30% B in 30 min; A = 0.1% TFA in H$_2$O, and B = MeCN (system 2). The elution time (t_R) of the intact radioligand was determined by co-injection with a sample of the labelling reaction solution.

4.3.2. Tumor Induction in SCID Mice

A suspension of freshly harvested AsPC-1 (~150 μL, 5×10^6) or MiaCapa-2 (~150 μL, 3.5×10^6) cells in normal saline was subcutaneously inoculated in the flanks of 6-week-old SCID mice (NCSR "Demokritos" Animal House; group A = 11 mice, 20.34 ± 1.63 g body weight; group B = 4 mice, 22.81 ± 0.25 g body weight). After 3–4 weeks, palpable tumors (group A, AsPC-1: 0.23 ± 0.11 g; group B: MiaCapa-2: 0.14 ± 0.05 g) had developed at the inoculation sites, and biodistribution was performed.

4.3.3. Biodistribution in SCID Mice Bearing AsPC-1 and MiaCapa-2 Xenografts

At the day of biodistribution, a bolus of [^{99m}Tc]Tc–DT1 (185 kBq, 10 pmol total peptide, in vehicle: saline/EtOH = 9:1 *v/v*) was intravenously injected in the tail of group A mice, together with the vehicle (100 μL; control group: four mice). The rest of group A mice were treated with Entresto 30 min prior to radioligand co-injection with Lis (200 μg Lis dissolved in 100 μL vehicle; Entresto + Lis-group: four mice), or with Lis plus excess NT (200 μg Lis and 100 μg NT dissolved in 100 μL vehicle; block group: three mice). Animals were euthanized at 4 h pi, and blood samples, organs of interest, and AsPC-1 tumors were dissected, weighed, and counted in the gamma counter. Biodistribution data was calculated as percent of injected activity per gram tissue (% IA/g) with the aid of suitable standards of the injected activity, using the Microsoft Excel program. Results represent mean values ± SD, *n* = 4.

Mice of group B (four animals with MiaCapa-2 tumors) were treated with the Entresto + Lis combination, as described above, and the same protocol was followed.

4.3.4. Statistical Analysis

For statistical analysis of biological results, a two-way ANOVA with multiple comparisons was used, applying Tukey's post-hoc analysis (GraphPad Prism Software, San Diego, CA, USA); *p* values of <0.05 were considered to be statistically significant.

All animal studies were performed in compliance to European guidelines in supervised and licensed facilities (EL 25 BIO 021), whereas the study protocols were approved by the Department of Agriculture and Veterinary Service of the Prefecture of Athens (revised protocol number 1609 approved on 24 April 2019 for the stability studies and revised protocol number 1610 approved on 24 April 2019 for biodistribution and imaging studies).

5. Conclusions

Pancreatic cancer, and in particular PDAC, is a devastating disease with five-year survival below 5%. Typically, cancer has already spread without symptoms until the time of diagnosis, and prognosis is poor. Consequently, molecular tools for diagnosis and therapy—theranostics—of PDAC are urgently needed to improve survival rates for patients. In the present work, we have evaluated the NT(7–13)-based radiotracer [^{99m}Tc]Tc–DT1 in NTS1R-positive pancreatic cell and mice models, given that overexpression of the NTS1R target has been documented in PDAC. We selected AsPC-1 cells amongst a panel of human pancreatic cancer cell lines as our study model, based on the superior NTS1R-specific uptake of [^{99m}Tc]Tc–DT1 in these cells. Next, we were able to markedly stabilize [^{99m}Tc]Tc–DT1 in mice circulation through the administration of two clinically established inhibitors, namely Entresto (for NEP inhibition) and Lis (for ACE inhibition). Last but not least, we could induce notable increases in the NTS1R-specific uptake of [^{99m}Tc]Tc–DT1 in AsPC-1 tumors xenografted in mice compared with controls. These findings are in favor of clinical translation of the protease-inhibition concept in PDAC patients.

References

1. Vincent, J.P.; Mazella, J.; Kitabgi, P. Neurotensin and neurotensin receptors. *Trends Pharmacol. Sci.* **1999**, *20*, 302–309. [CrossRef]
2. Kitabgi, P. Targeting neurotensin receptors with agonists and antagonists for therapeutic purposes. *Curr. Opin. Drug Discov. Devel.* **2002**, *5*, 764–776. [PubMed]
3. Evers, B.M. Neurotensin and growth of normal and neoplastic tissues. *Peptides* **2006**, *27*, 2424–2433. [CrossRef] [PubMed]
4. Reubi, J.C.; Waser, B.; Friess, H.; Buchler, M.; Laissue, J. Neurotensin receptors: A new marker for human ductal pancreatic adenocarcinoma. *Gut* **1998**, *42*, 546–550. [CrossRef]

5. Ishizuka, J.; Townsend, C.M., Jr.; Thompson, J.C. Neurotensin regulates growth of human pancreatic cancer. *Ann. Surg.* **1993**, *217*, 439–445. [CrossRef] [PubMed]

6. Ehlers, R.A.; Kim, S.; Zhang, Y.; Ethridge, R.T.; Murrilo, C.; Hellmich, M.R.; Evans, D.B.; Townsend, C.M., Jr.; Mark Evers, B. Gut peptide receptor expression in human pancreatic cancers. *Ann. Surg.* **2000**, *231*, 838–848. [CrossRef] [PubMed]

7. Reubi, J.C.; Waser, B.; Schaer, J.C.; Laissue, J.A. Neurotensin receptors in human neoplasms: High incidence in Ewing's sarcomas. *Int. J. Cancer* **1999**, *82*, 213–218. [CrossRef]

8. Gui, X.; Guzman, G.; Dobner, P.R.; Kadkol, S.S. Increased neurotensin receptor-1 expression during progression of colonic adenocarcinoma. *Peptides* **2008**, *29*, 1609–1615. [CrossRef]

9. Morgat, C.; Chastel, A.; Molinie, V.; Schollhammer, R.; Macgrogan, G.; Velasco, V.; Malavaud, B.; Fernandez, P.; Hindie, E. Neurotensin receptor-1 expression in human prostate cancer: A pilot study on primary tumors and lymph node metastases. *Int. J. Mol. Sci.* **2019**, *20*, 1721. [CrossRef]

10. Souaze, F.; Dupouy, S.; Viardot-Foucault, V.; Bruyneel, E.; Attoub, S.; Gespach, C.; Gompel, A.; Forgez, P. Expression of neurotensin and NT1 receptor in human breast cancer: A potential role in tumor progression. *Cancer Res.* **2006**, *66*, 6243–6249. [CrossRef]

11. Nikolaou, S.; Qiu, S.; Fiorentino, F.; Simillis, C.; Rasheed, S.; Tekkis, P.; Kontovounisios, C. The role of neurotensin and its receptors in non-gastrointestinal cancers: A review. *Cell Commun. Signal.* **2020**, *18*, 68. [CrossRef] [PubMed]

12. Reubi, J.C.; Waser, B.; Schmassmann, A.; Laissue, J.A. Receptor autoradiographic evaluation of cholecystokinin, neurotensin, somatostatin and vasoactive intestinal peptide receptors in gastro-intestinal adenocarcinoma samples: Where are they really located? *Int. J. Cancer* **1999**, *81*, 376–386. [CrossRef]

13. Reubi, J.C. Peptide receptors as molecular targets for cancer diagnosis and therapy. *Endocr. Rev.* **2003**, *24*, 389–427. [CrossRef]

14. Zhang, J.; Singh, A.; Kulkarni, H.R.; Schuchardt, C.; Müller, D.; Wester, H.J.; Maina, T.; Rösch, F.; van der Meulen, N.P.; Müller, C.; et al. From bench to bedside-the Bad Berka experience with first-in-human studies. *Semin. Nucl. Med.* **2019**, *49*, 422–437. [CrossRef] [PubMed]

15. Granier, C.; van Rietschoten, J.; Kitabgi, P.; Poustis, C.; Freychet, P. Synthesis and characterization of neurotensin analogues for structure/activity relationship studies. Acetyl-neurotensin-(8–13) is the shortest analogue with full binding and pharmacological activities. *Eur. J. Biochem.* **1982**, *124*, 117–124. [CrossRef]

16. Cutler, C.S.; Hennkens, H.M.; Sisay, N.; Huclier-Markai, S.; Jurisson, S.S. Radiometals for combined imaging and therapy. *Chem. Rev.* **2013**, *113*, 858–883. [CrossRef]

17. Maes, V.; García-Garayoa, E.; Blauenstein, P.; Tourwé, D. Novel ^{99m}Tc-labeled neurotensin analogues with optimized biodistribution properties. *J. Med. Chem.* **2006**, *49*, 1833–1836. [CrossRef]

18. Alshoukr, F.; Rosant, C.; Maes, V.; Abdelhak, J.; Raguin, O.; Burg, S.; Sarda, L.; Barbet, J.; Tourwé, D.; Pelaprat, D.; et al. Novel neurotensin analogues for radioisotope targeting to neurotensin receptor-positive tumors. *Bioconjug. Chem.* **2009**, *20*, 1602–1610. [CrossRef]

19. de Visser, M.; Janssen, P.J.J.M.; Srinivasan, A.; Reubi, J.C.; Waser, B.; Erion, J.L.; Schmidt, M.A.; Krenning, E.P.; de Jong, M. Stabilised In-111-labelled DTPA- and DOTA-conjugated neurotensin analogues for imaging and therapy of exocrine pancreatic cancer. *Eur. J. Nucl. Med. Mol. Imaging* **2003**, *30*, 1134–1139. [CrossRef]

20. Achilefu, S.; Srinivasan, A.; Schmidt, M.A.; Jimenez, H.N.; Bugaj, J.E.; Erion, J.L. Novel bioactive and stable neurotensin peptide analogues capable of delivering radiopharmaceuticals and molecular beacons to tumors. *J. Med. Chem.* **2003**, *46*, 3403–3411. [CrossRef]

21. Jia, Y.; Shi, W.; Zhou, Z.; Wagh, N.K.; Fan, W.; Brusnahan, S.K.; Garrison, J.C. Evaluation of DOTA-chelated neurotensin analogs with spacer-enhanced biological performance for neurotensin-receptor-1-positive tumor targeting. *Nucl. Med. Biol.* **2015**, *42*, 816–823. [CrossRef] [PubMed]

22. Maschauer, S.; Prante, O. Radiopharmaceuticals for imaging and endoradiotherapy of neurotensin receptor-positive tumors. *J. Label. Comp. Radiopharm.* **2018**, *61*, 309–325. [CrossRef] [PubMed]

23. Couder, J.; Tourwé, D.; Van Binst, G.; Schuurkens, J.; Leysen, J.E. Synthesis and biological activities of psi (CH$_2$NH) pseudopeptide analogues of the C-terminal hexapeptide of neurotensin. *Int. J. Pept. Protein Res.* **1993**, *41*, 181–184. [CrossRef]

24. Schubiger, P.A.; Allemann-Tannahill, L.; Egli, A.; Schibli, R.; Alberto, R.; Carrel-Remy, N.; Willmann, M.; Blauenstein, P.; Tourwé, D. Catabolism of neurotensins. Implications for the design of radiolabeling strategies of peptides. *Q. J. Nucl. Med.* **1999**, *43*, 155–158.

25. Kostelnik, T.I.; Orvig, C. Radioactive main group and rare earth metals for imaging and therapy. *Chem. Rev.* **2019**, *119*, 902–956. [CrossRef]

26. de Jong, M.; Breeman, W.A.; Kwekkeboom, D.J.; Valkema, R.; Krenning, E.P. Tumor imaging and therapy using radiolabeled somatostatin analogues. *Acc. Chem. Res.* **2009**, *42*, 873–880. [CrossRef] [PubMed]

27. Baum, R.P.; Kulkarni, H.R. THERANOSTICS: From Molecular Imaging Using Ga-68 Labeled Tracers and PET/CT to Personalized Radionuclide Therapy-The Bad Berka Experience. *Theranostics* **2012**, *2*, 437–447. [CrossRef]

28. Nock, B.A.; Nikolopoulou, A.; Reubi, J.C.; Maes, V.; Conrath, P.; Tourwé, D.; Maina, T. Toward stable N$_4$-modified neurotensins for NTS1-receptor-targeted tumor imaging with ^{99m}Tc. *J. Med. Chem.* **2006**, *49*, 4767–4776. [CrossRef]

29. Maina, T.; Nikolopoulou, A.; Stathopoulou, E.; Galanis, A.S.; Cordopatis, P.; Nock, B.A. [^{99m}Tc]demotensin 5 and 6 in the NTS1-r-targeted imaging of tumours: Synthesis and preclinical results. *Eur. J. Nucl. Med. Mol. Imaging* **2007**, *34*, 1804–1814. [CrossRef]

30. Gabriel, M.; Decristoforo, C.; Woll, E.; Eisterer, W.; Nock, B.; Maina, T.; Moncayo, R.; Virgolini, I. [^{99m}Tc]demotensin VI: Biodistribution and initial clinical results in tumor patients of a pilot/phase I study. *Cancer Biother. Radiopharm.* **2011**, *26*, 557–563. [CrossRef]

31. Checler, F.; Vincent, J.P.; Kitabgi, P. Degradation of neurotensin by rat brain synaptic membranes: Involvement of a thermolysin-like metalloendopeptidase (enkephalinase), angiotensin-converting enzyme, and other unidentified peptidases. *J. Neurochem.* **1983**, *41*, 375–384. [CrossRef] [PubMed]

32. Skidgel, R.A.; Engelbrecht, S.; Johnson, A.R.; Erdös, E.G. Hydrolysis of substance P and neurotensin by converting enzyme and neutral endopeptidase. *Peptides* **1984**, *5*, 769–776. [CrossRef]

33. Schindler, L.; Bernhardt, G.; Keller, M. Modifications at Arg and Ile give neurotensin(8-13) derivatives with high stability and retained NTS1 receptor affinity. *ACS Med. Chem. Lett.* **2019**, *10*, 960–965. [CrossRef]

34. Kitabgi, P.; De Nadai, F.; Rovere, C.; Bidard, J.N. Biosynthesis, maturation, release, and degradation of neurotensin and neuromedin N. *Ann. N. Y. Acad. Sci.* **1992**, *668*, 30–42. [CrossRef] [PubMed]

35. Kitabgi, P.; Dubuc, I.; Nouel, D.; Costentin, J.; Cuber, J.C.; Fulcrand, H.; Doulut, S.; Rodriguez, M.; Martinez, J. Effects of thiorphan, bestatin and a novel metallopeptidase inhibitor JMV 390-1 on the recovery of neurotensin and neuromedin N released from mouse hypothalamus. *Neurosci. Lett.* **1992**, *142*, 200–204. [CrossRef]

36. Kitabgi, P. Inactivation of neurotensin and neuromedin N by Zn metallopeptidases. *Peptides* **2006**, *27*, 2515–2522. [CrossRef] [PubMed]

37. Paschoalin, T.; Carmona, A.K.; Rodrigues, E.G.; Oliveira, V.; Monteiro, H.P.; Juliano, M.A.; Juliano, L.; Travassos, L.R. Characterization of thimet oligopeptidase and neurolysin activities in B16F10-NEX2 tumor cells and their involvement in angiogenesis and tumor growth. *Mol. Cancer* **2007**, *6*, 44. [CrossRef]

38. Berti, D.A.; Morano, C.; Russo, L.C.; Castro, L.M.; Cunha, F.M.; Zhang, X.; Sironi, J.; Klitzke, C.F.; Ferro, E.S.; Fricker, L.D. Analysis of intracellular substrates and products of thimet oligopeptidase in human embryonic kidney 293 cells. *J. Biol. Chem.* **2009**, *284*, 14105–14116. [CrossRef]

39. Kanellopoulos, P.; Kaloudi, A.; Jong, M.; Krenning, E.P.; Nock, B.A.; Maina, T. Key-protease inhibition regimens promote tumor targeting of neurotensin radioligands. *Pharmaceutics* **2020**, *12*, 528. [CrossRef]

40. Suda, H.; Aoyagi, T.; Takeuchi, T.; Umezawa, H. Letter: A thermolysin inhibitor produced by actinomycetes: Phosphoramidon. *J. Antibiot. (Tokyo)* **1973**, *26*, 621–623. [CrossRef]

41. Millar, J.A.; Derkx, F.H.; McLean, K.; Reid, J.L. Pharmacodynamics of converting enzyme inhibition: The cardiovascular, endocrine and autonomic effects of MK421 (enalapril) and MK521. *Br. J. Clin. Pharmacol.* **1982**, *14*, 347–355. [CrossRef]

42. Cornelissen, B.; Knight, J.C.; Mukherjee, S.; Evangelista, L.; Xavier, C.; Caobelli, F.; Del Vecchio, S.; Rbah-Vidal, L.; Barbet, J.; de Jong, M.; et al. Translational molecular imaging in exocrine pancreatic cancer. *Eur. J. Nucl. Med. Mol. Imaging* **2018**, *45*, 2442–2455. [CrossRef]

43. Gu, J.; Noe, A.; Chandra, P.; Al-Fayoumi, S.; Ligueros-Saylan, M.; Sarangapani, R.; Maahs, S.; Ksander, G.; Rigel, D.F.; Jeng, A.Y.; et al. Pharmacokinetics and pharmacodynamics of LCZ696, a novel dual-acting angiotensin receptor-neprilysin inhibitor (ARNi). *J. Clin. Pharmacol.* **2010**, *50*, 401–414. [CrossRef]

44. McMurray, J.J.; Packer, M.; Solomon, S.D. Neprilysin inhibition for heart failure. *N. Engl. J. Med.* **2014**, *371*, 2336–2337. [CrossRef] [PubMed]

45. Froberg, A.C.; van Eijck, C.H.J.; Verdijsseldonck, M.C.C.; Melis, M.; Bakker, W.H.; Krenning, E.P. Use of neurotensin analogue In-111-DTPA-neurotensin (In-111-MP2530) in diagnosis of pancreatic adenocarcinoma. *Eur. J. Nucl. Med. Mol. Imaging* **2004**, *31* (Suppl. 2), S392.

46.   Büchegger, F.; Bonvin, F.; Kosinski, M.; Schaffland, A.O.; Prior, J.; Reubi, J.C.; Blauenstein, P.; Tourwé, D.; García Garayoa, E.; Bischof Delaloye, A. Radiolabeled neurotensin analog, ^{99m}Tc-NT-XI, evaluated in ductal pancreatic adenocarcinoma patients. *J. Nucl. Med.* **2003**, *44*, 1649–1654. [PubMed]

47.   Roques, B.P.; Noble, F.; Dauge, V.; Fournie-Zaluski, M.C.; Beaumont, A. Neutral endopeptidase 24.11: Structure, inhibition, and experimental and clinical pharmacology. *Pharmacol. Rev.* **1993**, *45*, 87–146.

48.   Roques, B.P. Zinc metallopeptidases: Active site structure and design of selective and mixed inhibitors: New approaches in the search for analgesics and anti-hypertensives. *Biochem. Soc. Trans.* **1993**, *21 Pt 3*, 678–685. [CrossRef]

49.   Nock, B.; Maina, T.; Krenning, E.; de Jong, M. In vivo enzyme inhibition - a new promising route toward higher diagnostic sensitivity and therapeutic efficacy of tumor-directed radiopeptides. *J. Nucl. Med.* **2014**, *55*, 121–127. [CrossRef] [PubMed]

50.   Lymperis, E.; Kaloudi, A.; Sallegger, W.; Bakker, I.L.; Krenning, E.P.; de Jong, M.; Maina, T.; Nock, B.A. Radiometal-dependent biological profile of the radiolabeled gastrin-releasing peptide receptor antagonist SB3 in cancer theranostics: Metabolic and biodistribution patterns defined by neprilysin. *Bioconjug. Chem.* **2018**, *29*, 1774–1784. [CrossRef]

51.   Geer, S. Evaluation of the Neurotensin Receptor-1 as Target for Molecular Imaging and Radiotherapy of Pancreatic and Prostate Cancer. Ph.D. Thesis, Friedrich-Alexander-Universität, Erlangen-Nürnberg, Germany, 24 September 2018.

52.   Prignon, A.; Provost, C.; Alshoukr, F.; Wendum, D.; Couvelard, A.; Barbet, J.; Forgez, P.; Talbot, J.N.; Gruaz-Guyon, A. Preclinical evaluation of ^{68}Ga-DOTA-NT-20.3: A promising PET imaging probe to discriminate human pancreatic ductal adenocarcinoma from pancreatitis. *Mol. Pharm.* **2019**, *16*, 2776–2784. [CrossRef] [PubMed]

53.   Renard, E.; Dancer, P.A.; Portal, C.; Denat, F.; Prignon, A.; Goncalves, V. Design of bimodal ligands of neurotensin receptor 1 for positron emission tomography imaging and fluorescence-guided surgery of pancreatic cancer. *J. Med. Chem.* **2020**, *63*, 2426–2433. [CrossRef] [PubMed]

54.   Valkema, R.A.; Maina, T.; Nock, B.A.; de Blois, E.; Melis, M.L.; Konijnenberg, M.W.; Koolen, S.L.W.; Peeters, R.P.; de Herder, W.W.; de Jong, M. Clinical translation of the pepprotect: A novel method to improve the detection of cancer and metastases by peptide scanning under the protection of enzyme inhibitors. *Eur. J. Nucl. Med. Mol. Imaging* **2019**, *46*, S701–S702. [CrossRef]

Publisher's Note: MDPI stays neutral with regard to jurisdictional claims in published maps and institutional affiliations.